

Springer Remote Sensing/Photogrammetry

S. Hazra

A. Mukhopadhyay

A.R. Ghosh

D. Mitra

V.K. Dadhwal *Editors*

Environment and Earth Observation

Case Studies in India

 Springer

Springer Remote Sensing/Photogrammetry

More information about this series at <http://www.springer.com/series/10182>

S. Hazra · A. Mukhopadhyay · A.R. Ghosh
D. Mitra · V.K. Dadhwal
Editors

Environment and Earth Observation

Case Studies in India

 Springer

Editors

S. Hazra
School of Oceanographic Studies
Jadavpur University
Kolkata
India

D. Mitra
Marine and Atmospheric Studies
Indian Space Research Organisation
Dehradun
India

A. Mukhopadhyay
School of Oceanographic Studies
Jadavpur University
Kolkata, West Bengal
India

V.K. Dadhwal
Indian Space Research Organisation
National Remote Sensing Centre
Hyderabad
India

A.R. Ghosh
Department of Science and Technology
Kolkata, West Bengal
India

ISSN 2198-0721 ISSN 2198-073X (electronic)
Springer Remote Sensing/Photogrammetry
ISBN 978-3-319-46008-6 ISBN 978-3-319-46010-9 (eBook)
DOI 10.1007/978-3-319-46010-9

Library of Congress Control Number: 2016951647

© Springer International Publishing Switzerland 2017

This work is subject to copyright. All rights are reserved by the Publisher, whether the whole or part of the material is concerned, specifically the rights of translation, reprinting, reuse of illustrations, recitation, broadcasting, reproduction on microfilms or in any other physical way, and transmission or information storage and retrieval, electronic adaptation, computer software, or by similar or dissimilar methodology now known or hereafter developed.

The use of general descriptive names, registered names, trademarks, service marks, etc. in this publication does not imply, even in the absence of a specific statement, that such names are exempt from the relevant protective laws and regulations and therefore free for general use.

The publisher, the authors and the editors are safe to assume that the advice and information in this book are believed to be true and accurate at the date of publication. Neither the publisher nor the authors or the editors give a warranty, express or implied, with respect to the material contained herein or for any errors or omissions that may have been made.

Printed on acid-free paper

This Springer imprint is published by Springer Nature
The registered company is Springer International Publishing AG
The registered company address is: Gewerbestrasse 11, 6330 Cham, Switzerland

Editorial

Among the modern and emerging disciplines of natural science, remote sensing technologies have become a significant and worldwide tool for various approaches towards monitoring, assessment and conservation of natural resources and environment. Remote sensing makes it possible to collect information about an object or a phenomenon without making physical contact with it. This phenomenon is especially helpful in the case of monitoring areas which are difficult to access or sometimes simply inaccessible. With the availability of remotely sensed data from different sensors of various platforms with a wide range of spatiotemporal, radiometric, and spectral resolutions has made remote sensing perhaps, the best source of data for large-scale applications and study. Recent advances made in microwave sensing, hyperspectral imaging and high spatial resolution offer promising techniques to cultivate various aspects related to monitoring large-scale environment in a fruitful and cost-effective way. Applying remote sensing in understanding hydrological processes, several oceanic features along with mapping inventory of water resources across different spatial and temporal scales can bring about tremendous outputs. In the field of forestry and agriculture, terrain analysis, forest management, updating of existing forest and agricultural inventories, vegetation cover type discrimination, delineation of burned areas and mapping of cleared areas are done applying various techniques of remote sensing. Climate change and climate-induced disasters have become a menace for the present-day scientists. Remote sensing seems to be the most efficient tool for studying, monitoring and hence formulating preventive strategies for combating such phenomenon.

This book would not have seen the light without the assistance of the Department of Science and Technology, Govt. of West Bengal. The active participation of National Remote Sensing Centre (NRSC), Hyderabad; Indian Institute of Remote Sensing (IIRS), Dehradun and Jadavpur University, West Bengal is also humbly acknowledged.

Contents

Part I Remote Sensing of Landscape and Environment

Geospatial Analysis for Industrial Site Suitability Using AHP Modeling: A Case Study	3
Chalantika L. Salui and Punnya Brata Hazra	
Standalone Open-Source GIS-Based Tools for Land and Water Resource Development Plan Generation	23
Arati Paul, V.M. Chowdary, Dibyendu Dutta and J.R. Sharma	
Downscaling of Coarse Resolution Satellite Remote Sensing Thermal Data	35
Sandip Mukherjee, P.K. Joshi and R.D. Garg	
Future Projection of Rainfall by Statistical Downscaling Method in a Part of Central India	57
Sananda Kundu, Deepak Khare and Arun Mondal	

Part II Remote Sensing of Agriculture and Forestry

Identification of Crop Types with the Fuzzy Supervised Classification Using AWiFS and LISS-III Images	73
Arun Mondal, Deepak Khare and Sananda Kundu	
Application of Remote Sensing in Assessing the Impacts of Mahatma Gandhi National Rural Employment Guarantee Act (MGNREGA), in Ratlam District, Madhya Pradesh, India	87
Bhaskar Sinha, Deep Narayan Singh, Anoma Basu and Mili Ghosh	
Mangrove Forest Cover Changes in Indian Sundarban (1986–2012) Using Remote Sensing and GIS	97
Kaberi Samanta and Sugata Hazra	

Change Detection of Vegetation Cover Using Synthetic Color Composite with Some Other Techniques	109
A.S. Seikh, A. Halder and S. Mukhopadhyay	

Part III Remote Sensing of Coast and Ocean

Estimation of Air-Sea CO₂ Exchange and Decadal Change of Surface Water fCO₂ in a Shallow Continental Shelf Using in Situ and Remote Sensing Data During Winter	123
Anirban Akhand, Sudip Manna, Partho Pratim Mondal, Abhra Chanda, Sachinandan Dutta, Sourav Das, Sugata Hazra, Debasish Mitra, P.V. Nagamani, K.H. Rao, S.B. Choudhury and V.K. Dadhwal	

Identification of River Discontinuity Using Geo-Informatics to Improve Freshwater Flow and Ecosystem Services in Indian Sundarban Delta	137
Tuhin Bhadra, Anirban Mukhopadhyay and Sugata Hazra	

Comparative Assessment of Morphological and Landuse/Landcover Change Pattern of Sagar, Ghoramara, and Mousani Island of Indian Sundarban Delta Through Remote Sensing	153
Rituparna Hajra, Amit Ghosh and Tuhin Ghosh	

Part IV Remote Sensing of Natural Hazards

A Comparative Evaluation of Weight-Rating and Analytical Hierarchical (AHP) for Landslide Susceptibility Mapping in Dhalai District, Tripura	175
Kapil Ghosh, Shreya Bandyopadhyay and Sunil Kumar De	

Micro Level Vulnerability Assessment of a Community Living in Mousuni Island in the Indian Sundarban: An Integrated Study Employing Geoinformatics	195
Bimalesh Samanta, Shouvik Das and Sugata Hazra	

Analyzing Trends of Urbanization and Concomitantly Increasing Environmental Cruciality—A Case of the Cultural City, Kolkata	215
Richa Sharma, P.K. Joshi and Sandip Mukherjee	

Part V Remote Sensing of Wild Habitat

Habitat Suitability Modelling for Sambar (<i>Rusa unicolor</i>): A Remote Sensing and GIS Approach	231
Ekwal Imam	

Snow Leopard Habitat Modeling Using Neuro-Fuzzy Technique and a Comparative Analysis Between Traditional Overlay and Neuro-Fuzzy Technique—A Case Study of Chamoli and Pithorgarh District of Uttarakhand 247
S. Sen, G. Areedran and C.K. Singh

Index 265

Introduction

The urge for the acquisition of information regarding any object or even a phenomenon undergoing in and around that object without making any physical contact with the object dates back to 1840s when primitive photographs were used to be taken from cameras secured to tethered balloons in order to carry out topographic mapping. However, with the advancement of technology, attempts of satellite-based imaging started its venture in the 1950s. The term 'remote sensing' was then coined for the first time in the United States of America. Among the various possible definitions of the term 'remote sensing', the most lucid one states that it is the art and science of identifying, observing and measuring an object without coming into direct contact with it. Now the field of 'remote sensing' has a vast expanse and it has become indispensable in various earth science based disciplines such as geology, oceanography, ecology, marine science, hydrology, agriculture and forestry. Remote sensing has also found a wide spread application in the fields such as military, intelligence, crime management, commercial, economic, planning and so forth. The present book is an attempt to assemble various scholarly works throwing light on the several technologies and applications of remote sensing which can benefit the modern-day environmental scientists for better understanding and monitoring of the earth and earthly processes. The edited chapters of the present book are subclassified into five separate domains: 'remote sensing of landscape and environment', 'remote sensing of agriculture and forestry', 'remote sensing of coast and ocean', 'remote sensing of natural hazards' and lastly 'remote sensing of wild habitat'. Brief introductions about the theme of each and every chapter under these subcategories are discussed in this chapter.

'Landscape and environment' are perhaps the two most important spheres, where the use and significance of remote sensing was long understood. Multifarious activities take place in both short-term and long-term temporal scale which needs to be monitored over a large spatial scale. This is where it was first realized that the in situ data collection process will not merely serve the purpose of knowing each and every nook and corner of a large spatial extent. Moreover, monitoring at a fixed short-term scale was also many a times not feasible by in situ methods. Thus remote sensing emerged as a very efficient tool which coupled with in situ data collection

led to give rise to a strong wing of environmental monitoring. In this book, four chapters are assembled in this subcategory of 'Remote Sensing of Landscape and Environment'. Salui and Hazra in their chapter discussed the identification of a suitable site for industrial purpose by means of multi-criteria decision-making using advanced hierarchical process. Various information like land use/land cover database has been generated using IRS P6-LISS-III satellite images of 2009 and 2011 and several other factors such as soil, land capability, hydro-geomorphology and population density were taken into account to finally suggest suitable areas for industrial prospect. It will promote a higher socioeconomic condition of the local people in the study area retaining the possibilities for sustainable development. Similarly Paul et al. in their chapter reported about preparation of 'Land and Water Resource Development Plan Generation' with the help of a standalone open-source GIS based tool like that of Map Window GIS that can be customized through dot net programming. This chapter mainly emphasizes on the fact that how several information layers in spatial database can be stacked together and based on a set of logical conditions, a suitable land and water resource development plan can be extracted from them (for a particular study area), which could be beneficial for the policymakers. In another chapter, Mukherjee et al. dealt with an acute problem of downscaling coarse resolution satellite remote sensing thermal data. They pointed out that high-resolution thermal imagery is though available but their temporal resolution is very low. On the contrary on daily basis coarse resolution thermal imagery is available. This chapter aimed to provide a comprehensive account of thermal remote sensing data downscale techniques so as to bridge these two types of datasets (one having higher spatial resolution and the other having higher temporal resolution) and how they can also be used for thematic mapping, geospatial modeling and scenario generation including climate change. Lastly, Kundu et al. discussed a very important climatic phenomenon, i.e., the rainfall of a specified area. Through their chapter they tried to predict the long-term future rainfall based on the historical past data. Statistical downscaling model (SDSM) has been applied to estimate the future rainfall using general circulation model (GCM).

Like landscape and environment, 'agriculture and forestry' is also one of the most crucial domains of natural science. Agricultural science and forestry emerged as subjects of tremendous importance in the last century, as both these heads are almost directly related to human livelihood and sustenance along with a far-reaching impact on the global climate. Four chapters comprise this category in the present book, out of which two dealt with agriculture and other two regarding forestry. Mondal et al. discussed about the identification of crop types implementing the fuzzy supervised classification upon the IRS P6, AWiFS and LISS-III Images. Crop identification in a particular area is a difficult task by simply using the survey method and at the same time it is extremely essential for planning and management of water resources. Hence, this type of study is enormously helpful for the policymakers to sustain the agriculture productivity. Sinha et al. on the other hand tried to assess the Impacts of Mahatma Gandhi National Rural Employment Guarantee Act (MGNREGA) in a particular district of Central India. MGNREGA is the first ever demand driven livelihood act that guarantees 100 days of employment

in every rural household. Under this scheme several dug wells were built in respective farmer's agricultural land in order to enhance the availability of water for sustainable agriculture especially in the semi-arid and arid regions. This chapter tried explicitly to quantify the benefits that the rural population could utilize due to these measures in the form of increased irrigated area, crop productivity and cropping intensity. In the field of forestry, Samanta and Hazra tried to assess the minute changes taking place in the mangrove forest cover of Indian Sundarban. In this chapter, they have categorized six major classes of forest cover by supervised and unsupervised classification of the mangrove forest area: dense forest, degraded forest, saline blanks, water body, sand (beaches/dunes) and mud flats. The sequences of forest cover changes within these subclasses were minutely studied in this chapter. In another chapter, Seikh et al. reported the positive sides as well as the limitations in the technique of change detection of vegetation cover using synthetic color composite. They also associated the normalized difference vegetation index (NDVI) index comparison and vectorization process in their analysis.

Another important domain where a wide arena of remote sensing application is used by scientists throughout the globe is the 'coast and ocean'. Several coastal processes and biogeochemistry of oceans are being monitored nowadays by remote sensing. Since these areas cover a large spatial extent of the globe, remote sensing application has become inevitable to monitor and measure several parameters whose dynamics are very crucial from the perspective global climate and earthly processes. Also the dynamic nature of the coast requires to be monitored in a temporal domain and remote sensing data with high temporal resolution is most suitable to address this issue. In this segment, we have three contributions. Akhand et al. tried to figure out the variability of fugacity of carbon dioxide in the continental shelf waters of the northern Bay of Bengal with the help of remote sensing data. CO₂ is one the most studied gas of the atmosphere owing to its greenhouse properties and its potential to substantially alter the global climate by means of global warming. This region, the northern Bay of Bengal off the West Bengal coast, has a very shallow bathymetry and acquiring in situ data is very cumbersome. The authors have tried to explore the relationship between water surface CO₂ concentration (which in turn is very crucial as the rate of exchange of CO₂ between the sea surface and the atmosphere determines the residence time of CO₂ in the atmosphere) with sea surface temperature. The decadal change in CO₂ concentration of the water surface is also assessed through remote sensing data in this chapter. Bhadra et al. carried out a very interesting work in the Indian Sundarbans delta trying to identify the discontinuity of river network in his area by means of remotely sensed imageries and extracting several water indices from them. The river flow in the delta especially the source of freshwater enhances the flow-dependent ecosystem services in this region. Thus identifying the regions of discontinuity would enable the policymakers to go for apt measures that can rejuvenate the defunct courses of the river and nourish the delta with more fresh water. In another chapter, Hajra et al. tried to delineate the morphological change dynamics of three crucial islands lying within the Indian Sundarban deltaic landmass namely Sagar, Ghoramara and Mousani Island. The geomorphic and the land use type changes

over a long temporal scale have been analyzed with the help of remotely sensed imageries in order to formulate the strategic planning for the sustenance of these islands.

One of the most crucial aspects of natural science that has received foremost attention of various scientists in the last few decades is the 'natural hazards'. Especially with the ongoing climate change the frequency and occurrences of natural calamities such as cyclone, landslides due to excessive rainfall, storm surges, etc., have increased manifold leading to both loss of life and property. Thus this domain has a special significance and in the present date various strategic planning and analysis of hazards are being carried out with the help of remote sensing and GIS. In this book there are three chapters that are devoted to natural hazards. Ghosh et al. tried to assess the landslide susceptibility of a landslide prone zone by using weight-rating and analytical hierarchical processes. They took into account different causative factors like lithology, road buffer, slope, relative relief, rainfall, fault buffer, land use/land cover and drainage density to prepare the final susceptibility map. This type of landslide susceptibility map delineates the potential areas of landslide occurrence which is considered to be the first step for landslide hazard management. In another chapter, Samanta et al. computed the composite vulnerability (VR_c) which is a product of physical, as well as socioeconomic vulnerability at community level of Mousuni Island situated in the Indian Sundarban which is under accelerating threat of climate change related impacts. Factors such as severe coastal erosion, repeated breach of embankments, cyclones, storm surge and inundation causing loss of lives, properties and displacement and migration of families have been considered in this study. This type of study is expected to help in planned adaptation that can be taken up by administrators and policymakers for reducing the risks due to climate change. Lastly, Sharma et al. dealt with an essential aspect of urban expansion and tried to quantify the degradation of the overall environment of the city of Kolkata (one of the most populous and polluted cities of India) by analyzing various remotely sensed imageries. An environmental cruciality indicator (ECI) was developed for this study using the vegetation indices and the land surface temperature (LST) and based on its variability along with some other environmental variables such as the moisture intensity of the surface, greenness and the built-up intensity, the overall degradation of the micro-climate has been assessed for this metropolis.

Last but not least, a very interesting aspect has been covered in this book, i.e., the application of remote sensing in wild habitat. Imam et al. has argued that the concept of wildlife species conservation starts with the identification of their suitable habitat as it provides essential information for wildlife refuge design and management. In this study multiple logistic regression is integrated with remote sensing and geographic information system to evaluate the suitable habitats available for Sambar (*Rusa unicolor*) in Chandoli tiger reserve, Maharashtra, India. Layers of different variables such as land use land cover, forest density, proximity to disturbances and water resources and a digital terrain model were created from satellite and topographic sheets. These layers along with GPS location of Sambar presence/absence and multiple logistic regression (MLR) techniques were

integrated in a GIS environment to model habitat suitability index of Sambar. In similar study, Sen et al. tried to optimize the habitat suitability for an endangered species as per the International Union for Conservation of Nature's (IUCN) Red List, named snow leopard (*uncia uncia*). In this study a neuro-fuzzy model has been developed using the MATLAB ANFIS editor to determine the suitable habitat zones for snow leopards in the Himalayan state.

Thus on the whole it can be stated that this book comprises a wide variety of chapters where various tools of remote sensing and GIS have been utilized to find solutions of multifarious problems covering several aspects of environment. Readers of interdisciplinary domain are expected to find interest in this book due to its heterogeneity in the subjects covered. Finally, the book has been written in a very eloquent language for better understanding of a wide spectrum of readers.

Part I
Remote Sensing of Landscape and
Environment

Geospatial Analysis for Industrial Site Suitability Using AHP Modeling: A Case Study

Chalantika L. Salui and Punnya Brata Hazra

Abstract This study attempts the land suitability mapping for the industrial sitting. To facilitate this, base level spatial information, i.e., land use/land cover database has been generated using on-screen interpretation technique from multi-season (Kharif, Rabi, and Zaid) IRS P6—LISS-III satellite images of 2009 and 2011. Information have also been taken for existing infrastructural (transportation) and administrative territorial information up to mouza level, existing industries with their polluting categories (Red, Orange, Green, Exempted, and Proposed), Soil, Land capability, Hydro-geomorphology, and Population density. The study has been conducted on Contai-I block of Purba Medinipur District, West Bengal, INDIA, with the main objective of multicriteria decision-making for industrial site suitability analysis using Advanced Hierarchical Process. The variables are being assigned individual weightage by AHP weightage matrix. Hierarchical weightage mapping has provided with a final suitability map for future industrial prospect. The study area belongs to a backward district in terms of industrial development. So, suggested suitable areas can promote a higher socioeconomic condition of the block retaining the possibilities for sustainable development.

Keywords Suitability mapping · Multi-criteria-decision-making · Hierarchical process · Suitability analysis · Weightage matrix · Sustainable development

1 Introduction

Industrial development of an area makes significant change in the socioeconomic identity of the dwellers. But, setting up of an industry is the outcome of a long background analysis because it should not hamper the sustainable development and

C.L. Salui (✉) · P.B. Hazra
West Bengal State Council of Science and Technology, Department of Science
and Technology, Government of West Bengal, Bikash Bhavan, Salt Lake,
Kolkata-91, India
e-mail: chalantikal@gmail.com

© Springer International Publishing Switzerland 2017
S. Hazra et al. (eds.), *Environment and Earth Observation*,
Springer Remote Sensing/Photogrammetry, DOI 10.1007/978-3-319-46010-9_1

ecological balance. This includes demand for industrialization of that area to replace agricultural production as well as magnitude of fulfillment of industrial requirements. Other parameters are profit maximization of industrial production as well as the environmental quality assurance of the area (Gupta et al. 2002). This study will take care of all the parameter where the last two parameters will be considered according to the characteristics of the proposed industry to be setup. As a case study, Contai-I block of Purba Medinipur district has been taken (Fig. 1). This district is mostly a low agricultural productive zone (District Statistical Handbook 1999 and 2000). So, for the socioeconomic development of the district, development of secondary sector like industry should be encouraged. For the purpose of industrial planning, the selection should be acceptable by the industrialists but it should not affect the local environment and inhabitants adversely as well. Here an attempt has been taken to get such a balanced scenario for the setup of an industry. A decision modeling has been executed for the purpose. This is ‘Advanced Hierarchical Process (AHP)’ where all the variables with their categories or sub-variables have been assigned individual weightage as per their hierarchy (Laha 2012). The hierarchical comparison is run through a weightage matrix which ultimately provides weightage for a specific variable. All these weightage

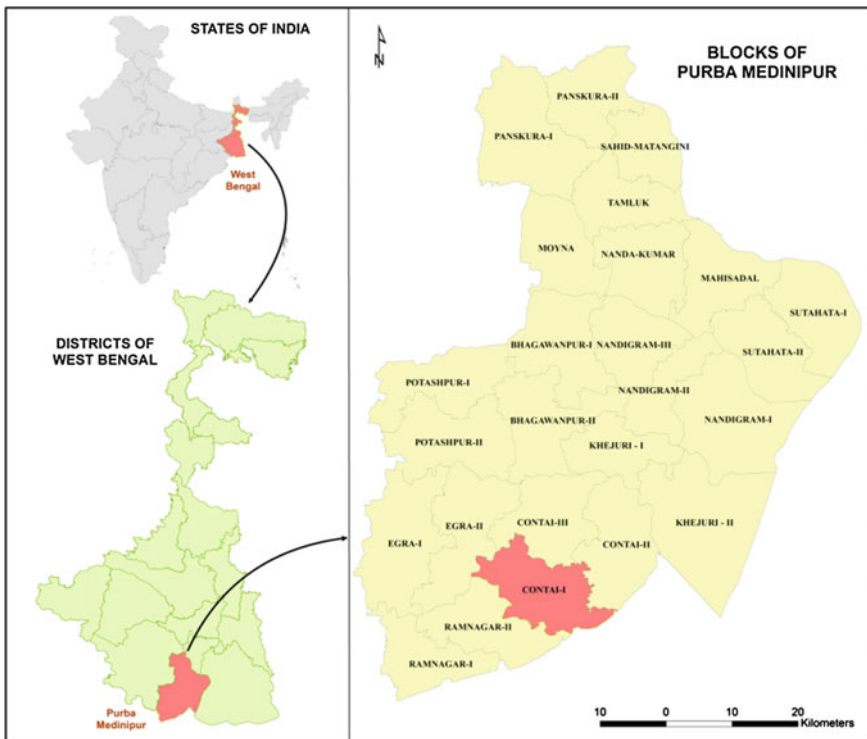


Fig. 1 Study area

calculations have been done here as raster pixels. So, each pixel covering the study area is carrying weightage for each variable. Thus, total step wise calculations here are conducted for individual pixel and accordingly come with the output of magnitude of priority. This prioritization of such spatial entity can be very much helpful for such a block level developmental planning.

2 Study Area

Contai I is the southern block of Purba Medinipur District, West Bengal, India, (Table 1) with coastal lofty sand dunes. Contai means ‘Sand bound reefs’ or sand walls (Fig. 1). This block is surrounded by Bay-of-Bengal in the southern portion whereas, Ramnagar-II, Egra-II, Contai-II, and Contai-III on the other sides.

This is a backward district in terms of industrial development. Only a few small industries (Table 2) are sparsely distributed over the entire block.

Table 1 Demographic data

Geographical area	155.27 km ²
Total population	170,848
Male population	88,110
Female population	82,733
Density of population	1100/km ²
No. of Gram Panchayat	8
No. of Mouza	225

Source Census of India (2011)

Table 2 Industry types

Sl. No.	Industry type	Pollution category	Area (m ²)
1	Rice mill	Industry (orange)	4815.76
2	Rice mill	Industry (orange)	2711.39
3	Oil mil	Industry (green)	2347.18
4	Rice mill	Industry (orange)	2792.33
5	Saw mill	Industry (orange)	3682.64
6	Rice mill	Industry (orange)	8457.93
7	Saw mill	Industry (orange)	4330.14
8	Saw mill	Industry (orange)	4411.07
9	Rice mill	Industry (orange)	3925.45
10	Saw mill	Industry (orange)	4249.20
11	Polythene industry	Industry (red)	485.62
12	Cashew factory	Non-polluting industry	809.37

Source Land use mapping for Land Bank, DST, WBSCST, Govt. of West Bengal

3 Aims and Objectives

Main objective of this study is to prioritize the areas for industrial setup. Attempt has been made to study the Multi-Criteria-Decision-Making for Industrial Site Suitability Analysis using Weightage Variables. All the variables have been run through a decision modeling to get individual weightage to be assigned. This study will help to suggest locations for the establishment of industries to plan for a higher status of industrial development where retention of environmental quality has been taken into consideration. Hence, the output will be serving the planners with existing industrial detailing along with the proposed sites to be taken under consideration with their location information.

4 Database

Land Use/Land Cover mapping as well as infrastructure mapping has been conducted with multi-season satellite image, Survey of India topographical sheets and other co-lateral data as well as sufficient field verification. Multi-season satellite images (Kharif, Rabi, and Zaid) which have been analyzed are of three seasons of IRS-LISS-III of 2008–09 (Table 3). Multi-season image interpretation gives the cropping frequency in a year like single crop, multicrop, etc.

Other data used are

- Hydro-Geomorphology Map taken from Project Report District Environmental Atlas, Purba Medinipur District, West Bengal, WBSCST (West Bengal State Council of Science and Technology), DST (Dept. of Science and Technology), Govt. of West Bengal, 2006
- Soil Map taken from Project Report District Environmental Atlas, Purba Medinipur District, West Bengal, WBSCST, DST, Govt. of West Bengal, 2006
- Land Capability Map taken from Project Report District Environmental Atlas, Purba Medinipur District, West Bengal, WBSCST, DST, Govt. of West Bengal, 2006
- Population data from Census of India, 2001
- Data on existing industries provided by Land and Land Records Depts., Govt. of West Bengal
- Land use/Land cover data from Land use mapping for Land Bank project, WBSCST, DST, Govt. of West Bengal

Table 3 Imagery details

Satellite	Sensor	Date of pass
IRS-P6	LISS-III	23.03.2009
IRS-P6	LISS-III	30.10.2008
IRS-P6	LISS-III	03.02.2009

5 Methodology

The primary base layers have all been prepared based on RS-GIS analysis. The land use/land cover, infrastructure mapping have been done using the on-screen analysis of satellite images as enlisted in the database section. Single and multiple cropping areas have been detected using temporal analysis from satellite images of different seasons. All these layers were spatially correlated on the GIS platform. GPS has been also used to correlate the data with real-world scenario. After the generation of base layers as the parameters, the decision-making process was run through a modeling, which is known as Advanced Hierarchical Process or AHP (Fig. 2).

AHP Decision modeling:

Analytical Hierarchy Process (AHP) is one multi-criteria-decision-making method that was originally developed by Prof. Thomas L. Saaty. This is a method to derive ratio scales from paired comparisons. Inputs can be obtained from actual measurements such as price, weight, etc., or from subjective opinion such as satisfaction, feelings, and preferences. The ratio scales are derived from the principal eigenvectors and the consistency index derived from the principal eigenvalue. The normalized principal eigenvectors are called priority vectors. As it is normalized, the sum of all elements in priority vector is 1. The priority vector shows relative weights among the things that we compare (Saaty 1987).

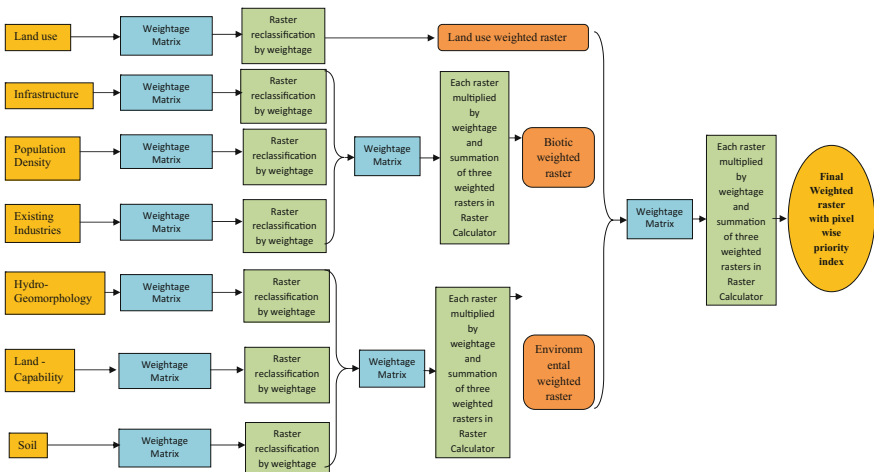


Fig. 2 Methodology flow-chart of the decision modeling

6 Weightage Analysis

Weightage matrix is a matrix where value is assigned on the basis of hierarchical relation in between two variables. Relational value is assigned out of 10. So, a value assigned to a particular relation gives 1/10th of that value to its inverse relation in a weightage matrix. The variables here have been taken here as per their hierarchical position. Like infrastructure, population density, existing industries, hydro-geomorphology, land capability, and soil rasters have been considered as the variables of first hierarchy. Land use has been directly taken in second hierarchy. Infrastructure, population density, and existing industries have been calculated to get biotic variables of second hierarchy. Hydro-geomorphology, land capability, and soil rasters have been calculated to get an output of environmental variable of second hierarchy. Finally these three variables of second hierarchy are run through model (Fig. 3) to get a final priority weightage raster. Logic behind the assignment of hierarchical values for the variables is elaborated below.

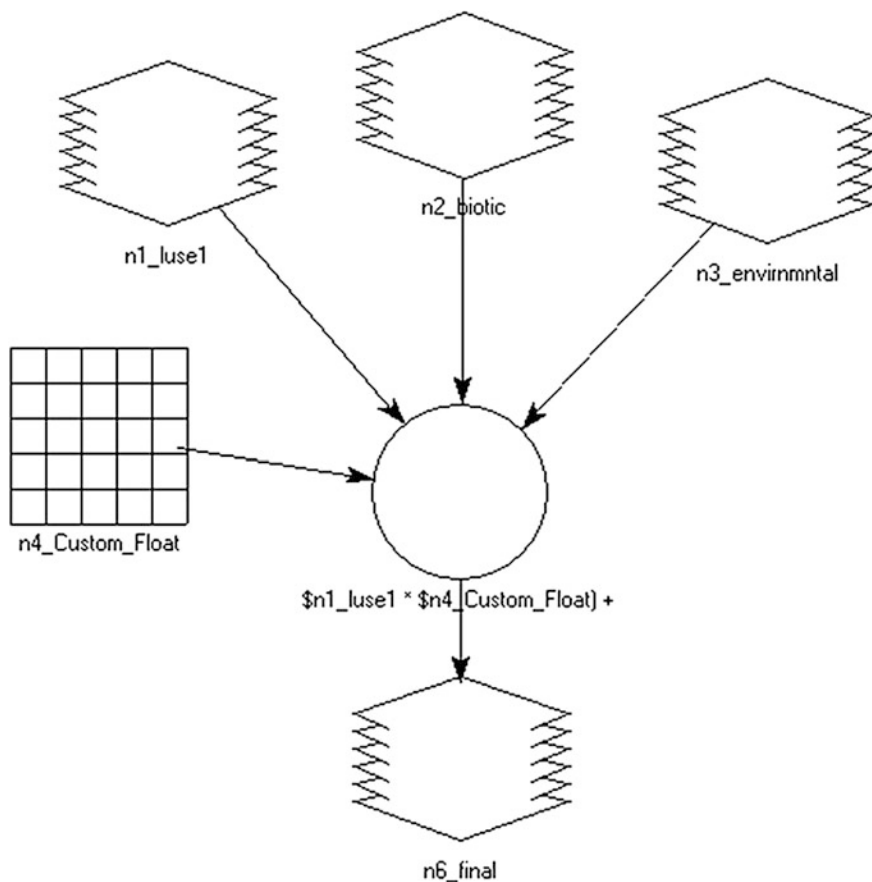


Fig. 3 Model used to get weighted raster output

6.1 Land Use/Land Cover

The variables under this unit are settlement, single crop, multicrop, horticulture, forest, waste land, and water bodies. Physiographically, the block is a flat alluvial plain gently grading to the coastal tract of the Bay of Bengal. The land is not sufficiently good for cultivation and scarcity of soil moisture is there (Chakrabarti 1991). That is why; this block has a huge area with a single season cropping. Main uplifted dune areas are used for major settlements. Double crop areas are facilitated by mainly canal and stream irrigation. So, areas adverse for agriculture and other primary source of income will get more importance for industrial setup. Thus, the hierarchy of categories from highest to least importance is Wasteland, single crop, horticulture, water bodies, forest, and settlement (Fig. 4). Following weightage matrix shows the outcome of weightage for these variables (Table 4a, b).

6.2 Infrastructure

There are two state highways running through this block. These are State Highway-4 (Total length-12.25 km) which is connecting Bajkul and Digha and

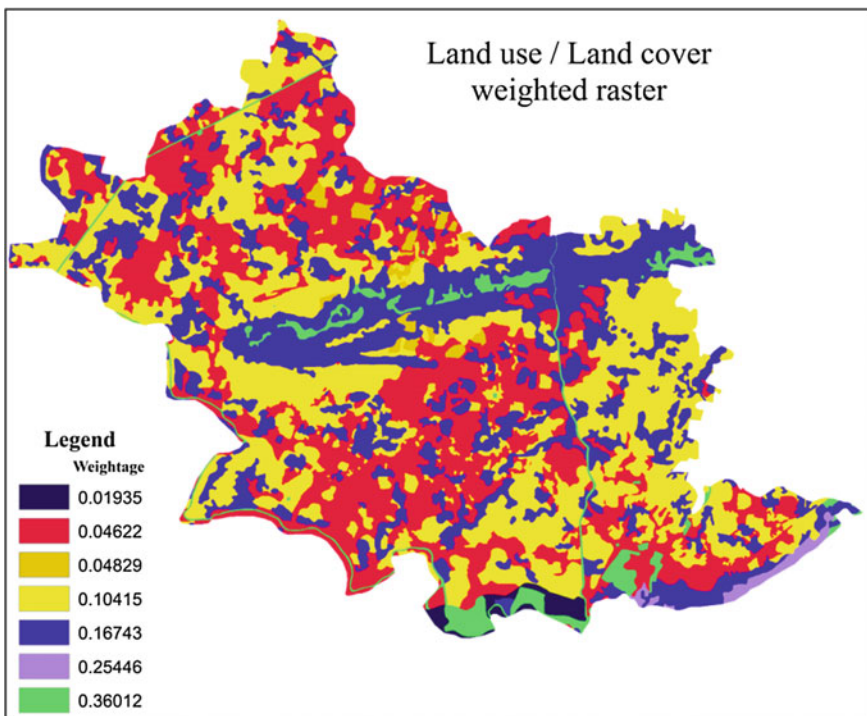


Fig. 4 Weighted raster for Land use/land cover of Contai-I block

Table 4 (a) Weightage matrix along with their sum. (b) Weightage matrix along with their average

(a)									
	Settlement	Single crop	Multicrop	Horti-culture	Forest	Wasteland	Water bodies		
Settlement	1	5	2	7	0.5	8	0.33333		
Single crop	0.20	1	0.16667	2	0.125	4	0.11111		
Multicrop	0.5	6	1	3	0.2	7	0.14286		
Horticulture	0.14286	0.5	0.33333	1	0.16667	5	0.2		
Forest	2	8	5	6	1	9	0.5		
Waste land	0.125	0.25	0.14286	0.2	0.11111	1	0.1		
Water bodies	3	9	7	5	2	10	1		
SUM	6.96786	29.75	15.64286	24.2	4.10278	44	2.3873		
(b)									
	Settlement	Single crop	Multicrop	Horticulture	Forest	Wasteland	Water bodies	SUM	AVRG
Settlement	0.143	0.168	0.12785	0.2892	0.1218	0.1818	0.1396	1.172	0.167
Single crop	0.03	0.033	0.01065	0.0826	0.0304	0.0909	0.0465	0.32	0.046
Multicrop	0.071	0.201	0.06392	0.1239	0.0487	0.1591	0.0598	0.729	0.104
Horticulture	0.021	0.0168	0.02130	0.0413	0.0406	0.1136	0.0838	0.338	0.048
Forest	0.287	0.2689	0.31963	0.2479	0.2437	0.2046	0.2094	1.78	0.254
wasteland	0.018	0.0084	0.00913	0.0082	0.0270	0.0227	0.0419	0.135	0.019
Water bodies	0.431	0.3025	0.44748	0.2066	0.4874	0.2272	0.4189	2.521	0.360

another one, i.e., SH 5 (Total length-16.65 km) which is connecting Junput and Egra. About 100 km of metal main roads are distributed over the entire block (Land use mapping for Land Bank report, WBCST 2014). Motorable embankment cum road has been constructed parallel to coast. Tamluk-Digha section of South Eastern Railway (Length-10.97 km) is passing through Contai Municipality. Multiple buffers have been created around the infrastructures. Metalled road and rail have buffers of 0.5, 1, 3, and 5 km (Fig. 5a); whereas, unmetalled roads are having buffers of 0.5, 1, 3, and 7 km (Fig. 5b). These buffers are assigned with weightage (Table 5) according to the accessibility to the transport (Fig. 5c).

6.3 Population Density

Highest density of population is 5440 persons/km² come under Contai municipal area. Out of the other villages, highest population density can be seen in Gimagere village with 53 persons/km². The lowest density of population is found to be in Maharampur village which is only 0.23 persons/km² (Land use mapping for Land

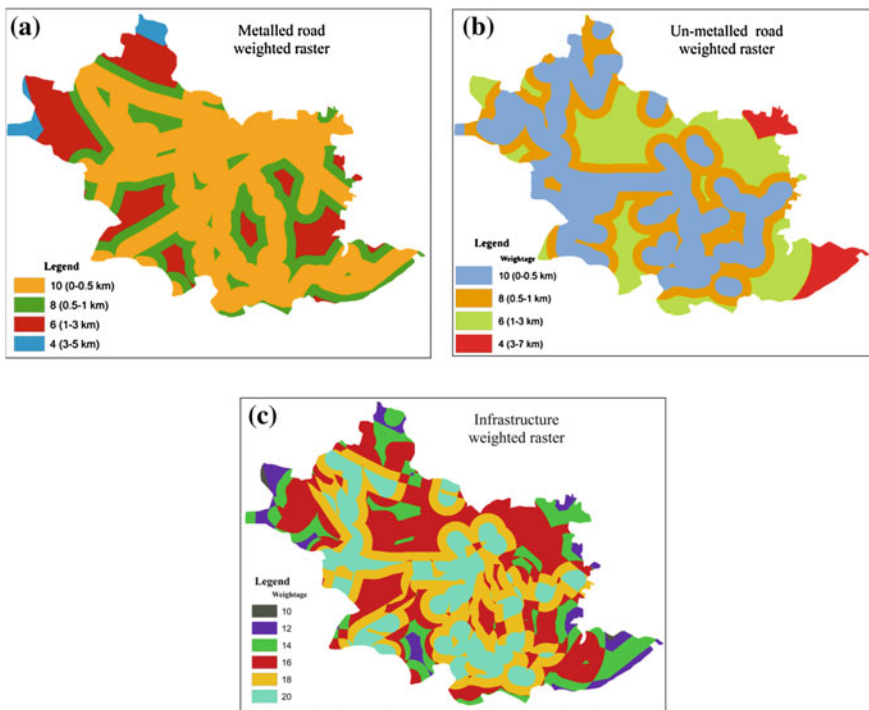


Fig. 5 a Weighted raster for metalled road. b Weighted raster for unmetalled road. c Weighted raster for infrastructure of Contai-I block

Table 5 Weightage of buffer area

	Weightage	4	6	8	10
Buffer area in km	Metal and rail	3.0–5.0	1.0–3.0	0.5–1.0	0–0.5
	Unmetalled	3.0–7.0	1.0–3.0	0.5–1.0	0–0.5

Bank report, WBCSST 2014). High population density does not encourage the industrial setup, whereas; very low population should have the priority provided that it has surrounding enough population to supply labor (Fig. 6). So, medium to low density of population can motivate industrialization (Table 6).

6.4 Existing Industries

Industry should be setup beyond 1 km of any existing industry to get environmental clearance. So, here 1 km buffers have been calculated around all existing industries (Fig. 7). Within this 1 km buffer, weightage for industrial setup will be 0, whereas; beyond this, the value has been assigned as 10 (Table 7).

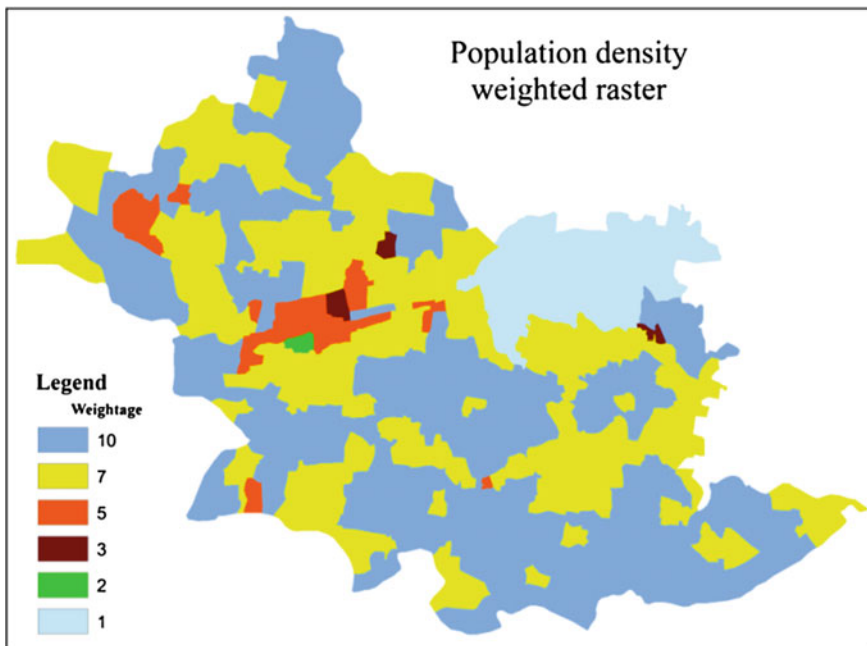
**Fig. 6** Weighted raster for population density of Contai-I block

Table 6 Weightage of population density

Population density	01.00–10.00	10.01–20.00	20.01–30.00	30.01–40.00	40.01–50.00	More than 50.01
Weightage	10	7	5	3	2	1

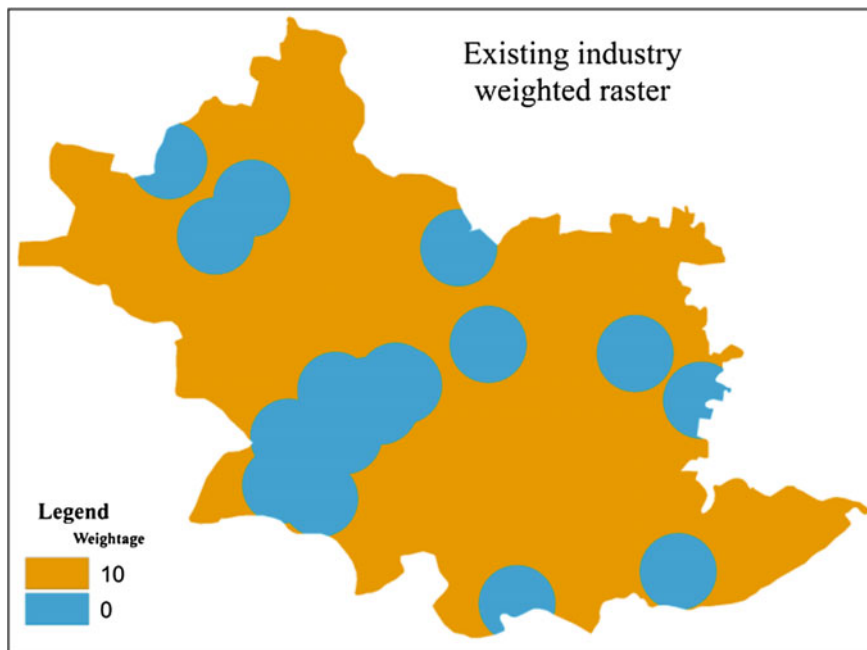


Fig. 7 Weighted raster for existing industrial buffer of Contai-I block

Table 7 Weightage of buffer around existing industry

Buffer around existing industry	Weightage
0.0–1.0 km	0
More than 1.0 km	10

6.5 Hydro-Geomorphology

This part of coastal tract of Purba Medinipur district constitutes part of the meso-tidal coastal plain characterized by the presence of successive rows of dunes, beach ridge with intervening clayey tidal flats due to the fluctuation in the regression of the sea during the Holocene time (District Environmental Atlas Report, WBCST, DST, GoWB 2006). The coastal portion of the block is Active Marine Coastal Plain with poor ground water potentiality. In the south-western corner, there is a patch of Older Beach Ridge with also a poor ground water

potentiality. Further Northward, an Ancient Inter tidal flat with low ground water potentiality is extended up to Ancient Dune Complex to the north (Watershed Atlas of India 1990). This dune complex is mainly major settlement area having very poor ground water potentiality and agricultural possibility. Northward from this East–West extended dune complex, the Inactive fluvio-tidal flat starts which have a better ground water prospect having a good prospect for industrial sitting (Fig. 8). Other hierarchy can be seen from the following weightage matrix (Table 8a, b).

6.6 Soil

Here, the soils have been developed in alluvium, laid by the rivers of Haldi and Rupnarayan. They are by and large salt impregnated due to diurnal tidal flow of sea water through creeks and sub-tributaries. They are deep, fine loamy to fine in texture, imperfectly to poorly drained, with moderate to very strong salinity hazards. The soil changes follow the hydro-geomorphology. The Active Marine Coastal Plain is with Aquic Ustrisamments soil which is very deep, moderately well-drained sandy soil having severe erosion and strong salinity having very low weightage. The Older Beach Ridge has soils of Fine Aeric Haplaquepts characterized by very deep, poor/imperfectly drained, fine soils with moderate salinity. The Ancient Dune Complex is characterized by Typic Ustrisamments which is

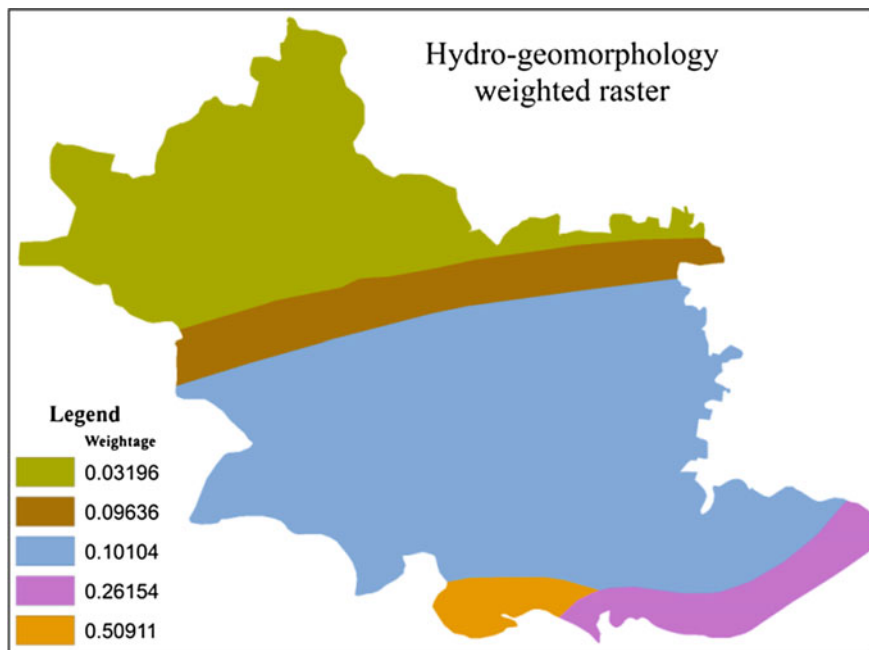


Fig. 8 Weighted raster for hydro-geomorphology of Contai-I block

Table 8 (a) Weightage matrix. (b) Weightage matrix along with the sum and average

(a)					
	AITF	IFTF	ADC	AMCP	OBR
AITF	1	6	0.5	0.2	0.25
IFTF	0.166667	1	0.333333	0.1	0.125
ADC	2	3	1	0.5	0.142857
AMCP	5	10	5	1	0.125
OBR	4	8	7	8	1
SUM	12.166667	28	13.833333	9.8	1.642857

(b)							
	AITF	IFTF	ADC	AMCP	OBR	SUM	AVRG
AITF	0.082191	0.214285	0.0361445	0.0204081	0.152173	0.5052	0.101040
IFTF	0.013698	0.035714	0.0240961	0.0102040	0.076086	0.1598	0.031960
ADC	0.164383	0.107142	0.0722891	0.0510204	0.086956	0.48179	0.096358
AMCP	0.410958	0.357142	0.3614458	0.1020408	0.076086	1.30767	0.261535
OBR	0.328767	0.285714	0.5060242	0.8163265	0.608695	2.54552	0.509105

very deep, well-drained sandy soils on moderately sloping coastal plain with sandy surface, severe erosion, and slight salinity (DEA Report, WBSCST, DST, GoWB 2006). These two should carry moderate to low priority for industry. Rest of the block comprising Inter-tidal flat and Fluvio-tidal flats is composed of Fine Vertic Haplaquepts which is very deep, very poorly drained, and fine cracking soils (Table 9a, b). So, this should be taken under the highest priority zone (Fig. 9).

6.7 Land Capability

The land capability classification is an interpretative grouping of soils mainly based on the inherent soil characteristics, external land features, and environmental factors that limit the use of land. On the basis of physiographic, the three land capability classes are II, III, and V. Depending on the severity of limitations of erosion (e), wetness (w), and soil rooting zones (s) factors, these capability classes are again subdivided into subclasses (DEA Report, WBSCST, DST, GoWB 2006). Here, the Marine Coastal Plain is characterized by Ves. Here, land with some limitations suitable for pasture and grazing as well as limitation of erosion and soil rooting zone like salinity. So, it carries the lowest priority. Vs represent the same with only limitation of soil rooting like salinity having a moderate to low priority. IIes lies on the eastern part of Ancient Dune Complex where moderately good cultivable land with major limitations of erosion and soil rooting zone like salinity. This should be taken under moderate to high priority (Fig. 10). Rest of the block is having land capability type IIIs representing moderately good cultivable land with major limitation of soil rooting zone like texture (Table 10a, b). Thus this unit should carry the highest weightage.

Table 9 (a) Priority zone matrix. (b) Sum and average of priority zone matrix

(a)				
	Fine Vertic Haplaquepts	Typic Ustipsamments	Aquic Ustipsamments	Fine Aeric Haplaquepts
Fine Vertic Haplaquepts	1	0.2	0.1	0.125
Typic Ustipsamments	5	1	0.142857	0.166667
Aquic Ustipsamments	10	7	1	0.25
Fine Aeric Haplaquepts	8	6	4	1
SUM	24	14.2	5.242857	1.541667

(b)						
	Fine Vertic Haplaquepts	Typic Ustipsamments	Aquic Ustipsamments	Fine Aeric Haplaquepts	SUM	AVRG
Fine Vertic Haplaquepts	0.041666666	0.01408450	0.0190735	0.081081	0.155905	0.038976
Typic Ustipsamments	0.208333333	0.07042253	0.0272479	0.108109	0.414112	0.103528
Aquic Ustipsamments	0.416666666	0.49295774	0.1907357	0.162162	1.262522	0.315631
Fine Aeric Haplaquepts	0.333333333	0.42253521	0.7629428	0.648649	2.167459	0.541865

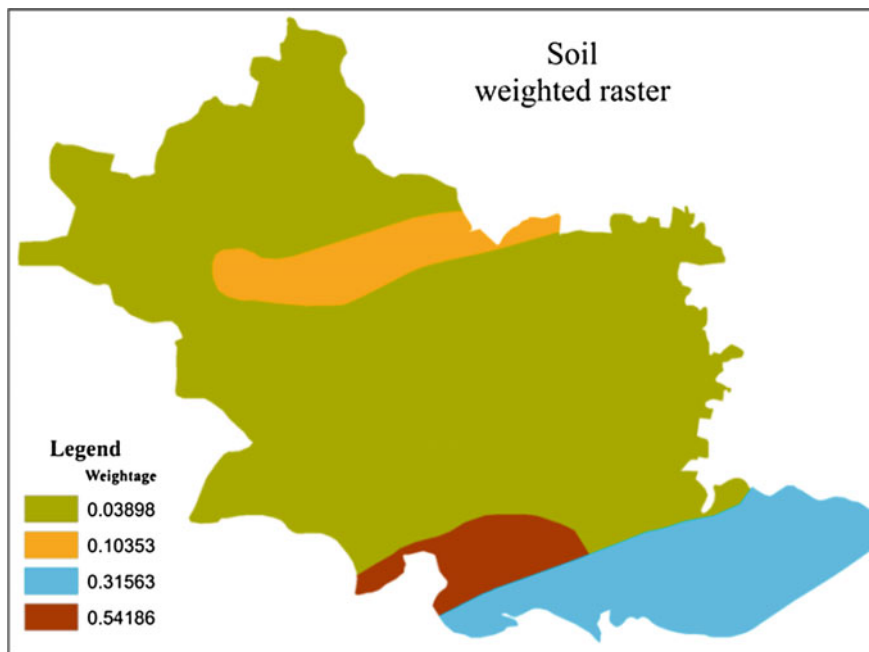


Fig. 9 Weighted raster for soil of Contai-I block

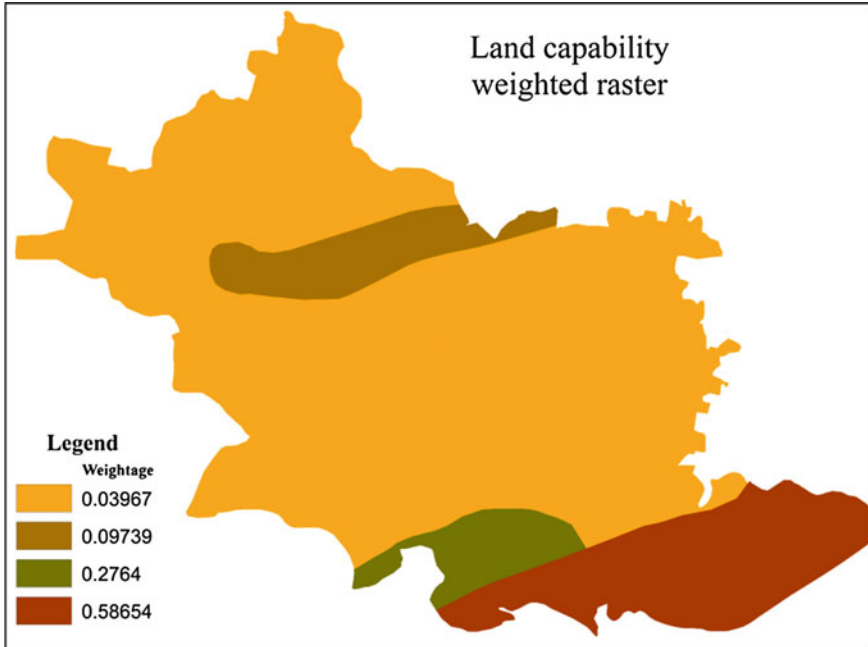


Fig. 10 Weighted raster for land capability of Contai-I block

Table 10 (a) Weightage matrix. (b) Sum and average of weightage matrix

(a)						
	III _s	III _{es}	Ves	Vs		
III _s	1	0.25	0.1	0.166667		
III _{es}	4	1	0.166667	0.125		
Ves	10	6	1	5		
Vs	6	8	0.2	1		
SUM	21	15.25	1.466667	6.291667		
(b)						
	III _s	III _{es}	Ves	Vs	SUM	AVRG
III _s	0.047619048	0.016393443	0.068181803	0.026490118	0.158684411	0.039671
III _{es}	0.19047619	0.06557377	0.113636565	0.019867549	0.389554075	0.097389
Ves	0.476190476	0.393442623	0.681818027	0.794701945	2.346153071	0.586538
Vs	0.285714286	0.524590164	0.136363605	0.158940389	1.105608444	0.276402

6.8 Biotic

This is the weighted average (Table 11a, b) of infrastructure, population density, and existing industries (Fig. 11a).

Table 11 (a) Weightage matrix of infrastructure, population density and existing industries. (b) Weightage matrix of infrastructure, population density, and existing industries along with sum and average

(a)					
	Infrastructure	Population density	Existing industry		
Infrastructure	1	0.166667	8		
Population density	6	1	10		
Existing industry	0.125	0.1	1		
SUM	7.125	1.266667	19		

(b)					
	Infrastructure	Population density	Existing industry	SUM	AVRG
Infrastructure	0.14035087	0.131579176	0.421052632	0.692982685	0.230994
Population density	0.84210526	0.789473476	0.526315789	2.157894529	0.719298
Existing industry	0.01754386	0.078947348	0.052631579	0.149122786	0.049707

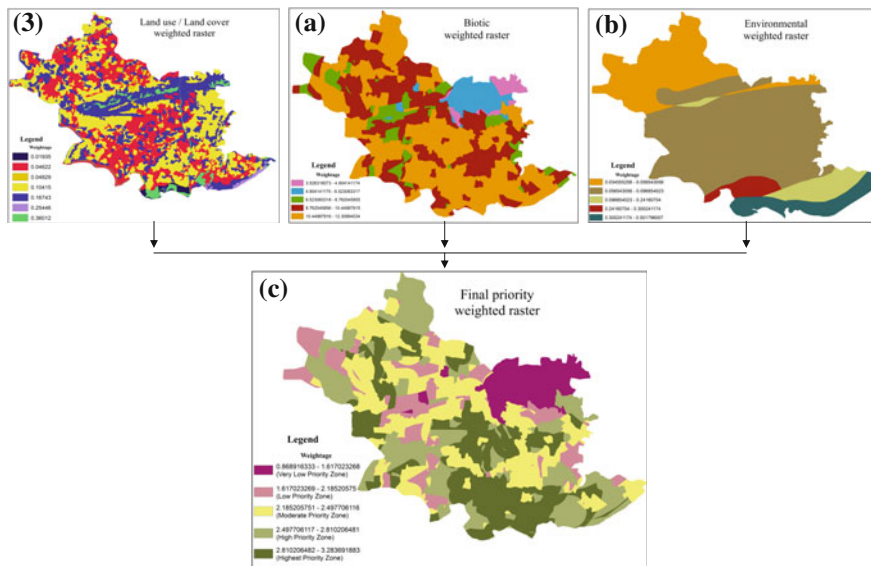


Fig. 11 a Weighted raster showing the priority mapping of biotic parameters. b Weighted raster showing the priority mapping of environmental parameters. c Final weighted raster of priority zoning for industrialization in Contai-I block

6.9 Environmental

This is the weighted average (Table 12a, b) of hydro-geomorphology, soil, and land capability (Fig. 11b).

6.10 Final Industrial Priority Variables

At the third hierarchy or final weightage matrix (Table 13a, b), three variables of second hierarchy have been taken. These are land use/land cover, biotic and environmental variables. Weighted average of these three variables has given the pixel based final priority index (Fig. 11c).

Table 12 (a) Weightage matrix of environmental parameters. (b) Weightage matrix of environmental parameters along with their sum and average

(a)					
	Hydro-geom	Land capability	Soil		
Hydro-geom	1	6	4		
Land capability	0.166667	1	0.142857		
Soil	0.25	7	1		
SUM	1.416667	14	5.142857		
(b)					
	Hydro-geom	Land capability	Soil	SUM	AVRG
Hydro-geom	0.705882187	0.428571429	0.77777777	1.912231415	0.637410472
Land capability	0.117647266	0.071428571	0.02777777	0.216853589	0.07228453
Soil	0.176470547	0.5	0.1944444	0.870914997	0.290304999

Table 13 (a) Combined weightage matrix. (b) Combined weightage matrix along with sum and average

(a)					
	Land use	Biotic	Environmental		
Land use	1	0.166667	0.125		
Biotic	6	1	0.2		
Environmental	8	5	1		
SUM	15	6.166667	1.325		
(b)					
	Land use	Biotic	Environmental	SUM	AVRG
Land use	0.066666667	0.02702708	0.094339623	0.18803336	0.062678
Biotic	0.4	0.16216215	0.150943396	0.71310555	0.237702
Environmental	0.533333333	0.81081076	0.754716981	2.09886108	0.699620

6.11 Results and Discussion

Multi-Criteria-Decision-Making is the decision modeling on the basis of the importance of individual variables. All these variables are subdivided into categories for which individual weightage are assigned according to their feasibility for the establishment of industries by reclassification module of ArcGIS 10.1 and ERDAS 8.4 software. As per the methodology of AHP modeling, the variables are multiplied by its respective weightage and all the multiplied weightages are summed up to get the output weighted raster. All these output rasters as per hierarchy are given below.

Infrastructure, population density, and existing industry buffer weighted rasters have been multiplied by calculated weightage and then run summation to get output biotic weighted raster. Same way, the hydro-geomorphology, soil, and land capability weighted rasters have been multiplied by their calculated weightage values and summed up to get environmental weighted raster. Final priority raster have been calculated by same raster calculations on land use/land cover, biotic, and environmental weighted rasters. The model of this raster calculation has been shown accordingly.

7 Conclusion

Such an analysis can enhance spatial decision support system with a higher accuracy which can be fruitful from the entrepreneur point of view ensuring environmental quality. Here decision has been taken on the basis of certain physical factors, as well as, anthropogenic factors though the pollution category of the proposed industry should also be taken under consideration. Other variables are taken according to the requirement of the industry, like distance from the core commercial area, distance from raw material source area, accessibility to water body/river/canals for the disposal, local socioeconomic and political environment of the area, industrial policies, and profit in production. Here we have just tried to show the methodology toward making a decision in GIS environment where as many as logical and associated criteria can be added. So, this study enlightens the decision-makers a path toward a suitability analysis for further industrial development of the block.

Acknowledgments Thanks are due the Secretary, Dept. of Science and Technology, GoWB for kind permission to present this paper in the National Seminar on Remote Sensing and Environment, Organized by School of Oceanographic studies, Jadavpur University and also to publish the full paper. Views in this paper are primarily author's own and not necessary of the organization to which they belong.

References

- Bureau of Applied Economics & Statistics (1999 and 2000) GoWB: District Statistical Handbook, Medinipur District
- Census of India (2011) West Bengal- A Census View- Purba Medinipur District
- Chakrabarti P (1991) Morpho-stratigraphy of coastal quaternaries of West Bengal and Subarnarekha Delta. Orissa, Indian J Earth Sci 18(3–4):219–225
- Gupta AK, Inakollu VS, Misra J, Yunus M (2002) Environmental risk mapping approach: risk minimization tool for development of industrial growth centers in developing countries. J Clean Prod 10(5):271–281
- Laha C (2012) Forest suitability analysis through AHP spatial decision modeling. Application of remote sensing and GIS in resource management. University of North Bengal, pp 33–44
- Satty RW (1987) The analytic hierarchy process—what it is and how it is used. Math Model 9(3–5):161–176
- Unpublished Project Report (2006) District Environmental Atlas, Purba Medinipur District, West Bengal, West Bengal State Council of Science & Technology, DST, Govt. of West Bengal
- Unpublished project report (2014) Land use mapping for Land Bank, West Bengal State Council of Science and Technology, DST, Govt. of West Bengal
- Watershed Atlas of India (1990) All India Soil and Land-use Survey, Department of Agriculture and Cooperation, GOI

Standalone Open-Source GIS-Based Tools for Land and Water Resource Development Plan Generation

Arati Paul, V.M. Chowdary, Dibyendu Dutta and J.R. Sharma

Abstract Land and water which are extremely important natural resources are depleting at a fast rate. This has triggered the need to conserve these resources and utilise them optimally. Proper planning that involves strategies for achieving a desired set of goals, and management of these resources are required for sustainable development of any geographical area at watershed scale. Remote sensing and Geographic Information System (GIS)-based techniques have the potential to generate as well as to analyse geospatial data that serve as key inputs for generation of land and water resource development plans at the watershed level. However, planning authorities are adopting conventional methods for planning due to lack of GIS knowledge which is time consuming. Thus, the proposed customised open-source GIS tools not only help in bridging the knowledge gap but also help in generation of land and water resource development plans in short time. MapWindowGIS is a unique standalone open-source GIS component that can be customised through dot net programming. In the present study, MapWinGIS is used to develop Land Resource Development (LRD) and Water Resource Development (WRD) plan generation tools. These tools employ a set of logical conditions over a set of input layers to produce WRD and LRD action plans for a chosen area. A spatial database, pertaining to the Kuchai block of Saraikela district, Jharkhand India is used for generation of land and water resources development plan. These plans involve the generation of alternate land use and demarcation of areas suitable for artificial recharge. Thus, the tool enables to integrate together spatial data from diversified sources in order to analyse and produce meaningful information for decision makers to support their planning activity.

Keywords LRD · WRD · Natural resources · Open source · GIS

A. Paul (✉) · V.M. Chowdary · D. Dutta
Regional Remote Sensing Centre—East, Kolkata, India
e-mail: aratipaul@yahoo.com

J.R. Sharma
National Remote Sensing Centre, Hyderabad, India

© Springer International Publishing Switzerland 2017
S. Hazra et al. (eds.), *Environment and Earth Observation*,
Springer Remote Sensing/Photogrammetry, DOI 10.1007/978-3-319-46010-9_2

1 Introduction

Sustainable development of land and water resources is necessary to maintain and improve land productivity as well as to conserve soil and water resources. Soil degradation and high surface runoff can be caused by a variety of factors including inadequate forest cover and uncontrolled grazing. Moreover, accelerated soil erosion has an adverse effect on the productivity of land. Hence an alternate land-use plan, in addition to water resource development plan, is sometimes necessary for the optimum use of a watershed.

Most of the studies carried out at the watershed level in India involve site-specific techniques based on intuition, experience and thumb rules, which may have serious environmental implications (Bali and Karale 1977; Singh et al. 1990). However, geospatial technologies such as remote sensing and geographic information systems (GIS) have shown their proven potential for generating sustainable LRD and WRD plans (Krishnamurthy et al. 2000; Anbazhagan et al. 2005; Shankar and Mohan 2005; Chowdary et al. 2009). The critical analysis of thematic maps derived from satellite data interpretation and socio-economic parameters are extremely crucial in this regard. It helps to identify problems as well as potential of the thematic information in terms of availability, sensitivity, severity, and criticality of resources. This facilitates optimum utilisation of resources and transfers the benefits to people in the watershed area.

Particularly, land-use information obtained from satellite images allowed decision-makers to devise plans for sustainable natural resource management (Joerin et al. 2001; Jansen and Di 2004). Integrated water resource development plan that involves identifying suitable zones for artificial recharge using GIS is extremely important as it makes watershed management not only simpler but also more effective. Multi-criteria analysis at spatial context was carried out in GIS by several researchers in solving conflict situations that arose during planning (Janssen and Rietveld 1990; Joerin et al. 2001; Chowdary et al. 2009; Rout et al. 2012).

For the past few years, the world of GIS has experienced many free and open-source GIS software tools, which helped GIS to reach out to a large number of people and created a significant impact on the society. Customised GIS applications were developed in many fields, viz. civil engineering projects (Jabbar 2011), potential risk assessment of water resources due to contaminants (Marchant et al. 2013), ground water quality assessment (Rabah et al. 2013) and natural resource management (Paul et al. 2014). Hence in the present study, customised tools are developed using open-source GIS component in order to generate LRD and WRD plans for any chosen area that might bridge the knowledge gap between policy makers and GIS professionals. The LRD Plan generation tool generates alternate land-use plan while the WRD plan generation tool demarcates the suitable zones for taking up location-specific activities such as check dam, percolation tank, underground barrier, etc., for artificial recharge in a natural boundary like a watershed.

2 Study Area and Spatial Data Used

In the present study, spatial database pertaining to the Kuchai block of Saraikela district, Jharkhand (Fig. 1) is used for the generation of land and water resource development plans. The geographical extent of the study area lies between 85° 30' 40" E, 22° 56' 36" N and 85° 50' 28" E, 22° 43' 37" N. Remote sensing and GIS techniques were utilised for generation of various thematic resource maps in conjunction with collateral data. Data integration and generation of development plans were carried out in GIS environment. The data acquired from multi-spectral sensors, viz. LISS-III (23 m resolution), LISS-IV (5.6 m resolution), panchromatic sensor, viz. CARTOSAT-1 (2.5 m resolution) of the Indian Remote Sensing Satellite (IRS) series were extensively used for generating spatial databases under different national projects coordinated by the National Remote Sensing Center, India and were used in the present study.

Multi-date satellite data covering the area under study is considered necessary to guard against any information loss and improve data sensitivity. Inputting the spatial data generated from various sources is the foremost step for GIS analysis. Spatial layers such as land use/land cover (LU/LC), soil, drainage order, slope, geology (structural layer), runoff potential layer and ground water potential (GWP) layers are used in the present study. For WRD plan generation, spatial layers such as LU/LC, soil, slope and drainage order (buffer layer) are considered as requisite layers while runoff potential layer and geology (structural layer) are considered as optional. Information on existing LU/LC and its spatial distribution forms the basis for any developmental planning. In the present study, LU/LC mapped using three season LISS-III data of 2005–2006 by Jharkhand Space Application Centre (JSAC) as part of NRSC sponsored NR-CENSUS project was considered. Major portion of the study area is upland and devoid of natural vegetation. Paddy is the main crop during *kharif* season.

Hydro-geomorphological maps depict major geomorphic units, landforms and provide an understanding of the processes relating to groundwater occurrence as

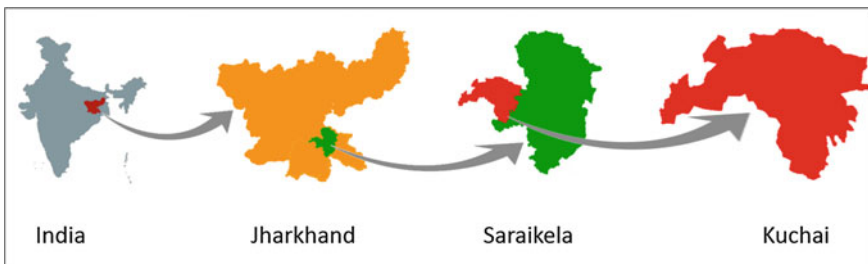


Fig. 1 Index map of the study area

well as groundwater prospects. Such maps depicting prospective zones for groundwater targeting are essential as a basis for land-use planning. Based on the morphological expressions in the satellite data, geomorphological map prepared at 1:50000 scale is used. Digital elevation model (DEM) is one of the important parameters for developmental activities and was derived from CARTOSAT-1 stereo pair. The elevation data is very much essential for generating slope map, which is an essential parameter for generating land and water resources development plan. CARTOSAT-1 stereo pair, supplied with Rational Polynomial Coefficients (RPC) were used for generation of DEM at 10 m resolution. That subsequently is used for generation of slope map in the area under study using standard procedures available in the Erdas Imagine software. Slope map of the study area, categorised into eight classes as per Integrated Mission for Sustainable Development guidelines (IMSD 1995), was derived using DEM. Satellite images are ortho-rectified first to remove effects of image perspective and relief. This ortho-rectified image (i.e. planimetrically correct image) enables accurate measurement of distances, angles and areas and was used as an input to produce drainage network. Strahler's method was adopted for stream ordering as it is an important parameter in planning of artificial recharge structures (Strahler 1964). These natural resource (NR) maps were used to produce the utilitarian type of maps to serve planning decisions. They were derived in some cases by the direct translation of single thematic map (Table 1) and in others either by the combination of two or more thematic maps, or chosen parameters of different themes, particularly as in case of the runoff potential map and the ground water potential maps (Table 2).

Table 1 Information sources for land and water resources planning

Data/map	Source	Spatial/non-spatial
Digital elevation model	CARTOSAT-1 stereo data	Spatial
Geological map	Rajiv Gandhi National Drinking Water Mission	Spatial
Geomorphological map		Spatial
Structures/lineaments		Spatial
Soil	NBSS & LUP, India	Spatial
Land use/cover	NR census	Spatial
Drainage map	IRS LISS IV	Spatial
Surface water bodies		Spatial
Watershed map	CARTO-DEM	Spatial
Meteorological data	Indian Met. Dept. (IMD)	Spatial
Settlement location	IRS LISS IV/CARTOSAT	Spatial
Transport network		Spatial
Village boundaries	Census directorate	Spatial
Population		Non-spatial

Table 2 Derived spatial databases required LRD and WRD planning

Derived map	Theme map	Remarks
Slope	Digital elevation model	Derived from DEM
Land capability map	Soil, slope and climate maps	Digital aggregation
Land irrigability	Soil, slope, landform, groundwater	Digital aggregation
Groundwater potential	Geology, geomorphology, bore well litholog and yield data	Integration of thematic maps and point database
Drainage density	Drainage network	Strahler method
Surface water potential	Slope, soil map, land use, rainfall and micro-watershed boundary	Natural Resources Conservation Service-Curve Number (NRCS-CN) technique through integration of layers

3 Methodology for Development of LRD and WRD Tools

LRD and WRD plans are generated by integrating different thematic layers according to the set of logical conditions highlighting suitability of a particular land-use or artificial recharge activity in the area under study. The logical conditions for integrating spatial layers in the GIS environment are presented in Tables 3 and 4 respectively. GIS is an analytical tool capable of performing storing, spatial

Table 3 Land resources plan development generation—conditions

Existing land use	Soil Perm.	GWP (m ³ /h)	Slope (%)	Geomorphic units	Proposed LU
Single crop	Low/moderate	12–24	0–1	Pediplain/valley fills/buried pediplain	Intensive agriculture
Single crop, fallow	Low/moderate/high	3–12	0–3	Pediplain/dissected plateau/buried pediment/pediment	Agro-horticulture
Single crop, fallow wasteland	Low/moderate/high	3–12	3–10		Agro-forestry
Land with/without scrub, gullied land, stony waste	Moderate/high	<3–6	0–5		Silvopasture
Land with/without scrub, mining waste areas, barren land	High	<3–6	5–35	Pediment	Fuel and fodder plantation

operations, spatial queries, data linkages, data matching and output generation. A GIS can perform all these operations because it uses geography or space as a common key between the databases. The data sets are linked only if they relate to the same geographical area. Further, the important purpose of a GIS is to combine together spatial data from diversified sources. This helps in describing and analysing data to make predictions with models and in providing support for decision makers. Thus, a GIS model is a process of combining a set of input themes with a function to produce an output theme:

$$\text{Output} = f(\text{two or more input themes}) \quad (1)$$

MapWindowGIS is a standalone open-source GIS component that is customised through dot net programming in the present study to develop LRD and WRD plan generation tools. LRD and WRD plans have been generated through respective tools by inputting the requisite thematic layers. Hence, for integration of the layers, attributes in the thematic layers need to be in a specific format failing which tools generate suitable error messages. Subsequently, thematic layers are integrated to generate a new union layer having the attributes of all the themes where logical conditions are applied. This union layer is extremely important as this layer helps in evaluating the suitability of the particular area for a specific action plan. Further, the dissolve operation of GIS tool is performed on the respective LRD and WRD action plans as shown in the map area of respective tools. A provision is also made in the tool for storing initial output and dissolved output at the prescribed location. The overall methodology for generation of LRD and WRD tools is shown as a flowchart in Fig. 2.

4 Customised GIS Tools for Generation of Developmental Plans

4.1 LRD Plan Generation Tool

For the generation of LRDP, thematic layers pertaining to LU/LC, soil, slope, and GWP are mandatory. These layers with specific attributes are selected and executed through the input module of LRDP tool (Fig. 3). The LRDP layer with or without the dissolve operation is generated and stored in a particular location. The path of the generated layers is displayed on the tool's screen while the dissolved layer is shown in the map area of the tool (Fig. 3). The background process of the LRDP generation tool is depicted in Fig. 4. The tool checks the availability of the required attribute in a specific format for each layer, in the absence of which it generates a suitable message (Fig. 5) and the system prompts for the correct input. The 'HELP' document attached along with the tool provides the details of each input layer and its format.

Table 4 Water resources development plan generation—conditions

Drain order	Soil Perm.	Slope (%)	Land use	Runoff potential	Structure	Action plan
Second/third	Moderate to high	<10	Agricultural areas	Medium/low		Check dam (in agricultural areas)
Second/third	Moderate to high	<10	Forest areas	Medium/low		Check dam (in forest areas)
Second/third	High	<3	Waste lands	Medium/low	Lineament and fractures preferred	Percolation tank (across streams)
	High	<3	waste lands	Medium/Low	Same as above	Percolation tank (in wasteland areas)
	Low	0–3	Agricultural areas	Medium/low	Lineament and fractures should be avoided	Farm pond (without seepage control)
	Moderate to high	0–3	Agricultural areas	Medium/low	Same as above	Farm pond (with seepage control)
Fourth–seventh	Sandy/gravel river bed	0–3				Subsurface dykes (underground barrier)

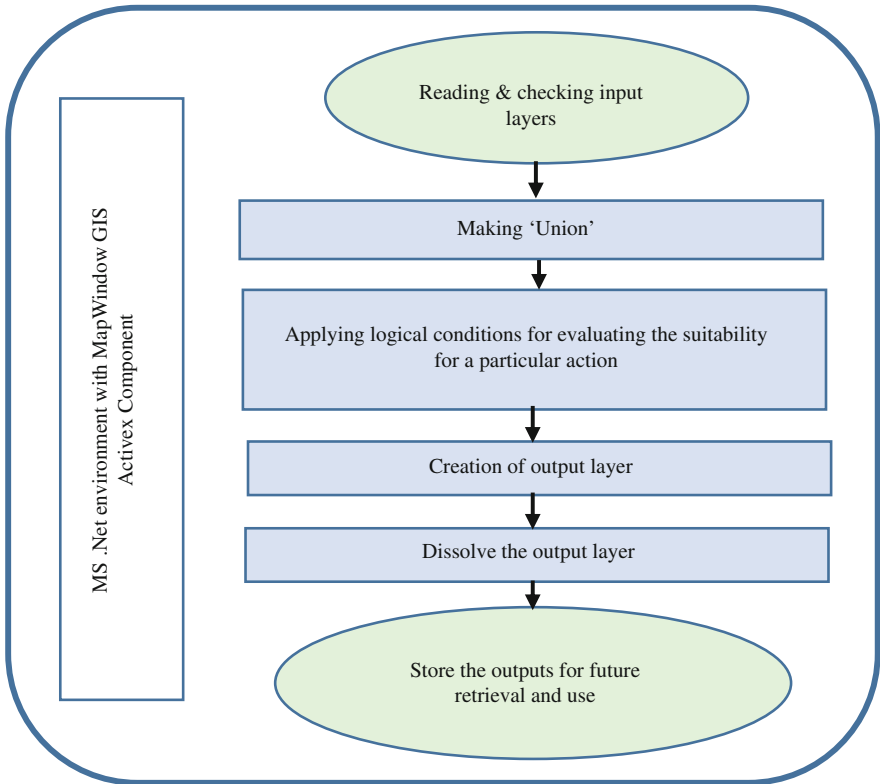


Fig. 2 Schematic representation of methodology

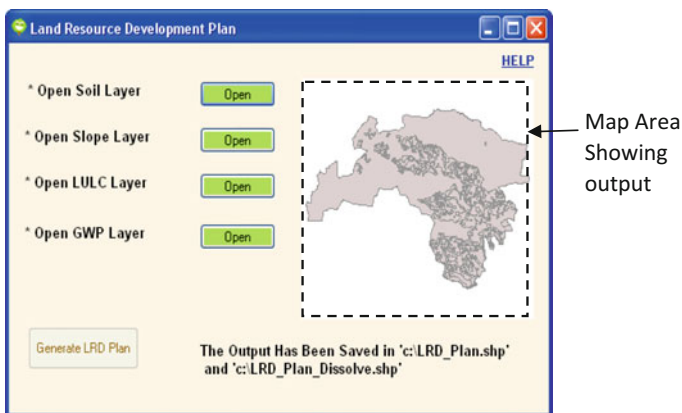


Fig. 3 LRD plan generation tool

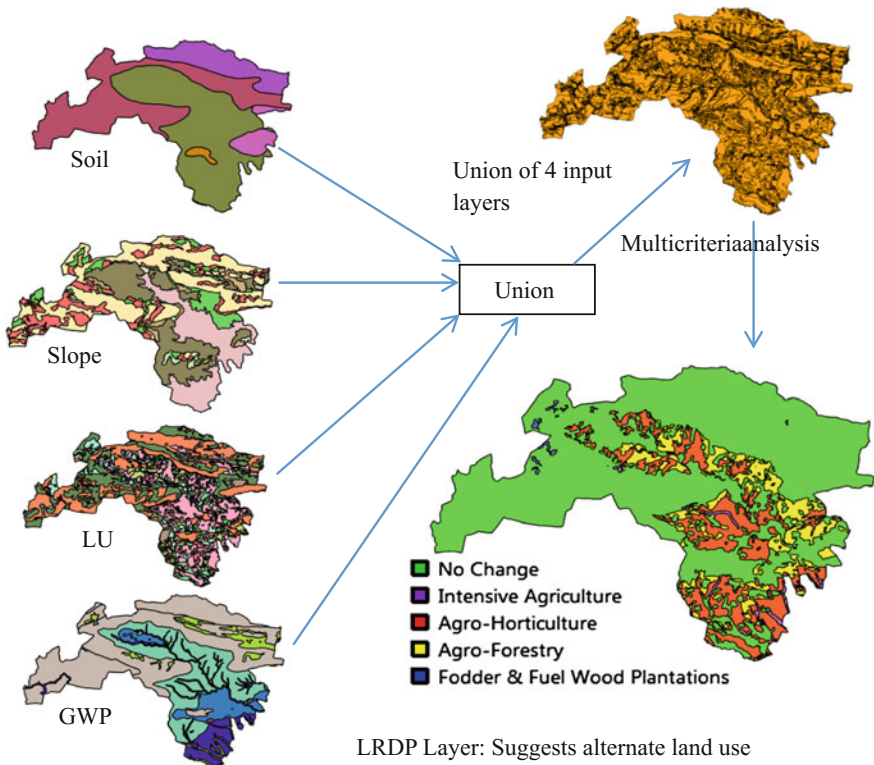


Fig. 4 LRDP generation process

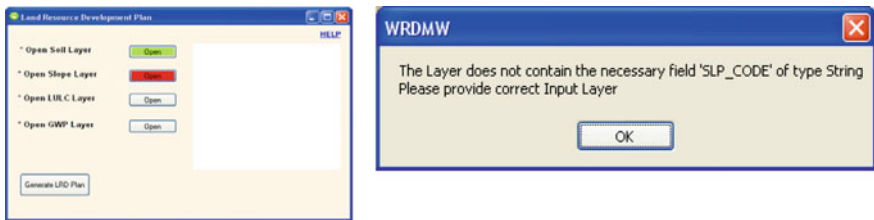


Fig. 5 LRD plan generation tool shows prompts for the correct input layer

4.2 WRD Plan Generation Tool

For the WRD plan generation, spatial layers such as LU/LC, soil, slope, drainage order (Buffer layer) are considered to be the requisite layers, while the runoff potential layer and geology (structural layer) are considered to be optional. Once the requisite input layers are selected from the tool (Fig. 6), validation of input

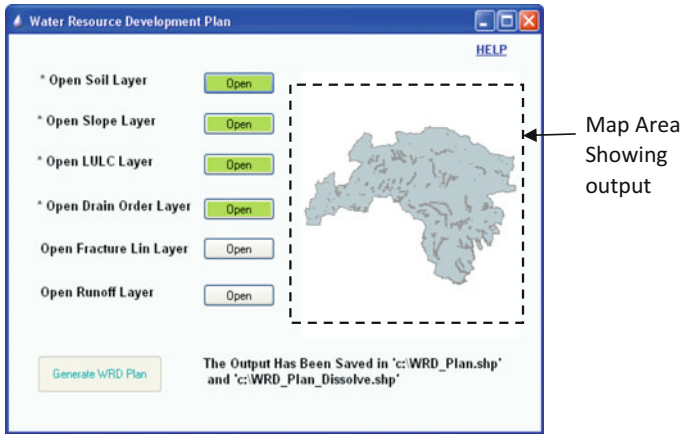


Fig. 6 WRD plan generation tool

parameters is performed. In case wrong input layers are selected, suitable error messages will be generated. The 'HELP' document contains details of the input data formats. If input layer selection is correct, the tool generates WRDP as well as dissolved WRDP layers and stores them as in case of the LRDP tool. The background process of the WRDP generation is depicted in Fig. 7.

All the required layers are integrated one by one through the 'Union' operation for both LRDP and WRDP generation tools, which is a computationally complex process. Hence, it is advisable to use these tools only for a small geographical area such as micro-watershed, block or village level to avoid long processing time. Generation of development plans through conventional methods is a tedious process as many controlling parameters must be independently derived and integrated. Hence, in the present study, standalone open-source GIS based tools is proposed for land and water resources development planning, which involves generation of alternate land-use and demarcation of areas suitable for artificial recharge.

Although, these specific action plans involve application of a set of criteria resulting from the GIS analysis of scientific factors, they need to be integrated with social factors as well. This associational analysis not only helps in a better understanding of the cause and effect related to problems or limitations, but also helps in assessing the potential for betterment that exists in the area under study. An attempt has been made for the generation of a water resource development plan through an integrated analysis by combining the different thematic layers using the Boolean logics in GIS. Detailed field inspection while implementation of plans at micro level, however, is likely to improve results of this analysis.

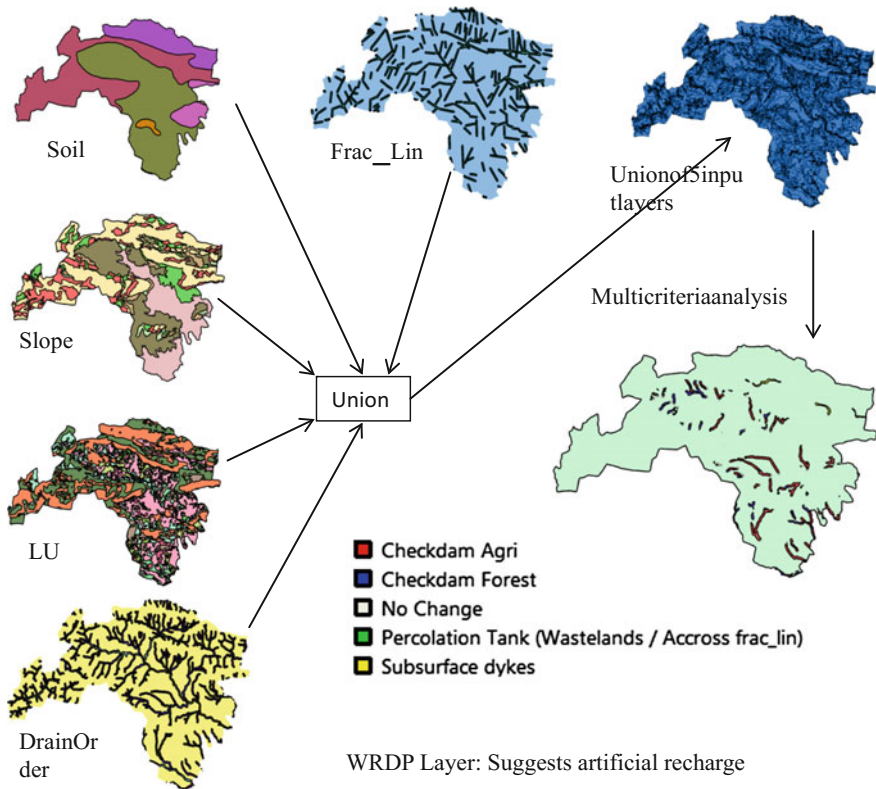


Fig. 7 WRDP generation process

5 Conclusion

Land and water resources planning is usually done by various government agencies through conventional methods, and are limited when it comes to GIS expertise. The full version of GIS software is not always desirable for decision-makers due to technical and financial constraints. Development of customised GIS tools and its access to the planners may address these issues to a greater extent. In the recent past, geospatial technologies have become effective tools by either substituting or supplementing the conventional technology with reasonably faster and efficient methods of survey and inventory in the domain of land and water resources planning, conservation, development, management and utilisation. Further, efforts are continued to develop customised tools to use remotely sensed data in a more optimal and efficient way for as many applications as possible to ensure that these techniques are used as powerful and inevitable tools for integration of the diverse spatial database. Customised tools developed in the present study are useful for

generation of action plans at the watershed, or administrative (*panchayat* or the block) level. Persons with a limited GIS background can also use these tools for effective planning of natural resources.

Acknowledgments The authors duly acknowledge Jharkhand Space Application Centre (JSAC), Jharkhand, India for the data which has been used to carry out the present work.

References

- Anbazhagan S, Ramasamy SM, Das Gupta S (2005) Remote sensing and GIS for artificial recharge study, runoff estimation and planning in Ayyar basin, Tamil Nadu, India. *Environ Geol* 48:158–170
- Bali YP, Karale RL (1977) A sediment yield index for choosing priority basins. *IAHS-AISH Publ* 222:180
- Chowdary VM, Ramakrishnan D, Srivastava YK, Chandra V, Jeyaram A (2009) Integrated water resources development plan for sustainable management of Mayurakshi Watershed, India using remote sensing and GIS. *Water Resour Manag* 23:1581–1602
- IMSD (1995) Integrated mission for sustainable development (IMSD) technical guidelines. NRSA, Hyderabad
- Jabbar A (2011) Using geographic information system (GIS) to manage civil engineering projects. *Eng Technol J* 29(7):1276–1289
- Jansen LJM, Di GA (2004) Obtaining land-use information from a remotely sensed land cover map: results from a case study in Lebanon. *Int J Appl Earth Obs Geoinf* 5:141–157
- Janssen R, Rietveld P (1990) Multicriteria analysis and geographical information systems: an application to agriculture land-use in Netherlands. In: Scholten HJ, Stillwell JCH (eds) *Geographical information systems for urban and regional planning*. Kluwer Academic Publishers, Dordrecht, pp 129–139
- Joerin F, Thériault M, Musy A (2001) Using GIS and outranking multicriteria analysis for land-use suitability assessment. *Int J Geogr Inf Sci* 15(2):153–174
- Krishnamurthy J, Mani A, Jayaraman V, Manivel M (2000) Groundwater resources development in hard rock terrain—an approach using remote sensing and GIS techniques. *J Appl Geol* 2 (3/4):204–215
- Marchant P, Banks VJ, Royse KR, Quigley SP (2013) The developed of aGIS methodology to assess the potential for water resource contamination due to new development in the 2012 Olympic Park Site, London. *Comput Geosci* 51:206–215
- Paul A, Chowdary VM, Chakraborty D, Dutta D, Sharma JR (2014) Customization of freeware GIS software for management of natural resources data for developmental planning a case study. *Int J Open Inf Technol* 2(4):25–29. ISSN: 2307-8162
- Rabah F, Budwan AE, Ghabayen S (2013) Customized standalone GIS-based tool for ground water quality assessment: Gaza Strip as a case study. *J Softw Eng Appl* 6(5):243–250
- Rout J, Ojha A, Pradhan S, Samal RN (2012) GIS for rural development and spatial planning system. *Geospatial World, Application (Utilities)*
- Shankar MNR, Mohan G (2005) A GIS based hydrogeomorphic approach for identification of site-specific artificial-recharge techniques in the Deccan Volcanic Province. *J Earth Syst Sci* 114(5):505–514
- Singh G, Venkataramanan C, Sastry G, Joshi BP (1990) Text book on manual of soil and water conservation practices. Oxford & IBH publishing Co. Pvt. Ltd., New Delhi, p 387
- Strahler AN (1964). Quantitative geomorphology of drainage basins and channel networks. In: Chow VT (ed) *Hand book of applied hydrology* Sections 4–11. McGraw Hill, New York

Downscaling of Coarse Resolution Satellite Remote Sensing Thermal Data

Sandip Mukherjee, P.K. Joshi and R.D. Garg

Abstract Satellite-based moderate to high resolution thermal imagery is absolutely important for various environmental applications. At present, the availability of high-spatial resolution thermal image (<250 m) is limited and the temporal resolution of such images is low. However, open-source coarser spatial resolution (1000 m) with high receptivity thermal image (~1 day) is freely available. To bridge this trade-off, the downscaling of coarse resolution thermal image is required. This chapter elaborates on different thermal image downscaling methods. It also touches upon the applicability of downscaled thermal images over various landscapes with an emphasis on agricultural drought mapping, soil moisture mapping, and urban center detection. Such data products can also be used for thematic mapping, geospatial modeling, and scenario generation including climate change. This chapter aims to provide a comprehensive account of thermal Remote Sensing data downscale techniques. The authors anticipate wide usage and usefulness of these algorithms for understanding of thermal processes, and a step forward for agricultural, climate, and environmental studies.

Keywords Downscaling · Land surface temperature · Thermal remote sensing · Drought · Soil moisture · Urban heat island

S. Mukherjee (✉) · P.K. Joshi
Department of Natural Resources, TERI University, New Delhi, India
e-mail: sandip.iirs@gmail.com

P.K. Joshi
School of Environmental Sciences, Jawaharlal Nehru University, New Delhi, India

R.D. Garg
Department of Civil Engineering, Indian Institute of Technology, Roorkee, India

1 Introduction

Remote Sensing data collection is carried out in different parts of electromagnetic radiation (EMR). The energy of the sun is made to interact with the surface materials on the earth after which it goes back to the sensor. The reflected, emitted, or backscattered (Jensen 2006) energy coming from the visible/near infrared (VNIR), thermal infrared (TIR), and microwave parts of the EMR is received by the sensor to form an image. The capability of the sensor is defined by four types of resolutions, namely: spectral resolution, spatial resolution, radiometric resolution, and temporal resolution. Spectral resolution is the number and width of the EMR bands, spatial resolution deals with minimum areal unit detection capability, radiometric resolution is the quantization level and temporal resolution is the revisit period of any sensor. Satellite imageries (including information captured in thermal band) can be used for generating various biophysical variables which are essential for environmental monitoring and scientific applications. Land Surface Temperature (LST) is one such biophysical variable derived using information from the thermal bands (Morrow and Friedl 1998; Anderson et al. 2008).

Thermal data/LST is used for environmental monitoring applications (Luvall and Holbo 1989; Coudert et al. 2008), estimation of other biophysical parameters (Yang and Wang 2011) and studies related to climate change (Julien et al. 2006; Weng 2009). The advantages of satellite Remote Sensing derived LST over other methods of assessment are its continuous measurements (Ormsby 1981), spatial representation (Ottlé and Vidal-Madjar 1992), surface kinetic temperature measurements (Liyanaage and Manawadu 2011), and its ability to provide information about the surface properties of different materials (Nasipuri et al. 2006).

In the recent discussions of environmental process-based modeling, LST has become very crucial for the monitoring of vegetation health (Rajapakse et al. 2002; Hope et al. 2005), understanding effects of climatic variability on crop growth (Abuzar et al. 2009), phenological studies (Badeck et al. 2004), monitoring coastal climatic hazards (Embury et al. 2012), detecting wild fire (Pinol et al. 2005), and monitoring volcanic activities (Wright et al. 2002). Medium-to-high resolution LST information is also the prerequisite for urban studies (Chen et al. 2006; Caihua et al. 2011), agriculture management (Rojas et al. 2011), forest and agriculture burnt area estimation (Ichoku et al. 2003), active fire detection (Wooster et al. 2012), water stress monitoring in crop land (Dragutin and Eitzinger 2007), evapotranspiration monitoring (Anderson et al. 2012), drought assessment (Sobrino et al. 2007; Karnieli et al. 2010), surface energy flux (Muramatsu et al. 2006) and regional energy balance modeling (Li et al. 2005), spatiotemporal pattern of soil moisture (Hulley et al. 2010), detection of coal fires (Zhang et al. 1997; Prakash et al. 1999), thermal anomalies of the surface associated with underground fires (Prakash et al. 1995), and detection of buried hot features (Prakash et al. 1995). In order to understand the aforementioned applications, a wide range of medium-to-high resolution LST or thermal data products are used successfully.

Thermal images which are currently available on a daily basis (temporal resolution of 1–2 days or less) have a moderate to coarse (≥ 500 m) spatial resolution. Due to physical and technological constraints, the acquisition of moderate-to-high resolution LST/thermal data is a challenging task (Liang 2004). TIR sensors measure long wave (3.0–14.0 μm) emitted energy from the ground surface. This is because atmospheric windows are present between 0.8 and 14.0 μm , the maximum emission of the earth occurring at approximately around 9.0 μm . The designs of thermal sensors are therefore preferred for these wavelengths.

It can be explained by Planck's theory of thermodynamics (Lillesand and Kiefer 1994) that the spatial resolution of such a large wavelength (thermal) sensor is coarse in comparison to a smaller wavelength (visible- and near-infrared) sensor. The availability of thermal images (Table 1) with a spatial resolution <250 m from the current satellite sensors is limited and the temporal resolution of these sensors are 15 days and/or more (Agam et al. 2007a; Mukherjee et al. 2014a). It creates a trade-off between the spatial and the temporal resolution of available sensors in the thermal Remote Sensing domain (Fig. 1).

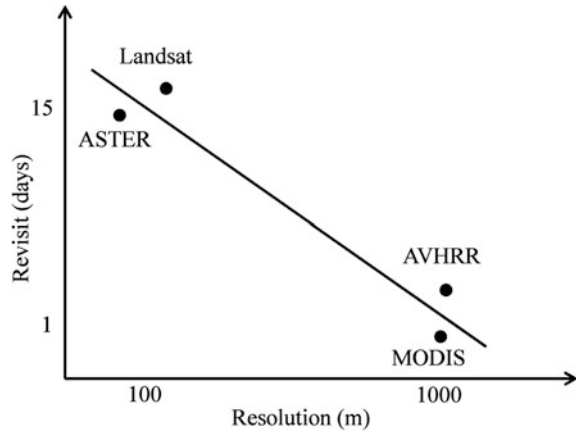
A thermal imagery of coarse resolution receives mixed signals from a variety of land features or materials situated within a pixel, resulting in the thermal mixture effect (Zhan et al. 2013). Therefore, for environmental applications, one needs

Table 1 Characteristics of different satellite sensors providing information in TIR region

Satellite	Sensor	Spatial resolution (m)		Temporal resolution (days)	Operational status
		VNIR	TIR		
Landsat 7	ETM+	30	60	16	Stripping in image
Terra	ASTER	15	90	On demand	Operational
Landsat 8	OLI & TIRS	30	100	16	Operational
Landsat 5	TM	30	120	16	Non-operational
Aqua/Terra	MODIS	250	1000	1	Operational
NOAA	AVHRR	1000	1000	1	Operational
Envisat	AATSR	1000	1000	2–3	Non-operational
Meteosat-8	MSG SEVIRI	1000	3000	<1	Operational
GEOS	GEOS imager	–	5000	15	Operational
INSAT 3A	VHRR & CCD	1000	8000	<1	Operational

AVHRR Advanced Very High Resolution Radiometer; *ASTER* Advanced Spaceborne Thermal Emission and Reflection Radiometer; *ETM+* Enhanced Thematic Mapper Plus; *Envisat AATSR* Environmental Satellite Advanced Along-track Scanning Radiometer; *GOES* Geostationary Operational Environmental Satellites; *INSAT VHRR* Indian National SATellite Very High Resolution Radiometer; *MODIS* MODerate-resolution Imaging Spectroradiomete; *MSG SEVIRI* Meteosat Second Generation Spinning Enhanced Visible and Infrared Imager and *TM* Thematic Mapper

Fig. 1 Trade-off between spatial and temporal resolution



moderate to fine spatial resolution thermal imagery along with relatively high-temporal resolution (Kustas et al. 2003; Agam et al. 2007a; Yang et al. 2010a). To a great extent, such applications were being taken care of by using thermal imagery provided by the Landsat 5/7 satellites sensors. However, since May 31, 2003, technical difficulties have occurred in the scan line of the Landsat 7 satellite (60 m spatial resolution in thermal band) which have resulted in the stripping in thermal imagery. Landsat TM 5 (120 m spatial resolution in thermal band) has been nonoperational since November 8, 2011. Thus, it is difficult to use the data from the Landsat ETM+ sensor for research and operational applications (Agam et al. 2007a). Though the recent thermal infrared sensor (TIRS) of the Landsat 8 satellite (since 11 Feb 2013) provides thermal images at a 100 m resolution, the temporal resolution is 16 days. Due to periodic cloud cover (Moran et al. 1996), it is difficult to use this imagery for the routine monitoring of the environmental processes. Moreover, there is no new program and/or forthcoming launch which would focus on the polar orbiting Remote Sensing satellite system working on thermal wavelengths. The airborne thermal sensors are available, but these have restricted applications to limited geographic extent and many countries have free flying restrictions for the collection of Remote Sensing data. Hence, it is necessary to look for alternative thermal datasets to monitor the long-term environmental phenomena. In this regard, the downscaling of thermal data or LST is necessary.

2 Downscaling

The term ‘downscaling’ is commonly used by various climate scientists (Hewitson and Crane 1996; Wood et al. 2004). Downscaling is a term which refers to deriving local to regional scale information from a global scale model output (Hewitson and

Crane 1996). There are two main approaches that are adopted while processing geospatial datasets—dynamic downscaling and empirical statistical downscaling.

Dynamic downscaling deals with obtaining local, regional, or numerical model in a higher spatial resolution from the output of a Global Climatic Model (GCM). The high-resolution output is able to simulate the local scenario in larger details. This process does not assume any historic relationship. This process is also called numerical downscaling or nested modelling (Benestad et al. 2008). Empirical statistical downscaling establishes statistical relationships between the local climate variables and the large-scale predictors. These relationships are applied to the output of the GCM experiments to simulate future characteristics of the local climate. Various analog methods like regression analysis and neural network are used to establish this relationship.

In the context of Remote Sensing, downscaling refers to an improvement in the spatial resolution of satellite images. It is decrease in pixel size of remotely sensed images (Atkinson 2013). In the thermal domain, the term downscaling is synonymous with sharpening (Agam et al. 2007a), disaggregation (Merlin et al. 2010), spatial resolution enhancement (Nichol 2009), unmixing (Eckmann et al. 2009), subpixel (Kustas et al. 2003), and fusion (Jing and Cheng 2010). All of these refer to the processes of increasing information content by enhancing the spatial resolution of thermal images. Zhan et al. (2013) reviewed studies related to remotely sensed LST downscaling procedure, taxonomy, issues, and caveats. Various terminologies used by the researchers and its associated percentage of utilization representing LST downscaling is shown in Fig. 2.

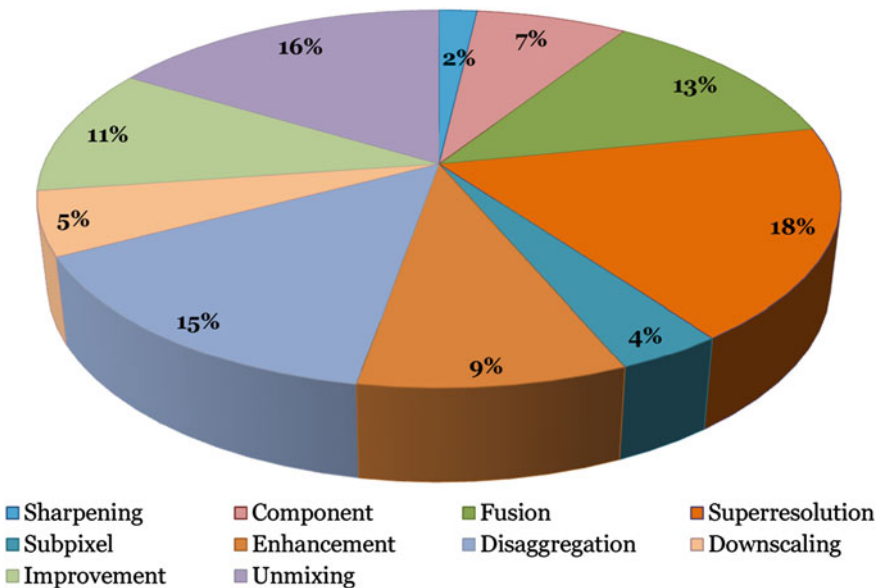


Fig. 2 Terminologies used by various researchers in this field of research. Source Zhan et al. (2013)

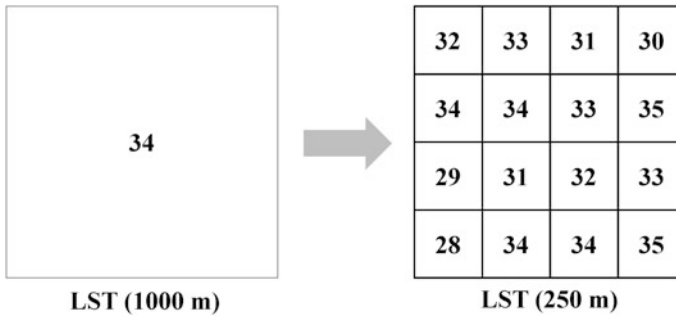


Fig. 3 Pictorial representation of downscaling LST. A 1000 m resolution LST pixel is downscaled to 250 m resolution

A pictorial representation of LST downscaling procedure is shown in the Fig. 3. For downscaling thermal data or LST, an empirical/statistical approach is widely used which involves correlating temperature (LST) with vegetation indices (Kustas et al. 2003; Yang et al. 2010b, 2011), fractional vegetation cover (Agam et al. 2007a), emissivity (Inamdar and French 2009; Nichol 2009), principal component of VNIR radiance (Zakšek and Oštir 2012), surface albedo, built-up index, and NDVI (Normalized Difference Vegetation Index) (Zhu et al. 2013), etc. Most of the researchers have utilized a physical relationship-based statistical downscaling technique assuming that the relationship between LST and vegetation indices are scale invariant.

3 Methods of Downscaling Thermal Data/LST

Downscaling LST data refers to increasing the spatial resolution by disaggregating the pixels using statistical and physically based models (Merlin et al. 2010; Atkinson 2013). Major studies have been carried out using physically based LST downscaling models (Kustas et al. 2003; Anderson et al. 2004; Agam et al. 2007a, b; Yang et al. 2010a, b; Dominguez et al. 2011; Jeganathan et al. 2011; Essa et al. 2012;2013; Rodriguez-Galiano et al. 2012; Zakšek and Oštir 2012; Zhu et al. 2013). Existing literature suggests that most of the studies utilize the property of the vegetation index (NDVI, fc) and the LST relationship to downscale LST. Due to the availability of VI at a fine resolution, it is used as a proxy data to derive the LST at the resolution of the VI image (Yang et al. 2010b).

The algorithms are applied over various levels (DN, radiance or LST) of thermal data (Zhan et al. 2013). Among the most noted works, the DisTrad (Disaggregation

of radiometric temperature) procedure has been applied for disaggregation of radiometric surface temperature (Kustas et al. 2003; Anderson et al. 2004). The basis of the DisTrad algorithm is the unique relationship between the NDVI and the LST. The algorithm was modified to propose a new method named as TsHARP (Temperature Sharpening) algorithm (Agam et al. 2007a). The TsHARP technique was tested over extensive homogeneous corn/soybean fields of Central Iowa, USA during the crop growing season. A modification of the TsHARP algorithm was proposed using the local variant and applied to downscale the thermal imagery of the mixed agricultural landscape of India (Mukherjee 2008, 2015b; Jeganathan et al. 2011). The downscaling model was developed based on aggregated ASTER data and tested on MODIS data to downscale the thermal imagery of 1000 m to 250 m spatial resolution.

Yang et al. (2010a) suggested a downscaling model based on the temperature vegetation-space triangular relationship over no-stressed canopy cover landscape. Merlin et al. (2010) considered the LST difference between non-photosynthetically and photosynthetically active vegetation fraction derived from a time series Formosat-2 shortwave data to downscale the MODIS LST. Mukherjee et al. (2014a) applied and compared various regression-based downscaling models over heterogeneous landscapes of India located in the humid tropical climate. The study suggested a least median square (LMS) regression-based downscaling model for disaggregating pixels of LST imagery to overcome landscape heterogeneity.

An end-member index-based technique using genetic algorithm and self-organizing feature map artificial neural network (GA-SOFM-ANN) was tested on ASTER and MODIS LST images (Yang et al. 2010b, 2011). Ghosh and Joshi (2014) downscaled the LST of the Landsat ETM+ sensor using narrowband reflectance information derived from the hyperspectral sensor EO1-Hyperion using three regression algorithms, such as partial least square regression, gradient boosting machine, and support vector machine. Rodriguez-Galiano et al. (2012) and Mukherjee et al. (2015) have utilized geostatistical algorithm to downscale the LST using the NDVI. Bindhu et al. (2013) proposed a nonlinear method (NL-DisTrad) and downscaled the satellite-derived LST of MODIS with a resolution of 960 m to the scale of Landsat 7 ETM+ at 60 m resolution over Indian landscapes.

3.1 LST Downscaling Model

The LST downscaling model was developed based on the well-documented observation of the inverse relationship between the LST and the NDVI (Kustas et al. 2003; Agam et al. 2007a, b) and strong correlation between these two variables (Karnieli et al. 2006). The nature of this relationship and the coefficients are scene and site specific. Therefore, the downscaling function was generated from the

thermal imagery itself to be downscaled (Agam et al. 2007a). A subpixel-based sample selection criterion was adopted during regression analysis to screen out the pixels that have higher intrapixel variability and belong to water bodies. The NDVI pixels with the most subpixel uniformity, i.e., having the least subpixel variability ($CV \leq 25\%$) were considered as samples for regression analysis (Kustas et al. 2003). A linear ordinary least square (OLS) regression function was developed to relate the LST and the NDVI at coarse resolution. The residual LST of fitted regression model at coarse resolution was calculated using the difference between the predicted and the actual LST. The residual LST was introduced to the regression model due to the dependency of the spatial variability of the LST on various environmental factors other than the NDVI such as soil moisture (Mukherjee et al. 2014a). The regression model developed at coarse resolution was applied to fine resolution NDVI to predict the LST at finer resolution. Finally, the residual LST of corresponding coarse resolution pixel is added to the predicted LST of fine resolution to increase the accuracy of the downscaled data. The algorithm of the downscaling model is listed in Eqs. 1–4. The schematic representation of the LST downscaling model is given in Fig. 4.

$$\hat{LST}_{CR_i} = a + b \times NDVI_{CR_i} \tag{1}$$

$$\Delta \hat{LST}_{CR_i} = LST_{CR_i} - \hat{LST}_{CR_i} \tag{2}$$

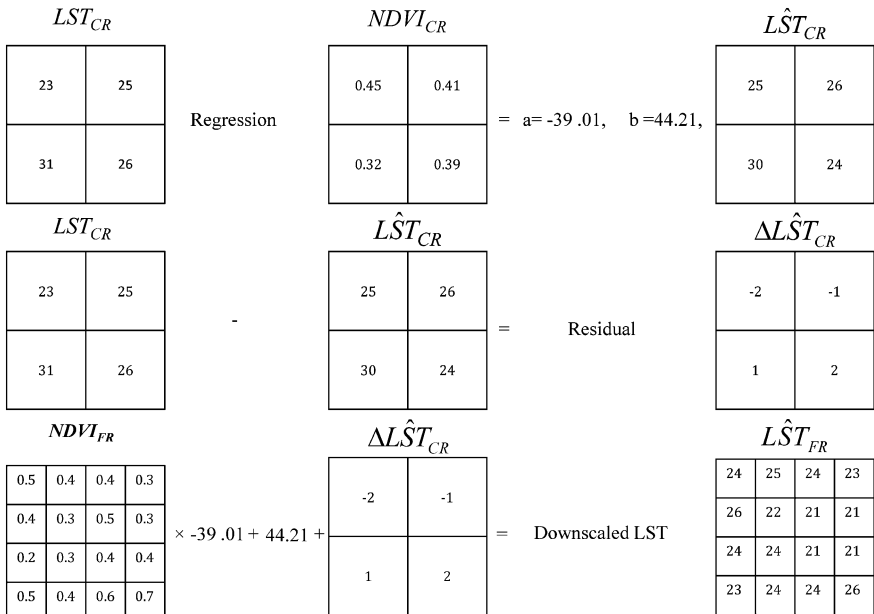


Fig. 4 Schematic representation of LST downscaling model

Table 2 LST downscaling models

Model	Description	Method	Parameter	Remarks	References
DisTrad (Disaggregation of Radiometric Temperature)	This model was developed for the first time to downscale thermal data while working in agricultural fields of Oklahoma, USA	A second-order polynomial regression model, this provides better fit in upper and lower tails of the LST-NDVI distribution	Radiometric temperature and NDVI	Can be used for homogeneous landscapes, but not suitable for heterogeneous landscapes	Kustas et al. (2003), Mukherjee (2008)
TsHARP (Temperature Sharpening)	It is a modification of DisTrad algorithm. It uses f_c instead of NDVI. This model was tested over growing agricultural landscapes of Central Iowa, USA	Simple least square regression function (i.e., OLS) which assumes polynomial function is more sensitive to outliers compare to linear function	LST and f_c	Suitable for homogeneous agricultural landscapes, but produce good result over heterogeneous landscape	Agam et al. (2007a), Mukherjee (2008)
TsHARP _{LM} (Temperature Sharpening with Local Model)	It is a modification of TsHARP algorithm for better applicability in mixed agricultural landscapes where firm size is small. The model was tested over Indian heterogeneous landscapes for the first time	A moving window-based regression technique considering local neighborhood. Local variant of LST and NDVI were considered for parameter estimation to overcome heterogeneity. Overlapping and nonoverlapping window size of 3×3 , 5×5 , 7×7 , and 9×9	LST and NDVI	Suitable for homogeneous as well as heterogeneous agricultural landscapes. But some box-like structure appeared in the downscaled LST image	Mukherjee (2008), Jeganathan et al. (2011)
LMS _{DS} (Least Median Square-Based Downscaling)	The model was first applied over Indian humid tropical region	A less outlier sensitive robust regression function (LMS regression)	LST and NDVI	Suitable for homogeneous and heterogeneous landscapes	Mukherjee et al. (2014a)

(continued)

Table 2 (continued)

Model	Description	Method	Parameter	Remarks	References
PR _{DS} (Pace Regression-Based Downscaling)	In this model, a clustering analysis procedure is used to evaluate each variable and estimate their contribution to the overall regression	PACE (Projection Adjustment by Contribution Estimation) regression model	LST and NDVI	Suitable for heterogeneous landscapes but it does not produce higher accuracy during downscaling LST	Mukherjee et al. (2014a)
M5P _{DS} (M5 Rule based Downscaling)	A data mining approach (decision tree) is used for downscaling of LST. NDVI/LST relationship may vary over various LULC classes and studies have found that this relationship is not well-defined over heterogeneous landscapes. It can find out similarity patterns within the sample data which can be used for training of variables	M5P decision tree rule	LST, NDVI, SAVI, and <i>f_c</i>	Suitable for heterogeneous landscapes efficiently to downscale LST	Mukherjee et al. (2015)
MLP _{DS} (Multilayer Perceptron Downscaling)	This technique is mostly used in machine learning and/or pattern recognition. It is a modified form of the standard linear perceptron algorithm and can discriminate variables that are not linearly separable	Multilayer perceptron utilizing a supervised learning procedure	NDVI, SAVI, <i>f_c</i> , and LST	Suitable for heterogeneous landscapes efficiently to downscale LST. It can be tested over homogeneous landscapes to understand the performance	Mukherjee et al. (2015)

(continued)

Table 2 (continued)

Model	Description	Method	Parameter	Remarks	References
RK _{ps} (Regression-Kriging Based Downscaling)	It assumes that if NDVI-LST relationship model is perfect, there should not be any bias or residual at coarse resolution. Gaussian filter, neural network, and differential weighting function are applied on residual LST before adding to predicted LST at fine resolution	Regression-Kriging using OLS/generalized least square (GLS) regression model	LST and NDVI	Suitable for heterogeneous and homogeneous landscapes to downscale LST. The major advantage is that no artificial box-like appearance is seen in the downscaled LST image	Mukherjee et al. (2015)

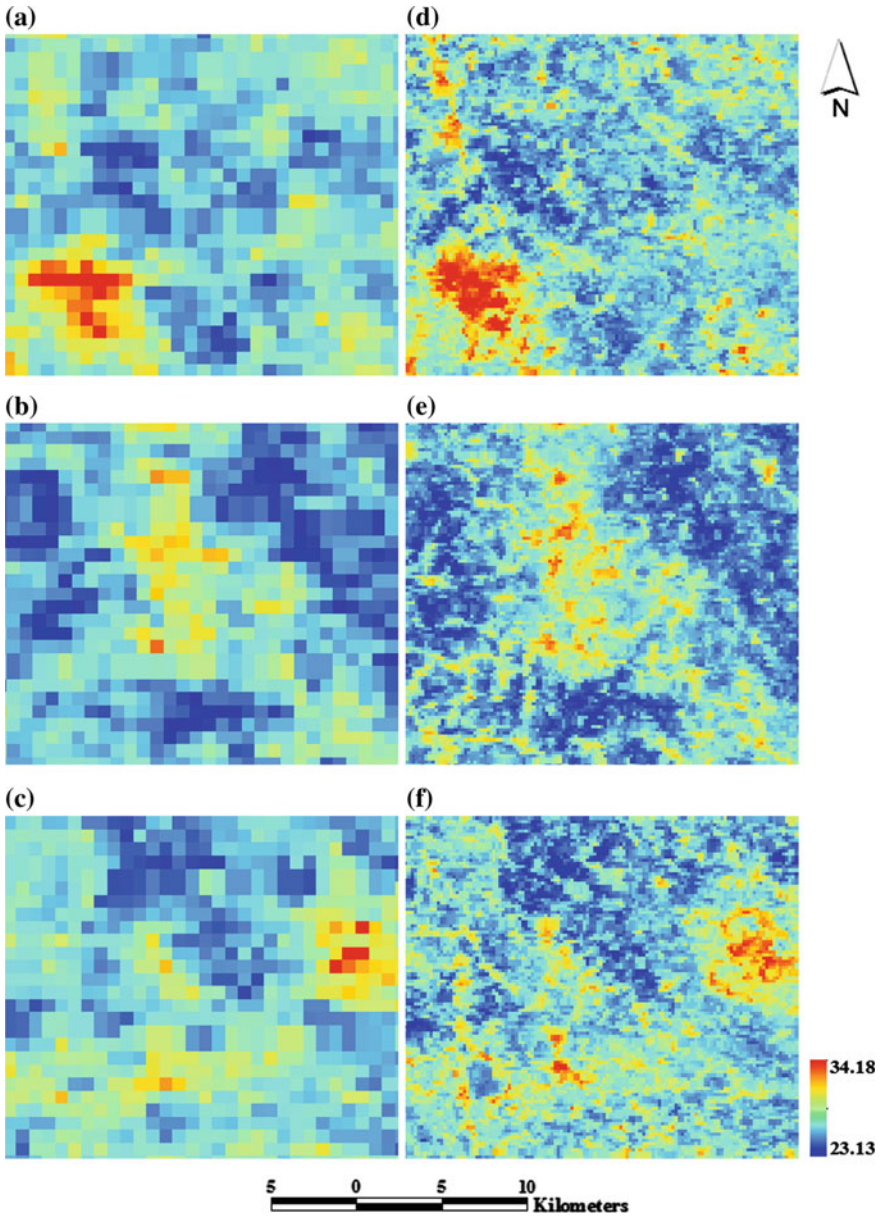


Fig. 5 a–c Actual MODIS LST of 1000 m of 26th February 2010 and d–f downsampled MODIS LST of 250 m resolution using RK_{DS} model. The area is located in the eastern part of Uttar Pradesh under humid tropical climate

$$\hat{LST}_{FR_i} = a + b \times NDVI_{FR_i} \quad (3)$$

$$\hat{LST}_{DFR_i} = \hat{LST}_{FR_i} + \Delta\hat{LST}_{CR_i} \quad (4)$$

where $NDVI_{CR}$ is the coarse resolution NDVI, \hat{LST}_{CR} is the predicted LST at coarser resolution, LST_{REF} is the reference LST, $\Delta\hat{LST}_{CR}$ is the residual LST, $NDVI_{FR}$ is the finer resolution NDVI and \hat{LST}_{FR} is the predicted LST at finer resolution, \hat{LST}_{DFR} is the downscaled LST of fine resolution and ‘a’ and ‘b’ are slope and intercept of the regression model. i stands for individual pixel (i th pixel).

The description of various thermal data or the LST downscaling models such as (i) Regression-based model (DisTrad, TsHARP, TsHARP_{LM}, LMS_{DS}, and PR_{DS}) (ii) Decision tree-based model (M5P) (iii) Geostatistical model (RK_{DS}), and (iv) Hybrid model (MLP_{DS}) are given in the Table 2. The model characteristics, algorithms, parameters used in the model and their applicability over various landscapes are also described in this section. The models are grouped into above-mentioned categories depending on their nature and characteristics.

The models demonstrated in the Table 2 can be used for downscaling thermal data or the LST. Figure 5 shows the actual (1000 m) and the downscaled MODIS (250 m) LST image. The downscaled image shows similar pattern with the actual MODIS image, but the information content is higher.

4 Application of Thermal Data Downscaling

MODIS LST of 1000 m resolution can be downscaled using the methodology explained in Sect. 3. The selection of method should be based on the degree of heterogeneity over the landscape, the biophysical parameters available and the algorithm to be used. The Remote Sensing community can take up the downscaling methodology for various environmental and natural resource monitoring applications. The theme of the research can be extended to different applications listed in Table 3 using satellite-based open-source LST.

In this chapter, application of such downscaled LST products has been demonstrated for drought, soil moisture, and urban mapping on a regional scale. The downscaled MODIS LST provides larger details as compared to the actual LST while maintaining a similarity in the overall pattern. The actual and downscaled LST are used to derive vegetation health Index (VHI) (Kogan 2001) and temperature vegetation dryness index (TVDI) (Sandholt et al. 2002) for drought intensity and soil moisture status mapping (Figs. 6 and 7). Information content increases in the fine resolution VHI and TVDI maps due to the high intra-pixel variability. Field

Table 3 Application of downscaled LST models and research areas

Application	References
<p>Surface energy budget</p> <p>It is a process of estimating the energy coming from the sun to the earth's climate system and reaching back to atmosphere to maintain the balance between incoming and outgoing energy</p>	Muramatsu et al. (2006), Anderson et al. (2008)
<p>Evapotranspiration</p> <p>It is a process which includes the sum of evaporation and transpiration from vegetation from the earth's land and water surface to the atmosphere</p>	Anderson et al. (2012), Bindhu et al. (2013)
<p>Drought</p> <p>It refers to a prolonged period of deficient precipitation with declining soil moisture content and causes extensive damage to crops, resulting in loss of yield</p>	Karnieli et al. (2010), Mukherjee et al. (2014b)
<p>Soil moisture</p> <p>Soil moisture is a key parameter required for the meteorology, hydrology, and agriculture-related applications</p>	Sandholt et al. (2002), Hulley et al. (2010)
<p>Urban climate and heat island</p> <p>The core of urban area/cities is warmer than the periphery and surrounding rural areas which form an urban heat island. It affects the micro and mesoscale climatic impact on urban environment</p>	Sharma and Joshi (2014), Imhoff et al. (2010)
<p>Crop management</p> <p>Crop growth monitoring, assessment of crop water stress and crop health evaluation</p>	Abuzar et al. (2009), Dragutin and Eitzinger (2007)
<p>Wild fire</p> <p>A wildfire/forest fire is an uncontrolled extensive size fire in an area of combustible vegetation that occurs in a wilderness area</p>	Robinson (1991), Pinol et al. (2005)
<p>Landscape ecology</p> <p>It is a science of studying and improving the relationships between environment and ecological processes</p>	Quattrochi and Luvall (1999), Kerr and Ostrovsky (2003)
<p>Burnt area estimation</p> <p>The crop residue burning is a common practice in developing countries. Estimation of burnt area is important for environment</p>	Roy (1999), Ichoku et al. (2003)
<p>Vegetation phenology, dynamics, and change</p> <p>Phenology is the study of periodic behavior of plant/vegetation and identifies how they are influenced by seasonal pattern of climate. Decadal change in vegetation and its dynamics is also important for the climate change and land cover-related studies</p>	Badeck et al. (2004), Julien et al. (2011)
<p>Volcanic eruptive activity</p> <p>Volcanic eruptions are an important phenomenon which needs to be studied. The developments in thermal remote sensing techniques have expanded the monitoring capability of volcanoes through satellite image</p>	Wright et al. (2002, 2004)

(continued)

Table 3 (continued)

Application	References
Coal fire Coal fire is a serious natural hazard which affects the economic, social and ecological environment. It is an underground fire, often seen in coal mine due to lightning, grass or forest fires	Prakash et al. (1995, 1999)
Defence-related Monitoring of defence-related features is an important application of thermal Remote Sensing	Khanafer and Vafai (2002)

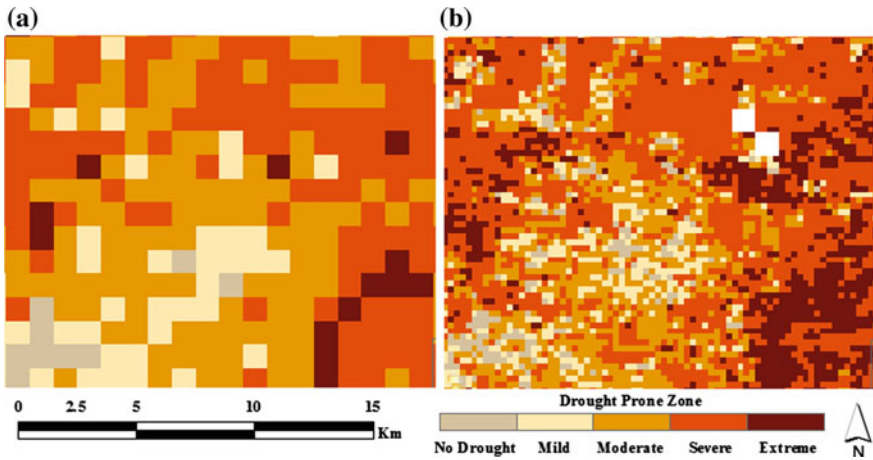


Fig. 6 Drought intensity maps **a** MODIS data (1000 m) and **b** downscaled data (250 m). The area is located in the eastern part of Rajasthan state, India. Larger spatial details and drought intensity information is observed in the downscaled drought map

scale agricultural drought intensity could be easily delineated from the downscaled data. This downscaled data is useful for drought and soil moisture mapping on a regional scale.

Downscaled LST is found to be useful for urban mapping. Location of urban centers, shape, and size of town/cities are better visible in downscaled LST data (Fig. 8). The visualization of temperature differences among urban, suburban, and rural areas is better in the downscaled data. Small built-up areas are detectable in 250 m resolution downscaled LST. The urban sprawl development along the road alignment can also be clearly demarcated. This data is also helpful for mapping of SUHI and its intensity estimation.

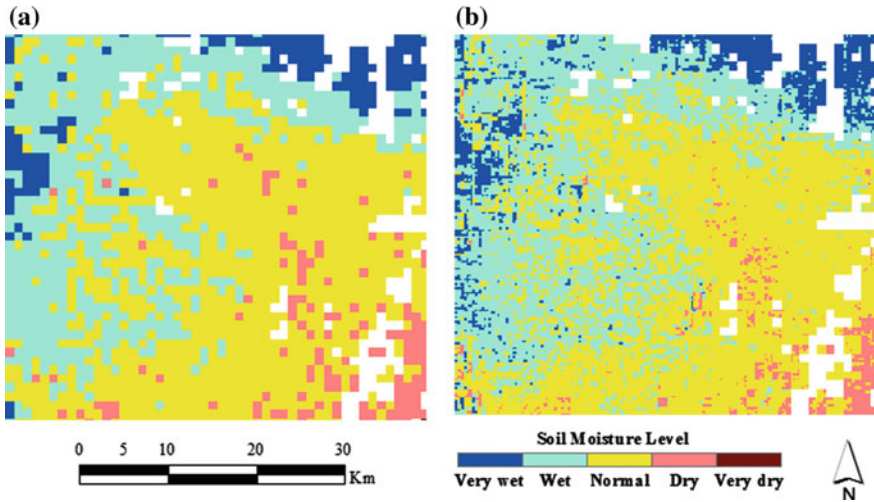


Fig. 7 Soil moisture maps **a** actual MODIS data (1000 m) and **b** downscaled data (250 m). The area is located in the eastern part of Rajasthan state, India. Higher spatial details and soil moisture information is observed in the downscaled soil moisture map

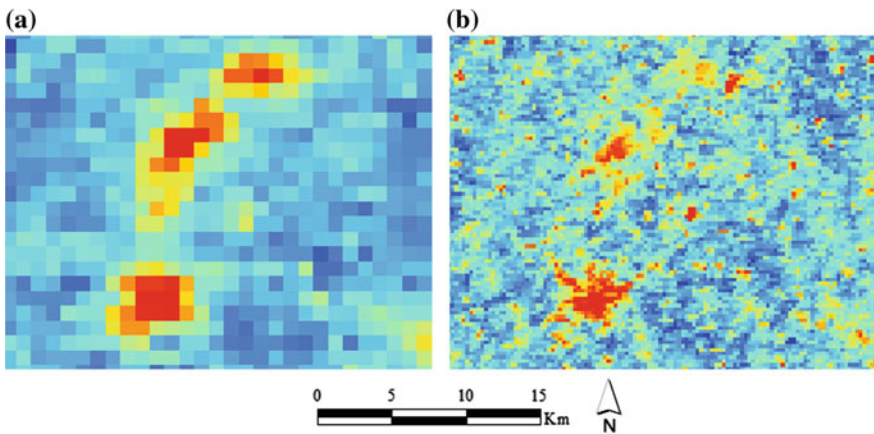


Fig. 8 **a** Actual MODIS data of 1000 m spatial resolution and **b** downscaled data of 250 m resolution. The area is located in the Southern part of Punjab state, India. The urban centers, urban sprawl and other small built-up structures are better visualized in the downscaled LST data

5 Future of Thermal Data Downscaling

The frequently available optical and downscaled LST (around 250 m spatial resolution) will certainly increase the probability of daily or weekly monitoring of environmental processes and other related phenomenon. Some of the immediate

requirements are monitoring of indices like drought and forest fire, assessment of soil moisture content, and urban heat island phenomenon. The high frequency spatiotemporal aspect of the environment-related information of the patterns and their variability will help decision makers for effectively managing and formulating policies for the affected areas and adequate land use planning. The downscaled LST will also be helpful for urban planning and management which is one of the most recent environmental concerns as it is expected to add to the magnitude of global environmental warming. This technique will certainly increase the utilization of the EOS thermal data for the agriculture and environment-related applications to promote the goal of the ‘Synergy Program’ of NASA.

Mapping and continuous monitoring of drought and soil moisture status is very critical for decision makers and planners (Kalluri et al. 2003) in order to decide on implementing water conservation and drought response measures. In this regard, we need continuous research and innovation in downscaling the thermal data. The methods demonstrated in this chapter are well researched and would certainly be helpful for understanding regional soil moisture and drought patterns, its intensity variation over space and time in a daily or weekly manner. Such mechanisms would also enhance the management, planning, and policy formation procedures. This will also help the decision makers to create the mechanism for periodic monitoring and prepare action plans for the management of urban planning and environmental management.

References

- Abuzar M, O’Leary G, Fitzgerald G (2009) Measuring water stress in a wheat crop on a spatial scale using airborne thermal and multispectral imagery. *Field Crops Res.* 112:55–65
- Agam N, Kustas WP, Anderson MC, Li F, Neale CMU (2007a) A vegetation index based technique for spatial sharpening of thermal imagery. *Remote Sens Environ* 107:545–558
- Agam N, Kustas WP, Anderson MC, Li F, Colaizzi PD (2007b) Utility of thermal sharpening over Texas high plains irrigated agricultural fields. *J Geophys Res* 112:1–10
- Anderson MC, Neale CMU, Li F, Norman JM, Kustas WP, Jayanthi H, Chavez J (2004) Upscaling ground observations of vegetation water content, canopy height, and leaf area index during SMEX02 using aircraft and Landsat imagery. *Remote Sens Environ* 92:447–464
- Anderson MC, Norman JM, Kustas WP, Houborg J, Starks PJ, Agam N (2008) A thermal-based Remote Sensing technique for routine mapping of land-surface carbon, water and energy fluxes from field to regional scales. *Remote Sens Environ* 112:4227–4241
- Anderson MC, Allen RG, Morse A, Kustas WP (2012) Use of Landsat thermal imagery in monitoring evapotranspiration and managing water resources. *Remote Sens Environ* 112:50–65
- Atkinson PM (2013) Downscaling in remote sensing. *Int J Appl Earth Obs Geoinfo* 22:106–114
- Badeck FW, Bondeau A, Bottcher K, Doktor D, Lucht W, Schaber J, Sitch S (2004) Responses of spring phenology to climate change. *New Phytol* 162:295–309
- Benestad RE, Hanssen-Bauer I, Chen D (2008) Empirical-statistical downscaling, vol 41. World Scientific, Singapore
- Bindhu VM, Narasimhan B, Sudheer KP (2013) Development and verification of a non-linear disaggregation method (NL-DisTrad) to downscale MODIS land surface temperature to the

- spatial scale of Landsat thermal data to estimate evapotranspiration. *Remote Sens Environ* 135:118–129
- Caihua Y, Yonghong L, Weijun Q, Weidong C, Cheng L (2011) Application of Urban thermal environment monitoring based on remote Sensing in Beijing. *Procedia Environ. Sci.* 11:1424–1433
- Chen XL, Zhao HM, Li PX, Yin ZY (2006) Remote Sensing image-based analysis of the relationship between urban heat island and land use/cover changes. *Remote Sens Environ* 104:133–146
- Coudert B, Ottlé C, Briottet X (2008) Monitoring land surface processes with thermal infrared data: Calibration of SVAT parameters based on the optimisation of diurnal surface temperature cycling features. *Remote Sens Environ* 112(3):872–887
- Dominguez A, Kleissl J, Luvall JC, Rickman DL (2011) High-resolution urban thermal sharpener (HUTS). *Remote Sens Environ* 115(7):1772–1780
- Dragutin TM, Eitzinger J (2007) Modelling temperatures of crop environment. *Ecol Model* 202:465–475
- Eckmann TC, Roberts DA, Still CJ (2009) Estimating subpixel fire sizes and temperatures from ASTER using multiple endmember spectral mixture analysis. *Int J Remote Sens* 30(22):5851–5864
- Embury O, Merchant CJ, Corlett GK (2012) A reprocessing for climate of sea surface temperature from the along-track scanning radiometers: Initial validation, accounting for skin and diurnal variability effects. *Remote Sens Environ* 116:62–78
- Essa W, Verbeiren B, Kwast JVD, Voorde TVD, Batelaan O (2012) Evaluation of the DisTrad thermal sharpening methodology for urban areas. *Int J Appl Earth Obs Geoinf* 19:163–172
- Essa W, Kwast JVD, Verbeiren B, Batelaan O (2013) Downscaling of thermal images over urban areas using the land surface temperature–impervious percentage relationship. *Int J Appl Earth Obs Geoinf* 23:95–108
- Ghosh A, Joshi PK (2014) Hyperspectral imagery for disaggregation of land surface temperature with selected regression algorithms over different land use land cover scenes. *ISPRS J Photogramm Remote Sens* 96:76–93
- Hewitson BC, Crane RG (1996) Climate downscaling: techniques and application. *Climate Res* 7:85–96
- Hope A, Engstrom R, Stow D (2005) Relationship between AVHRR surface temperature and NDVI in Arctic tundra ecosystems. *Int J Remote Sens* 26(8):1771–1776
- Hulley GC, Hook SJ, Baldridge AM (2010) Investigating the effects of soil moisture on thermal infrared land surface temperature and emissivity using satellite retrievals and laboratory measurements. *Remote Sens Environ* 114(7):1480–1493
- Ichoku C, Kaufman YJ, Giglio L, Li Z, Fraser RH, Jin JZ, Park WM (2003) Comparative analysis of daytime fire detection algorithms using AVHRR data for the 1995 fire season in Canada: perspective for MODIS. *Int J Remote Sens* 24(8):1669–1690
- Imhoff ML, Zhang P, Wolfe RE, Bounoua L (2010) Remote sensing of the urban heat island effect across biomes in the continental USA. *Remote Sens Environ* 114(3):504–513
- Inamdar AK, French A (2009) Disaggregation of GOES land surface temperatures using surface emissivity. *Geophys Res Lett* 36(2)
- Jeganathan C, Hamm NAS, Mukherjee S, Atkinson PM, Raju PLN, Dadhwal VK (2011) Evaluating a thermal image sharpening model over a mixed agricultural landscape in India. *Int J Appl Earth Obs Geoinf* 13:178–191
- Jensen JR (2006) *Remote sensing of the environment: an earth resource perspective* (second edn). Prentice Hall
- Jing LH, Cheng QM (2010) A technique based on non-linear transform and multivariate analysis to merge thermal infrared data and higher-resolution multispectral data. *Int J Remote Sens* 31(24):6459–6471
- Julien Y, Sobrino JA, Verhoef W (2006) Changes in land surface temperatures and NDVI values over Europe between 1982 and 1999. *Remote Sens Environ* 103:43–55

- Julien Y, Sobrino JA, Jiménez-Muñoz J-C (2011) Land use classification from multi temporal Landsat imagery using the Yearly Land Cover Dynamics (YLCD) method. *Int J Appl Earth Obs Geoinf* 13:711–720
- Kalluri S, Gilruth P, Bergman R (2003) The potential of remote sensing data for decision makers at the state, local and tribal level: experiences from NASA's Synergy program. *Environ Sci Policy* 6(6):487–500
- Karnieli A, Bayasgalan M, Bayarjargal Y, Agam N, Khudulmur S, Tucker CJ (2006) Comments on the use of the Vegetation Health Index over Mongolia. *Int J Remote Sens* 27:2017–2024
- Karnieli A, Agam N, Pinker RT, Anderson M, Imhoff ML, Gutman GG, Panov N, Goldberg A (2010) Use of NDVI and Land surface temperature for drought assessment: merits and limitations. *J Clim* 23:618–633
- Kerr JT, Ostrovsky M (2003) From space to species: ecological applications for remote sensing. *Trends Ecol Evolut.* 18(6):299–305
- Khanafer K, Vafai K (2002) Thermal analysis of buried land mines over a diurnal cycle. *IEEE Trans Geosci Remote Sens* 40(2):461–473
- Kogan FN (2001) Operational space technology for global vegetation assessment. *Bull Am Meteorol Soc* 82(9):1949–1964
- Kustas WP, Norman JM, Anderson MC, French AN (2003) Estimating subpixel surface temperatures and energy fluxes from the vegetation index-radiometric temperature relationship. *Remote Sens Environ* 85:429–440
- Li F, Kustas WP, Prueger JH, Neale CM, Jackson TJ (2005) Utility of remote sensing-based two-source energy balance model under low- and high-vegetation cover conditions. *J. Hydrometeor.* 6(6):878–891
- Liang S (2004) Quantitative remote sensing of land surfaces. John Wiley & Sons. INC., Publication
- Lillesand TM, Kiefer RW (1994) Remote sensing and image interpretation. Wiley
- Liyanage PKNC, Manawadu L (2011) Spatial variability of surface temperature—use of thermal remote sensing as an alternative to measure surface temperature: a case study of Colombo. LAP Lambert Academic Publishing, Sri Lanka. ISBN 978-3-8454-4313-3
- Luvall JC, Holbo HR (1989) Measurements of short-term thermal responses of coniferous forest canopies using thermal scanner data. *Remote Sens Environ* 27(1):1–10
- Merlin O, Duchemin B, Hagolle O, Jacob F, Coudert B, Chehbouni G, Dedieu G, Garatuza J, Kerr Y (2010) Disaggregation of MODIS surface temperature over an agricultural area using a time series of Formosat-2 images. *Remote Sens Environ* 114(11):2500–2512
- Moran MS, Rahman AF, Washburne JC, Kustas WP (1996) Combining the Penman-Monteith equation with measurements of surface temperature and reflectance to estimate evaporation rates of semiarid grassland. *Agri. For. Meteorol.* 80:87–109
- Morrow N, Friedl MA (1998) Modeling biophysical controls on land surface temperature reflectance in grasslands. *Agri. For. Meteorol.* 92(3):147–161
- Mukherjee S (2008) Multi-resolution technique for disaggregation of thermal image using vegetation index. M.Sc. Thesis, IIRS and ITC joint programme
- Mukherjee S (2015). Downscaling of coarse resolution open source remotely sensed satellite-based land surface temperature data. Ph.D. Thesis. TERI University
- Mukherjee S, Joshi PK, Garg RD (2014a) A comparison of different regression models for downscaling Landsat and MODIS land surface temperature images over heterogeneous landscape. *Adv Space Res* 54:655–669
- Mukherjee T, Mukherjee S, Mukhopadhyay A, Roy AK, Dutta S (2014b) Drought monitoring of Chhattisgarh using different indices based on remote sensing data. Climate change and biodiversity: proceedings of IGU Rohtak Conference, vol. 1, Advances in Geographical and Environmental Sciences, Springer Japan
- Mukherjee S, Joshi P, Garg RD (2015) Regression-kriging technique to downscale satellite-derived land surface temperature in heterogeneous agricultural landscape. *IEEE J Sel Topics Appl Earth Observ in Remote Sens.* doi:[10.1109/JSTARS.2015.2396032](https://doi.org/10.1109/JSTARS.2015.2396032)

- Muramatsu K, Nakayama S, Kaihotsu I (2006) A case study of estimating thermal energy budget in Mongolian plateau using LANDSAT 7/ETM+ data. *Adv Space Res* 38:2191–2195
- Nasipuri P, Majumdar TJ, Mitra DS (2006) Study of high-resolution thermal inertia over western India oil fields using ASTER data. *Acta Astronaut* 58(5):270–278
- Nichol J (2009) An Emissivity modulation method for spatial enhancement of thermal satellite images in urban heat Island Analysis. *Photogramm. Eng. Remote Sens.* 75:547–556
- Ormsby JP (1981) The use of Landsat-3 thermal data to help differentiate land covers. *Remote Sens Environ* 12(2):97–105
- Ottlé C, Vidal-Madjar D (1992) Estimation of land surface temperature with NOAA 9 data. *Remote Sens Environ* 40(1):27–41
- Pinol J, Beven K, Viegas DX (2005) Modelling the effect of fire-exclusion and prescribed fire on wildfire size in Mediterranean ecosystems. *Ecol Model* 183:397–409
- Prakash A, Sastry RGS, Gupta RP, Saraf AK (1995) Estimating the depth of buried hot feature from thermal IR Remote Sensing data, a conceptual approach. *Int J Remote Sens* 16(13):2503–2510
- Prakash A, Gens R, Vekerdy Z (1999) Monitoring coal fires using multi-temporal night-time thermal images in a coal field in North-west China. *Int J Remote Sens* 20(14):2883–2888
- Quattrochi DA, Luvall JC (1999) Thermal infrared Remote Sensing for analysis of landscape ecological processes: methods and applications. *Landscape Ecol* 14(6):577–598
- Rajapakse RMSS, Tripathi NK, Honda K (2002) Spectral characterization and LAI modeling for the tea (*Camellia sinensis* (L) O. Kuntze) Canopy. *Int J Remote Sens* 23(18):3569–3578
- Robinson JM (1991) Fire from space: global fire evaluation using infrared remote sensing. *Int J Remote Sens* 12(1):3–24
- Rodriguez-Galiano V, Pardo-Iguzquiza E, Sanchez-Castillo M, Chica-Olmo M, Chica-Rivas M (2012) Downscaling Landsat 7 ETM+ thermal imagery using land surface temperature and NDVI images. *Int J Appl Earth Obs Geoinf* 18:515–527
- Rojas O, Vrieling A, Rembold F (2011) Assessing drought probability for agricultural areas in Africa with coarse resolution remote sensing imagery. *Remote Sens Environ* 115(2):343–352
- Roy DP (1999) Multi-temporal active-fire based burn scar detection algorithm. *Int J Remote Sens* 20(5):1031–1038
- Sandholt I, Rasmussen K, Andersen J (2002) A simple interpretation of the surface temperature/vegetation index space for assessment of surface moisture status. *Remote Sens Environ* 79:213–224
- Sharma R, Joshi PK (2014) Identifying seasonal heat islands in urban settings of Delhi (India) using remotely sensed data—An anomaly based approach. *Urban Climate*. 9:19–34
- Sobrino JA, Gomez M, Munoz JCJ, Olioso A (2007) Application of a simple algorithm to estimate daily evapotranspiration from NOAA-AVHRR images for the Iberian Peninsula. *Remote Sens Environ* 110:139–148
- Weng Q (2009) Thermal infrared remote sensing for urban climate and environmental studies: methods, applications, and trends. *ISPRS J Photogramm Remote Sens* 64:335–344
- Wood AW, Leung LR, Sridhar V, Lettenmaier DP (2004) Hydrological implications of dynamical and statistical approaches to downscaling climate model outputs. *Clim Change* 62:189–216
- Wooster MJ, Xu W, Nightingale T (2012) Sentinel-3 SLSTR active fire detection and FRP product: Pre-launch algorithm development and performance evaluation using MODIS and ASTER datasets. *Remote Sens Environ* 120:236–254
- Wright R, Flynn L, Garbeil H, Harris A, Pilger E (2002) Automated volcanic eruption detection using MODIS. *Remote Sens Environ* 82:135–155
- Wright R, Flynn LP, Garbeil H, Harris AJ, Pilger E (2004) MODVOLC: near-real-time thermal monitoring of global volcanism. *J Volcanol Geoth Res* 135(1):29–49
- Yang J, Wang Y (2011) Estimating evapotranspiration fraction by modeling two-dimensional space of NDVI/albedo and day–night land surface temperature difference: A comparative study. *Adv Water Resour* 34(4):512–518
- Yang H, Cong Z, Liu Z, Lei Z (2010a) Estimating sub-pixel temperatures using the triangle algorithm. *Int J Remote Sens* 31(23):6047–6060

- Yang G, Pu R, Huang W, Wang J, Zhao C (2010b) A novel method to estimate subpixel temperature by fusing solar-reflective and thermal infrared Remote Sensing data with an artificial neural network. *IEEE Trans Geosci Remote Sens* 48:2170–2178
- Yang G, Pu R, Zhao R, Huang W, Wang J (2011) Estimation of subpixel land surface temperature using an endmember index based technique: a case examination on ASTER and MODIS temperature products over a heterogeneous area. *Remote Sens Environ* 115(5):1202–1219
- Zakšek K, Oštir K (2012) Downscaling land surface temperature for urban heat island diurnal cycle analysis. *Remote Sens Environ* 117:114–124
- Zhang X, Genderen JLV, Kroonenberg SB (1997) A method to evaluate the capability of Landsat-5 TM band 6 data for sub-pixel coal fire detection. *Int J Remote Sens* 18(15):3279–3288
- Zhan W, Chen Y, Zhou J, Wang J, Liu W, Voogt J, Zhu X, Quan J, Li J (2013) Disaggregation of remotely sensed land surface temperature: literature survey, taxonomy, issues, and caveats. *Remote Sens Environ* 131:119–139
- Zhu S, Guan H, Millington AC, Zhang G (2013) Disaggregation of land surface temperature over a heterogeneous urban and surrounding suburban area: a case study in Shanghai. *China Int J Remote Sens* 34(5):1707–1723

Future Projection of Rainfall by Statistical Downscaling Method in a Part of Central India

Sananda Kundu, Deepak Khare and Arun Mondal

Abstract Rainfall is one of the important parameters of climate and hydrological studies. Distribution and intensity of the rainfall vary from place to place. The present study involves prediction of future rainfall using past historical data. The study area is a part of the Narmada river basin in the central part of India. Three rainfall stations (Betul, Hoshangabad and Raisen) are taken for this study. Statistical Downscaling Model (SDSM) has been applied to estimate the future rainfall using General Circulation Model (GCM). Observed data (rainfall) and National Centre for Environmental Prediction (NCEP) data are used from 1961 to 2001. Hadley Centre Coupled Model, version 3 (HADCM3) of A2 emission scenario is also used during 1961–2099. The period of calibration and validation of the model is 1961–1989 and 1990–2001, respectively. The performance of the downscaling technique is estimated by Root Mean Square Error (RMSE), Normalized Mean Square error (NMSE) and Nash–Sutcliffe coefficient (NASH) and Correlation Coefficient (CC) methods. The bias correction technique has been applied in this study. The prediction results are illustrated for the period of 2020s, 2050s and 2080s time scale. The results of future rainfall project increasing trend in three different stations.

Keywords SDSM · GCM · NCEP and HADCM3

1 Introduction

Proper assessment of climatic parameters is very difficult for future time periods. But their changing pattern can be explained due to their interrelationship with other parameters. Climate change indicates a change in the properties of climate that

S. Kundu (✉) · D. Khare · A. Mondal

Department of Water Resources Development and Management, Indian Institute of Technology, Roorkee, India
e-mail: sanandakundu@gmail.com

© Springer International Publishing Switzerland 2017

S. Hazra et al. (eds.), *Environment and Earth Observation*,

Springer Remote Sensing/Photogrammetry, DOI 10.1007/978-3-319-46010-9_4

persists for a long period, may be decades or longer because of natural variation or due to human activity, as given by Intergovernmental Panel on Climate Change (IPCC 2007). The global climate change has shown its severity in many places and has raised concern to study the change of various climate parameters. There is an increase in population, which is raising the food and water demand. Changes in the climate are affecting rainfall and temperature that influence food production and water availability. Variation in the spatial and temporal distribution of water may worsen the situation. There is a higher rate of concentration of carbon dioxide and trace gases with the changing climate (Kamga 2001), and it may affect the water resources in the future. Changes in the rainfall and temperature pattern have resulted in elaborate studies. According to the IPCC (2007), interseasonal, inter-annual and spatial variation of precipitation are observed in Asia in the last few decades. The climate change is influencing the water balance of a region and for the future, proper planning should be carried out. Different models are there for estimating the complex process of a hydrologic system (Arnold and Allen 1996). The effect of human interference is observed in many studies that have caused changes in temperature and resultant variation in the spatial distribution of rainfall and thus affecting the future runoff (Hulme et al. 2002; Fowler et al. 2005). Different types of climate changes study are available. Most of the studies are related to a past climate scenario and future probable scenario using different climatic parameters. Past climatic trend and related analysis have been done by different researchers (Akinremi et al. 2001; Kipkorir 2002; González et al. 2008; Conway et al. 2009; Kumar et al. 2010; Kumar and Jain 2010; Zhang et al. 2012; Padmavathi and Virmani 2013; Bisht et al. 2013; Kundu et al. 2014, 2015; Mondal et al. 2014a; Wei et al. 2014; Dashtpagerdi et al. 2014). The General Circulation Models (GCMs) are not used directly in the local hydrological models (Carter et al. 1994) due to coarse resolution of the data; statistical downscaling methods serve the purpose as it is able to relate the global climate variables with the regional climate variables. Various methods are available to downscale into fine resolution (local scale) from coarse resolution (regional scale) data. Multiple Linear Regression (MLR), Artificial Neural Networks (ANN) and Support Vector Machine (SVM) are the reputed methods for climate downscaling techniques. These methods have been applied in different study areas in the world by various researchers (Schoof and Pryor 2001; Kostopoulou et al. 2007; Goyal and Ojha 2010, 2012; Anandhi et al. 2009; Mishra et al. 2014; Duhan and Pandey 2014; Mondal et al. 2014b). The SDSM is used widely for climate downscaling all over the globe. However, the performance of the model and representation of the results is limited in SDSM tool in previous works. In this study, model performance and better representation of results have been added for improved analysis of the study.

The objective of the study is to set up the model with past rainfall data and predict the rainfall in the future. SDSM is based on MLR concept which is used for downscaling to predict the future rainfall using A2 scenario of HadCM3 data, which is also a GCM type of data. Output results have been analysed in different time periods after checking the model performance with good accuracy.

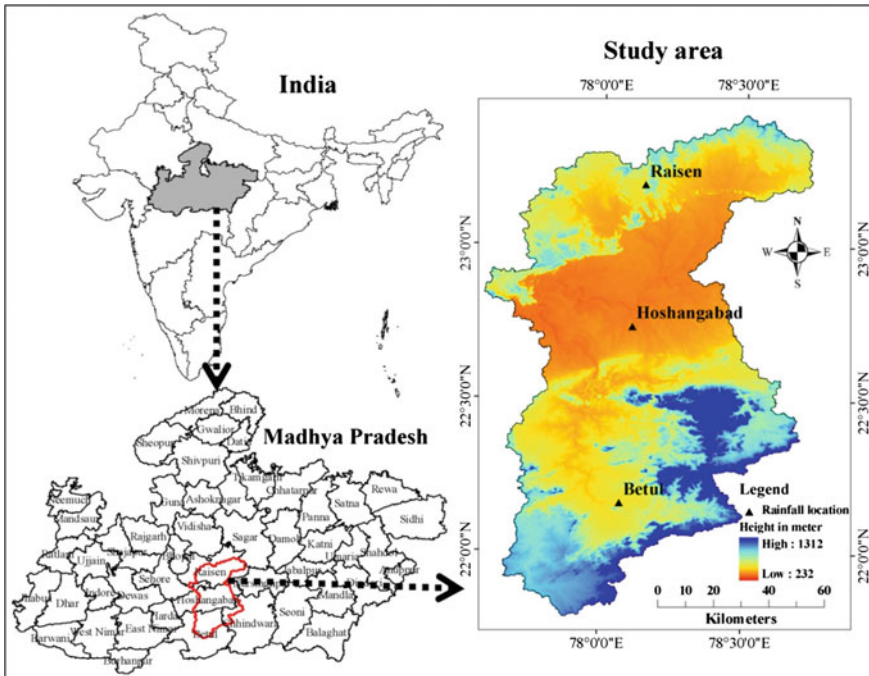


Fig. 1 Study area

2 Study Area

The study is located in a part of the Narmada river basin in Madhya Pradesh state, India. The latitudinal longitudinal extensions are $21^{\circ}47'24''$ to $23^{\circ}26'06''N$ and $77^{\circ}34'44''$ to $78^{\circ}42'21''E$, which is covering $12,290 \text{ km}^2$ areas (Fig. 1). The major part of the area is lying in three districts (Betul, Hoshangabad and Raisen) of Madhya Pradesh. It experiences a subtropical nature of climate with hot, dry summer and a cool dry winter. Rainfall and temperature varies from 900 to 1150 mm and 19.5 to $32.5 \text{ }^{\circ}\text{C}$ annually (last 40 years average data). Elevation range varies from 267 m to 1308 m and clay and sandy clay types of soil are found there.

3 Used Data and Methodology

3.1 Data Details

The NCEP grids are used to get the data from 1961 to 2001 (predictor) on a scale of $2.5^{\circ} \times 2.5^{\circ}$ and the HADCM3 grid has the scale of $2.5^{\circ} \times 3.75^{\circ}$ obtained from the

Table 1 Locations and Information of stations

Sl no.	Station name	Lat. (N)	Long. (E)	Alt (m)	Duration of data	Data type
1	Betul	21.18	78.06	437	1961–01	Rainfall
2	Hoshangabad	22.73	78.08	313	1961–01	
3	Raisen	23.26	78.12	433	1961–01	

Canadian Climate Impacts Scenarios. Total NCEP or GCM (HADCM3) variables of every grid is given in the Table 2. Therefore, the NCEP and HADCM3 grid scales are different. The daily observed rainfall data were obtained for the 3 stations for 41 years (1961–2001) from the Indian Meteorological Department (IMD). Details of the stations are given below (Table 1).

3.2 Method

3.2.1 The Statistical DownScaling Model (SDSM)

Analysis was done with the A2 scenario with the model output from 1961 to 2099. The NCEP grid points and HADCM3 grid points' locations do not match, thus Inverse Distance Weighted (IDW) method (Willmott et al. 1985) of interpolation was applied prior to the use of GCM outputs in prediction by regridding the HADCM3 points to the NCEP grids (Fig. 2).

The A2 scenario was used in the analysis of future projection of climate. The A2 scenario has a higher concentration of atmospheric CO₂ and this condition is similar to the Indian environment and many have used A2 scenario to study in India (Anandhi et al. 2009; Kannan and Ghosh 2011; Raje and Mujumdar 2011; Meenu et al. 2013).

The observed station data were considered as predictands with the NCEP (predictor) variable from 1961 to 2001 for annual climatic analysis. Among the variables of the NCEP data, only highly correlated data were selected as the predictors. The selected NCEP data were then standardized. Then calibration and validation of the model were done and the same process is repeated with the GCM data. The future climate data is obtained by the trained models and bias correction is carried out (Fig. 1). Bias correction was applied to the predicted data. Model obtained future rainfall of the decades from 2011 to 2099 of three stations was taken.

The Statistical DownScaling Model (SDSM) is a decision support tool method based on the on multiple linear regression technique, which was developed by Wilby et al. (2002). The SDSM model integrates multiple linear regression and weather generator. The five major steps of downscale in SDSM are, (i) initial screening of the predictor variables; (ii) calibration of the SDSM model; (iii) observed data synthesis (predictor variables); (iv) future data generation from the predictors that are obtained

Table 2 Selected predictor variables

Sl. No.	Atmospheric pressure level	NCEP/GCM Variables	Name	Unit
A.	1013.25 hPa (1)	MSL pressure	mslp	Pa
B.	1000 hPa (6)	Wind speed (Geostrophic)	p_f	m/s
		Zonal (Eastward) velocity (U-component)	p_u	m/s
		Meridional (Northward) velocity (V-component)	p_v	m/s
		Vorticity	p_z	s ⁻¹
		Wind direction	p_th	degree
		Divergence	p_zh	s ⁻¹
C	850 hPa (8)	Wind speed (Geostrophic)	p8_f	m/s
		Zonal (Eastward) velocity (U-component)	p8_u	m/s
		Meridional (Northward) velocity (V-component)	p8_v	m/s
		Vorticity	p8_z	s ⁻¹
		Wind direction	p8_th	degree
		Divergence	p8_zh	s ⁻¹
		Geopotential height	p850	m
		Relative humidity	r850	%
D	500 hPa (8)	Wind speed (Geostrophic)	p5_f	m/s
		Zonal (Eastward) velocity (U-component)	p5_u	m/s
		Meridional (Northward) velocity (V-component)	p5_v	m/s
		Vorticity	p5_z	s ⁻¹
		Wind direction	p5_th	
		Divergence	p5_zh	s ⁻¹
		Geopotential height	p500	m
		Relative humidity	r500	%
E	Near surface (3)	Specific humidity	shum	g/kg
		Mean temperature	temp	°C
		Relative humidity	rhum	%

from the GCM; (v) statistical analyses and diagnostic testing of the scenarios of climate change.

Suitable predictor selection is important for predictand downscaling and it is considered as an important process in deciding the generated predictands' character. In the SDSM, predictor selection is an iterative process and is partially dependent on the user's judgment Wilby et al. (2002). Predictor selection is done on the basis of the analysis of partial correlation, correlation and scatter plots between the predictands and predictors. The daily observed NCEP data from 1961 to 2001 is applied for predictor selection. The partial correlation is given as (Afifi and Clark 1996),

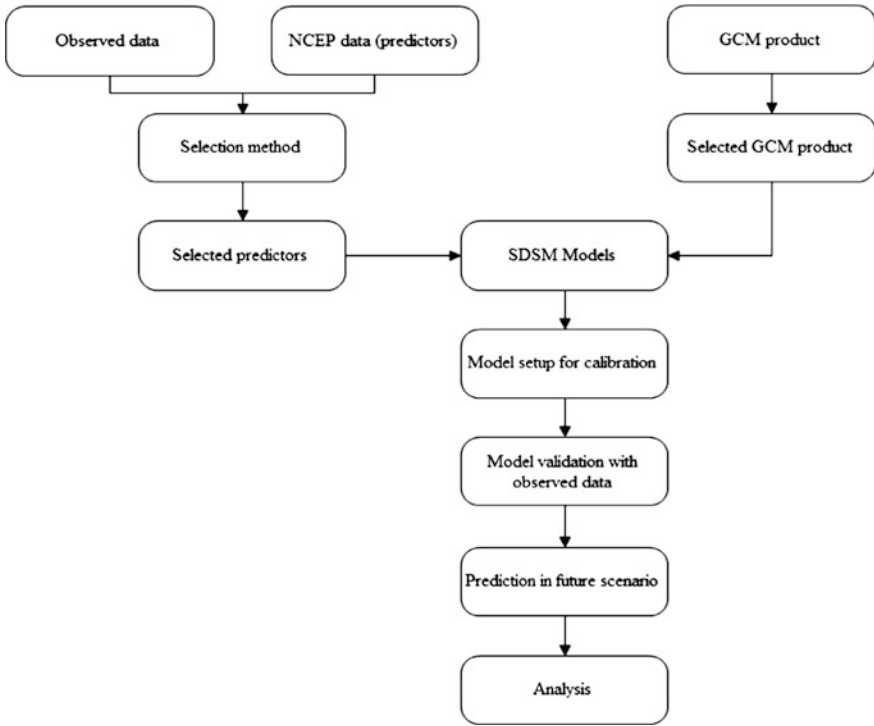


Fig. 2 Flow chart of methodology

$$R_{ij,k} = \frac{R_{ij} - R_{ik}R_{jk}}{\sqrt{(1 - R_{ik}^2)(1 - R_{jk}^2)}} \tag{1}$$

The R_{ij} shows the correlation coefficient between i and j , the partial correlation is between i and j , when controlling for the third variable of k . The value of p is estimated by the transfer of the correlation R to establish the t -statistic with the degree of freedom of $n - 2$. This method is used for eliminating any one of the predictors in the partial correlation with n observations (Hessami et al. 2008).

$$t = \frac{R}{\sqrt{\frac{1-R^2}{n-2}}} \tag{2}$$

The t -test method is used to calculate p -value, to analyse the observed and simulated data. High partial correlation indicates a strong association between the predictor and the predictand while a low p -value indicates low occurrence chances

of such association. The association strength of the predictors varies from month to month and the p -value of less than 0.05 is considered as practically less significant. In case there is higher correlation and low p -value, scatter plots are utilized to determine the presence of outliers or to find out whether it can be useful in downscaling.

3.3 Model Performance

The SDSM calibration and validation is assessed by four performance indexes used by other researchers such as, Root mean square error (RMSE), Normalized Mean Square error (NMSE) and Nash–Sutcliffe coefficient (NASH) and correlation coefficient (CC) (Duhan and Pandey 2014) during the period between 1961–1989 and 1990–2001 data.

(a) Root mean square error is given as

$$\text{RMSE} = \sqrt{\frac{1}{N} \sum_{i=1}^N (y_i - \hat{y}_i)^2} \quad (3)$$

(b) Normalized Mean Square error is

$$\text{NMSE} = \frac{\frac{1}{N} \sum_{i=1}^N (y_i - \hat{y}_i)^2}{(S_{\text{obs}})^2} \quad (4)$$

(c) Nash–Sutcliffe coefficient is

$$\text{NASH} = 1 - \frac{\frac{1}{N} \sum_{i=1}^N (y_i - \hat{y}_i)^2}{\frac{1}{N} \sum_{i=1}^N (y_i - \bar{y}_i)^2} \quad (5)$$

(d) Correlation coefficient

$$\text{CC} = \frac{N \sum (y_i \times \hat{y}_i) - (\sum y_i) \times (\sum \hat{y}_i)}{\sqrt{[N \sum y_i^2 - (\sum y_i)^2] \times [N \sum \hat{y}_i^2 - (\sum \hat{y}_i)^2]}} \quad (6)$$

Where, y_i and \hat{y}_i show the time series of the observed and simulated predictands, respectively, and the N represents the sample size of the training and testing data. A small value of the RMSE and NMSE depicts that the discrepancy is less between the observed and predicted series; hence it will provide better accuracy for prediction while in case of NASH and CC the higher values give better accuracy.

3.4 Scenario Generation

The simulated HadCM3 A2 GCMs data are used with the validated regression model for generating future rainfall scenario of the area, assuming that the predictor–predictand relationship will remain valid in future climatic condition. A daily synthetic rainfall of twenty ensembles is generated for 139 years from 1961 to 2099. These ensemble values are then averaged and separated into three periods, such as, 2020s (2011–2040), 2050s (2041–2070) and 2080s (2071–2099).

4 Results and Discussions

4.1 Predictor Selection

Predictor selection is an essential process for downscaling and it is said that a variable can be considered as a predictor if there exists a relationship between the predictor and the predictand (Wetterhall et al. 2005). Selection of predictors is done on the basis of some factors such as (i) majority of predictors should remain physically related to the local-scale elements and should be realistically GCM simulated, (ii) predictors should be available from the datasets and output archives of GCM, (iii) remain highly correlated to the predicted data (Table 3).

4.2 Model Performance

For developing the SDSM, the data were used for calibration and validation during 1961–1989 and 1990–2001. The three stations of Betul, Hoshangabad and Raisen were used for the downscaling. The observed and predicted monthly rainfall using

Table 3 Selected predictor variables

Sl. No.	Predictors	Full name of predictors	Sl. No.	Predictors	Full name of predictors
1	Mslp	Mean sea level pressure	6	shum	Specific humidity
2	p_z	Vorticity (surface)	7	p5_v	Zonal wind at 500 hPa
3	p500	Geopotential height at 500 hPa	8	p5_z	Vorticity at 500 hPa
4	p850	Geopotential height at 850 hPa	9	p8_z	Vorticity at 850 hPa
5	rhum	Surface relative humidity	10	p8_th	Wind direction at 850 hPa

SDSM during the calibration and validation of Betul, Hoshangabad and Raisen are given in the Fig. 3. It can be deduced from the given graphs that the predicted values of the validation are very close to the observed values for all the three stations. For calibration also the observed and predicted values are quite close.

The RMSE ranges from 18.72 to 28.34 (calibration) and from 25.94 to 38.82 (validation) while the NMSE varies from 1.62 to 4.23 for calibration and 3.56 to 6.65 for validation. The NASH values range from 0.945 to 0.950 (calibration) and from 0.941 to 0.946 (validation). Lastly, the CC values range from 0.949 to 0.959 in calibration and from 0.943 to 0.951 in validation (Table 4).

4.3 Future Scenario

In SDSM, Betul shows similar mean to the observed mean in 2011–2020 and continuously increasing rainfall is observed with little drop between 2031–40 and 2081–90. In Hoshangabad, there is a gradual increase with little decline in 2041–50 and the highest increase is observed in 2091–99. Raisen experienced increased rainfall than the observed mean and highest increase is expected in 2081–90. There is a decrease in 2020–30 and again 2051–60 (Fig. 4). However, increasing rainfall projection is found in all the stations.

4.4 Future Projection of Rainfall in Different Months

Monthly projected rainfall is given in the Fig. 4, presented as the mean of 30 years' time slice. Here, 2020s indicate the mean of 2011–2040, 2050s indicate mean of 2041–2070 and 2080s indicate mean of 2071–2099. Future projected rainfall shows increase in all the three stations of Betul, Hoshangabad and Raisen. The August month shows highest rise in rainfall in 2050s and 2080s followed by September, which are a part of monsoon months. However, July indicates decrease in future projected rainfall (Fig. 5).

4.5 Comparison of Past and Future Rainfall

The past rainfall trend is showing a decrease and future rainfall is indicating a gradual increase annually with few fluctuations in three stations (Fig. 6). High rainfall of 1717 and 1705 mm in 2065 and 2081 is observed in the Betul station while average projected rainfall is 1089 mm. Similarly, the maximum rainfall of 1805 mm in 2097 in Hosangabad and 2184 mm in 2081 in Raisen is observed.

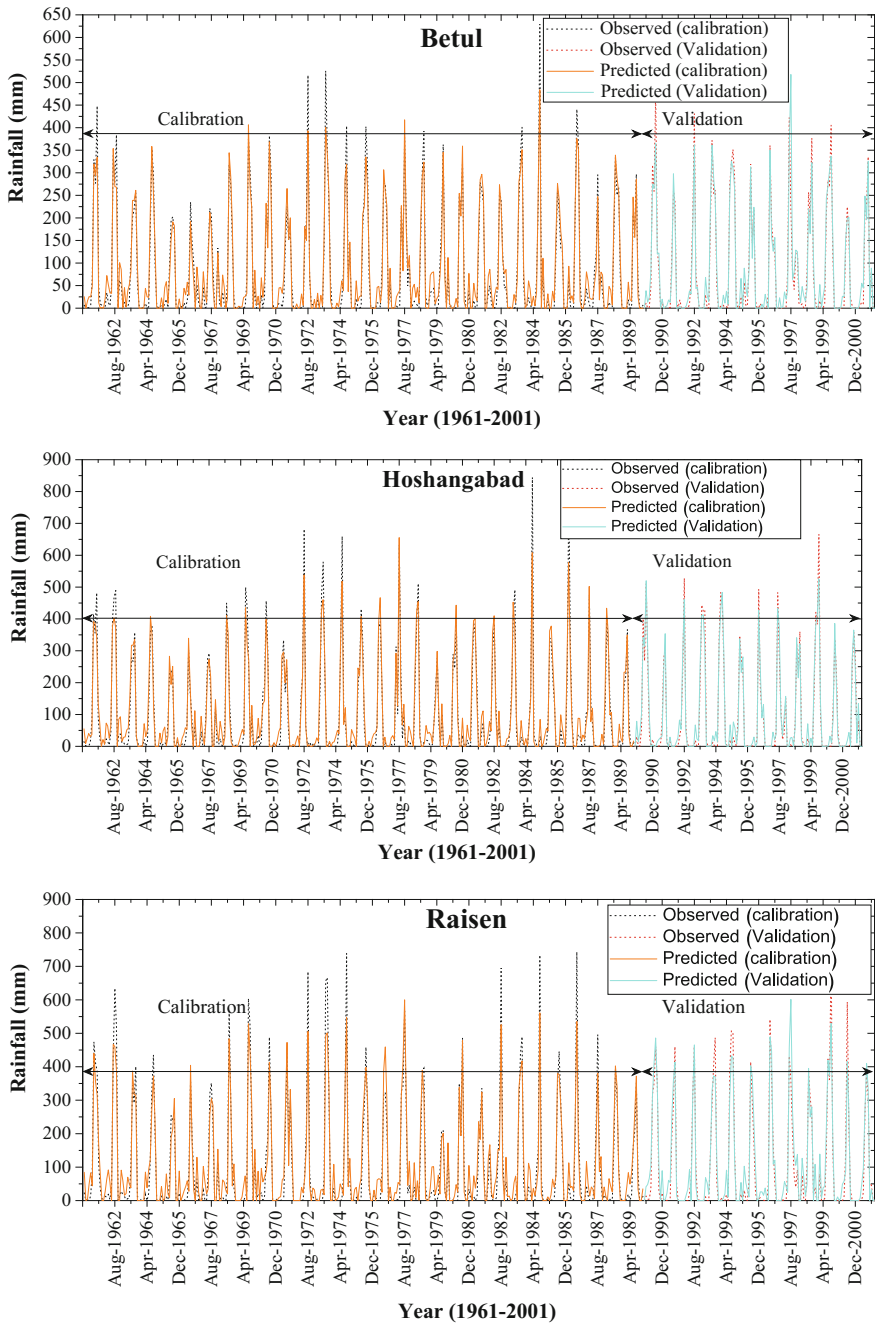


Fig. 3 Calibration and validation of SDSM rainfall

Table 4 Model performance

Stations	RMSE		NMSE		NASH		CC	
	A	B	A	B	A	B	A	B
Betul	21.360	36.500	4.230	5.210	0.947	0.942	0.959	0.950
Hoshangabad	28.340	38.820	2.210	6.650	0.950	0.946	0.953	0.951
Raisen	18.720	25.940	1.620	3.560	0.945	0.941	0.949	0.943

A Calibration and B Validation

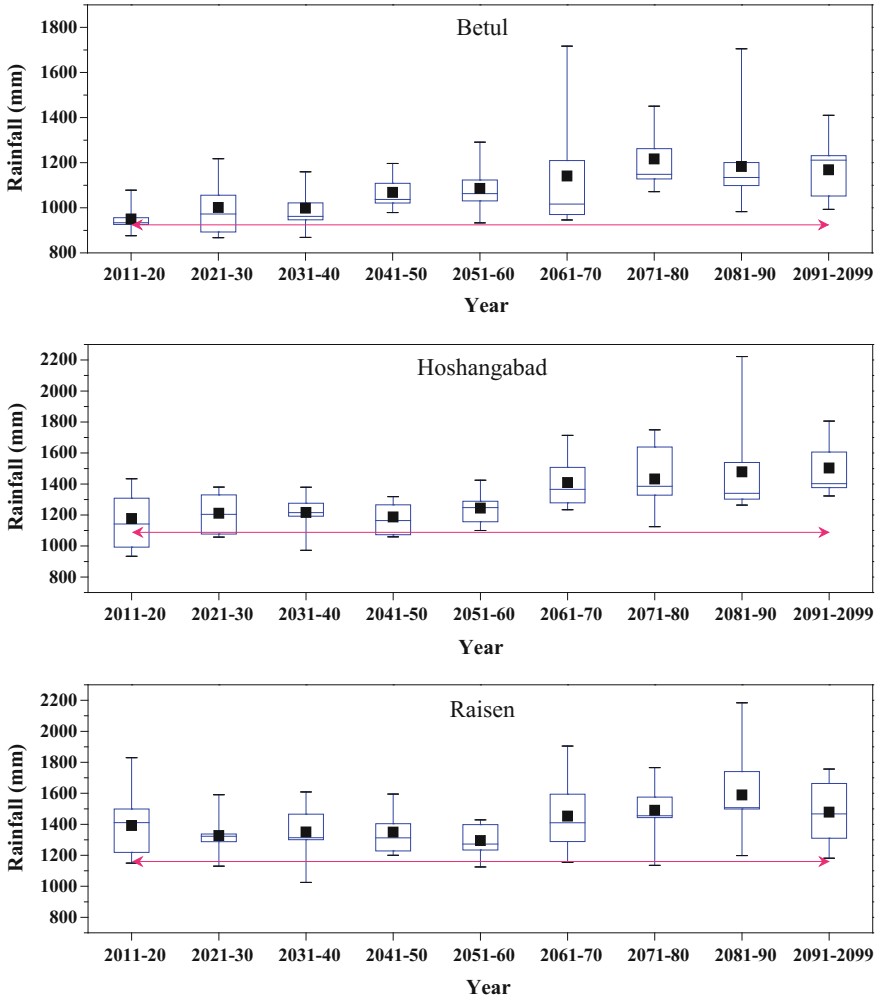


Fig. 4 Box plots of the decades showing changes in future downscaled rainfall (2002–2099) by SDSM

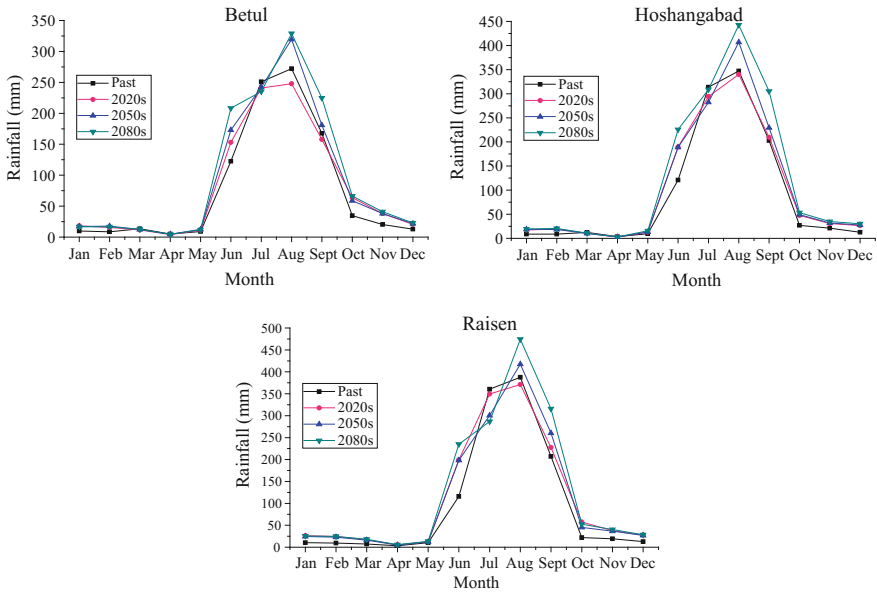


Fig. 5 Monthly rainfall variation during past and future periods

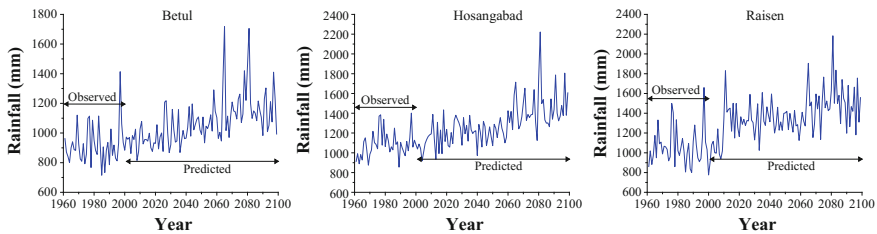


Fig. 6 Past and future annual rainfall trend

Projected increase of the rainfall trend in future might be due to more carbon emission attributable to rapid development of the country.

5 Conclusion

SDSM is a reputed model for downscaling using GCM climatic data for future prediction. It is widely used in different parts of the world for climate change studies. During calibration and validation, model performance was good. The results of the model are indicating gradually increasing trend of rainfall of three stations in the future in different periods (2020s, 2050s and 2080s) than the past

observed data. During the monsoon period (June to September), 2050s and 2080s periods are showing more rainfall in comparison to past for three stations except the month of July. It is known that uncertainties are there in climate change projection, but some estimation of future change is possible that is also very important. The higher change rate in the future may cause problem in future water availability. This study helps in estimating the change of rainfall in this area in future and will help in management processes.

Acknowledgments The authors are thankful to the Water Portal for the rainfall data and to the Pacific Climate Impacts Consortium (PCIC) for providing the GCM and NCEP Data.

References

- Afifi AA, Clark V (1996) Computer-aided multivariate analysis (3rd edition). Chapman and Hall (p 480). *Biometrical J* 39(7):875–876. doi:[10.1002/bimj.4710390716](https://doi.org/10.1002/bimj.4710390716)
- Akinremi OO, McGinn SM, Cutforth HW (2001) Seasonal and spatial patterns of rainfall trends on the Canadian prairies. *J Clim* 14(9):2177–2182
- Anandhi A, Srinivas VV, Nagesh KD, Nanjundiah RS (2009) Role of predictors in downscaling surface temperature to river basin in India for IPCC SRES scenarios using support vector machine. *Int J Clim* 29:583–603
- Arnold JG, Allen PM (1996) Estimating hydrologic budgets for three Illinois watersheds. *J Hydrol* 176(1–4):57–77
- Bisht H, Nain AS, Gautam S, Puranik HV (2013) Agro-climatic zonation of Uttarakhand using remote sensing and GIS. *J Agromet* 15(1):30
- Carter TR, Parry ML, Harasawa H, Nishioka S (1994) IPCC technical guidelines for assessing climate change impacts and adaptations. University College, London
- Conway D, Persechino A, Ardoin-Bardin S, Hamandawana H, Dieulin C, Mahe' G (2009) Rainfall and water resources variability in sub-Saharan Africa during the twentieth century. *J Hydrometeor* 10:41–59
- Dashtpagerdi MM, Kousari MR, Vagharfard H, Ghonchepour D, Hosseini ME, Ahani H (2014). An investigation of drought magnitude trend during 1975–2005 in arid and semi-arid regions of Iran. *Environ Earth Sci*. doi:[10.1007/s12665-014-3477-1](https://doi.org/10.1007/s12665-014-3477-1)
- Duhan D, Pandey A (2014) Statistical downscaling of temperature using three techniques in the Tons River basin in Central India. *Theor Appl Clim*. doi:[10.1007/s00704-014-1253-5](https://doi.org/10.1007/s00704-014-1253-5)
- Fowler HJ, Ekström M, Kilsby CG, Jones PD (2005) New estimates of future changes in extreme rainfall across the UK using regional climate model integrations. 1: Assessment of control climate. *J Hydrol* 300:212–233
- González JM, Cháidez JJN, Ontiveros VG (2008) Analysis of rainfall trends (1920–2004) in Mexico. *Investigaciones Geográficas, Boletín del Instituto de Geografía UNAM* 65:38–55
- Goyal MK, Ojha CSP (2010) Evaluation of various linear regression methods for downscaling of mean monthly precipitation in arid Pichola watershed. *Nat Resour* 1(1):11–18
- Goyal MK, Ojha CSP (2012) Downscaling of surface temperature for lake catchment in an arid region in India using linear multiple regression and neural networks. *Int J Clim* 32:552–566
- Hessami M, Gachon P, Ouarda TB, St-Hilaire A (2008) Automated regression-based statistical downscaling tool. *Environ Model Softw* 23(6):813–834
- Hulme M, Jenkins GJ, Lu X, Turnpenny JR, Mitchell TD, Jones RG, Lowe J, Murph JM, Hassell D, Boorman P, McDonald R, Hill S (2002) Climate change scenarios for the United Kingdom: the UKCIP02 scientific report, Tyndall Centre for Climate Change Research, School of Environmental Sciences, University of East Anglia, Norwich, UK: 120

- IPCC (Intergovernmental Panel on Climate Change) (2007) Climate change: impacts, adaptation and vulnerability. Contribution of Working Group II to the Fourth Assessment Report of IPCC. Cambridge, United Kingdom and New York, USA, p 976
- Kamba FM (2001) Impact of greenhouse gas induced climate change on the runoff of the Upper Benue River (Cameroon). *J Hydrol* 252:145–156
- Kannan S, Ghosh S (2011) Prediction of daily rainfall state in a river basin using statistical downscaling from GCM output. *Stoch Environ Res Risk Assess* 25(4):457–474
- Kipkorir EC (2002) Analysis of rainfall climate on the Njemps Flats, Baringo District, Kenya. *J Arid Environ* 50:445–458
- Kostopoulou E, Giannakopoulos C, Anagnostopoulou C, Tolika K, Maheras P, Vafiadis M, Founda D (2007) Simulating maximum and minimum temperatures over Greece: a comparison of three downscaling techniques. *Theor Appl Clim* 90:65–82
- Kumar V, Jain SK (2010) Trends in seasonal and annual rainfall and rainy days in Kashmir Valley in the last century. *Quatern Int* 212:64–69
- Kumar V, Jain SK, Singh Y (2010) Analysis of long-term rainfall trends in India. *Hydrol Sci J* 55 (4):484–496
- Kundu S, Khare D, Mondal A, Mishra PK (2015) Analysis of spatial and temporal variation in rainfall trend of Madhya Pradesh, India (1901–2011). *Environ Earth Sci*. doi:10.1007/s12665-014-3978-y
- Kundu S, Khare D, Mondal A, Mishra PK (2014) Long term rainfall trend analysis (1871–2011) for Whole India. In *Climate Change and Biodiversity* (pp 45–60). Springer, Japan. doi:10.1007/978-4-431-54838-6_4
- Meenu R, Rehana S, Mujumdar PP (2013) Assessment of hydrologic impacts of climate change in Tunga-Bhadra river basin, India with HEC-HMS and SDSM. *Hydrol Process* 27(11): 1572–1589
- Mishra PK, Khare D, Mondal A, Kundu S (2014) Multiple Linear regression based statistical downscaling of daily precipitation in a canal command. In *Climate Change and Biodiversity* (pp 73–83). Springer, Japan. doi:10.1007/978-4-431-54838-6_6
- Mondal A, Khare D, Kundu S, Meena PK, Mishra PK, Shukla R (2014b) Impact of climate change on future soil erosion in different slope, land use, and soil-type conditions in a part of the Narmada River Basin, India. *J Hydrol Eng*. doi:10.1061/(ASCE)HE.1943-5584.0001065
- Mondal A, Khare D, Kundu S (2014a) Spatial and temporal analysis of rainfall and temperature trend of India. *Theor Appl Clim* 1–16. doi:10.1007/s00704-014-1283-z
- Padmavathi P, Virmani SM (2013) Impact of climate change on safflower (*Carthamus tinctorius* L) in India and Mexico. *J Agromet* 15(1):58
- Raje D, Mujumdar PP (2011) A comparison of three methods for downscaling daily precipitation in the Punjab region. *Hydrol Process* 25:3575–3589
- Schoof JT, Pryor SC (2001) Downscaling temperature and precipitation: a comparison of regression-based methods and artificial neural networks. *Int J Climatol* 21:773–790
- Wei W, Chen L, Zhang H, Chen J (2014) Effect of rainfall variation and landscape change on runoff and sediment yield from a loess hilly catchment in China. *Environ Earth Sci*. doi:10.1007/s12665-014-3451-y
- Wetterhall F, Halldin S, Xu CY (2005) Statistical precipitation downscaling in central Sweden with the analogue method. *J Hydrol* 306:174–190
- Wilby RL, Dawson CW, Barrow EM (2002) SDSM—A decision support tool for the assessment of regional climate change impacts. *Environ Model Software* 17:147–159
- Willmott CJ, Rowe CM, Philpot WD (1985) Small-scale climate maps: a sensitivity analysis of some common assumptions associated with grid-point interpolation and contouring. *Am Cartog* 12:5–16
- Zhang Q, Li J, Singh VP, Xu C (2012) Copula-based spatio-temporal patterns of precipitation extremes in China. *Int J Climatol* 33(5):1140–1152. doi:10.1002/joc.3499

Part II
Remote Sensing of Agriculture and
Forestry

Identification of Crop Types with the Fuzzy Supervised Classification Using AWiFS and LISS-III Images

Arun Mondal, Deepak Khare and Sananda Kundu

Abstract Proper crop identification is a difficult task in a particular area by using the survey method, and it is essential for planning and management of water resources. Types of crops may be dynamic in any area during a season, and it also depends on the cultivator. The current study is the identification of spatial crops in Rabi season using multi-temporal satellite imagery. Different types of crops have different reflectance in the electromagnetic spectrum. A single crop shows different reflectance in different time of the growing period. The region of interest for the analysis is a part of the Narmada River basin of Madhya Pradesh covering an area of about 20,558 km². Land use classification was carried out using LISS-III satellite imagery and demarcation of the agricultural lands of the study area was done. Multi-temporal AWiFS satellite data (9 images) were used for extracting the crop types from October 23, 2011 to March 10, 2012 and NDVI method was applied to the AWiFS satellite data. Different crops have shown different NDVI values during Rabi season. Wheat and soyabean were observed to be the major crops during Rabi season in the study area. Locations (sample points) of different crops were taken from the field survey at the same time period (Rabi). Fuzzy Supervised Classification (FSC) method was applied for identifying the major five crops using NDVI outputs. The results of the accuracy assessment give the overall accuracy and Kappa statistics about 85.60 % and 0.79 respectively.

Keywords Crop identification · Reflectance · AWiFS · NDVI · FSC

A. Mondal (✉) · D. Khare · S. Kundu
Department of Water Resources Development and Management,
Indian Institute of Technology, Roorkee, India
e-mail: arun.iirs@gmail.com

© Springer International Publishing Switzerland 2017
S. Hazra et al. (eds.), *Environment and Earth Observation*,
Springer Remote Sensing/Photogrammetry, DOI 10.1007/978-3-319-46010-9_5

1 Introduction

The demand for food will increase in the coming decades due to the rapid increase of population in the developing parts of the world (Rounsevell et al. 2005; Searchinger et al. 2008). To keep up with this growing demand, there needs to be an increase in the production of agricultural needs using limited agricultural land in the near future. A proper irrigation system is vital in increasing the agricultural production as it is particularly helpful during seasons of drought or in the water stressed areas. The development of irrigation system is important for agricultural management strategies that help to adapt to a changing climate (Evans 1998). So, it is important to measure the actual arable land of a particular area (Salmon et al. 2015).

India has a dominant agricultural economy. Different types of crops are grown in the same place and thus, it becomes difficult to identify individual crops on the same date through simple digital classifications. Identification of agricultural land derived from digital classification techniques using Remote Sensing has been done by many researchers (Mondal et al. 2014a; Qiu et al. 2014; Mondal et al. 2014b).

To identify and separate various crops, the differences in the spectral signatures should be recognized. According to Wardlow et al. (2007) and Masialetti et al. (2010), crop mapping is very difficult from a single date image. The problem of mixed pixels during classification creates a problem for crop mapping. Different techniques like neural network, fuzzy classification, etc., may help in the estimation of the area of a particular land cover class in fine and coarse resolution images (Dadhwal et al. 2002).

The Normalised Difference Vegetation Index (NDVI) method was also used for the classification of different types of vegetation in the high resolution image (Vincent and Pierre 2003). Wardlow et al. (2007) also used NDVI on the monthly series data of Moderate-resolution Imaging Spectroradiometer (MODIS) from the agricultural field. The NDVI is a very useful index for crop mapping (Reed et al. 2003) and many researches were done with NDVI from the temporal images for crop mapping (Bradley et al. 2007; Wardlow and Egbert 2008). Crop identification with the NDVI method was also used by Ying et al. (2010) from the temporal data sets and crop classification was done from the AWiFS data by Panigrahy et al. (2009) with the help of crop calendar and growth season of crops. Kundu et al. (2014) used NDVI for crop identification from the AWiFS data. Proper classification is also required for identifying crops and for solving the problems of mixed pixels. Fuzzy classification is useful in such cases and can give better accuracy (Wang 1990).

The main objective of this study is the extraction of agricultural land from the suitable land use map. Then identification of the spatial crops from extracted agricultural land in Rabi season uses multi-temporal satellite images with the NDVI method and supervised Fuzzy classification on the basis of the spectral growth profile of crops. Field verification is applied for generating the actual accuracy of the method.

2 Study Area

The study area spans about 20,558 km² covering major areas of the Harda, Dewas, East Nimar (Khandwa) and West Nimar (Khargone) districts and is a part of the Narmada river basin of the state of Madhya Pradesh (MP) in India. The study area also covers parts of the Barwani, Sehore and Indore districts and is situated in the southwestern part of MP. The extension of the basin area is from 21°23'7.7" to 22° 55'08" N latitude and 75°21'07" to 77°21'17" E longitude (Fig. 1). The Digital Elevation Model (DEM) of the area shows the highest elevations in the northern and southern margins and low elevations in the central part. The highest elevation is about 982 m in the north and the lowest elevation is 108 m. Areas surrounding the Narmada riverbed have the lowest elevation.

The area has a similar subtropical climate as experienced by the state of MP. The Harda district experiences an average rainfall of 916 mm and the temperature varies

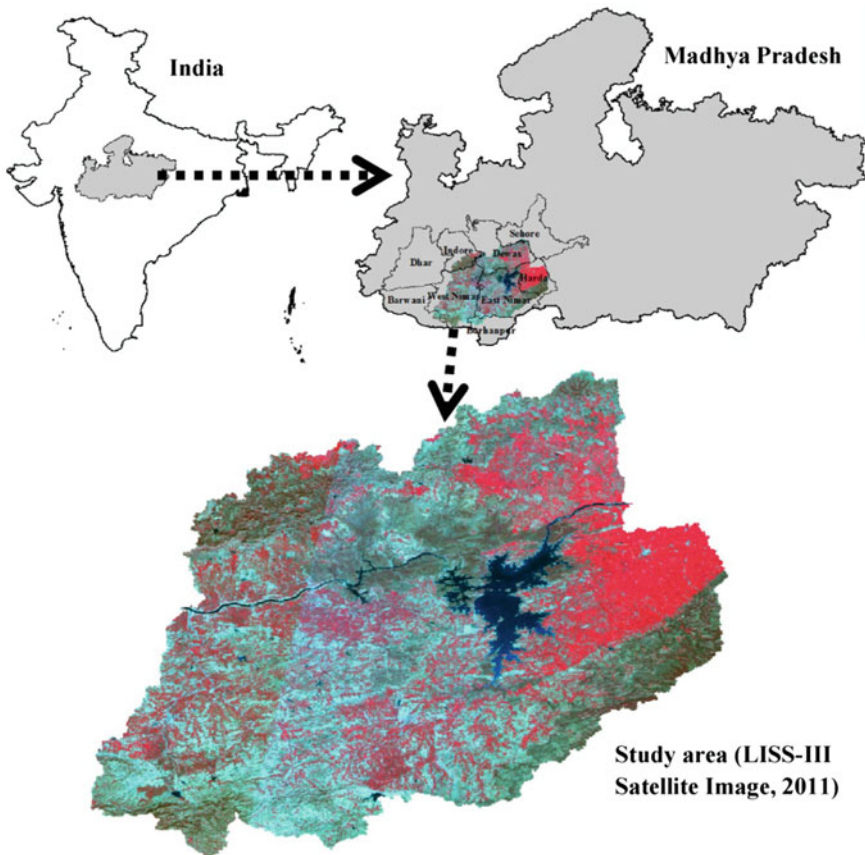


Fig. 1 Study area

from 12 to 47 °C. Average annual rainfall in East Nimar (Khandwa) is about 980 mm. The north of the district gets more rainfall than the south. The temperature of Khandwa varies from 42 °C in summer to 10 °C in winter. West Nimar (Khandwa) experiences a transitional type of climate between the wet and dry tropical climate and subtropical climate. The temperature ranges from 40 °C in summer to 15 °C and less in winter. The district experiences about 914 mm of rainfall. The state has a mainly agricultural economy producing variety of crops and seeds. The major crops produced here are soya bean, wheat, rice, gram, cotton, maize, rapeseed, etc. Some minor forest productions are also found here.

3 Methodology

LISS-III and AWiFS data sets were used in the study, which were georeferenced with the UTM projection zone 43 and WGS 84 datum. The images were registered with the Root Mean Square Error (RMSE) of 0.5 pixel. After that, the radiometric normalization was done. Then classification was performed on the corrected LISS-III images with a good accuracy and agricultural land was extracted from the classified images. The NDVI method was further applied on agricultural land of the 9 temporal images of the AWiFS data to obtain a spectral growth profile of various crops at different growing stages. These images were then further classified with the Fuzzy Supervised Classification (FSC) method using ground samples of crops during same time period (Rabi season) and accuracy assessment with Kappa statistics was done. Training samples collected from the field for type of crops were used in the accuracy assessment (Fig. 2). Details of the data used in the study are given in Table 1.

3.1 Preprocessing of Data

DN value is first converted into spectral radiance (L_{λ}) by checking the gain value from the approved ranges from the NASA of $L_{\max_{\lambda}}$ and $L_{\min_{\lambda}}$. The formula used is (Chander and Markham 2003; Melesse 2004; NASA 2004; Mukhopadhyay et al. 2014)

$$L_{\text{TOA}} = \left(\frac{L_{\max_{\lambda}} - L_{\min_{\lambda}}}{\text{QCAL}_{\max} - \text{QCAL}_{\min}} \right) * (\text{DN} - \text{QCAL}_{\min}) + L_{\min_{\lambda}} \quad (1)$$

Here,

$L_{\max_{\lambda}}$ is the maximum radiance (in $\text{Wm}^{-2}\text{sr}^{-1}\mu\text{m}^{-1}$)

$L_{\min_{\lambda}}$ is the minimum radiance (in $\text{Wm}^{-2}\text{sr}^{-1}\mu\text{m}^{-1}$)

QCAL_{max} is the maximum DN value, and

QCAL_{min} is the minimum DN value

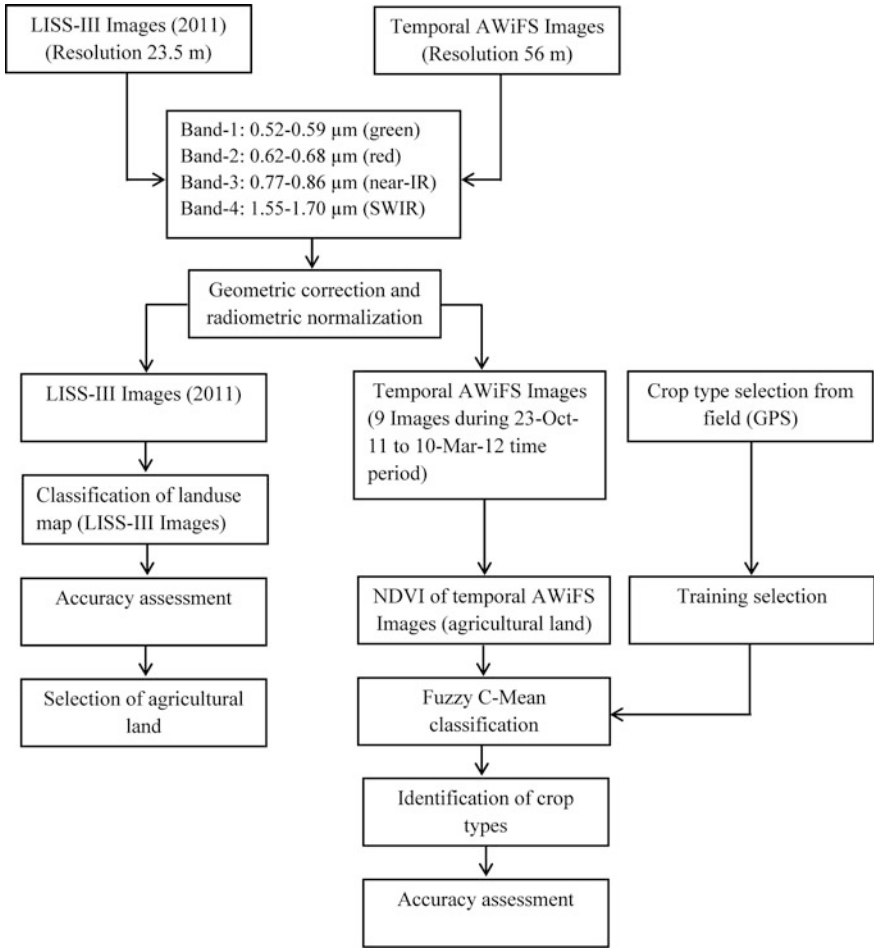


Fig. 2 Methodology

Table 1 Data used

AWiFS				
Sl No.	Date	Band	Wavelength (μm)	Resolution (m)
1	23-Oct-11	2-5	0.52-0.59 (green)	60
2	11-Nov-11	2-5	0.62-0.68 (red)	60
3	21-Nov-11	2-5	0.77-0.86 (near-IR)	60
4	10-Dec-11	2-5	1.55-1.70 (SWIR)	60
5	24-Dec-11	2-5		60
6	12-Jan-12	2-5		60
7	5-Feb-12	2-5		60
8	20-Feb-12	2-5		60
9	10-Mar-12	2-5		60

The reflectance value is then obtained from the radiance by using the following equation (Sobrino et al. 2004).

$$\rho = \frac{L_{\text{TOA}} \pi d^2}{\text{ESUN}_\lambda \cos \theta_z T_z} \quad (2)$$

Here,

ρ is the reflectance

d^2 is the earth sun distance (AU)

ESUN_λ is the band dependent exoatmospheric irradiance ($\text{Wm}^{-2}\mu\text{m}^{-1}$)

θ_z is the solar zenith angle (deg)

T_z shows the atmospheric transmission between ground and TOA

$$d = 1.001672 * \sin\left(\frac{2\pi(J - 93.5)}{356}\right) \quad (3)$$

Here, J is the Julian day.

3.2 NDVI Method

The NDVI is useful in identifying vegetation because of the absorption of chlorophyll in the red spectrum and the high reflection in the near infrared spectrum which helps in differentiating between the types of vegetation. The NDVI is an indicator of the vegetation health and hence is important in crop identification. It is given as:

$$\text{NDVI} = \frac{\rho_{\text{nir}} - \rho_{\text{red}}}{\rho_{\text{nir}} + \rho_{\text{red}}} \quad (4)$$

Here, ρ_{nir} represents the spectral reflectance of the near infrared band and ρ_{red} is the spectral reflectance of the red band (Zeng et al. 2010).

3.3 Fuzzy Supervised Classification

Fuzzy Supervised Classification (FSC) algorithm was applied in the study for classification (Wang 1990). Homogeneity is not much important in selection of training sites of FSC. Statistical parameters of more than one class can be generated using the site and training can be previously defined for land use with fuzzy

representation. The training data are represented as a fuzzy partition matrix. The fuzzy covariance and fuzzy mean of each class is calculated as:

$$\mu_c^* = \frac{\sum_{i=1}^n f_c(x_i)x_i}{\sum_{i=1}^n f_c(x_i)} \tag{5}$$

where n is the total number of sample pixel measurement vectors, f_c shows the membership function of class c , and x_i represents a sample pixel measurement vector ($1 \leq i \leq n$). The fuzzy covariance matrix is expressed as:

$$\sum_c^* = \frac{\sum_{i=1}^n f_c(x_i)(x_i - \mu_c^*)(x_i - \mu_c^*)^T}{\sum_{i=1}^n f_c(x_i)} \tag{6}$$

The calculation of fuzzy mean for class c , requires a multiplication of a sample pixel measurement vector x by its membership grade in c , $f_c(x)$ before adding it to the sum. For calculating the fuzzy covariance matrix for class c , $(x_i - \mu_c^*)(x_i - \mu_c^*)^T$ is used to multiply with $f_c(x)$ before adding it. The fuzzy mean and fuzzy covariance matrix are the extensions of conventional mean and covariance matrix. When the $f_c(x) = 0$ or 1 , (5) and (6) represent the conventional mean and covariance matrix.

A fuzzy set is described by its membership function and to perform a fuzzy partition, a membership function should be given for each class. Here, the membership functions are defined on the basis of the maximum likelihood classification with the fuzzy mean and fuzzy covariance matrix by replacing the conventional mean and covariance matrix. The membership function of class cover c is defined as:

$$f_c(x) = \frac{P_c^*(x)}{\sum_{i=1}^m P_i^*(x)} \tag{7}$$

$$P_i^*(x) = \frac{1}{(2\pi)^{N/2} |\sum_i^*|^{1/2}} \cdot \exp \left[-\frac{1}{2} (x - \mu_i^*)^T \sum_i^{*-1} (x - \mu_i^*) \right] \tag{8}$$

where N is considered as the dimension of pixel vectors, m shows the number of predefined classes and $1 \leq i \leq m$.

The membership grades of the x pixel vector is dependent on the position of x in the spectral space. The $f_c(x)$ exponentially increases with the decrease of $(x - \mu_i^*)^T \sum_i^{*-1} (x - \mu_i^*)$, i.e., the Mahalanobis distance between x and class c . The $\sum_{i=1}^m P_i^*(x)$ is a normalizing factor.

3.4 Accuracy Assessment

The images are classified into five classes: water body, settlement, vegetation, agricultural land and fallow lands, which have been validated with the field observation. The accuracy assessment is done with the Producer's accuracy, the User's accuracy and the Kappa coefficient. The error matrices are used to compare the relation between the ground truth/known reference data to the corresponding results of the automated classification (Congalton and Green 1999; In Lillesand and Keifer 2000). This is one of the most common means of accuracy assessment (Lillesand and Kiefer 2000; Jensen 1996).

The Kappa coefficient is also used for the accuracy assessment. This technique is the measurement of the difference between the actual agreement between an automated classifier and the reference data and the chance agreement between a random classifier and the reference data (Lillesand and Keifer 2000). The Khat statistic is calculated as

$$\hat{k} = \frac{N \sum_{i=1}^r x_{ii} - \sum_{i=1}^r (x_{i+} \cdot x_{+i})}{N^2 - \sum_{i=1}^r (x_{i+} \cdot x_{+i})} \quad (9)$$

where

- r is the number of rows in the error matrix
- x_{ii} is the number of observations in row i and column i ,
- x_{i+} is represented as the total observation in row i
- x_{+i} is total observation in column i
- N denotes the total number of observation involved in the matrix

4 Results and Discussion

4.1 Land Use Classification

The LISS-III image was digitally classified into 8 land use classes which are water body, settlement, forest, double crop land, Rabi crop, Kharif crop, scrub and waste land. The highest area was covered by the Kharif crop (26.41 %) followed by the scrub (25.56 %) and the double crop land (21.33 %). The Rabi crop also occupies a major area of about 7.25 % of the land. The major water body of Indira Sagar Dam lies toward the east of the study area. The Kharif crops are observed in major parts of the south and in some areas of the northeast while the double crop lands occupy the east and the northwestern parts of the area. Forests follow a pattern of location in the southeast and to the north of the Indira Sagar dam. The land use classification is given in the Fig. 3.

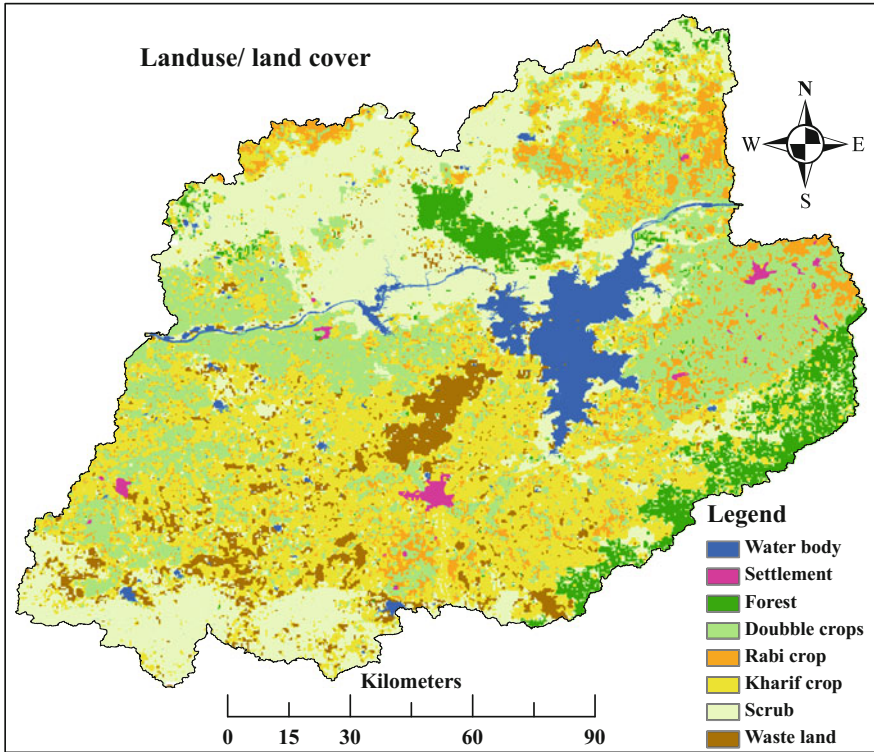


Fig. 3 Land use classification

4.2 Identification of Crops

The agricultural land was extracted from the classified land use of the LISS-III image to generate NDVI profile. Differences in the spectrotemporal curves are observed in the Fig. 4, where the spectral reflectance in NDVI varies for different crops. The vegetables usually take less time to mature, which is reflected in the downward curve of vegetables in the month of February while the other crops have higher spectral reflectances.

The highest spectral reflectance is found in the case of paddy and wheat during the months of December and January when these crops reach their mature stages. Most of the agricultural lands were located near the Narmada river basin. During the Rabi season, the main source of water for cultivation is the irrigation system, which is designed near the main river. Rainfall is very less during the Rabi season in the middle part of India. In the particular study area, the Indira Sagar dam was constructed to serve the purpose of both irrigation and hydropower generation.

NDVI maps are shown in the Fig. 5 during the Rabi season using nine consecutive intervals of real-time satellite imagery. More intense cultivation is

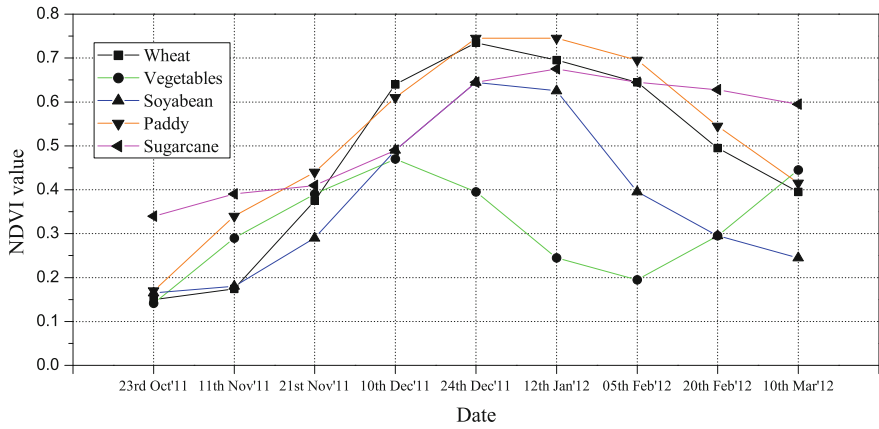


Fig. 4 Spectrotemporal curves of different crops

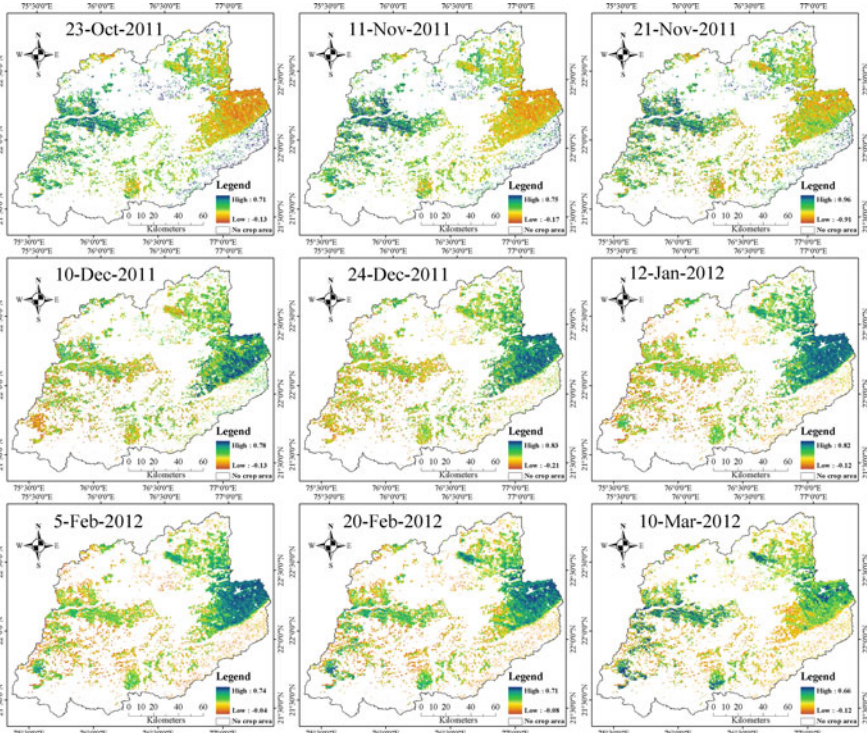


Fig. 5 NDVI maps (October 23, 2011 to March 10, 2012)

observed in the eastern part of the study area. The NDVI value is less due to the initial stage of crops in the period between October 23, 2011 and November 11, 2011. Crops are seen to be growing gradually and the NDVI value is seen increasing between December 10, 2011 and February 20, 2012. Finally, the NDVI value has decreased due to the harvesting of the crop as observed in the image on March 10, 2012.

The NDVI image is further classified by the FSC method into 5 different crop-lands such as wheat, vegetables, soyabean, paddy and sugarcane. Soyabeans are found to have occupied maximum area (42.38 %), followed by wheat (34.11 %), vegetables, paddy and sugarcane. Table 2 gives the area covered by different crops.

Table 2 Area covered by crop

Sl No.	Crop type	Area (km ²)	Area (%)
1	Wheat	2004.68	34.11
2	Vegetables	523.03	8.90
3	Soyabean	2490.44	42.38
4	Paddy	447.00	7.61
5	Sugarcane	411.46	7.00
	Total	5876.62	100

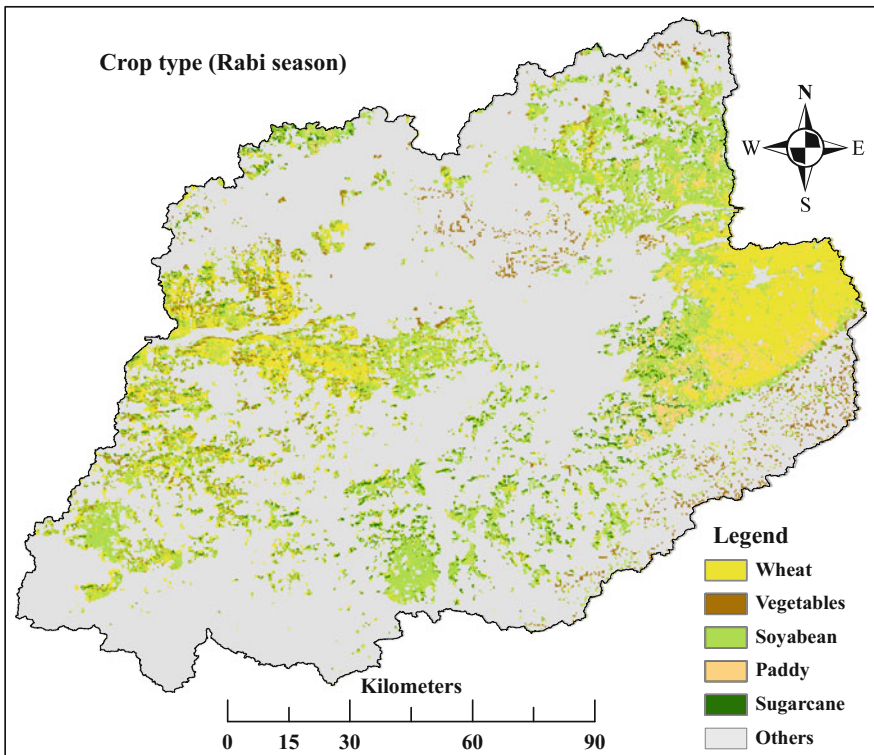


Fig. 6 Classified crop types

Table 3 Strength of agreement of the Kappa statistics

Sl. no	Kappa statistic	Strength of agreement
1	<0.00	Poor
2	0.00–0.20	Slight
3	0.21–0.40	Fair
4	0.41–0.60	Moderate
5	0.61–0.80	Substantial
6	0.81–1.00	Almost perfect

Source Landis and Koch (1977)

Table 4 Accuracy assessment

Class name	Reference totals	Classified totals	Number of correct points	Producer's accuracy (%)	User's accuracy (%)
Wheat	37	38	32	86	84
Vegetables	10	11	9	90	82
Soyabean	46	44	38	83	86
Paddy	9	9	8	89	89
Sugarcane	8	8	7	88	88
Total	110	110	94	NA	NA

NA Not applicable

The identified crops within the agricultural land are given in the Fig. 6 classified by the FSC method. Crop profiles generated with the NDVI help in the identification of different crops. A total of 110 samples have been taken from the field for all the 5 crops classified in the image. The Producer's and the User's accuracy for different crops are above 75 %. The overall accuracy is 85 % and the overall Kappa is 0.79 which indicates a substantial category of classification (Table 3). The User's and the Producer's accuracy have been assessed for five types of crops and their values vary from 82 % to 89 % and 83 % to 90 %, respectively (Table 4).

5 Conclusion

Remote Sensing data helps in the identification of different crops in a particular area from the temporal satellite images to obtain crop profiles. Crop identification and mapping is necessary as it gives a picture of the agriculture of a region and helps in future planning. The present study showed the spectral profile through NDVI on 9 images, which indicated the health of different crops in the period from October 2011 to March 2012. The difference in the spectral reflectance for different crops helped in the crop identification.

The NDVI profile was drawn to the extracted agricultural land area from the classified LISS-III image. The FSC method was done on the stacked single NDVI image to give specific crop types and their spatial distribution within the study area with the accuracy assessment. Microwave and Hyperspectral Remote Sensing have also been used for the identification of crops. However, multi-temporal image analysis is considered to be more beneficial as the Microwave and Hyperspectral studies are expensive and are suitable when the area under observation is considerably smaller.

Acknowledgments The authors are thankful to the National Remote Sensing Centre (NRSC) for providing the AWiFS and LISS-III satellite images. The authors are also thankful to the CSIR for financial assistance.

References

- Bradley BA, Jacob RW, Hermance JF, Mustard JF (2007) A curve fitting procedure to derive inter-annual phonologies from time series of noisy satellite NDVI data. *Remote Sens Environ* 106:137–145
- Chander G, Markham B (2003) Revised Landsat-5 TM Radiometric Calibration Procedures and post-calibration Dynamic Ranges. *IEEE T Geosci Remote* 41(11):2674–2677
- Congalton RG, Green K (1999) *Assessing the accuracy of remotely sensed data: principles and practices* Lewis Publishers, Boca Raton
- Dadhwal VK, Singh RP, Dutta S, Parihar JS (2002) Remote Sensing based crop inventory: a review of Indian experience. *Trop Ecol* 43(1):107–122
- Evans LT (1998) *Feeding the ten billion: plants and population growth*. Cambridge University Press, Cambridge, UK
- Jensen JR (1996) *Introduction to digital image processing: a remote sensing perspective*. Prentice-Hall, Englewood Cliffs, New Jersey
- Kundu S, Khare D, Mondal A, Mishra PK (2014) Crop Identification by Fuzzy C-Mean in Ravi Season using Multi-Spectral Temporal Images. In: Pant et al. (eds): *Topic in Advances in intelligent systems and computing*. Third international conference on soft computing for problem solving, 2014. Springer, India, pp 391–401. doi:[10.1007/978-81-322-1768-8_35](https://doi.org/10.1007/978-81-322-1768-8_35)
- Landis JR, Koch GG (1977) The measurement of observer agreement for categorical data. *Biometrics* 159–174
- Lillesand TM, Kiefer RW (2000) *Remote sensing and image interpretation*. Wiley, pp 572–576
- Masialeti I, Egbert S, Wardlow BD (2010) A comparative analysis of phonological curves for major crops in Kansas. *Gisci Remote Sens* 47(2):241–259
- Melesse AM (2004) Spatiotemporal dynamics of land surface parameters in the Red river of the north basin. *Phys Chem Earth* 29:795–810
- Mondal A, Khare D, Kundu S, Mishra PK (2014a) Detection of land use change and future prediction with Markov chain model in a part of Narmada River Basin, Madhya Pradesh. In: Singh et al. (eds) *Landscape ecology and water management*. IGU conference, 2013. Springer, Japan, pp 3–14. doi:[10.1007/978-4-431-54871-3_1](https://doi.org/10.1007/978-4-431-54871-3_1)
- Mondal A, Khare D, Kundu S, Mishra PK, Meena PK (2014b) Land use change prediction and its impact on surface run-off using fuzzy c-mean, Markov chain and curve number methods. In: Pant et al. (eds) *Topic in advances in intelligent systems and computing*. Third international conference on soft computing for problem solving, 2014. Springer, India, pp 365–376. doi:[10.1007/978-81-322-1768-8_35](https://doi.org/10.1007/978-81-322-1768-8_35)

- Mukhopadhyay A, Mondal A, Mukherjee S, Khatua D, Ghosh S, Mitra D, Ghosh T (2014) Forest cover change prediction using hybrid methodology of geoinformatics and Markov chain model: a case study on sub-Himalayan town Gangtok. India. *J Earth Syst Sci* 123(6):1349–1360
- NASA (2004) Landsat project science office. Landsat 7 science data users handbook. Chapt. 11-data products. (http://1tpwww.gsfc.nasa.gov/IAS/handbook/handbook_htmls/chapter11.html:11.1–11.4)
- Panigrahy RK, Ray SS, Panigrahy S (2009) Study on utility of IRS-P6 SWIR band for crop discrimination and classification. *J Indian Soc Remote* 37(2):325–333
- Qiu B, Fan Z, Zhong M, Tang Z, Chen C (2014) A new approach for crop identification with wavelet variance and JM distance. *Environ Monit Assess* 186(11):7929–7940
- Reed BR, White MA, Brown JF (2003) Remote Sensing phenology. In: Schwartz MD (ed) *Phenology: an integrative environmental science*. Kluwer Academic Publishers, New York, NY, pp 365–381
- Rounsevell M, Ewert F, Leemans R, Reginster I, Metzger M (2005) Future scenarios of European agricultural land use: I. estimating changes in crop productivity. *Agric Ecosyst Environ* 107:101–116
- Salmon JM, Friedl MA, Froking S, Wisser D, Douglas EM (2015) Global rain-fed, irrigated, and paddy croplands: A new high resolution map derived from Remote Sensing, crop inventories and climate data. *Int J Appl Earth Obs* 38:321–334
- Searchinger T, Heimlich R, Houghton RA, Dong F, Elobeid A, Fabiosa J, Tokgoz S, Hayes D, Yu TH (2008) Use of U.S. Croplands for biofuels increases greenhouse gases through emissions from land-use change. *Science* 319:1238–1240
- Sobrino JA, Jiménez-Muñoz JC, Paolini L (2004) Land surface temperature retrieval from LANDSAT TM 5. *Rem Sens Environ* 90(4):434–440
- Vincent S, Pierre F (2003) Identifying main crop classes in an irrigated area using high resolution image time series. In: *Geoscience and remote sensing symposium, 2003. IGARSS'03. Proceedings. IEEE International IEEE*. pp 252–254
- Wang F (1990) Fuzzy supervised classification of remote sensing images. *IEEE T Geosci Remote* 28(2):194–201
- Wardlow B, Egbert S (2008) Large-area crop mapping using time-series MODIS 250 m NDVI data: an assessment for the U.S. Central Great Plains. *Rem Sens Environ* 112:1096–1116
- Wardlow B, Egbert S, Kastens J (2007) Analysis of time-series MODIS 250 m vegetation index data for crop classification in the U.S. Central Great Plains. *Rem Sens Environ* 108:290–310
- Ying L, Xiuwan C, Hongwei D, Lingui M (2010) An improved multi temporal masking classification method for winter wheat identification. *International Conference on Audio Language and Image Processing (ICALIP'10)*, pp 1648–1651
- Zeng Y, Huang W, Zhan F, Zhang H, Liu H (2010) Study on the urban heat island effects and its relationship with surface biophysical characteristics using MODIS imageries. *Geo Spat Inf Sci* 13(1):1–7

Application of Remote Sensing in Assessing the Impacts of Mahatma Gandhi National Rural Employment Guarantee Act (MGNREGA), in Ratlam District, Madhya Pradesh, India

Bhaskar Sinha, Deep Narayan Singh, Anoma Basu and Mili Ghosh

Abstract The Mahatma Gandhi National Rural Employment Guarantee Act, (MGNREGA) is the first ever demand-driven livelihood act that guarantees 100 days of employment in every rural household. It also aims to achieve sustainable livelihood by addressing the causes of chronic poverty as well as strengthening of the natural resource base. The assets created under the MGNREGA related to water and soil conservation and management have contributed to an increased availability of water for sustainable agriculture especially in the semi-arid and arid regions. Dug well at the farmer's land, locally known as Kapil Dhara, is one of the highly demanded assets created under the MGNREGA in the state of Madhya Pradesh. Dug wells have benefitted the rural population in form of increased irrigated area, crop productivity, and cropping intensity. An integrated approach based on remote sensing (RS) and field survey was used to assess the impact of dug wells toward change in cropped area and cropping intensity. Six sampling units representing one/two micro-watershed has been randomly selected for in-depth study. Interpretation of RS data has shown that there has been an increase in double crop area after the MGNREGA intervention in five selected sampling units spread in two blocks of the Ratlam district. Watershed with diverse

B. Sinha (✉) · D.N. Singh · M. Ghosh
Department of Ecosystem and Environment Management,
Indian Institute of Forest Management, Post Box: 357,
Nehru Nagar 462003, Bhopal, India
e-mail: bhaskarsinha@hotmail.com; bsinha@iifm.ac.in

A. Basu
Agriculture Vertical, NABARD Consultancy Services, NABARD Building,
Bandra Kurla Complex, Bandra East, Mumbai 400051, Maharashtra, India

water recharge activities recorded comparatively higher impact of dug wells as compared to watershed that had lesser associated water recharge activities. The analysis further revealed that application of RS and watershed approach in planning can enhance sustainability of assets created under the MGNREGA.

Keywords MGNREGA · Sustainability · Dug well (Kapil Dhara) · Remote sensing · Watershed

1 Introduction

Mahatma Gandhi National Rural Employment Guarantee Act, (MGNREGA) is the first ever demand-driven employment guarantee act that aims at enhancing the livelihood security of people in rural areas by guaranteeing 100 days of wage employment in a financial year to every rural household whose adult members volunteer to do unskilled manual work. It ensures sustainable livelihood through creation of assets that aims at strengthening rural infrastructure and natural resource base, besides mitigating the causes of chronic poverty like drought, flood, deforestation, poor rural connectivity, etc. The MGNREGA assets pertaining to water and soil conservation have provided multiple environmental benefits that include groundwater recharge, additional water storage in tanks (Kareemulla et al. 2009; Bassi and Kumar 2010), increased soil fertility and soil organic carbon (Kumar et al. 2011; Esteves et al. 2013), increase in agricultural biodiversity (Kareemulla et al. 2010).

Assets created under MGNREGA are implemented under 16 different categories and can be further categorized as asset under individual ownership (one that is implemented at beneficiary level) and asset under community ownership (one that is implemented at community level). Individual assets related to water harvesting structures bring direct benefits to the beneficiary in terms of increased agricultural productivity and income. Dug wells, locally known as Kapil Dhara is implemented at the beneficiary level and is one of the majorly implemented activities in Madhya Pradesh (Samarthan 2010). Dug wells have significantly contributed toward increased agricultural production and livelihood in the state since its inception (Sinha et al. 2010). Therefore, it is important to ensure that the benefits derived from water harvesting structures is sustained and properly monitored since this constitutes about 60 % of MGNREGA works (GoI 2013). It is also well known that planning of any water or soil conservation and harvesting activity should be done following the principles of watershed management for greater benefits. In this regard, application of remote sensing (RS) and geographical information system (GIS) technology coupled with field observations can be of immense use in planning and monitoring the sustainability of such water harvesting structures like Kapil Dhara on watershed basis (Adinarayana et al. 1995; Khan et al. 2001; Randhir et al. 2001; Vittala et al. 2008).

It is against this background that the study was undertaken to evaluate the sustainability of dug wells (Kapil Dhara) on a watershed basis using RS and GIS techniques along with field survey. The present study was conducted in six sampling units representing one/two micro-watershed randomly selected in two blocks of the Ratlam district. The district of Ratlam was brought under the implementation of the MGNREGA in the third phase of its implementation since April 1, 2008.

2 Methodology

The present study was conducted in the district of Ratlam during the year 2011–2012. The base year for the study was taken as year 2006–2007. The district selection was made in consultation with related field officers. Further, Ratlam is a part of Malwa region that is known for its low groundwater level, soil moisture, rainfall, and harsh climatic conditions which further make it an ideal site for studying the impacts of dug wells. From the district, two blocks; Sailana and Bajana were selected on the basis of the highest number of the MGNREGA activities since its implementation (Fig. 1a). Further, six sampling units were randomly selected (three from each block) based on secondary data collected from the implementing agencies in the selected blocks of Ratlam district for further in-depth analysis. The sampling units were a composite cluster of *Gram Panchayat* (GP) and micro-watershed. In each selected GP, all the micro-watersheds (as delineated in the National Watershed Atlas by Central Ground Water Board) corresponding to the GP were taken up (Fig. 1b). The adjacent GPs were also included in the cases where the selected micro-watersheds extended up to these adjacent GPs in order to achieve a best fit overlap model thereby forming a Composite Primary Sampling Unit (CPSU).

In the present study, two separate research techniques were adopted and applied simultaneously. The first method covered collection of both primary and secondary data. The primary data was collected during field visits in selected *Gram Panchayats* with the help of structured and semi-structured questionnaires, seeking demographic data of the villager, the MGNREGA activity he is drawing benefit from, his total landholding (irrigated and nonirrigated), crops grown, and crop productivity. Secondary data was collected from the *Zilla Panchayat* office and other line departments (district and block levels).

The second method dealt with application of remote sensing for mapping the change in crop intensity, land cover and land use for the pre and the post MGNREGA interventions. The IRS LISS III imageries of Dec 2007 and Dec 2011 were used to generate land use land cover of the study area. The ISODATA (un-supervised) classification technique was applied for digital classification (Lillesand et al. 2004) and the entire district was classified into four land use land cover class (Level I Classes). The accuracy was calculated for the classified image at the district level based on reference map available. Sixty random verification points was generated for each class spared over entire image. The analysis of confusion matrix reflected the overall accuracy of 80.83 %. Furthermore, the land use classes in the

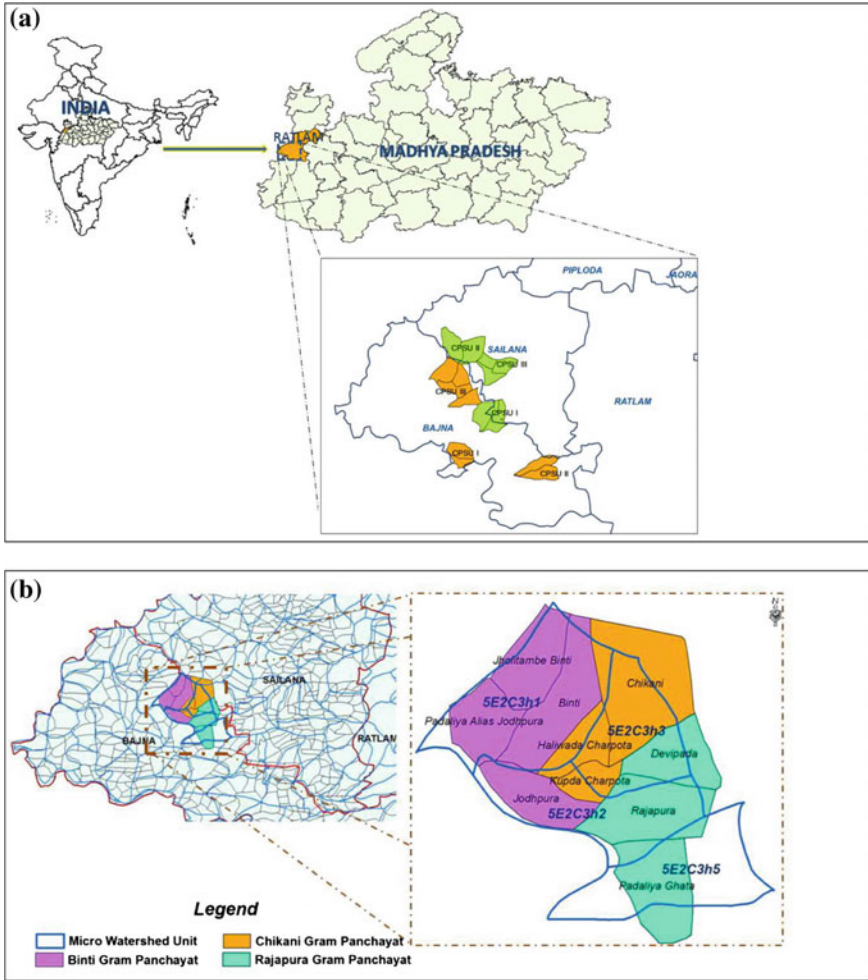


Fig. 1 a Location of composite sampling unit (CPSU). b Delineation of composite sampling unit (CPSU)

proximity of dug wells were validated by taking GPS points on the ground. The GIS analysis technique (Matrix analysis) in ERDAS Imagine was used to run post-classification change analysis. The change matrix was generated for district, blocks, and selected sampling units.

Both the results were compiled and analyzed separately and were presented individually. The results were comparable and they complemented each other's outcomes significantly. The analysis based on questionnaire survey is limited to the sampled GPs but the land use land cover maps and area statistics cover the entire CPSUs.

3 Results

3.1 Field Survey Results

Dug well (Kapil Dhara) is a water-related activity implemented at the beneficiary level and is one of the highly demanded works in Madhya Pradesh due to its direct impacts in agricultural productivity and household income. Being a water harvesting structure, its benefits is assumed to be more pronounced with presence of other water and soil conservation related activities in the selected watershed area (CPSU). Thus, among the various MGNREGA activities, the ones pertaining to water and soil conservation were included to assess the sustainability of dug wells (Table 1).

It was found that, CPSU II (Sailana block) and CPSU I and II (Bajana block) had the maximum variety of water and soil recharge activities (Table 1). So it is predicted that dug wells in these watershed units will perform better in terms of increased irrigated area, production, cropping intensity compared to other CPSUs. The major crops grown in the area were wheat and cotton so crop productivity was assessed in terms of average wheat and cotton yield. An increase in irrigated area, crop productivity, cropping intensity was recorded for all CPSUs post dug well implementation (Table 2). Further, the watershed units CPSU II (Sailana block) and CPSU I (Bajana block) recorded higher change in irrigated area. This is in agreement with the above assumption about performance of dug wells in selected watershed areas. The most visible impact of dug well is increase in water availability for irrigation of wheat. It was found that the average wheat yield is highest for CPSU II of both Bajana (27.5 q/ha) and Sailana block (16.3 q/ha). CPSU I of Bajana block recorded highest average cotton yield and change of cropping intensity. All these observations are in line with our assumption that dug wells in CPSU II of Sailana block and CPSU I and CPSU II of Bajana block have performed better in the set parameters due to variety of water and soil recharge activities taken up in these units.

Table 1 Total number of assets created in the six sampled CPSUs

Activities	Sailana block			Bajana block		
	CPSU I	CPSU II	CPSU III	CPSU I	CPSU II	CPSU III
Dug wells (Kapil Dhara)	22	33	22	72	54	65
Plantations	–	–	–	1	5	1
Horticulture plantations (Nandan Falyodyan)	–	–	–	–	12	–
Percolation tanks	–	1	–	3	3	–
Farm bunds	3	58	20	1	49	1
Watershed activities (Stop dam)	–	1	–	1	–	4
Ponds	6	4	3	4	–	2
Community wells	1	11	6	3	10	6

Table 2 Impact of water holding assets created under MGNREGA on agricultural performance

			Sailana block			Bajana block		
			CPSU I	CPSU II	CPSU III	CPSU I	CPSU II	CPSU III
Irrigated area (%)	Dug well (Kapil Dhara)	2006–2007	2	11	13	9	41	17
		2011–2012	48	68	43	58	83	42
Cropping intensity	Dug well (Kapil Dhara)	2006–2007	100	104	100	99	109	92
		2011–2012	144	133	108	103	130	110
Wheat yield (qt/ha)	Dug well (Kapil Dhara)	2006–2007	0	5	0	10	12.5	7.5
		2011–2012	12.1	16.3	13.8	20	27.5	17.2
Cotton yield (qt/ha)	Dug well (Kapil Dhara)	2006–2007	4.4	2.4	1.5	3.1	3.3	3.6
		2011–2012	11.2	6.5	4.6	8.6	7.3	6.2

4 Remote Sensing-Based Results

The field-based observations were further compared with observations obtained using RS and GIS techniques for district and CPSUs. The change in land use pattern were generated using RS and GIS between pre (2007) and post (2011) MGNREGA implementation. Ratlam district has a total geographical area of 4861 km² and it was further classified into four land use land cover classes (LULC) namely double crop, single crop, water body, and other LULC for the years 2007 and 2011 using ISODATA classification technique (Fig. 2). It was found that 77 % of the total geographical area of the district falls under agricultural land use. There was no significant change (+0.03 %) in agriculture area between the two years (2007 and 2011), however, the area under double crop increased by 10.5 % in the same period, due to increased availability of water for irrigation. A slight increase of area (0.15 %) under water body was found for the district of Ratlam that could be attributed due to the newly constructed water conservation structures (ponds, stop dams, and percolation tanks) (Fig. 2).

Similarly for CPSUs, an increase in area under double crop was found for five out of six sampled CPSUs (Fig. 3). In the block Sailana, increase in double crop area is almost double for CPSU I and is the highest among the other CPSUs. In Bajana block, CPSU I shows a decrease in the double crop area (Fig. 3) though the field data revealed a very slight increase in the area (Table 2). The dug well beneficiaries of this block utilized water mainly for the irrigation of cotton. As the growing period of cotton overlaps with the Rabi crop, the increase in cotton acreage was not reflected as an increase in the Rabi crop.

Further, an increase in area of water bodies was found in all six CPSUs post MGNREGA intervention (Fig. 3). This is consistent with the observation made in classified images at all the levels: watershed, block, and the district. Literature and field survey also revealed that significant number of water storage structures, viz.,

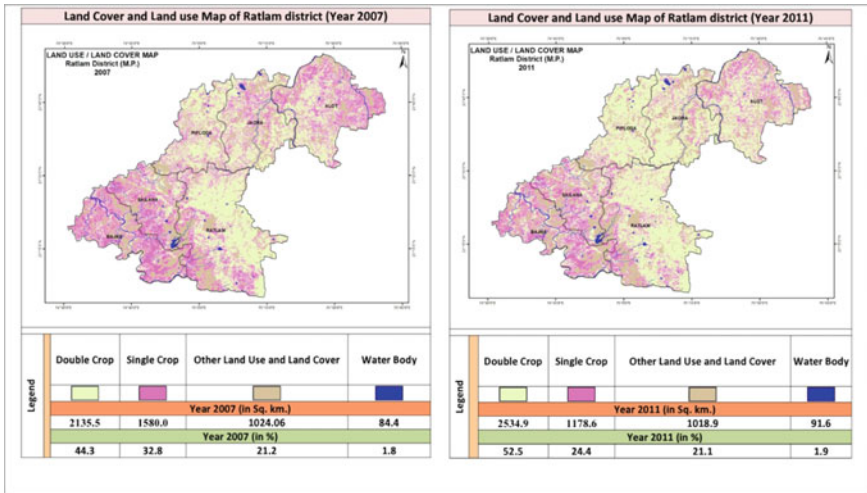


Fig. 2 Change in land cover/land use statistics of Ratlam district in 2007 and 2011



Fig. 3 Change in land cover/land use statistics of selected CPSUs in Sailana and Bajana block, Ratlam district in 2007 and 2011

ponds, percolation tanks, and dug wells had been created across the state of Madhya Pradesh including the Ratlam district.

A proximity analysis was applied using GIS techniques to analyze the impact of dug wells toward increase of double crop area (Table 3). The Global Positioning System (GPS) points of new dug wells recorded during the field survey was plotted in the classified land use map to study the increase in the double crop area surrounding the wells. A buffer of 200 and 500 m was created for all the 64 sampled dug wells spread across two blocks and was clipped to land use map for 2007 and

Table 3 Increase in double crop area due to sampled dug wells through proximity analysis for 500 and 200 m for the years 2007 and 2011

Distance from dug well (m)	500 m distance		200 m distance	
	2007	2011	2007	2011
Land use and land cover classes				
Double crop	28.8	35.8	39.5	44.9
Single crop	39.9	33.1	39.7	34.5
Forest (With dense scrub)	6.1	4.3	3.8	3.0
Waste/barren land (With open scrub)	21.3	22.4	12.6	13.9
Settlement and water body	4.0	4.3	4.4	3.7

2011, respectively. The result showed a significant increase in the double crop area for both the distance. Around 5.4 and 7 % area has increased in the proximity of 200 and 500 m, respectively, from dug well between the years 2007 and 2011.

5 Conclusions

The present study in the Ratlam district was undertaken to assess the sustainability of dug wells (Kapil Dhara) at the micro watershed scale through the integrated use of RS and GIS techniques. Dug wells were the most widely implemented beneficiary-oriented activity among all the MGNREGA works. The significant change in irrigated area, cropping intensity, and crop yield are the main indicators taken in this study for determining the sustainability of dug wells. The sustainability of dug well is more promising in CPSU II of both the Sailana and the Bajana block where a greater number and variety of water recharge and conservation activities have been taken up. Thus, performance of wells and its water availability in a particular watershed is an integrated function of the sum total of all the activities taken up in that watershed. The remote sensing mapping and proximity analysis indicated that farmers have intensified their cropping patterns during the Rabi season near the newly constructed dug wells, which was also observed during the field survey. The findings of field survey and remote sensing reinforce each other, implying that RS and GIS can be effective in monitoring and assessing the impact of MGNREGA at a larger scale (blocks/districts).

6 Recommendations

Time series analysis of land use and land cover change using RS along with integration of watershed component in GIS platform can be one of the effective approaches in prioritizing the watershed activity and monitoring the progress of any developmental activities. Among all various categories of the MGNREGA works, about 60 % works are related to water and soil conservation. Sustainability and

output of these assets can be further enhanced by adopting watershed approach during planning stage using remote sensing and GIS techniques in deciding the suitability of the sites. This would require the integration of accurate map of the village and the GP with the watershed and the administrative boundaries. Different relevant information and data available with other departments can be further integrated through RS and GIS toward effective planning and monitoring at block/district levels. Specifically, construction of dug wells should be well-monitored with respect to site suitability and supplemented with the creation of other water recharging assets like ponds, plantations, etc., in the watershed area to enhance their sustainability.

Acknowledgments The authors would like to acknowledge the Ministry of Rural Development (MoRD), India for the financial support as the content of the current paper is drawn from a larger project funded by the MoRD. The authors would also like to thank the director, IIFM for his guidance and support.

References

- Adinarayana J, Krishna NR, Rao KG (1995) An integrated approach for prioritisation of watersheds. *J Environ Manag* 44(4):375–384
- Bassi N, Kumar MD (2010) NREGA and rural water management in India: improving the welfare effects. Occasional paper, Institute for Resource Analysis and policy, Hyderabad
- Esteves T, Rao KV, Sinha B, Roy SS, Rao B, Jha S, Ravindranath NH (2013) Agricultural and livelihood vulnerability reduction through the MGNREGA. *Econ Pol Wkly* 48(52):94–103
- GoI (Government of India) (2013) The Mahatma Gandhi national rural employment guarantee act, 2005. <http://nrega.nic.in/netnrega/home.aspx>. Accessed 10 Mar 2014
- Kareemulla K, Reddy KS, Rao CR, Shalander K, Venkateswarlu B (2009) Soil and water conservation works through national rural employment guarantee scheme (NREGS) in Andhra Pradesh—an analysis of livelihoods impact. *Agric Econ Res Rev* 22:443–450
- Kareemulla K, Kumar S, Reddy KS, Rama Rao CA, Venkateswarlu B (2010) Impact of NREGS on rural livelihoods and agricultural capital formation. *Indian J Agric Econ* 65(3):524–539
- Khan MA, Gupta VP, Moharana PC (2001) Watershed prioritization using remote sensing and geographical information system: a case study from Guhiya. *India J Arid Environ* 49(3):465–475
- Kumar MD, Bassi N, Sivamohan MVK, Niranjana V (2011) Employment guarantee and its environmental impact: are the claims valid? *Econ Pol Wkly* 46(34):69–71
- Lillesand TM, Kiefer RW, Chipman JW (eds) (2004) *Remote sensing and image interpretation*. Wiley, USA
- Randhir TO, O'Connor R, Penner PR, Goodwin DW (2001) A watershed-based land prioritization model for water supply protection. *For Ecol Manag* 143(1):47–56
- Samarthan (2010) Impact assessment of MGNREGS in Madhya Pradesh. Samarthan, Centre for Development Support, Bhopal
- Sinha B, Basu A, Katiyar AS (2010) Impact assessment of MGNREGA's activities for ecological and economic security. Indian Institute of Forest Management, Bhopal
- Vittala SS, Govindaiah S, Gowd HH (2008) Prioritization of sub-watersheds for sustainable development and management of natural resources: an integrated approach using remote sensing, GIS and socio-economic data. *Curr Sci* 95(3):345–354

Mangrove Forest Cover Changes in Indian Sundarban (1986–2012) Using Remote Sensing and GIS

Kaberi Samanta and Sugata Hazra

Abstract The Indian Sundarban, a world heritage site, consists of an area of about 6312.768 km² (2012) out of which 2122.421 km² is covered by mangrove forests. The total forest cover of the Indian Sundarban, as assessed by Remote Sensing studies for the year 1986, was about 2246.839 km², which gradually declined to 2201.41 km² in 1996, to 2168.914 km² in 2001 and to 2122.421 km² in 2012. Strangely, there has been a loss of 124 km² of mangrove forest cover in spite of the significant addition of forest by plantation in the northern part and the emergent 'char lands' within the tidal creeks. But the erosion and submergence of the southern sea-facing mangrove islands is even more significant as a result of the strong coastal erosion and sea level rise. The present study identifies six major classes of forest cover by supervised and unsupervised classification of the mangrove forest area, which are Dense Forest, Degraded Forest, Saline Blanks, Water Body, Sand (beaches/dunes), and Mud flats. The principle sequence of forest cover change observed was the transformation of Dense Forest area to Degraded forest and then to Saline blanks, with an occasional reversal of change in isolated cases under specific conditions. Saline blank formation is most dominant in Herobhanga, Ajmalmari East, West and North West, Dulibhasani East and Dulibhasani with significant increase with time. Among the total land use change during the last 26 years, about 47 % of it have been the change of Dense Forest to Degraded Forest, Saline Blanks or Creeks, notwithstanding minor amount of regeneration in some cases. The saline blanks occupy about 12 % of the total changed area at the expense of Dense Forest, Degraded Forest, Creeks/Waterbody which may be due to increasing tidal inundation, an increase of temperature and a reduction of annual rainfall in the area probably in response to climate change.

Keywords Remote sensing · Sundarban · Mangrove · Saline blank · Climate change

K. Samanta (✉) · S. Hazra
School of Oceanographic Studies, Jadavpur University, Kolkata 700032, India
e-mail: samanta.kaberi@gmail.com

© Springer International Publishing Switzerland 2017
S. Hazra et al. (eds.), *Environment and Earth Observation*,
Springer Remote Sensing/Photogrammetry, DOI 10.1007/978-3-319-46010-9_7

1 Introduction

Mangrove Forests are unique bio-diverse ecosystems which support various ecosystem services for human well-being. Sundarban mangrove forest, the world's largest mangroves with an area covering 9630 km², is situated at the tide-dominated lower deltaic plain of the Ganges–Brahmaputra–Meghna delta extending from India to Bangladesh. Being one of the largest carbon sequesters of the globe, the change of mangrove forest cover, either by anthropogenic or natural drivers, appears to be a major concern for scientists. Satellite image processing and spatial analysis have proved to be effective methods for quantifying mangrove forest cover change (Ramsey and Jensen 1996; Lillesand and Kiefer 1994; Campbell 2002; Blasco et al. 1998). Jensen et al. (1991) observed that the Normalized Differential Vegetation Index (NDVI) calculated using SPOT XS imagery is correlated with canopy closure ($r = 0.91$), a surrogate for mangrove density. Ramsey and Jensen (1996) found that the NDVI is also related to the leaf area index ($r^2 = 0.84$), which is associated with canopy height. In this paper, the NDVI has been adopted for the actual estimation of the forest cover area intermixed with the degraded forest.

While there have been two major mangrove forest inventories assessed in southwest Bangladesh using aerial photography only a few studies of Sundarban mangrove forests have so far been conducted using satellite imagery (Islam et al. 1997; Giri et al. 2007; Iftekar and Saenger 2008). This study has quantified forest cover change from 1989 to 2000 using the Landsat Thematic Mapper (TM) and the Enhanced Thematic Mapper Plus (ETM+) images. It has used specifically two image processing techniques: NDVI differencing (Jensen 1996), maximum likelihood classification (Foody et al. 1992). Describing the reasons for changes in the spatial distribution of a mangrove ecosystem over time is an extremely complex task. Changes in mangrove forests are multidimensional and therefore, we must consider the biotic, geomorphic, and anthropogenic influences. Some researchers have described the distribution of mangrove species using a successional model which emphasizes on the biotic rather than the geomorphic characteristics.

The forest of Indian Sundarbans is mainly covered with mangroves. At present, the dominant mangrove species are *Avicennia* (Bain) *Excoecaria* (Gewa), *Bruguera* (Kankra), *Ceriops* (Passur), and *Phoenix* (Hental) (Giri et al. 2014) which occur prominently throughout the area with discontinuous a distribution of *Sonneratia* (Keora), *Dhundul* (*Xylocarpus*), and sporadic occurrences of *Heritiera* (Sundari). Among grasses and Palms, *Poresia* *Coaractata*, *Myriostachya* *Wightiana*, *Imperata* *Cylindrica*, *Phragmites* *Karka*, *Nypa* *fruticans* are well distributed. Besides the forest, there are extensive areas of brackish and freshwater marshes, intertidal mudflats, sandflats, sand dunes with typical dune vegetation, open grassland on sandy soils and raised areas supporting a variety of terrestrial shrubs and trees. In Remote Sensing images, the forests of the Indian Sundarbans have a very bright red vegetation signature. The reflectance values are quite high with a small range of variation. Therefore, the categorization in the vegetation reflectance values is difficult to achieve by simple classification methods. Mangrove vegetation gives bright

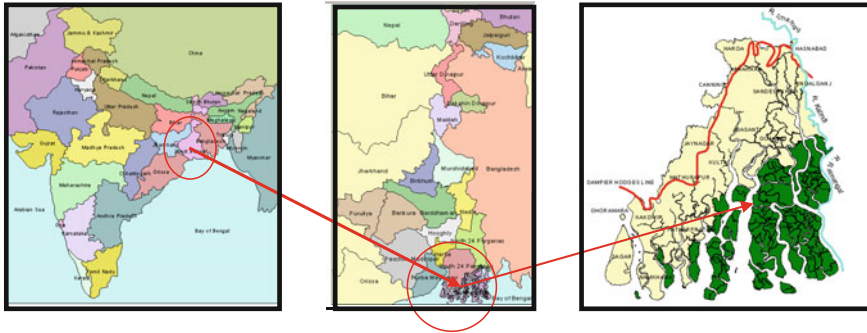


Fig. 1 Location map—Indian Sundarban

red (if dense) or pale red (if sparse) or orange color tone. They come across as irregular in shape with a smooth texture on satellite data and hence can be easily interpreted. The study area map of Sundarbans having forested areas out of the total Sundarban area is portrayed in Fig. 1.

2 Materials and Methods

This paper aims to evaluate the magnitude of change caused due to natural factors in the forest cover of the Indian Sundarban. The analysis has been done with the help of Remote Sensing data with relevant field observations. The classification has mainly been performed on the ERDAS imagine platform using both unsupervised and supervised techniques. The classification has been followed for all the individual island groups. The data products which have been used in this paper are:

Table 1 shows the details of satellite imagery used in the present study. NDVI analysis for the study area has been done to get the actual forest cover excluding the creeks and water bodies. An accuracy test was also done to confirm the procedure of classification (Mahdavi 2010). The satellite data procured were of similar tidal condition for the scale of the map and this helped in assessing the erosion and

Table 1 Details of satellite imagery

Sl. No.	Satellite data	Year and date of acquisition	Spatial resolution (m)
1	Landsat TM	January, 1986	30
2	Landsat TM	February, 1996	30
3	IRS 1D LISS III	January, 2001	23.5
4	IRS P6 LISS III	January, 2004	23.5
5	IRS P6 LISS III	January, 2009	23.5
6	IRS P6 LISS IV	February, 2012	5.8, resampled to 23.5

accretion of the forest areas of the Indian Sundarbans. All the data sets having individual forest-covered islands have been analyzed using unsupervised classification and subsequently confirmed by supervised classification techniques to specifically identify the dense forest cover, degraded forest, saline blanks, and creeks. The accuracy assessment was done and it came to be around 85 %.

3 Results and Discussion

Forest cover changes in the Indian Sundarbans is gradually decreasing due to several reasons which can be attributed to the non-anthropogenic or 'natural' changes (Pant et al. 2000; Sakthivel et al. 2010). The mean sea level at the Sagar Island Station measured from 1985 onwards till 2010 shows a rise by 2.6–4 mm/year (Bakshi et al. 2001; Allison et al. 2003). This may also be considered as a driving factor for coastal erosion, coastal flooding and the increase in number and area of tidal creeks (Semeniuk 1994) in this area. The salt water intrusions and subsequent drying are mainly causing the formation of saline blanks amidst the forested islands.

A study of the air temperature changes around the Sundarban and the adjacent Bay of Bengal from 1990 to 2000 indicates a clear rise at the rate of 0.019 °C per year which subsequently changed to 0.045 °C per year during the present decade (Hazra and Baksi 2003, Hazra et al. 2010). It was also observed that during the same time windows, the earlier rate of sea level rise at the rate of 3.14 mm/year has been surpassed by a much higher rate of 8 mm/year (Alam 2003; Pethick and Orford 2013). With a reduction of monsoonal rainfall, the island system has been experiencing the impact of an increased intensity of cyclonic storms and surges (Gopal and Chauhan 2006). All these factors have led to the sequential land loss of the mangrove forest-covered sediment starved islands of the Sundarban (Fig. 2).

The erosion is more prominent in the southern sea-facing side of the islands, while some amount of deposition by the slackening of flood tide is observed in the northern fringes and creeks as well. The intensity of erosion increases from the west to the east evidently as a consequence of the reduction of fresh water and sediment availability. A time series account (Table 2) of erosion of the mangrove forest-covered islands brings about the extent of the mangrove forest cover loss in the delta.

Thus the 2246.848 km² of area of the mangrove islands of 1986 has been reduced to 2122.4209 km² in 25 years accounting for 124 km² loss of mangrove forest from the Indian Sundarban. The main factor responsible for such forest cover loss happens to be erosion and submergence triggered by climate change and sea level rise in the sediment starved estuary (Roy et al. 2011; Akingbogun et al. 2012).

This may be apprehended that the above mentioned factors may be the cause for various changes which are occurring in the forest-covered islands of the Indian Sundarban, considerably protected from human interference. The classes which were taken for analysis of forest cover estimation in the present study are: 1. Dense

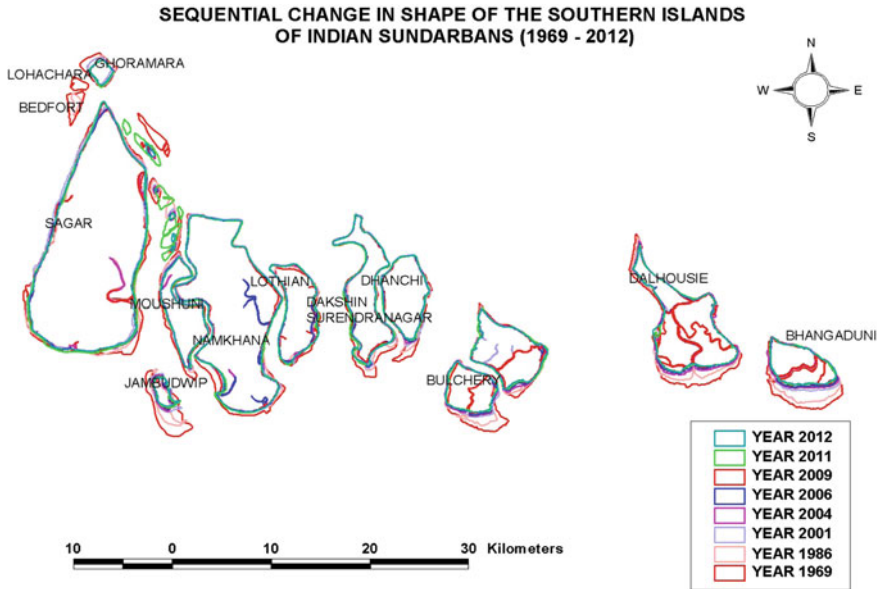


Fig. 2 Sequential change in shape of the Southern Islands of Indian Sundarbans (1969–2012)

Forest, 2. Degraded Forest, 3. Saline Blanks, 4. Water Body, 5. Sand (beaches/dunes), 6. Mud flats, and 7. Reclaimed land from forest.

The supervised classification has been carried out to identify the above features in the Sundarban forest part. (Iftekar and Saenger 2008). The observed general pattern of change is the transformation of the dense forest area to degraded forest and then to saline blanks. Basically the degraded forests are being transformed into saline blanks. The area under saline blanks is found to have increased by about 17.311 km² during the past 26 years. It is dominant in Herobhanga, Ajmalmari East–West and the North–West, Dulibhasani East and Dulibhasani West where the saline blanks have increased significantly. Major forest clearance of the mangrove area has been observed in Jambudwip under Namkhana block and Jharkhali island under the Basanti block which have significant human population. However, this conversion from forest land to deforested area took place before 2001. The details of forest cover types along with areas which underwent changes are given below with maps for individual island/block. Jambudwip, situated near to the Sagar Island of Hugli estuary, is under constant threat of coastal erosion and land loss. The total island area of 6.095 km² has reduced to 5.0035 km² registering about 18 % loss within a time window of 26 years. Figure 3 portrays the areal change of total forest cover in Indian Sundarban between the years 1986 and 2012. Figure 4 on the other

Table 2 Time series of erosion of mangrove forest-covered islands of Indian Sundarban

Sl. No	Forest-covered islands	1986	1996	2001	2004	2009	2012
1	Jambudwip	6.095	5.91	5.893	5.68	5.0338	5.0035
2	Herobhanga	49.04	48.358	48.359	48.377	47.6476	47.4222
3	Dalhousie	76.606	72.395	69.553	68.0927	65.9706	64.2414
4	Bhangaduni	40.447	35.157	31.629	29.556	27.1262	24.9164
5	Matla	402.85	396.86	395.54	397.08	394.12	394.252
6	Saznekhali North	132.96	132.43	131.38	132.071	128.469	128.857
7	Sudhyanyakhali	181.59	180.03	179.54	179.37	177.526	176.713
8	Gosaba	517.47	517.44	506.71	506.71	506.71	506.691
9	Jhilla	91.507	90.269	90.1774	90.1774	88.7888	88.7211
10	Katuajpuri	279.1	260.48	253.36	253.36	253.36	252.591
11	Ajmalhari West	25.864	26.144	25.561	25.999	25.707	23.8484
12	Ajmalhari east	78.583	77.336	76.87	76.65	75.5108	75.4959
13	Ajmalhari north west	48.306	47.803	47.3977	47.6	47.3269	47.3191
14	Bulchery	28.455	28.208	26.751	24.6908	22.8918	22.8195
15	Dulibhasani west	180.03	174.78	172.12	170.903	164.327	163.475
16	Dulibhasani east	37.299	37.712	37.874	36.1816	35.5245	34.0563
17	Dhanchi	36.503	35.467	35.26	34.848	31.9975	31.8329
18	Lothian	34.143	34.628	34.937	34.989	34.1673	34.1652

All areas given in km²

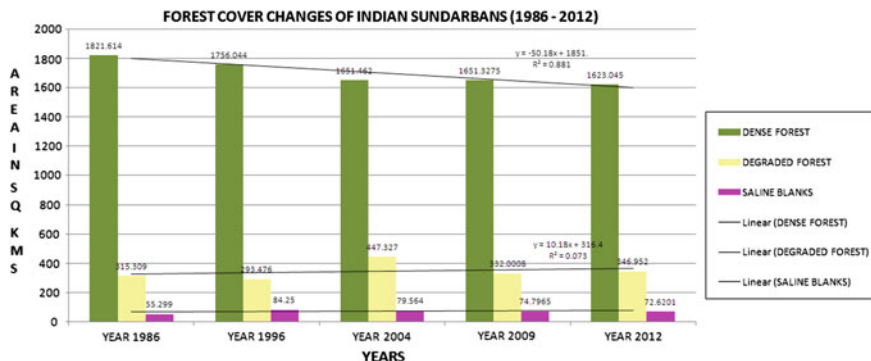


Fig. 3 Areal change of total forest cover in Indian Sundarban (1986–2012)

hand illustrates the forest cover changes of different islands in Indian Sundarban. Figures 5, 6, 7 and 8 portrays the land cover change significant islands between the same time span.

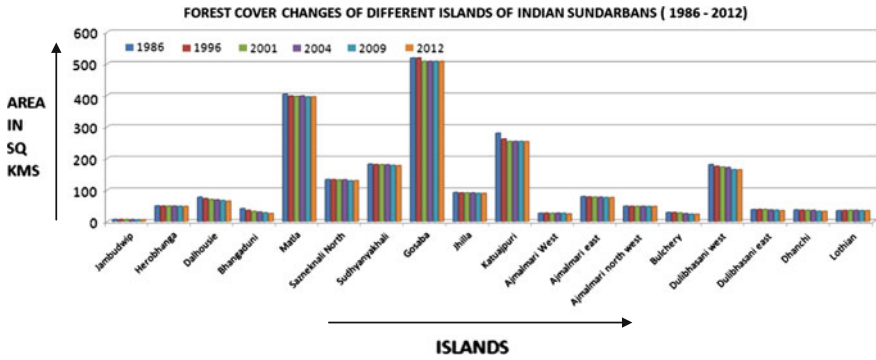


Fig. 4 Total forest cover changes of different islands in Indian Sundarban

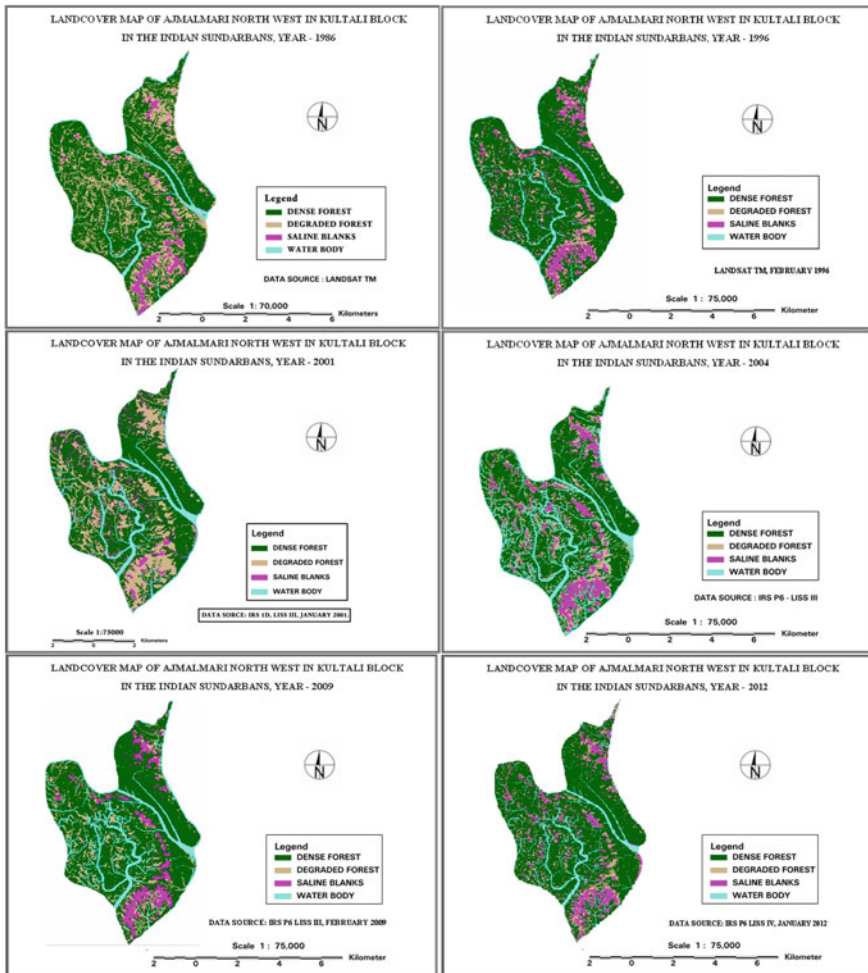


Fig. 5 Land cover map of Ajmalhari Northwest Island from 1986 to 2012

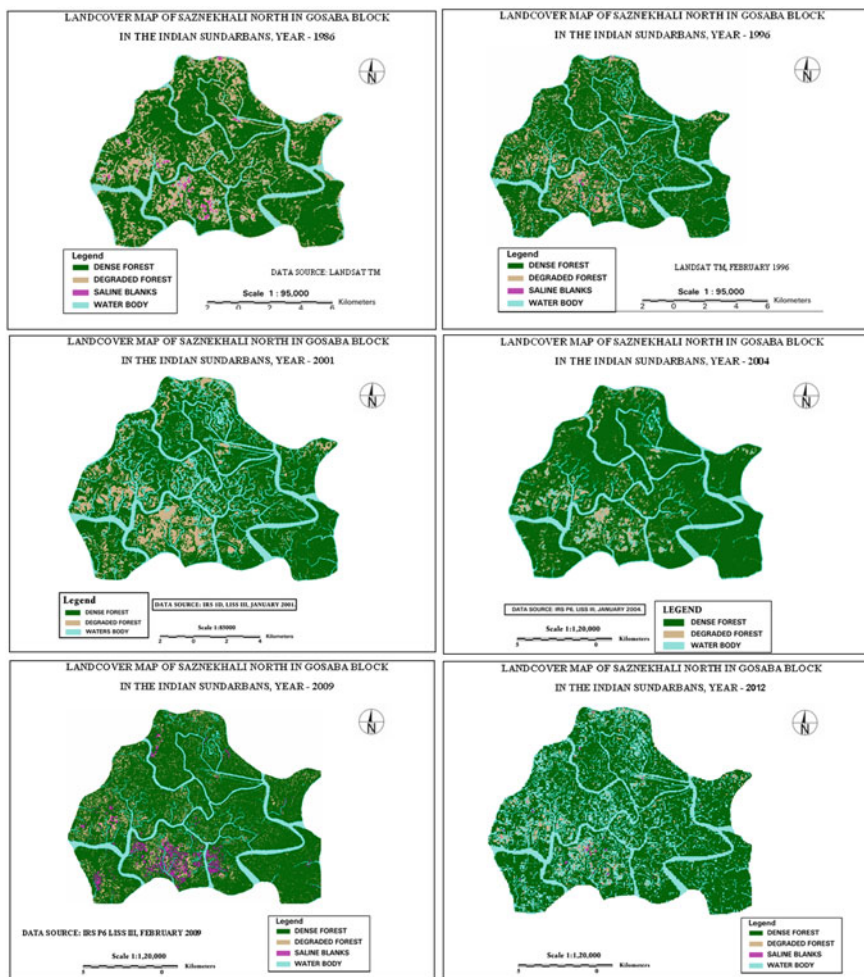


Fig. 6 Land cover map of Saznekhali North Island from 1986 to 2012

3.1 Discussion on Forest Cover Changes in the Indian Sundarban

The forest-covered part of the Indian Sundarban has been facing constant coastal erosion, tidal water intrusion. This has been particularly noticeable for the southern islands as the shapes are constantly changing. A total of what was 2246.848 km² of area of mangrove islands in 1986 has reduced to 2122.4209 km² in 25 years accounting for the loss of 124 km² of mangrove forest area from the Indian Sundarban. However, there is a discrepancy in the present data produced by the mapping division of the Forest Survey of India (FSI), 2011. The total forest area has

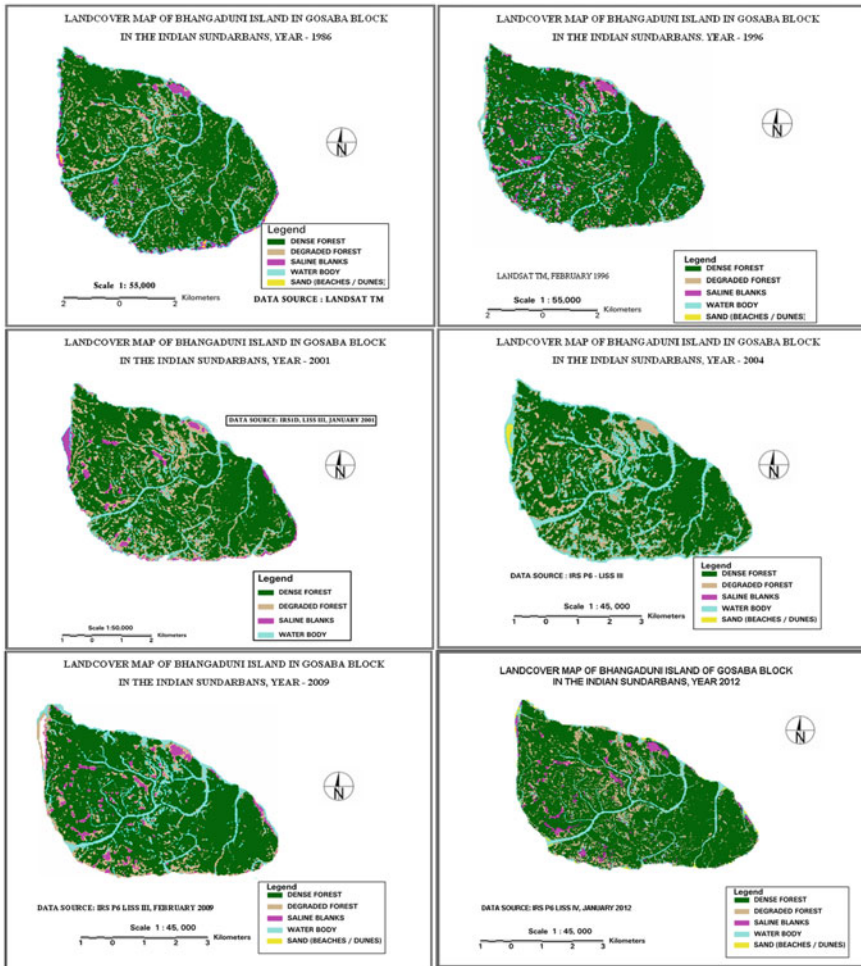


Fig. 7 Land cover map of Bhangaduni Island from 1986 to 2012

been shown as 2330.164 km² which is around 200 km² more than the present estimation. This discrepancy has been caused due to the constraint of resolution in mapping. While the FSI map included the minor creeks with widths less than 2 pixels of LISS III data in the forest area, the present exercise excluded 210 km² of the water area occupied by minor creeks with the help of higher resolution LISS IV data. It is believed the estimation of forest cover change would improve further with the help of further higher resolution data.

During the past 26 years, there has been a change of 31 % within the forest area while about 69 % has remained unchanged. In the total changed area, about 47 % of the change has taken place in the Dense Forest area as it has been converted to Degraded Forest, Saline Blanks and Creeks. The saline blanks occupy about 12 %

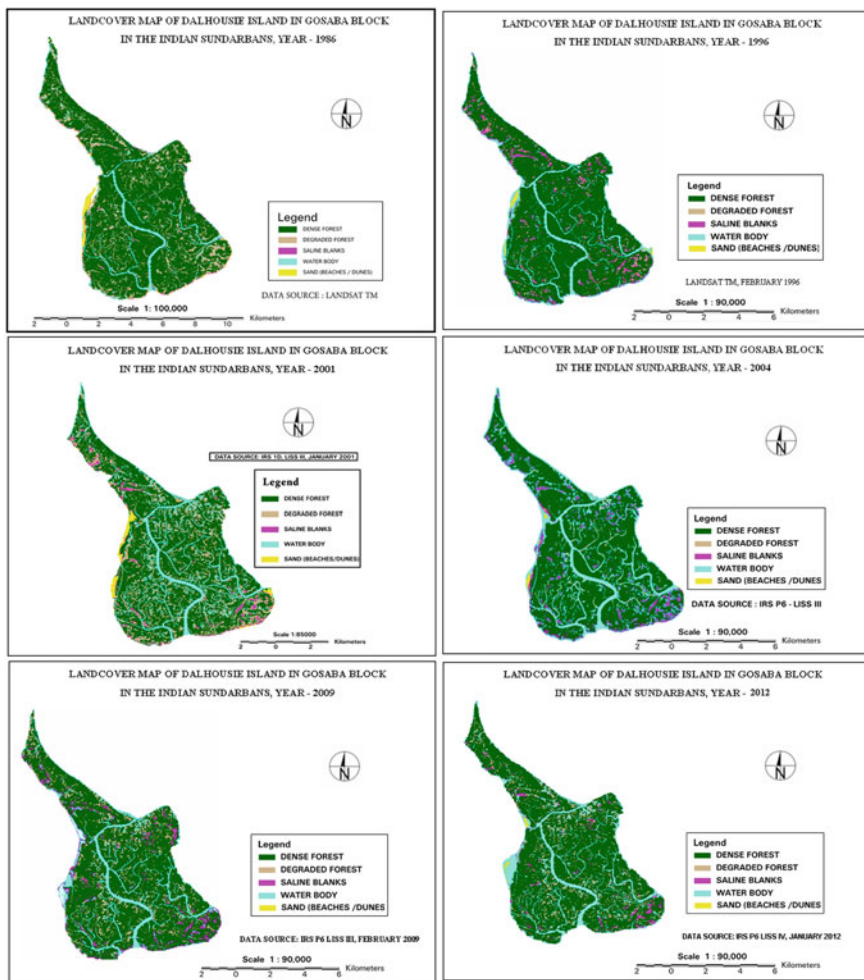


Fig. 8 Land cover map of Dalhousie Island from 1986 to 2012

of the total changed area at the expense of dense forest, degraded forest, creeks/water body. About 43 % of the total forest-covered area has undergone degradation in the past 26 years while at some places it has regenerated.

4 Conclusion

The forest cover of the Indian Sundarban has been declining in the recent years. The major change which has been observed is an overall depletion of the forest while within the forest area; there is a significant amount of saline blank formation which

can be attributed to the salt water intrusion and sea level rise. There is an increase in the creek area which is widening in some places which in turn increases the volume of water within the forested areas of the Indian Sundarban. The continuation of this process in response to climate change and sea level rise poses a serious threat to the carbon sequestration potential and other ecosystem services of this mangrove forest in future.

References

- Akingbogun AA, Kosoko OS, Aborisade DK (2012) Remote sensing and GIS application for forest reserve degradation prediction and monitoring. In: First FIG young surveyors conference knowing to create the future, Rome, pp 4–5
- Alam M (2003) Bangladesh country case study. Asian regional workshop for the preparation of national adaptation programme of action. Thimphu, Bhutan
- Allison MA, Khan SR, Goodbred SL Jr, Kuel SA (2003) Stratigraphic evolution of the Holocene Ganges-Brahmaputra lower delta plain. *Sediment Geol* 155:317–342
- Bakshi A, Hazra S, Sen G, Mukherjee AD (2001) Estimation of relative sea level rise from Tide Gauge data of Sagar island of Bay of Bengal. *J Coast Res*
- Blasco F, Gauquelin T, Rasolofoharinoro M, Denis J, Aizpuru M, Caldairou V (1998) Recent advances in mangrove studies using remote sensing data. *Mar Freshw Res* 49:287–296
- Campbell JB (2002) Introduction to remote sensing, 3rd edn. Taylor and Francis Ltd., London
- Foody GM, Campbell NA, Trodd NM, Wood TF (1992) Derivation and applications of probabilistic measures of class membership from the maximum likelihood classification. *Photogram Eng Remote Sens*. ISSN 0099-1112
- Giri C, Pega B, Zhu Z, Singh A, Tiensen LL (2007) Monitoring mangrove forest dynamics of the Sundarbans in Bangladesh and India using multi temporal satellite data from 1973 to 2000. *Estuar Coast Shelf Sci* 73(1):91–100
- Giri S, Mukhopadhyay A, Hazra S, Mukherjee S, Roy D, Ghosh S, Ghosh T, Mitra D (2014) A study on abundance and distribution of mangrove species in Indian Sundarban using remote sensing technique. *J Coast Conserv* 18:359–367. doi:10.1007/s11852-014-0322-3
- Gopal B, Chauhan M (2006) Biodiversity and its conservation in the Sundarban mangrove ecosystem. *Aquat Sci* 68(3):338–354
- Hazra S, Bakshi A (2003) Environmental refugees from vanishing islands. In: Environment and human security. Lancer Books, Delhi, pp 219–227
- Hazra S, Samanta K, Mukhopadhyay A, Akhand, A (2010) Temporal change detection (2001–2008) study of Sundarban. Unpublished report. WWF-India. http://www.icmpwb.org/main/pdf/ebook/WWF_FinalReportPDF.pdf
- Iftakar MS, Saenger P (2008) Vegetation dynamics in the Bangladesh Sundarbans mangrove: a review of forest inventories. *Wetlands Ecol Manag* 16(4):291–312
- Islam MJ, Alam MS, Elahi KM (1997) Remote sensing for change detection in the Sundarbans, Bangladesh. *Geocarto Int* 12(3):91–100
- Jensen JR (1991) Introductory digital image processing: a remote sensing perspective (2nd Edition), Upper Saddle River, N.J. Prentice Hall
- Jensen JR (1996) Thematic information extraction: image classification. *Introductory Digital Image Proc Remote Sens Perspect* 197–256
- Lillesand TM, Keifer RW (1994) Remote sensing and image interpretation. 5th edn. Wiley
- Mahdavi A (2010) IRS 1C image data applications for landuse/landcover mapping in Zagros region, case study: Ilam watershed, West of Iran. *Caspian J Env Sci* 8(1):35–41

- Pant DN, Groten SM, Roy PS (2000) Forest vegetation/landuse change detection and impact assessment in part of Western Himalaya. *Int Arch Photogram Remote Sens XXXIII(Part B7)*
- Pethick J, Orford JD (2013) Rapid rise in effective sea-level in southwest Bangladesh: its causes and contemporary rates. *Glob Planet Change 111:237–245*. doi:[10.1016/j.gloplacha.09.019](https://doi.org/10.1016/j.gloplacha.09.019)
- Ramsey E III, Jensen J (1996) Remote Sensing of mangroves: relating canopy spectra to site specific data. *Photogram Eng Remote Sens 62(8):939–948*
- Roy U, Mandal AK, Mukherjee S (2011) Detection and analysis of forest cover changes of Indian Sundarbans using satellite data. *J Environ Sci Eng 53(3):309–318*
- Sakthivel R, Manivel M, Jawahar N, Pugalanthi V, Ravichandran N, Anand VD (2010) Remote sensing and GIS based forest cover change detection study in Kalrayan hills, Tamil Nadu. *J Environ Biol 31(5):737–747*
- Semeniuk V (1994) Predicting the effect of sea-level rise on mangroves in northwestern Australia. *J Coast Res 1050–1076*

Change Detection of Vegetation Cover Using Synthetic Color Composite with Some Other Techniques

A.S. Seikh, A. Halder and S. Mukhopadhyay

Abstract This study intends to show the application of some techniques to observe vegetation cover change of an area. Monitoring vegetation cover change is necessary to identify the trend of loss or increase of the same. To fulfill the objective, LISS III images of alternate years have been used from 1997 to 2013. We have tried to identify the change by using synthetic color composite, normalized difference vegetation index (NDVI) index comparison, and vegetation cover mapping using vectorization process. The fundamental idea of synthetic color composite lies in the concept of color mixing. Artificial discreet colors have been assigned for the vegetation cover of different years, after applying NDVI model on those. The study includes a changing trend analysis using least square regression method. The vegetation cover of the area has also been vectorized to get the rate of change. The work concludes with more or less positive result, though there are some limitations. The techniques used are suitable for data of almost similar spatial resolution for the similar seasons. Change of vegetation cover as a whole can only be interpreted clearly with these methods.

Keywords Vegetation cover · Change · Color composite

1 Introduction

Change detection in statistical analysis is to identify the changes in the probability distribution of a time series. In Remote Sensing, change detection involves the process of identifying differences in the state of features by observing them at different times. This process can be accomplished either manually or with the aid of Remote Sensing software (Karl and Axel 2013).

A.S. Seikh · A. Halder (✉)

School of Oceanographic Studies, Jadavpur University, Kolkata, India
e-mail: halder.ananya1988@gmail.com

S. Mukhopadhyay

Department of Geography, North Eastern Hill University, Shilong, India

© Springer International Publishing Switzerland 2017

S. Hazra et al. (eds.), *Environment and Earth Observation*,

Springer Remote Sensing/Photogrammetry, DOI 10.1007/978-3-319-46010-9_8

There are various functional sectors of this technique. For the extraction of vegetation from the satellite imageries, NDVI is a well-known technique to enhance the chlorophyll concentration. A vegetation index model works to enhance the vegetation signal with the process of spectral transformation of surface reflectance. The vegetation Index model calculates the data from more than one bands. The NDVI (Tucker 1979) is a widely used technique which combines the red (R) and near-infrared (NIR) band. It is utilized for analyzing vegetation health, mapping, and land cover changes (Sellers et al. 1994; Running and Nemani 1988; Henderson-Sellers 1995).

The study aims to explain the vegetation cover change of an area using synthetic color composite, arithmetic model, and OLS (Ordinary least square method). Nayachara Island has been chosen as the study area. It is a newly emerged island in the Hooghly Estuary, of Haldia in the Purba Medinipur district of West Bengal.

2 Objectives

The study area has been selected for the purpose of the three main analyses which are as follows:

1. Change detection using synthetic color composite
2. Identification of changing trend using ordinary least-square method (OLS)
3. To identify the rate of vegetation change

3 Study Area

The study area is a newly emerged island in the Hooghly Estuary, of Haldia in the Purba Medinipur district of West Bengal, near the Haldia Dock complex, and Haldi river confluence. It is located between the latitude $21^{\circ} 54' 35''\text{N}$ – $22^{\circ} 1' 15''\text{N}$ and longitude $88^{\circ} 3' 30''\text{E}$ – $88^{\circ} 9' 52''\text{E}$ (Fig. 1).

4 Materials

LISS III images of the dry season during every alternate year from 1997 to 2013 have been used as the main data for this study.

5 Methodology

5.1 *Pre requisite of the Study*

LISS-III satellite images with 1-year interval have been collected and georeferenced to UTM, WGS1984 and 45 north zone accordingly. After atmospheric correction

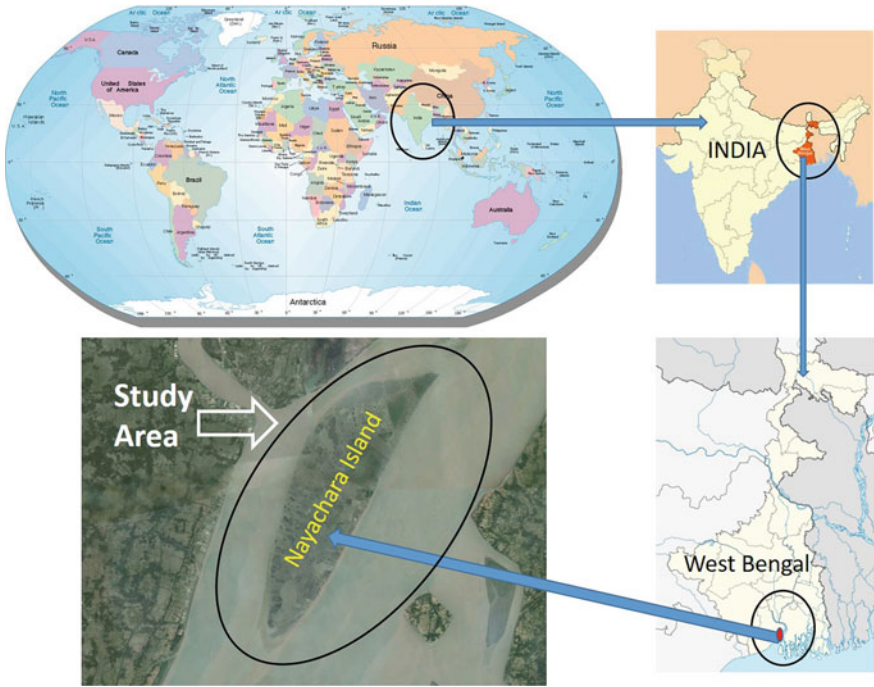


Fig. 1 Location map of study area

and extraction of the study area from the rectified images, all the dataset were resampled to spatial resolution 27 m (Fig. 2).

5.2 Normalized Difference Vegetation Index

The Normalized Difference Vegetation Index (NDVI) is commonly used for measure of vegetation of an area briefly (Justice et al. 1985; Goward et al. 1987; Loveland

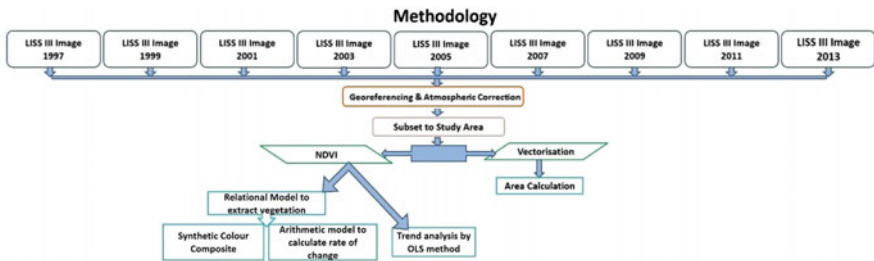


Fig. 2 Flow chart showing methodology

et al. 1991). In this study, the NDVI model has been applied on all the datasets for the extraction of vegetation cover area, using ERDAS Imagine. NDVI values vary from -1 to $+1$ while positive values nearer to $+1$ indicate healthy vegetation.

$$\text{NDVI} = (\text{NIR} - \text{R}) / (\text{NIR} + \text{R}) \quad (1)$$

5.3 *Relational Model*

It is a group of functions of the ERDAS Imagine Spatial Modeler. Among different types of relational functions, the greater than function has been used in this study. The relational greater than function has been applied on the NDVI images to extract greeneries (Fig. 3).

$$\text{Green vegetation} = \text{NDVI Image} \geq \text{vegetation threshold} \quad (2)$$

5.4 *Synthetic Color Composite*

The vegetation extracted NDVI images appears in the black and white shade. Extracted greeneries appear in white while the rest part has been kept black or color less. These images were recoded with unique values for vegetated and nonvegetated areas. Synthetic color used to apply artificial color from RGB combination over the white vegetated portion. Synthetic color composite was prepared by combining different synthetic colored images (at least three number of image for one single composite) of different year which aimed at the output showing vegetation cover change visually interpretable. Arithmetic (addition) function has been used to combine the recoded synthetic colored images. In this study, for a 3 year composite, the earliest year has been selected as layer 1 and assigned with blue, the second one with green, and the latest year (layer 3) with red. The composite has been laired as 321.

5.5 *Trend Analysis*

Trend Analysis has been done by ordinary least square (OLS) regression method using ARC GIS. The Positive, negative and not significant trends have been computed from the NDVI images. The positive trend was coded as $+1$ while the negative trend as -1 and the not significant as '0'.

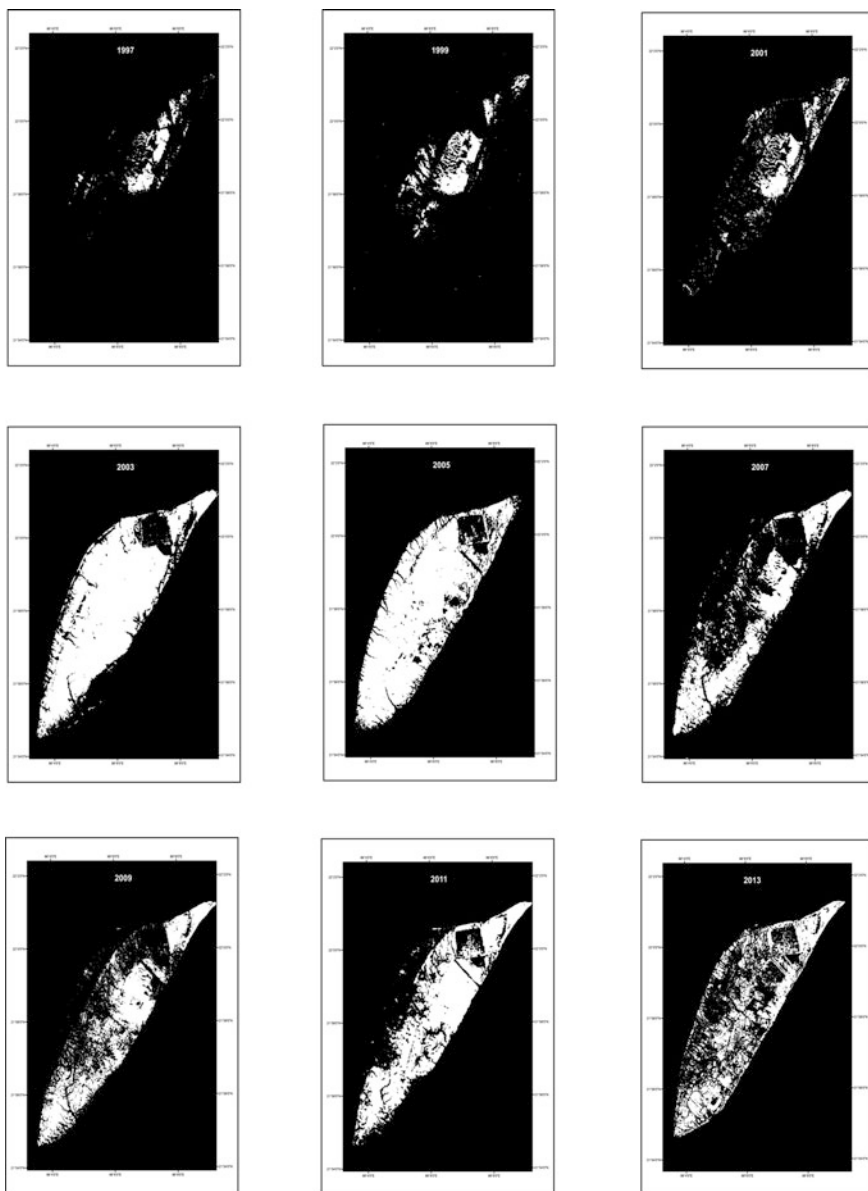


Fig. 3 Extracted greeneries using relational greater than model

5.6 Vectorisation/Digitization

To ascertain the area of Nayachara Island, satellite images of different years has been digitized using Arc GIS software.

6 Results and Discussion

In this study area, the vegetation covers include mainly grassland along with a few mangroves. The absence of high positive NDVI value has been noticed accordingly and therefore +0.2 was selected as the vegetation threshold. Synthetic color composite can be very effective for any spatiotemporal change identification, not only visually but also statistically. Following the standard RGB color combination chart (Fig. 4), the three year synthetic color composites exhibit (Table 1) different combination of vegetation change among different years (Fig. 5). The percentages of change (Table 2) have been figured out using the Raster calculation method.

Fig. 4 Standard RGB color composite

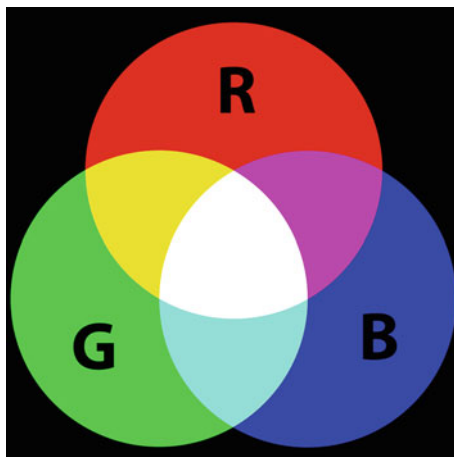








Table 1 Indications for color composite images

	Unchanged in three years
	Vegetation of the first year which vanished during the following years
	Vegetation which grew in the second year and vanished later on
	Vegetation that grew in the third (Latest) year
	Unchanged in the first two years
	Unchanged in the last two years
	Vegetation of the first year which vanished in the second but again grew in the third year

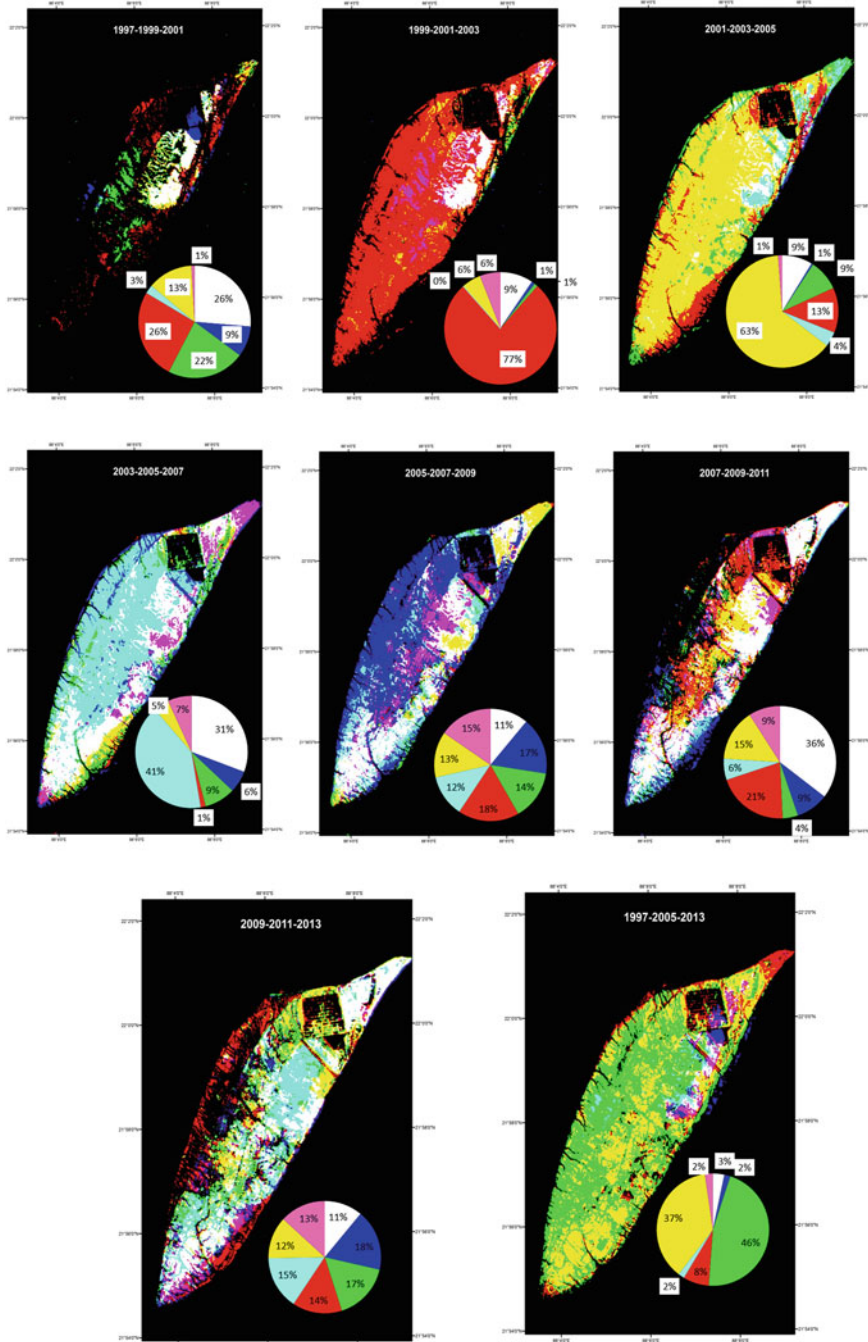
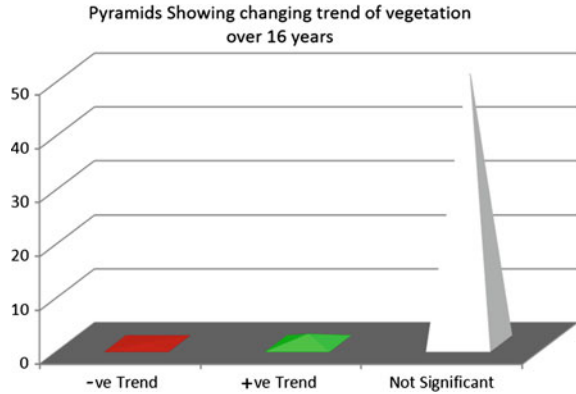


Fig. 5 Output of synthetic color composites

Table 2 Indications for color composite

Composite years	Unchanged in three years (%)	Veg. of the first year which vanished during the following years (%)	Veg. which grew in the second year and vanished later on (%)	Veg. that grew in the third (latest) year (%)	Unchanged in first two years (%)	Unchanged in last two years (%)	Veg. of the first year which vanished in the second but again grew in the third year (%)
1997-1999-2001	26	9	22	26	3	13	1
1999-2001-2003	9	1	1	77	0	6	6
2001-2003-2005	9	1	9	13	4	63	1
2003-2005-2007	31	6	9	1	41	5	7
2005-2007-2009	11	17	14	18	12	13	15
2007-2009-2011	36	9	4	21	6	15	9
2009-2011-2013	11	18	17	14	15	12	13
1997-2005-2013	3	2	46	8	2	37	2

Fig. 6 Trend of vegetation change



Very nominal positive (1.8 km²) and negative (0.2 km²) changes have been detected using the OLS method while the not significant trend (52 km²) is dominant in this area. Positive trend indicates gradual increase in vegetation while the negative trend shows gradual decrease. The not significant trend indicates change with no specific tendency (Fig. 6). The area calculated by digitization has matched with the same computed from pixels.

7 Concluding Remarks

The outer boundary of the Nayachara Island has been vectorized/digitized from satellite images of different years. Borderline comparison of 1997 and 2013 shows that total area of the island has decreased in the year 2013 which includes erosion along the eastern margin. The trend analysis output sketched out from NDVI images for 16 years also indicate a negative or decreasing vegetation trend in the eastern part (Fig. 7). Thus, it can be said that the raster calculation and the vector calculation are more or less similar confirming the same result.

A positive trend is found only at the extreme northern region of the island. However, there is no overall significant trend of vegetation change though the limitations of these techniques to identify vegetation cover change must be conceded. The FCC (False color Composite) images to be used as base data should be of same spatial resolution. Otherwise, the trend analysis will produce an erroneous output. In this study, all types of greeneries (including shrub and grass) have been considered as vegetation. Specification of vegetation type was not possible because of the limitation of these techniques for this purpose.

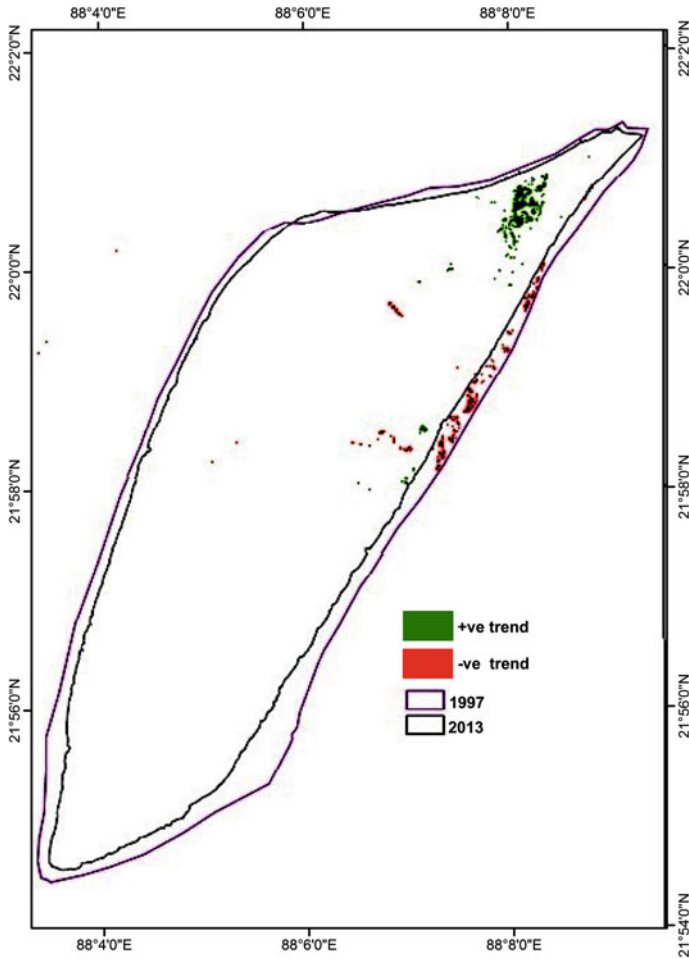


Fig. 7 Trend and digitized area

References

- Goward S, Dye D, Kerber A, Kalb V (1987) Comparison of North and South American biomes from AVHRR observations. *Geocarto Int* 1:27–39
- Henderson-Sellers A (1995) Global climate models and ‘dynamic’ vegetation changes. *Glob Change Biol* 1:63–75
- Justice C, Townshend J, Holben B, Tucker C (1985) Analysis of the phenology of global vegetation using meteorological satellite data. *Int J Remote Sens* 6:1271–1318
- Karl J, Axel A (2013) Change detection. http://wiki.landscapetoolbox.org/doku.php/remote_sensing_methods:change_detection
- Loveland T, Merchant J, Ohlen D, Brown J (1991) Development of a land-cover characteristics database for the conterminous U.S. *Photogram Eng Remote Sens* 57:1453–1463

- Running SW, Nemani RR (1988) Relating seasonal patterns of the AVHRR vegetation index to simulated photosynthesis and transpiration of forest in different climates. *Remote Sens Environ* 24:347–367
- Sellers PJ, Tucker CJ, Collatz GJ, Los S, Justice CO, Dazlich DA et al (1994) A global 1×1 NDVI data set for climate studies. Part 2—the adjustment of the NDVI and generation of global fields of terrestrial biophysical parameters. *Int J Remote Sens* 15:3519–3545
- Tucker CJ (1979) Red and photographic infrared linear combinations for monitoring vegetation. *Remote Sens Environ* 8:127–150

Part III
Remote Sensing of Coast and Ocean

Estimation of Air-Sea CO₂ Exchange and Decadal Change of Surface Water *f*CO₂ in a Shallow Continental Shelf Using in Situ and Remote Sensing Data During Winter

Anirban Akhand, Sudip Manna, Partho Pratim Mondal, Abhra Chanda, Sachinandan Dutta, Sourav Das, Sugata Hazra, Debasish Mitra, P.V. Nagamani, K.H. Rao, S.B. Choudhury and V.K. Dadhwal

Abstract The air-sea CO₂ exchange (*f*CO₂) was estimated in the outer estuary to offshore transition zone of the northern Bay of Bengal using in situ measurements and remote sensing data obtained from moderate resolution imaging spectroradiometer (MODIS) and advanced very high resolution radiometer (AVHRR). The in situ measurements were done during winter months (December, January and February) of the year 2011–12. Sea surface CO₂ fugacity (*f*CO₂), sea surface temperature (SST) and chlorophyll-*a* were measured in situ to develop an empirical relationship with *f*CO₂ but only the SST showed a significant correlation ($r^2 = 0.55$, $n = 64$, $p < 0.05$). This relationship was used to assess *f*CO₂ (water) and its temporal change in decadal scale from the year 2002–2003 to 2011–2012 of the winter months using remotely sensed SST data. The study area acted as a mild sink for atmospheric CO₂ at the mean rate of $-28 \mu\text{mol m}^{-2} \text{h}^{-1}$ (MODIS derived) to $-40 \mu\text{mol m}^{-2} \text{h}^{-1}$ (AVHRR derived). An overall winter-to-winter increasing trend of *f*CO₂ was observed in the last decade which is accompanied by a similar decrease in the chlorophyll-*a* concentrations.

Keywords Air-sea exchange · Fugacity of CO₂ · Chlorophyll-*a* · MODIS · AVHRR · Bay of Bengal

A. Akhand (✉) · S. Manna · A. Chanda · S. Dutta · S. Das · S. Hazra
School of Oceanographic Studies, Jadavpur University, 188 Raja S.C. Mallick Road,
Jadavpur, Kolkata 700032, West Bengal, India
e-mail: anirban.akhand@gmail.com

P.P. Mondal · D. Mitra
ISRO, Department of Space, Government of India, Indian Institute of Remote Sensing,
4 Kalidas Road, Dehradun 248001, Uttarakhand, India

P.V. Nagamani · K.H. Rao · S.B. Choudhury · V.K. Dadhwal
Department of Space, Government of India, National Remote Sensing Centre,
Indian Space Research Organization, Balanagar, Hyderabad 500 625, Telengana, India

1 Introduction

The role of oceans and their significance from the perspective of the global carbon cycle has long been realized. Recent studies emphasize on the fact that the oceans have been acting as a sink for 25–48 % of the anthropogenic emission of CO₂ ever since the days of the industrial revolution (Sabine et al. 2004; Canadell et al. 2007; Doney et al. 2009) with a present uptake rate of 1.5–2.0 Gt of carbon per year (Takahashi et al. 2009). Out of the total oceanic regime, the neritic zone always draws attention as it is the most biologically active zone of the ocean. The continental shelves, especially those with large river confluences, are considered to act as CO₂ pumps with a significant potential of CO₂ uptake (Cai 2003; Lohrenz and Cai 2006; De Grandpre et al. 2002). On the contrary, some observations show that the shelves act as net heterotrophic reservoirs as most of the river-borne particulate organic carbon is being respired here (Mackenzie et al. 2000; Zhai et al. 2005). However, Borges and Frankignoulle (2002) established a probable solution to this ambiguity as they observed that the proximal continental shelves tend to act as sources for CO₂ while the distal ones act the other way. Recent estimates by Laruelle et al. (2010) shows that the continental shelf areas act as a sink for CO₂ at the rate of -0.21 ± 0.36 PgC year⁻¹.

The Bay of Bengal (BoB) forms the eastern flank of the northern Indian Ocean, comprising an area of 2.2×10^6 km² (Shetye et al. 1991). The BoB is bounded by the largest mangrove forest of the world, i.e. Sundarban, in its northern coastal front. The Hugli Estuary, a tributary of the river Ganges, is the main artery of the Sundarban mangrove ecosystem which is dominated by the fresh water discharge from the Farakka dam, located 286 km upstream from the mouth of the river. Several other distributaries like Muriganga, Saptamukhi, Thakuran, Matla, Gosaba and Bidya have lost their original connections with the river Ganges because of siltation, and their estuarine character at present is maintained by the monsoonal runoff alone (Cole and Vaidyaraman 1966). Owing to the piles of sediments carried by the rivers, the continental shelf in this part of the Bay is extended to almost 100 km giving rise to shallow coastal waters.

Till date, several endeavours to estimate air-water CO₂ flux have been undertaken within the domain of the adjacent mangrove waters of the Sundarban deltaic system (Biswas et al. 2004; Mukhopadhyay et al. 2000, 2002). However, little attempt has been made so far to characterize the CO₂ exchange in the coastal margin of the Bay of Bengal. Akhand et al. (2012) conducted a short-term survey during the winter months and reported the study area as a net sink of CO₂ with an average influx rate of $14.03 \mu\text{mol m}^{-2} \text{h}^{-1}$. The scarcity of study in this area could be due to the difficulties in accessing the region owing to highly unstable weather conditions and ocean turbulence. Moreover, surface water distribution of sea surface CO₂ fugacity $f\text{CO}_2$ in such study areas is highly variable as they are influenced by several factors (hydrodynamic, meteorological, physical, chemical and biological). This makes the exact large-scale estimation of air-sea CO₂ flux based on the limited number of in situ measurements extremely difficult (Chen et al. 2011). The

tools of remote sensing on the other hand, measures the baseline parameters like sea surface temperature (SST), wind speed, wind direction and chlorophyll-*a* concentration (from ocean colour) (Carr 2001), which in turn could be used to monitor the $f\text{CO}_2$ distribution in surface water on monthly, seasonal and annual basis (Olsen et al. 2004).

Akhand et al. (2013) previously carried out a survey in the present study area and characterized the $f\text{CO}_2$ (water) and atmosphere-hydrosphere CO₂ flux during the winter months. In the present study, we took this endeavour one step forward to formulate an empirical relationship so as to implement the remote sensing tools and to not only assess the holistic scenario of the $f\text{CO}_2$ (water) distribution, but also to estimate the decadal change in the $f\text{CO}_2$ (water) distribution of the present study area. The in situ air and water $f\text{CO}_2$ along with SST and chlorophyll-*a* were measured during the winter months. The in situ measurement of $f\text{CO}_2$ (water) showed a linear relationship only with SST, which has been used in remote sensing estimation of $f\text{CO}_2$ (water) from the moderate resolution imaging spectrometer (MODIS) and advanced very high resolution radiometer (AVHRR) satellite image of SST for a comparison between two data sources. The in situ data is interpolated onto grids and combined with satellite data to produce monthly air-sea CO₂ flux maps in the northern Bay of Bengal. Moreover, the decadal change of water $f\text{CO}_2$ along with the phytoplankton standing stock (chlorophyll-*a*) has been studied for the winter months from the aqua MODIS satellite imagery.

2 Materials and Methods

2.1 *In Situ Measurements*

2.1.1 Sampling Strategy

Fifteen short cruises were conducted with fishing trawlers between 1 November, 2010–2011 and 29 February, 2011–2012. The sampling surveys were begun from the two coastal stations, namely Freasuregunje fishing harbour (21° 34' N, 88° 15' E) and Digha (21° 38' N, 88° 33' E) in West Bengal, India (Fig. 1). Each and every cruise was arranged to survey the longitudinal and latitudinal extent of the study area in a radial fashion. A uniform distance of about 2.5–3 km was maintained along the curvilinear track of sampling. The entire sampling was accomplished in the day time between 0800 h and 1400 h. The engine of the trawler was stopped for 15 min before each sampling. All the water samples were collected from a few centimetres below the sea surface in 300 ml BOD bottles and analyzed immediately on board.

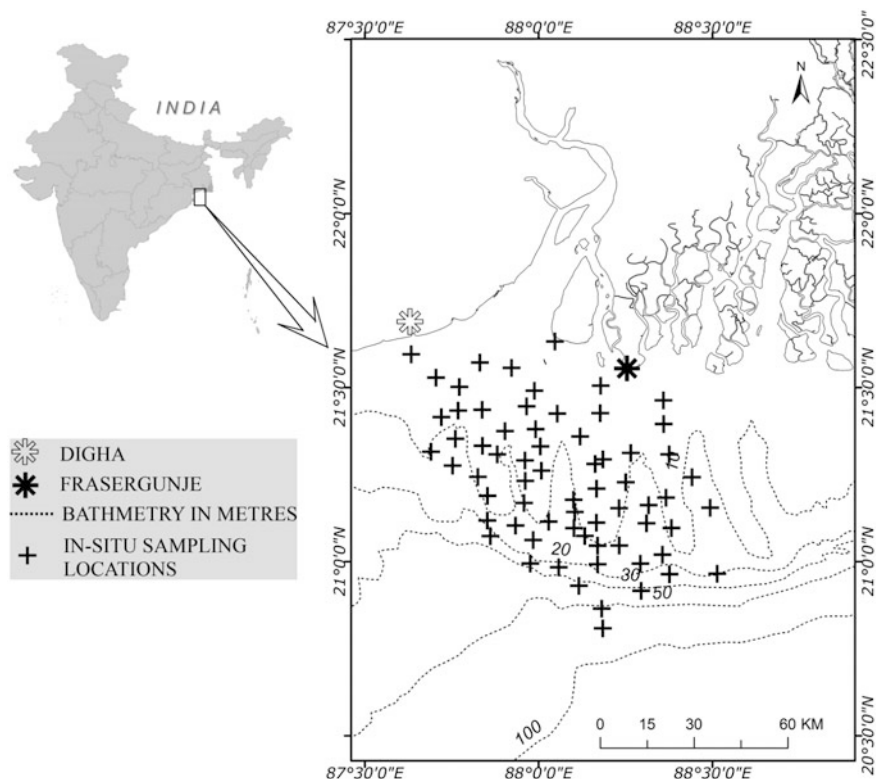


Fig. 1 Study area and sampling locations

2.1.2 Measurements and Analysis Protocol

Sea surface salinity (SSS) was measured using a Multikit (WTW Multi 340 i Set, EMERCK, Germany) fitted with the probe WTW Tetracon 325. pH and water temperature was also measured instantaneously with a micro-pH metre (pH 620, micro-pH metre, Eutech Instruments, Singapore) having a precision of 0.001. The glass electrode for pH measurements was calibrated daily in the NBS scale with technical buffers of pH 4.01 (Part no: 1.09475.0500, MERCK, Germany), pH 7.00 (Part no: 1.09477.0500, MERCK, Germany) and pH 9.00 (Part no: 1.09476.0500, MERCK, Germany) at controlled temperature of 25 °C. The pH readings taken on-board at the respective temperatures were corrected for the standard temperature of 25 °C. The total alkalinity (TALK) was measured using an automated titrator (905 Potentiometric Titrand, Metrohm, Switzerland). 0.1 N stock solution of HCl was standardized by preparing standard solution of known alkalinity with analytical grade Na₂CO₃ (EMERCK, Germany). Silicate and dissolved inorganic phosphate (DIP) were measured by standard spectrophotometric methods (Grasshoff 1983). The $f\text{CO}_2$ (water) was computed with the use of the software CO₂SYS.EXE

(Lewis and Wallace 1998), from the values of SSS, SST, atmospheric pressure, TAlk, pH, silicate and dissolved inorganic phosphate (DIP). The dissociation constants K_1 and K_2 are used according to Peng et al. (1987) and the correction for sulphate is implied as proposed by Khoo et al. (1977). These constants were deliberately chosen since the measured pH has been calibrated in NBS scale.

Samples for chlorophyll-*a* measurement were collected and preserved in the ice box in the dark. These samples were sent to the laboratory within 24 h of sampling and measured by spectrophotometric methods. The spectrophotometer was calibrated by a set of well preserved standard chlorophyll-*a* stock solutions of strength 2 μM , 5 μM , 10 μM and 20 μM . The standard solutions were prepared from lyophilized chlorophyll-*a* (C6144-1MG, Sigma chemicals, India). 2 L of each sample was passed through GF/F filter, extracted in 90 % acetone and measured with a spectrophotometer (Parsons et al. 1992).

The molar concentration of CO₂ ($\mu\text{mol mol}^{-1}$) in the overlying ambient air was determined by a non-dispersive infrared (NDIR) gas analyzer (Li-840A, Li-COR inc. USA), 10 m above the water surface level. The analyzer was calibrated before and after the completion of each cruise trip with the help of three gases—one having CO₂-free gas (N₂) and the other two having a certified reference standard of known concentration of CO₂ (300 and 600 ppm), where the medium gas was N₂ procured from Chemtron Science Laboratory Private Limited, India. The error in estimation was computed by means of a linear interpolation between the two standard calibrations and it varied between ± 0.04 %. The measured molar fraction of CO₂ is converted to $f\text{CO}_2$ (air) by using the virial equation of state (Weiss 1974). The data of air temperature, atmospheric pressure, relative humidity and wind velocity at 10 m from the water surface were logged by a weather station (WS-2350, La Crosse Technology, USA). Monthly mean values of atmospheric molar fraction of CO₂ ($x\text{CO}_2$) from *in situ* measurement were linearly regressed to obtain the latitudinal gradient of $x\text{CO}_2$. To convert the $x\text{CO}_2$ atm to $f\text{CO}_2$ atm, the water vapour pressure ($p\text{H}_2\text{O}$, in atm) was calculated from *in situ* temperature (T_{is} , in °C) according to Cooper et al. (1998) assuming a 0.3 % decrease between $p\text{CO}_2^{\text{atm}}$ and $f\text{CO}_2^{\text{atm}}$ to be sufficiently accurate (Weiss 1974).

$$p\text{CO}_2^{\text{atm}} = x\text{CO}_2^{\text{atm}} \times (p_{\text{atm}} - p\text{H}_2\text{O}) \quad (1)$$

$$p\text{H}_2\text{O} = 0.981 \exp\{14.32602 - 5306.83/(273.15 + T_{\text{is}})\} \quad (2)$$

2.2 Remotely Sensed Data

SST data were used from MODIS on board the Aqua satellite and AVHRR on board the NOAA Metop-A satellite. Advanced Scatterometer (ASCAT) coastal data products (at a spatial resolution of 12.5 km) were taken from KNMI OSI-SAF data repository for the estimation of wind speed in order to compute gas transfer velocity.

Daily Level-2 SST data of MODIS and AVHRR Level-1B Local Area Coverage (LAC) data set (at a spatial resolution of 1 km) were used for deriving monthly average during the period of our study. These monthly averaged SST data were used to assess $f\text{CO}_2$ water from SST using empirical relationship. The monthly composite level 3 MODIS data were used from the year 2002–2003 to 2011–2012 to evaluate winter-to-winter (average of November, December, January and February) change of $f\text{CO}_2$ water in decadal scale.

To assess the air-sea CO_2 flux, it is necessary to calculate the Ostwald solubility coefficient (β) and gas transfer velocity (k) along with $f\text{CO}_2$ of air and water. Among the parameters, β is the function of sea surface salinity (SSS) and SST, whereas k is the function of wind speed. As there is a dearth of remotely sensed data of SSS or they are available having coarse resolution, the in situ measured SSS has been interpolated within the selected study area in order to calculate the required β . The $f\text{CO}_2$ air was obtained from the linear interpolation of the in situ data ($n = 64$). Finally all the satellite derived data sets acquired at different resolution and the interpolated in situ data were resampled to a spatial resolution of 1100 m.

2.3 Empirical Relationship Between $f\text{CO}_2$ Water and Its Control

The primary driving force behind the ocean CO_2 uptake is the gradient of CO_2 levels (air-sea $f\text{CO}_2$ difference) between the ocean surface waters and the atmosphere. Key factors controlling this gradient are the solubility of CO_2 which is higher for cooler waters. Biological activities such as phytoplankton taking up CO_2 through photosynthesis and organisms releasing CO_2 through respiration also regulate the potential of surface absorption of CO_2 . These phenomena are described as physical pumps and biological pumps, respectively (Bates et al. 1998a, b; Hardman-Mountford et al. 2009; Sweeney 2002).

Amongst the possible control of $f\text{CO}_2$, only significant correlation was found between $f\text{CO}_2$, water and SST.

The regression equation established is as follows:

$$f\text{CO}_2 = 19.65 \times \text{SST} - 196.93 \quad (R^2 = 0.55, n = 64) \quad (4)$$

No significant correlation between $f\text{CO}_2$ of water and chlorophyll-*a* is justified as it was also observed by de la Paz et al. (2009) in the inner shelf of Loire Estuary. While working in the Ria de Vigo and adjacent shelf of northwestern Iberian Peninsula, Álvarez et al. (1999) experienced a similar trend and stated that as chlorophyll-*a* is affected by the sedimentation process and grazing, it should not be considered as a conservative parameter. This observation was also previously reported by Stephens et al. (1995) and Ono et al. (2004). Our study area, i.e. the northern Bay of Bengal, is severely affected by the sedimentation process and hence, this observation is quite relevant in this regard.

2.4 Estimation of Air-Sea CO₂ Flux

Flux (FCO_2 in $\mu\text{mol m}^{-2} \text{h}^{-1}$) across the air-sea was calculated according to the expression

$$FCO_2 = k \times \beta \times \Delta fCO_2 \quad (5)$$

where 'k' is the Gas Transfer Velocity (cm h^{-1}), 'β' is the Ostwald Solubility Coefficient ($\text{mol m}^{-3} \text{atm}^{-1}$) (Wanninkhof 1992) and ΔfCO_2 is the difference in partial pressure in CO₂ between water and air [fCO_2 (water) – fCO_2 (air)]. Gas transfer velocity 'k' (cm h^{-1}) was calculated according to the formula

$$k = 0.17 \times u_{10} \left(\frac{660}{Sc} \right)^{\frac{2}{3}} \quad \text{for } u_{10} \leq 3.6 \text{ ms}^{-1} \quad (6)$$

$$k = (2.85 \times u_{10} - 9.65) \left(\frac{660}{Sc} \right)^{0.5} \quad \text{for } 3.6 \leq u_{10} \leq 13 \text{ ms}^{-1} \quad (7)$$

where u_{10} is in m s^{-1} and the Schmidt number for CO₂ was evaluated as per the formula

$$Sc = A - Bt + Ct^2 - Dt^3 \quad (8)$$

where $A = 1992.1$, $B = 121.86$, $C = 3.54$, $D = 0.04227$ and t ($^{\circ}\text{C}$) = Temperature of water (Liss and Merlivat 1986). β was calculated according to the formula

$$\ln \beta = A_1 + A_2 \left(\frac{100}{T} \right) + A_3 \ln \left(\frac{T}{100} \right) + S \times \left[B_1 + B_2 \left(\frac{T}{100} \right) + B_3 \left(\frac{T}{100} \right)^2 \right] \quad (9)$$

where $A_1 = -60.2409$, $A_2 = 93.4517$, $A_3 = 23.3585$, $B_1 = 0.023517$, $B_2 = -0.023656$, $B_3 = 0.0047036$ and T = water temperature in Kelvin and S = salinity. Positive magnitude of FCO_2 interprets flux from water to air and vice versa.

3 Results and Discussion

3.1 Validation of fCO_2 (Water)

The negative ΔfCO_2 values indicate that the entire study area acted as a sink for atmospheric CO₂ during the winter season. Furthermore as atmospheric fCO_2 remained within a relatively narrow range ($380 \pm 9 \mu\text{atm}$), it could be ascertained that the ΔfCO_2 variation was controlled primarily by the fCO_2 of surface water as observed by Chou et al. (2011) in the East China Sea during the winter months.

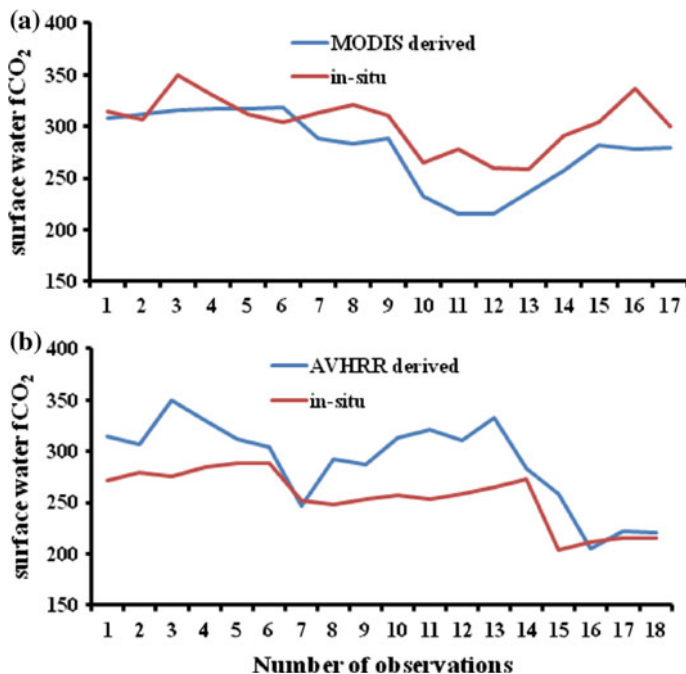


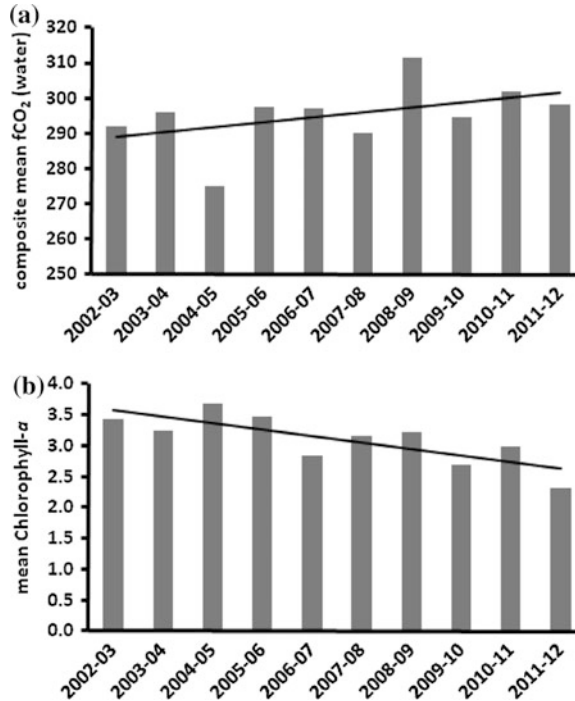
Fig. 2 Comparison between in situ and **a** MODIS and **b** AVHRR derived $f\text{CO}_2$ (water) (in μatm)

As $f\text{CO}_2$ water is the prime controlling parameter of air-sea CO_2 flux in this study, hence, the $f\text{CO}_2$ water values obtained from MODIS and AVHRR was validated with the suitable *in situ* data (Fig. 2). The *in situ* data used for validation were taken only within ± 1 h temporal interval of the satellite pass time (17 data out of 64 observations). The R^2 and RMSE of the AVHRR derived $f\text{CO}_2$ was found to be 0.64 and 48 μatm , whereas in case of MODIS, R^2 was 0.65 and RMSE was 41 μatm which indicates that MODIS is slightly better implementable for this study in this geo-specific region.

3.2 Decadal Change of $f\text{CO}_2$ (Water)

The long-term variability of the mean surface water $f\text{CO}_2$ in the northern coastal waters of the Bay of Bengal during the winter months was estimated assuming that the empirical relationship found holds true for the winter months of the last decade (2002–2003 to 2011–2012). The monthly composite satellite derived $f\text{CO}_2$ from the obtained algorithm for each of the winter months has been averaged to acquire the grand mean for every winter. In the month of January, 2005, the $f\text{CO}_2$ (water) was at its lowest (172 μatm) whereas in November, 2010, it was at its maximum

Fig. 3 Decadal change of **a** *f*CO₂ (water) (in μatm) and **b** Chlorophyll-*a* (in mg m⁻³) from 2002–03 to 2011–12 during winter



(364 μatm). A winter-to-winter increasing trend (Fig. 3a) was observed from year-wise plot of mean winter *f*CO₂ ($R^2 = 0.21, p < 0.05$). In relation to the *f*CO₂ trend, the mean surface *f*CO₂ content of the Bay of Bengal increased with a rate of 1 μatm year⁻¹ ($p < 0.05$). A significant decreasing trend (Fig. 3b) of the chlorophyll-*a* concentration in the study area was observed during the last decade ($R^2 = 0.61, p < 0.05$). Hence, the increase in *f*CO₂ (water) could be attributed to the lowering of phytoplankton biomass (chlorophyll-*a*), which in turn lowers the photosynthetic productivity.

3.3 Air-Sea CO₂ Exchange (FCO₂)

Figure 4 displays the air-sea CO₂ flux maps in the northern Bay of Bengal during winter. The computed air-sea CO₂ exchange rates show that the study area primarily acts as a sink for atmospheric CO₂ throughout the winter months; however, the influx of CO₂ from atmosphere towards the water body varied both temporally and spatially. In general the regions lying close to the shoreline acted as mild sinks as the river mouths are marked by organic matter rich freshwater having a high potential of *f*CO₂ (water) which slowly gets diluted towards the offshore upon mixing with the incoming seawater. Temporally, the sink strength of the study area increased from

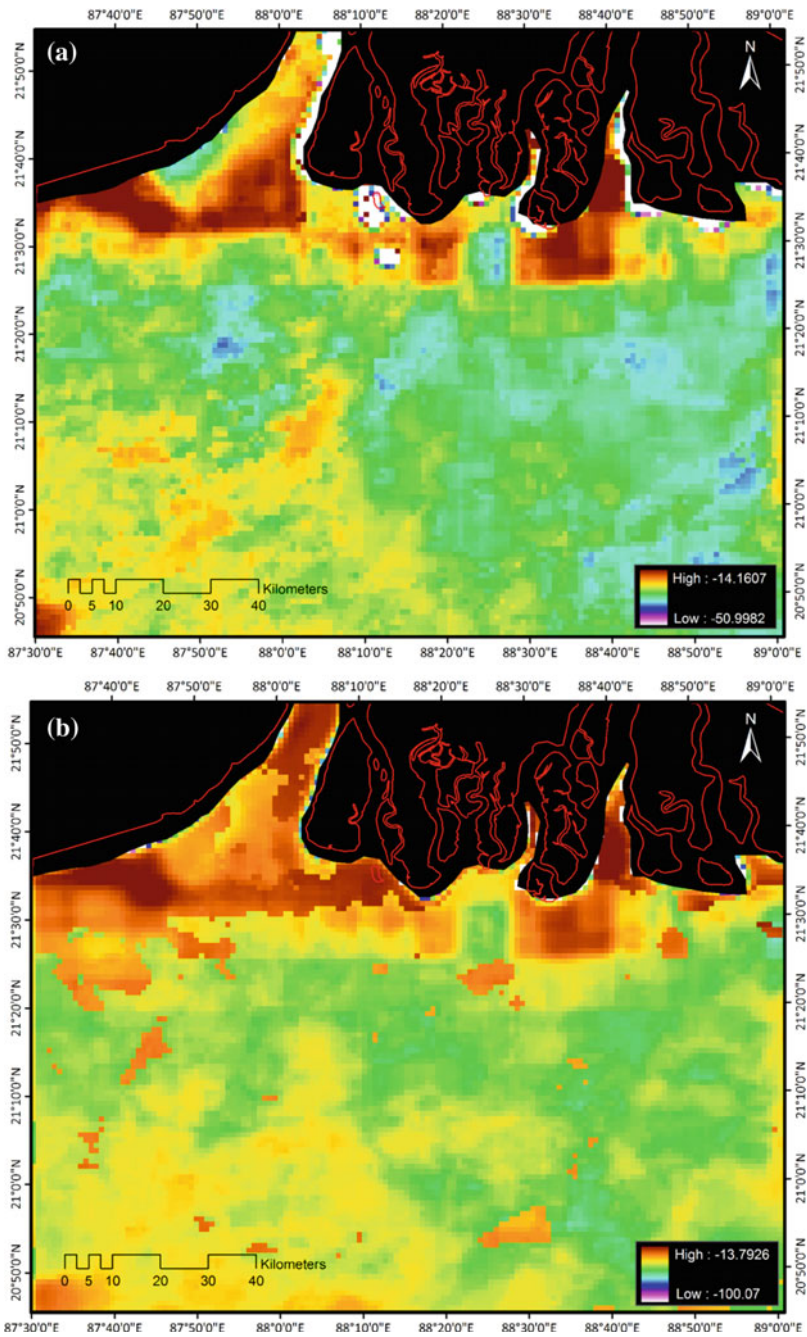


Fig. 4 Distribution of air-sea CO₂ exchange based on **a** MODIS derived $f\text{CO}_2$ and **b** AVHRR

Table 1 The AVHRR and MODIS derived mean monthly air-sea CO₂ exchange ($f\text{CO}_2$) [$\mu\text{mol m}^{-2} \text{h}^{-1}$] computed for four winter months

Remotely sensed data	November, 2011 Mean \pm S.D (range)	December, 2011 Mean \pm S.D (range)	January, 2012 Mean \pm S.D (range)	February, 2012 Mean \pm S.D (range)
AVHRR	-16 ± 11 (-1 to -117)	-47 ± 13 (-1 to -85)	-62 ± 17 (-3 to -157)	-43 ± 14 (-2 to -125)
MODIS	-7 ± 6 (-3 to -122)	-28 ± 7 (-1 to -74)	-43 ± 13 (-2 to -103)	-32 ± 10 (-1 to -126)

November till January and then it started degrading again. The highest rate of CO₂ exchange was observed in the month of January while November marked the lowest. Though the variation of air-sea CO₂ exchange followed the same trend, a discrepancy was observed between the MODIS and the AVHRR derived data. AVHRR derived fluxes were always higher than the MODIS derived ones with the highest difference being observed in the month of December (Table 1).

As a whole, the study area acted as a net sink for CO₂ at a rate of $-28 \mu\text{mol m}^{-2} \text{h}^{-1}$ (MODIS derived) to $-40 \mu\text{mol m}^{-2} \text{h}^{-1}$ (AVHRR derived). No previous data set on the Bay of Bengal, off the coast, related to the $f\text{CO}_2$ dynamics and its exchange with atmosphere is available in the literature. Hence, it is quite difficult to compare our findings with any observation from the past. In comparison with other recent studies in coastal seas, it can be concluded that the sink potential of the present study area was found to be weak. Chou et al. (2011) observed an average seaward flux of $-570 \pm 237 \mu\text{mol C m}^{-2} \text{h}^{-1}$ in the East China Sea, while the north eastern shelf of the Gulf of Cádiz acted as a source of CO₂ at the rate of $42 \mu\text{mol m}^{-2} \text{h}^{-1}$ during winter. Seasonal along with interannual studies need to be conducted to get a complete scenario.

Acknowledgments Authors are grateful to the National remote sensing Centre, (NRSC) Department of Space, Government of India for funding the research work. Abhra Chanda is grateful to the Department of Science and Technology, Govt. of India for providing the INSPIRE fellowship.

References

- Álvarez M, Fernández E, Pérez FF (1999) Air-sea CO₂ fluxes in a coastal embayment affected by upwelling: Physical versus biological control. *Oceanol Acta* 22(5):499–515
- Akhand A, Chanda A, Dutta S, Hazra S (2012) Air-water carbon dioxide exchange dynamics along the outer estuarine transition zone of Sundarban, northern Bay of Bengal, India. *Indian J Geo-Mar Sci* 41(2):111–116
- Akhand A, Chanda A, Dutta S, Manna S, Hazra S, Mitra D, Rao KH, Dadhwal VK (2013) Characterizing air-sea CO₂ exchange dynamics during winter in the coastal water off Hugli-Matla estuarine system in the northern Bay of Bengal. *J Oceanogr, India*. doi:[10.1007/s10872-013-0199-z](https://doi.org/10.1007/s10872-013-0199-z)

- Bates NR, Hansell DA, Carlson CA, Gordon LI (1998a) Distribution of CO₂ species, estimates of net community production, and air-sea CO₂ exchange in the Ross Sea polynya. *J Geophys Res* 103:2883–2896
- Bates NR, Takahashi T, Chipman DW, Knapp AH (1998b) Variability of pCO₂ on diel to seasonal time scales in the Sargasso Sea. *J Geophys Res* 103:15567–15585
- Biswas H, Mukhopadhyay SK, De TK, Sen S, Jana TK (2004) Biogenic controls on the air-water carbon dioxide exchange in the Sundarban mangrove environment, northeast coast of Bay of Bengal, India. *Limnol Oceanogr* 49(1):95–101
- Borges AV, Frankignoulle M (2002) Distribution and air-water exchange of carbon dioxide in the Scheldt plume off the Belgian coast. *Biogeochem* 59:41–67
- Cai W-J (2003) Riverine inorganic carbon flux and rate of biological uptake in the Mississippi River plume. *Geophys Res Lett* 30(2):1032. doi:[10.1029/2002GL016312](https://doi.org/10.1029/2002GL016312)
- Canadell JG, Quere C, Raupach MR, Field CB, Buitenhuis ET, Ciais P, Conway TJ, Gillett NP, Houghton RA, Marland G (2007) Contributions to accelerating atmospheric CO₂ growth from economic activity, carbon intensity, and efficiency of natural sinks. *Proc Nat Acad Sci USA* 104:18870–18886
- Carr ME (2001) Remote Sensing tools to study ocean biogeochemistry, The state of the art, Sessao Especial-Workshops, Anais X SBSR, Foz do Iguacu, 21–26, INPE, pp 779–784
- Chen L, Xu S, Gao Z, Chen H, Zhang Y, Zhan J, Li W (2011) Estimation of monthly air-sea CO₂ flux in the southern Atlantic and Indian Ocean using in-situ and remotely sensed data. *Remote Sens Environ* 115:1935–1941
- Chou WC, Gong GC, Tseng CM (2011) The carbonate system in the East China Sea in winter. *Mar Chem* 123:44–55
- Cooper DJ, Watson AJ, Ling RD (1998) Variation of pCO₂ along a North Atlantic shipping route (U.K. to Caribbean): a year of automated observations. *Mar Chem* 60:147–164
- Cole CV, Vaidyaraman PP (1966) Salinity distribution and effect of freshwater flows in the Hooghly River. Paper presented Proceedings Tenth Conference on Coastal Engineering, Tokyo (American Society of Civil Engineers, New York) pp 1312–1434
- De Grandpre MD, Olbu GJ, Beatty CM, Hammar TR (2002) Air-sea CO₂ fluxes on the US middle Atlantic bight. *Deep-Sea Res II* 49:4355–4367
- De la Paz M, Gómez-Parra A, Forja J (2009) Seasonal variability of surface fCO₂ in the Strait of Gibraltar. *Aquat Sci* 71(1):55–64
- Doney SC, Tilbrook B, Roy S, Metzl N, Le Quere C, Hood M, Feely RA, Bakker D (2009) Surface-ocean CO₂ variability and vulnerability. *Deep-Sea Res II* 56:504–511
- Grasshoff K (1983) Determination of nutrients. In: K. Gras-shoff, M. Ehrhard, K. Kremling [eds.], *Methods of seawater analysis*. Verlag Chemie, pp 125–187
- Hardman-Mountford N, Litt E, Mangi S, Dye S, Schuster U, Bakker D, Watson A (2009) Ocean uptake of carbon dioxide (CO₂). MCCIP Briefing Notes www.mccip.org.uk. Accessed 29 March 2015
- Khoo KH, Ramette RW, Culbertson CH, Bates RG (1977) Determination of hydrogen ion concentrations in seawater from 5 to 40 °C: standard potentials at salinities from 20 to 45%. *Anal Chem* 49(1):29–34
- Laruelle GG, Dürr HH, Slomp CP, Borges AV (2010) Evaluation of sinks and sources of CO₂ in the global coastal ocean using a spatially-explicit typology of estuaries and continental shelves. *Geophys Res Lett* 37:L15607. doi:[10.1029/2010GL043691](https://doi.org/10.1029/2010GL043691)
- Lewis E, Wallace DWR (1998) Program developed for CO₂ system calculations. ORNL/CDIAC—105. Carbon Dioxide Information Analysis Center, Oak Ridge National Laboratory, U.S. Department of Energy, Oak Ridge, Tennessee
- Liss PS, Merlivat L (1986) Air sea gas exchange rates: Introduction and synthesis. In: Buat-Menard P (ed) *The role of air sea exchange in geochemical cycling*, D. Reidel, Dordrecht, Holland, pp 113–129
- Lohrenz SE, Cai WJ (2006) Satellite ocean color assessment of air–sea fluxes of CO₂ in a river-dominated coastal margin. *Geophys Res Lett* 33:L01601. doi:[10.1029/2005GL023942](https://doi.org/10.1029/2005GL023942)

- Mackenzie FT, Ver LM, Lerman A (2000) Coastal-zone biogeochemical dynamics under global warming. *Int Geol Rev* 42:193–206
- Mukhopadhyay SK, Jana TK, De TK, Sen S (2000) Measurement of exchange of CO₂ in mangrove forest of Sundarbans using micrometeorological method. *Trop Ecol* 41(1):57–60
- Mukhopadhyay SK, Biswas H, De TK, Sen S, Jana TK (2002) Seasonal effects on the air–water carbon dioxide exchange in the Hooghly estuary, NE coast of Bay of Bengal, India. *J Environ Monit* 4:549–552
- Olsen A, Trinanes JA, Wanninkhof R (2004) Sea-air flux of CO₂ in the Caribbean Sea estimated using in-situ and remote sensing data. *Remote Sens Environ* 89:309–325
- Ono T, Saino T, Kurita N, Sasaki K (2004) Basin-scale extrapolation of shipboard pCO₂ data by using satellite SST and Chl a. *Int J Remote Sens* 25:3803–3815
- Parsons TR, Maita Y, Lalli CM (1992) A manual of chemical and biological methods for sea water analysis. Pergamon Press, New York
- Peng TH, Takahashi T, Broecker WS, Olafsson J (1987) Seasonal variability of carbon dioxide, nutrients and oxygen in the northern North Atlantic surface water: observations and a model. *Tellus* 39B:439–458
- Sabine CL, Feely RA, Gruber N, Key RM, Lee K, Bullister JL, Wanninkhof R, Wong CS, Wallace DW, Tilbrook B, Millero FJ, Peng TH, Kozyr A, Ono T, Rios AF (2004) The oceanic sink for anthropogenic CO₂. *Science* 305:367–371
- Shetye SR, Shenoi SSC, Gouveia AD, Michael GS, Sundar D, Nampoothiri G (1991) Wind driven coastal upwelling along the western boundary of the Bay of Bengal during southwest monsoon. *Cont Shelf Res* 11:397–408
- Stephens MP, Samuels G, Olson DB, Fine RA (1995) Sea-air flux of CO₂ in the North Pacific using shipboard and satellite data. *J Geophys Res* 100:13571–13583
- Sweeney C (2002) The annual cycle of surface water CO₂ and O₂ in the Ross Sea: A model for gas exchange on the continental shelves of Antarctic: Biogeochemistry of the Ross Sea. *Antarct Res Ser* 78:295–312
- Takahashi T, Sutherland S, Wanninkhof R, Sweeney C, Feely RA, Chipman DW, Hales B, Friederich G, Chavez F, Sabine C, Watson A, Bakker DCE, Schuster U, Metzi N, Yoshikawa-Inoue H, Ishii M, Midorikawa T, Nojiri Y, Körtzinger A, Steinhoff T, Hoppema M, Ollafson J, Arnarson TS, Tilbrook B, Johannessen T, Olsen A, Bellerby R, Wong CS, Delille B, Bates NR, de Baar HJW (2009) Climatological mean and decadal change in surface ocean pCO₂, and net sea–air CO₂ flux over the global oceans. *Deep-Sea Res II* 56:554–577
- Wanninkhof R (1992) Relationship between wind speed and gas exchange over the ocean. *J Geophys Res* 97:7373–7382
- Weiss RF (1974) Carbon dioxide in water and seawater. The solubility of a nonideal gas. *Mar Chem* 2:201–215
- Zhai WD, Dai MH, Cai WJ, Wang YC, Wang ZH (2005) High partial pressure of CO₂ and its maintaining mechanism in a subtropical estuary: The Pearl River estuary, China. *Mar Chem* 93:21–32

Identification of River Discontinuity Using Geo-Informatics to Improve Freshwater Flow and Ecosystem Services in Indian Sundarban Delta

Tuhin Bhadra, Anirban Mukhopadhyay and Sugata Hazra

Abstract The Indian Sundarban Delta (ISD) situated on the western tide-dominated part of the Ganges–Brahmaputra–Meghna delta, was formed by the sedimentation of the river Ganges and its tributaries. It is crisscrossed by several interlinked channels. Most of these rivers which used to nourish the delta have become defunct with the passage of time. To ensure sustainable flow and to enhance the flow-dependent ecosystem services in this region, the identification of the disconnected river reaches and their restoration is required. Keeping these perspectives in mind, this study has been conducted to identify the discontinuities in the flow paths of some major rivers using multispectral satellite imageries in geo-informatics platform. To extract the river network from the Landsat Thematic Mapper (TM) images, the water indexes like Normalized Difference Water Index (NDWI) and Modified Normalized Difference Water Index (MNDWI) have been calculated. These indexes use the differential spectral reflectance of water sensitive near-infrared and shortwave-infrared band with green band to identify the derelict paths. The spectral profiles of near-infrared band across these discontinuous stretches have been compared and validated with field data to map the actual blockages. The study reveals that the rivers Ichhamati, Jamuna, Bidyadhari, Noai, Suti, Kumarjol, Ghagramari, Karati, and Matla have been disconnected from their parent rivers and their courses are frequently interrupted by natural and man-made obstructions. River Adi Ganga is discontinuous in its middle stretches. The decayed river channels have been converted into ponds, agricultural fields, or aquaculture farms and have also been encroached by settlements. Restoration of these decayed channels may revitalize the river network and enhance the benefits of flow-dependent ecosystem services in the ISD.

Keywords Indian Sundarban delta · River discontinuity · Geo-informatics · NDWI · MNDWI

T. Bhadra (✉) · A. Mukhopadhyay · S. Hazra
School of Oceanographic Studies, Jadavpur University, 188 Raja S.C. Mallick Road
Jadavpur, Kolkata 700032, West Bengal, India
e-mail: tuhinbhadra.ju@gmail.com

1 Introduction

River network is the major controller of the earth surface. Discontinuities in the network restrict free flow of water and sediment and control river shape and function (Burchsted et al. 2014). River connectivity has an ecological importance to maintain the habitat quality of in stream and riparian biota. The concept of discontinuity and the importance of connectivity in a riverine system are well established in the ecological literature (Ward 1989; Pringle 2001, 2003; McGinness et al. 2002; Poole 2002; Ward et al. 2002; Jenkins and Boulton 2003; Tetzlaff et al. 2007; Fryirs 2013; Wohl and Beckman 2014). Apart from the ecologists, geomorphologists also describe the connectivity as sediment connectivity (Fryirs et al. 2007; Wohl and Beckman 2014) which explains the transfer of sediment between compartments in a river network (Fryirs 2013).

From the hydrological point of view, the connectivity represents free flow of water and water-driven energy, material and organism (Kondolf et al. 2006; Bracken and Croke 2007; Wohl and Beckman 2014). Fryirs (2013) describes three type of connectivity in a fluvial system. These are longitudinal connectivity (upstream–downstream connectivity), lateral connectivity (river–floodplain connectivity) and vertical connectivity (river–groundwater connectivity). The spatial extension of discontinuous stretches within a river change temporally. A large scale discontinuity may spatially be extended up to 10 km with a temporal extension of 10^5 years (Ouimet et al. 2007; Korup et al. 2010). The small scale discontinuities occur frequently with a spatial extension of less than 10 m and may exist 0 to 10 years (Burchsted et al. 2010, 2014; Wohl and Beckman 2014). Human activities have an intense impact on riverine connectivity. The construction of bridge and road over channel, conversion of decayed channel into agricultural field and encroachment of channel by settlement and fisheries discriminate the channel condition by altering its morphological and hydrological regime.

This paper focuses on the longitudinal connectivity of the rivers that used to nourish the Indian Sundarban Delta (ISD) with freshwater flow. The delta hosts the world's most unique mangrove ecosystem. Most of the rivers in the delta have disconnected from their upstream sources with the passage of time (Bhadra 2013; Bhadra et al. 2013; Gole and Vaidyaraman 1966; Gopal and Chauhan 2006; Hazra et al. 2015a, b). These disconnected river reaches have been identified using remotely sensed images and verified by field survey. To identify the disconnected areas, different water indexes have been run on multispectral satellite images. The spectral profiles of water sensitive near-infrared (NIR) band across the discontinuous reaches have been generated to demarcate the actual blockages. Identification of the disconnected reaches is essential to restore the river network. Restoration of this decayed network may revitalize the downstream ecosystem function and services by providing environmental flows within these river channels (Hazra et al. 2015a, b).

2 The Study Area and the Rivers

The ISD was formed during 11,000–3000 cal year BP (Goodbred and Kuehl 2000; Allison et al. 2003) by the sedimentation of the Ganges and its tributaries. The ISD is bounded by the river Hugli in the west and the International boundary between India and Bangladesh which more or less follows the Ichhamati–Raimangal–Harinbhanga river system in the east, the *Dampier-Hodges line* in the north and the Bay of Bengal in the south (Fig. 1). The geomorphology of this delta is unique with its vast alluvial plane, intricate river network, scattered meander cut-offs, abandoned paleo-channels and the world’s largest trans-boundary mangrove swamps, the Sundarban (Rudra 2014). The river system of the dynamic delta is formed by the distributary network, anabranching and avulsive channels that change their course with the development of the delta. The decay and rejuvenation of the river system depend on the availability of the upstream freshwater flow. Beside this, the huge number of population of the delta has an adverse effect that modifies the river channels from time to time.

The major rivers that used to nourish the delta are the Ichhamati, the Jamuna, the Bidyadhari–Kulti Gang–Matla system and the Adi Ganga (Fig. 3). The river Ichhamati takes off from the river Mathabhanga–Churni at Majhdia (23°24'15.55" N, 88°42'37.59"E) in the Nadia district and after flowing for 208 km towards south, it joins the river Kalindi near Hasnabad in the North 24 Parganas district (Fig. 3). The river Jamuna takes off from the river Hugli near Tribeni (22°59'24.95"N, 88° 24'33.78"E) (Fig. 3) in the Nadia district. Thereafter it flows towards east in a zigzag way and joins the river Ichhamati near Tipighat (22°50'31.08"N, 88°50' 31.57"E) (Fig. 3) in the North 24 Parganas district. The origin of the river Bidyadhari is not traceable at present. According to Rudra (2014), the river originates from the Mathura bill near Kalyani in the Nadia district. The river Nona, Suti, and Noai are three major tributaries of the river Bidyadhari. The river

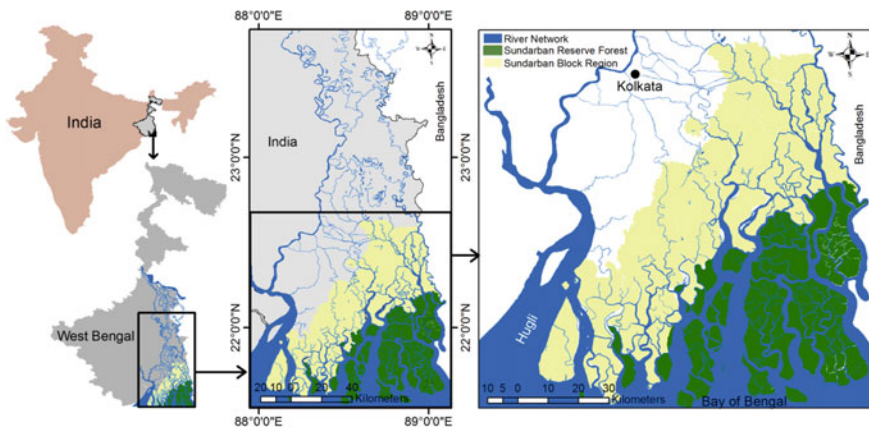


Fig. 1 Location of the study area

bifurcates at Tehatta ($22^{\circ}37'57.80''\text{N}$, $88^{\circ}37'35.72''\text{E}$) in the North 24 Parganas district. The western branch of the river used to discharge into the river Matla till the first half of the twentieth century whereas the eastern branch discharges into the river Kulti Gang (Rudra 2014). The Kumarjol Gang and the Ghagramari used to take off from the river Kulti Gang (Western arm of the river Bidyadhari) near Kulti ($22^{\circ}31'14.86''\text{N}$, $88^{\circ}41'28.27''\text{E}$) and Malancha ($22^{\circ}29'4.58''\text{N}$, $88^{\circ}47'9.68''\text{E}$) in the South 24 Parganas district respectively (Fig. 3). These two rivers joined to form the river Karatia near Kumarjol ($22^{\circ}28'41.54''\text{N}$, $88^{\circ}43'32.85''\text{E}$) (Fig. 3). The river Karatia was one of the major upstream sources of the river Matla. The river Jamuna and Bidyadhari were two major delta builder rivers as they largely contributed to raise the land of the Sundarban and the land to the east of the Kolkata respectively (Majumdar 1941). The river Adi Ganga takes off from the river Hugli at Garden reach ($22^{\circ}33'2.19''\text{N}$, $88^{\circ}19'29.04''\text{E}$) in Kolkata (Fig. 3). Thereafter it flows towards south–south east direction. Its degraded course is traceable up to Surjyapur ($22^{\circ}17'49''\text{N}$, $88^{\circ}27'43''\text{E}$) (Fig. 3) in the South 24 Parganas district (Bandyopadhyay 1996).

Though the river Bhagirathi–Hugli is the main river in deltaic West Bengal, it has an insignificant contribution in feeding the Sundarban as very little water from the river enters into the Sundarban via the river Muriganga and the Hataniya Doaniya channel. The connections of the river Ichhamati with the Ganga–Padma system and the river Jamuna–Bidyadhari–Adi Ganga with the Bhagirathi–Hugli system have been lost. The main flow of the river Ganges used to move through the course of the river Bhagirathi–Hugli till the end of the fifteenth century till the flooded Ganges started to get diverted along the Padma channel (Hist 1915). The eastward shifting of the Ganges flow commenced the decay of the river Bhagirathi–Hugli along with its three distributaries namely the Saraswati, the Jamuna–Bidyadhari, and the Adi Ganga.

The condition of the river Bhagirathi–Hugli has improved after the construction of the Farakka Barrage and the subsequent feeder canal in 1975. But the artificially recharged water was not enough to rejuvenate the three major distributaries which have been decayed with the passage of time. Losing the upstream discharge the character of these rivers is now maintained by the monsoonal runoff alone (Gole and Vaidyaraman 1966; Gopal and Chauhan 2006). They have also lost their glorious history as major navigational rout after their decay.

3 Material and Methods

Remote sensing techniques are widely used to map land surface water body all over the world. The thematic water body information extraction method which includes the thresholding of single band and the combination of multiple bands to distinguish the water body from the land surface (Rundquist et al. 1987; Li et al. 2013) has been used in the present study. Calculations of different water indexes

(Mcfeeters 1996; Xu 2006; Ji et al. 2009) have been performed by combining the water sensitive bands to identify the discontinuities.

Four Landsat TM images of 2010 (Path and Row Combination: 139/43, 138/43, 138/44 and 138/45) have been downloaded from the USGS server and used to identify the disconnected river reaches in this study. Before running the water index models on these images, the top-of-atmosphere (TOA) reflectance has been estimated as it gives better result than at-sensor spectral radiance (Li et al. 2013) (Fig. 2). The TOA reflectance has been obtained using the formula given below (Chander et al. 2009)

$$\rho_{\lambda} = \frac{\pi * L_{\lambda} * d^2}{ESUN_{\lambda} * \cos \theta_s}$$

where ρ_{λ} is the unit less TOA reflectance or planetary reflectance, L_{λ} is the spectral radiance at the sensor's aperture [Watts/(m²*ster* μ m)], d is the earth–sun distance in astronomical units, $ESUN_{\lambda}$ is mean exo-atmospheric solar irradiance [Watts/(m²* μ m)] and θ_s is the solar zenith angle in degrees.

Two water index methods namely McFeeters's Normalized Difference Water Index (NDWI) and Xu's Modified Normalized Difference Water Index (MNDWI) have been run on these corrected images to extract the water bodies and identify the disconnected reaches of the rivers (Fig. 2). Both of these two models utilize the green band (wave length: 0.520–0.600 μ m), water sensitive near-infrared (NIR) band (wave length: 0.520–0.600 μ m), and the short wave infrared (SWIR) band (wave length: 0.520–0.600 μ m). The green wavelength maximizes the reflectance of water body whereas the NIR and SWIR wavelengths are mostly absorbed by water body. McFeeters's NDWI model enhances the water body by contrasting the reflectance of the green and the NIR band. It also takes the advantage of the high

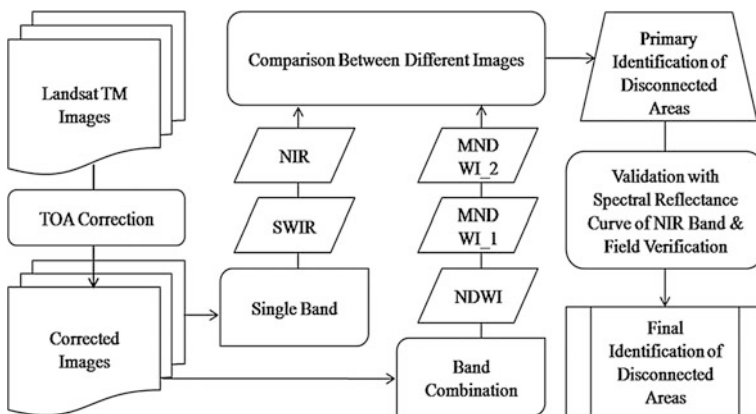


Fig. 2 Methodological framework for Identification of the disconnected river reaches

reflectance in the NIR of vegetation and soil features to restrict the background information (Li et al. 2013). McFeeters's NDWI (McFeeters 1996) is defined as

$$NDWI = \frac{\rho_{Green} - \rho_{NIR}}{\rho_{Green} + \rho_{NIR}} = \frac{Band2 - Band4}{Band2 + Band4} \text{ (For Landsat TM)}$$

where, ρ_{Green} is the reflectance of the green band and ρ_{NIR} is the reflectance of the NIR band.

As built-up features cannot be properly distinguishable from water body using McFeeters's NDWI model, Xu's MNDWI model has been used. Xu's MNDWI model utilizes the reflection difference of the green and the SWIR band to delineate the water body. Xu's MNDWI (Xu 2006) is defined as

$$MNDWI = \frac{\rho_{Green} - \rho_{SWIR}}{\rho_{Green} + \rho_{SWIR}}$$

$$MNDWI_1 = \frac{Band2 - Band5}{Band2 + Band5} \&$$

$$MNDWI_2 = \frac{Band2 - Band7}{Band2 + Band7} \text{ (For Landsat TM)}$$

where, ρ_{SWIR} is the reflectance of the SWIR band.

In this study, the model outcomes of NDWI, MNDWI_1 and MNDWI_2 of Landsat TM images have been compared to identify the disconnected reaches of the rivers (Fig. 2). The study reveals that MNDWI_1 gives a better contrast between land and water mass than other images. Finally, the MNDWI_1 model has been used to delineate the disconnected reaches. After delineating the area of obstruction from the output images, some spectral reflectance curve of the near-infrared (NRI) band (Band 4 of Land sat TM) have been drawn in some selected reaches of the rivers to validate the areas of disconnect (Figs. 2, 4, and 5). As the NIR is absorbed by water mass, it shows a trough in the profile where water is present. The NRI absorbance curve shows a peak due to the absence of water body and the presence of vegetation in the river channel. The field verification has also been carried out in some selected reaches to validate and map the disconnected areas within the river network of the study area (Fig. 2).

4 Results

The significantly disconnected river reaches in the lower part of the deltaic West Bengal have been identified in this study. Most of these reaches are permanently disconnected while some are seasonally disconnected. These disconnected reaches restrict the fresh water flow in the downstream of the delta. The major disconnected reaches of the delta have been highlighted in Fig. 3.

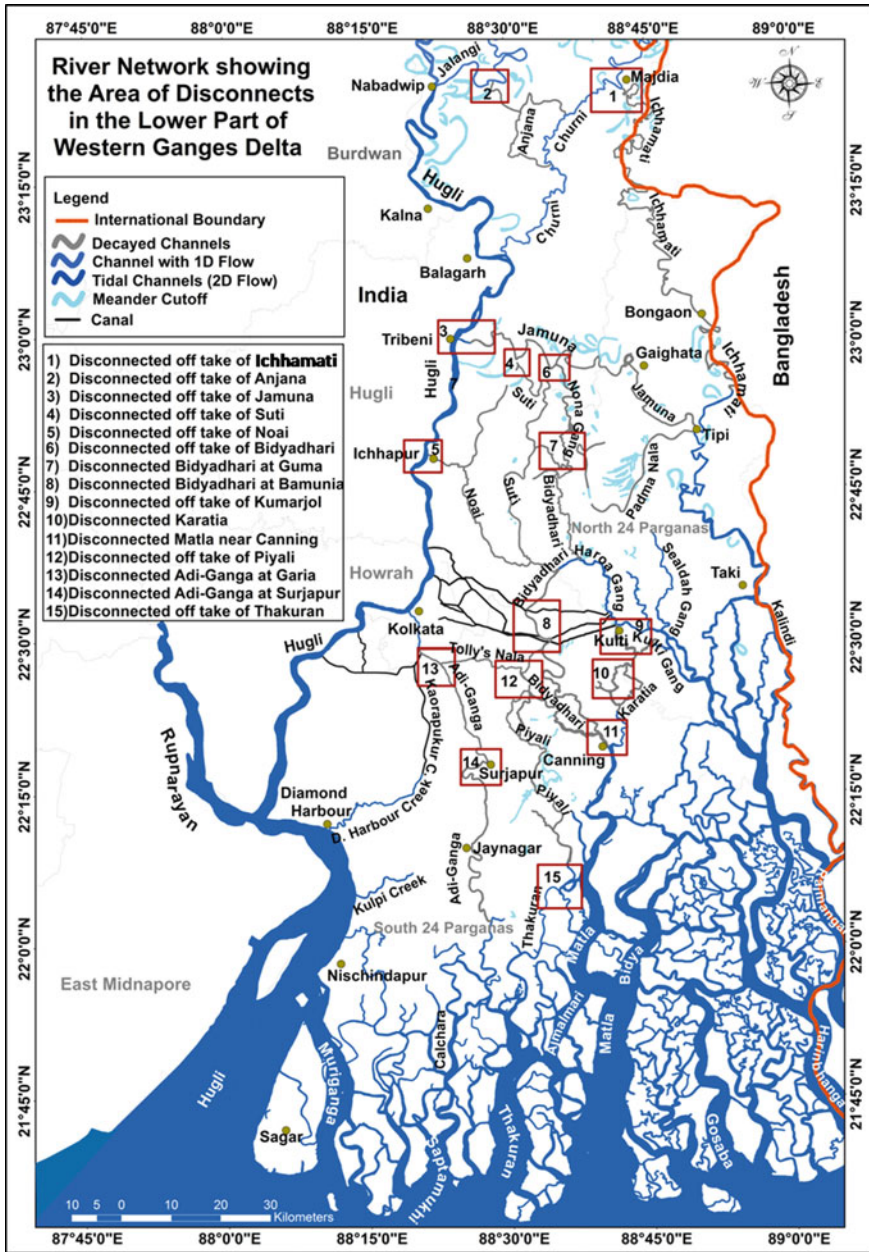


Fig. 3 River network and the disconnected areas in the surjapur part of Western Ganges Delta

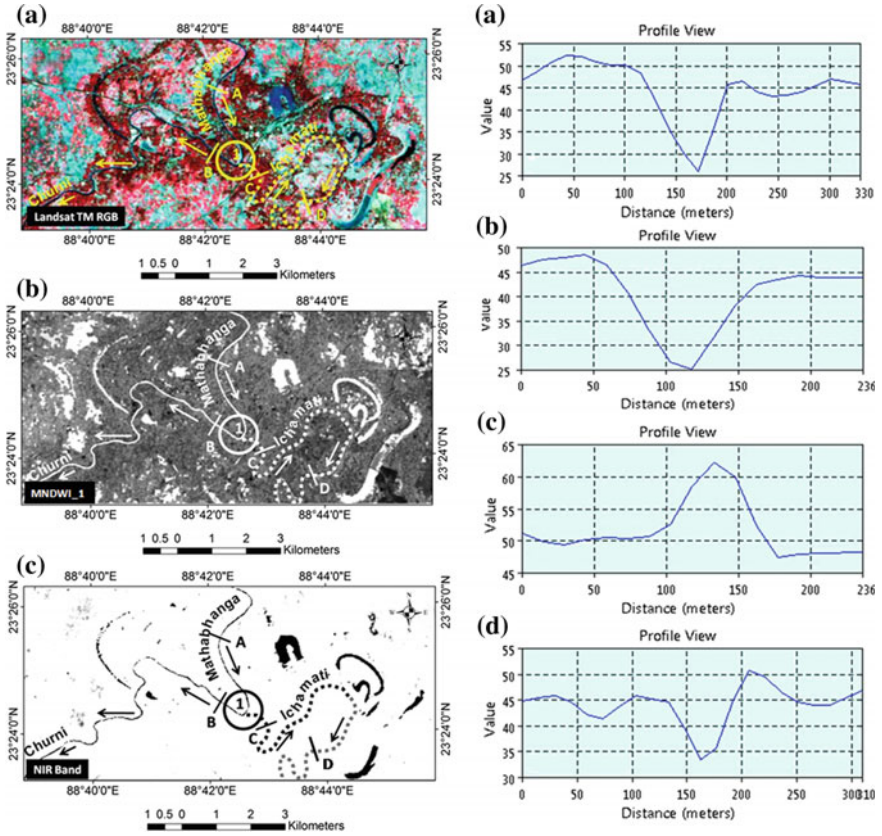


Fig. 4 RGB of land sat TM image **a**, MNDWI_1 **b** and NIR Band **c** of disconnected Reach-2. Graph 2A, 2B, 2C, and 2D are the spectral reflectance curve of NRI band of profile A, B, C, and D, respectively

The study reveals that the bed of the river Ichhamati is dry near its off-take point at Majdia (23°24'15.55"N, 88°42'37.59"E) (Figs. 3 and 4) and thereafter the river is frequently discontinuous up to 55 km downstream from its off-take. The river Jamuna is distinguishable up to a few kilometers from its off-take (22°59'27"N, 88°24'35"E) and thereafter its decayed course has been transformed into agricultural fields in a stretch from Candmari (22°59'17"N, 88°27'39"E) to Alaipur (23°0'8.76"N, 88°28'32.17"E) (Gray dotted line in Fig. 5c). The channel has become abandoned after Aliapur (Black dotted line in Fig. 5c). The course of the river Bidyadhari is not traceable up to Hijli (22°50'41"N, 88°36'31"E) which is located 17 km downstream from its off-take point near the Haringhata. The channel is further discontinuous up to 7 km downstream of Hijli. The upper 20 km of the western branch of the river Bidyadhari has mainly been encroached by fisheries and its lower 40 km up to its outfall at the river Matla has almost dried up (Fig. 3). Both of the rivers Kumarjol and

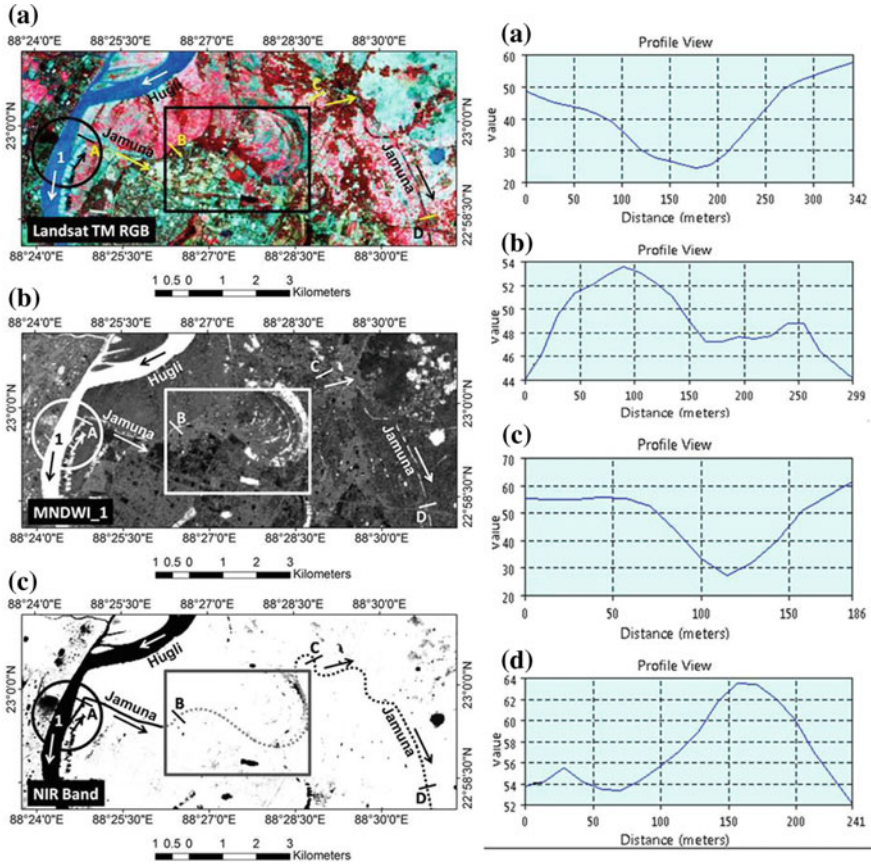


Fig. 5 RGB of Land sat TM image **a**, MNDWI_1 **b** and NIR Band **c** of disconnected Reach-3. Graph 2A, 2B, 2C, and 2D are the spectral reflectance curve of NRI band of profile A, B, C, and D, respectively

Ghagamari have been disconnected from the river Kulti Gang and the river channels have fully been decayed. A 10.5 km reach of the Kumarjol Gang from its off-take (22°31'17"N, 88°41'29"E) near Kulti to its confluence (22°28'41"N, 88°43'45"E) with the Ghagamari Khal near Joygram has completely been transformed into agricultural field (Figs. 3 and 6a). The condition of the Ghagrimary Khal is same as the Kumarjol Gang. The channel of the river Ghagamari is tidal up to 3 km downstream from its off-take point (22°29'05"N, 88°47'09"E) near Malancha. Thereafter, the course of the river Ghagamari has been converted into agricultural field up to its confluence with the river Kumarjol near Joygram (a 7.5 km reach). The course of the river Karatia is not traceable properly. From its origin to its confluence (22°19'45"N, 88°40'48"E) with the river Matla, the 25 km long river channel has been transformed into agricultural field in its upper reach and encroached by fisheries in its lower reach (Figs. 3 and 6b).

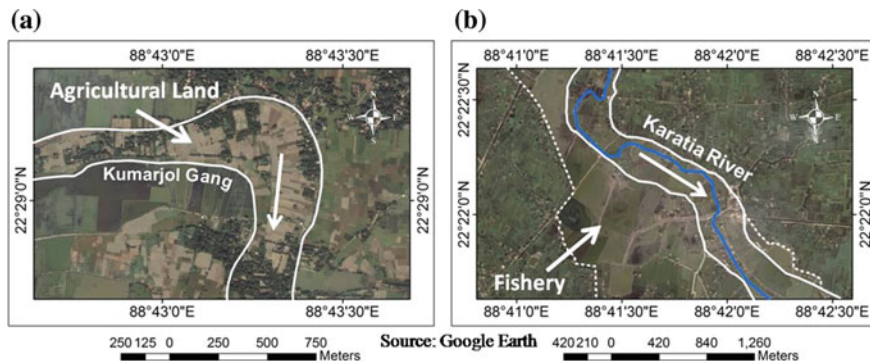


Fig. 6 Transformation of river course into agricultural land and fishery

The course of the river Adi Ganga is continuous from its off-take till Tollygunj ($22^{\circ}29'07''\text{N}$, $88^{\circ}20'31''\text{E}$) after which the channel exists from Kamalgaji to Surjapur ($22^{\circ}17'49''\text{N}$, $88^{\circ}27'43''\text{E}$) which is located 30 km downstream of Tollygunj. After Surjapur, the course of the river is not traceable properly.

Figures 4 and 5 show the dry course of the river Ichhamati near its off-take point and the disconnected river Jamuna respectively. Cross profiles of Figs. 4 and 5 represent the spectral reflectance of the near-infrared (NIR) in some selected cross-sections of the rivers Mathabhanga, Churni, Ichhamati, and Jamuna. Profiles A and B of Fig. 4 shows spectral trough of NIR (NIR absorbance $\sim 75\%$) due to the presence of water mass in the rivers Mathabhanga and Churni as they get a regular discharge from their upstream. But profiles C (Fig. 4) on the river Ichhamati shows a spectral peak (NIR reflectance $\sim 62\%$). The field observation reveals that the spectral peak is mainly due to the presence of Water Hyacinth in the channel.

In Fig. 5, profile A shows spectral trough of the NIR (NIR absorbance $\sim 75\%$) due to the presence of water mass in the river channel as it gets water from the river Hugli and this reach is tidal in nature. Profile C (Fig. 5) also shows a spectral trough (NIR absorbance $\sim 72\%$), but this is due to the presence of stagnant water in the channel. Profile B and D show a spectral peak (NIR reflectance $\sim 54\%$ & $\sim 64\%$) due to the presence of vegetation in the channel of the river Jamuna. The field observation reveals that the spectral peak of profiles B and D are due to the presence of paddy field and Water Hyacinth in the channel, respectively.

The spectral reflectance curve of the NIR band has been drawn on different river reaches in the study area to examine the channel condition and the water availability within the channel. The channel condition has also been verified by field investigation and with high resolution satellite images. Table 1 shows a summary of the NIR reflectance of some selected points in some selected river reaches along with their field observations.

It reveals that the NIR radiation is mainly absorbed by all the water bodies. The reflectance of the NIR radiation by the water mass in the selected river reaches

Table 1 NIR reflectance value (%) and field observation in some selected river points

River Name	CS	Latitude (N)	Longitude (E)	NIR reflectance	Field observation
Mathabhanga	A	23°25'06.08"	88°42'13.90"	~ 26 %	Flowing River
Churni	A	23°24'23.32"	88°42'19.41"	~ 25 %	Flowing River
Ichhamati	A	23°24'8.37"	88°42'56.15"	~ 62 %	Cultivated
	B	23°24'05.56"	88°44'21.55"	~ 44 %	Stagnant Water + W.H.
Jamuna	A	22°59'48.10"	88°24'50.01"	~ 25 %	Tidal Reach
	B	22°59'16.70"	88°27'40.27"	~ 54 %	Cultivated
	C	23° 0'14.16"	88°28'54.76"	~ 28 %	Stagnant Water
	D	22°59'31.74"	88°30'20.77"	~ 64 %	Water Hyacinth (W.H.)
Nona Gang	A	22°47'18.72"	88°36'27.72"	~ 59 %	Water Hyacinth
Bidyabhari	A	22°33'43.01"	88°32'51.61"	~ 25 %	Pond
	B	22°30'36.06"	88°33'8.04"	~ 57 %	Cultivated + W.H.
Suti	A	22°56'53.48"	88°31'33.96"	~ 28 %	Stagnant Water
	B	22°54'43.80"	88°34'21.52"	~ 73 %	Cultivated
Noai	A	22°38'17.56"	88°28'45.82"	~ 60 %	Water Hyacinth
	B	22°37'20.34"	88°32'4.35"	~ 20 %	Tidal Reach
Adi Ganga	A	22°32'39.98"	88°19'35.68"	~ 28 %	Tidal Reach
	B	22°21'39.87"	88°25'20.37"	~ 25 %	Stagnant Water
	C	22°20'34.92"	88°26'32.11"	~ 57 %	Water Hyacinth
	D	22°17'42.36"	88°26'36.83"	~ 54 %	Cultivated
Thakuran	A	22° 5'04.92"	88°33'50.96"	~ 52 %	Cultivated
	B	22° 1'49.98"	88°33'19.97"	~ 26 %	Tidal Reach
Kultigang	A	22°31'29.15"	88°42'52.42"	~ 23 %	Tidal Reach
Kumarjol	A	22°29'29.36"	88°42'19.42"	~ 52 %	Cultivated
Ghagramari	A	22°29'38.92"	88°45'35.43"	~ 75 %	Natural Vegetation
Karatia	A	22°26'55.80"	88°42'24.96"	~ 60 %	Cultivated

varies from 20 to 28 percent depending on the water depth, suspended sediments, chlorophyll concentration, water surface roughness, etc. Most of the selected river reaches show a high reflectance of the NIR radiation due to the presence of vegetation within the channel. The reflectance varies from 52 to 75 percent depending on the type of the vegetation. The field observation reveals that most of the selected river reaches have either been converted into agricultural field or occupied by Water Hyacinth (W.H.) and hence reflects the NIR radiation strongly. Point Ichhamati (B) where both water and Water Hyacinth are present shows a moderate reflectance (44 %) of the NIR radiation.

5 Discussion

Most of the rivers in the delta have been decayed as they have lost their connection with their parent rivers. This is mainly due to the siltation at the off-take point which raises the river bed higher than that of its parent river and interrupts the flow into the river. Their name and the lower reaches survive now mostly because of tidal contribution.

The bed of the river Ichhamati, at its off-take point, is about 9 m higher than the bed of its parent river, the Mathabhanga–Churni. It hampers the regular flow into the river Ichhamati which gets a little amount of flow from upstream only in monsoon months. The gradual reduction of upstream discharge from the river Ganges into the river Mathabhanga is another reason for the decay of the river Ichhamati. Besides this, an anthropogenic reason behind the silting up of the river bed is a railway accident in 1942 involving the Darjeeling mail and the North Bengal Express at the Majdia Railway Bridge on the river Ichhamati (Rudra 2008). The accident released huge amount of debris into the river bed and accelerated the gradual siltation of the river Ichhamati.

The most important delta builder, the river Jamuna has also been decayed by being disconnected from the river Bhagirathi–Hugli. The angular orientation of the channel at its off-take has been transformed into an obtuse one thus restricting the flow of the river Hugli into the river Jamuna. The river Bidyadhari was an important spill channel of the river Jamuna and it is also disconnected from its parent river Jamuna, at present. The excavation of the Kestopur canal in 1910 accelerated the death of the river Bidyadhari by cutting off a good portion of the salt lake spill area and interfering with the natural drainage from the north (Majumdar 1941). Besides this, the upper part of the western branch of the river Bidyadhari has been encroached by fisheries which further restrict the free flow into the channel.

Both the river Kumarjol and Ghagramari have been disconnected from the river Kulti Gang. These two rivers were the upstream freshwater source of the river Karatia. With the decay of the river Kumarjol and Ghagramari, the decay of the river Karatia began. The river Matla used to receive upstream freshwater from the river Bidyadhari through the western branch of the river Bidyadhari and the river Karatia. The river Matla started to dry up when the discharge from the western Bidyadhari and the Karatia into the river Matla had stopped. Figure 6 shows part of the rivers Kumarjol and Karatia which have been converted into agricultural field and fishery, respectively.

The problem of the river Adi Ganga is similar to that of the Jamuna. The flow of the river Hugli is restricted by the elevated bed and the obtuse angular bend of the river Adi Ganga at its off-take point. The tidal water from the river Hugli enters up to Tollygunj. Thereafter, the channel is treated as a drainage canal up to Garia. The Tollygunj–Garia reach has been further degraded by the construction of the Metro Railway pillars on the bed of the river Adi Ganga. The river is not traceable properly after Surjapur as its dry bed is encroached by agricultural fields.

This study reveals that the discontinuity of the rivers in the delta is not only due to the hydrological or morphological changes of its river system but also due to significant anthropogenic impacts which play a major role in changing the river network. The increasing population is gradually encroaching into the decayed river bed to build up their residences. The disconnected river channels are rapidly transforming into agricultural fields and aqua-cultural farms to fulfill the increasing demand of food and to generate more profit. The disconnected reaches reduce the services of the riverine ecosystems by limiting the freshwater flow from upstream. Disturbance in fresh water flow disrupts the process of drainage, navigation, sediment flushing, recycling of organic nutrients, carbon sequestration, etc. Decreasing freshwater flow increase the riverine and groundwater salinity by promoting the sea water intrusion. The saline river water and ground water cannot be utilized for drinking or irrigation purposes and hence restrict the food production. The increasing salinity also threatens the riverine and riparian freshwater-loving floral and faunal biodiversity. The restoration of the disconnected reaches is necessary to improve these ecosystem services by augmenting upstream freshwater flow in this region.

6 Conclusion

This study reveals that the remote sensing techniques have a great potential to detect the blockages in river channels. Three different normalized difference water indexes based on green, near-infrared (NIR), and shortwave-infrared (SWIR) bands of Landsat Thematic Mapper (TM) images have been calculated in this study to extract the water body and identify the areas of disconnect. The results indicate that the MNDWI_1 model based on the green (Band 2) and the near-infrared (Band 5) is the best indicator for water body extraction from Landsat TM images. After identifying the areas of disconnect, the results have been validated through the spectral profile of the near-infrared band and field observation in some selected reaches. The validation through field observation is necessary to map the actual disconnected areas.

The rivers of the delta which we have focused on in this paper have undergone almost total decay. Though the river Ichhamati gets a little amount of water from the river Mathabhanga–Churni during the monsoon months, its upper reach remains stagnant and is covered with Water Hyacinth during the other times of the year. The river Jamuna, the Bidyadhari, and the Adi Ganga remain as fragmented channels with stagnant water. Some parts of these rivers have been converted into agricultural fields, aquaculture farms, while other parts have been encroached by human settlements or remain as paleo-channels. The disconnected paths may be reclaimed to augment environmental flows from upstream to maintain the ecosystem functions and services of these rivers. The derelict channels may be restored to harvest rain

water within these channels. A proper management plan is required to reestablish the flow path by removing the blockages towards improving freshwater availability in the delta.

Acknowledgments The authors would like to express their heartfelt gratitude to the University Grants Commission (UGC), India and IUCN, India for providing fund to conduct the study. The authors are also indebted to the U.S. Geological Survey server (<http://glovis.usgs.gov/>) for providing the satellite images for this study. Special thanks are also due to Mr. Ratnadeep Ray for his remote sensing support. Kaberi Samanta, Subhajit Ghosh, Soumik Sarkar, Jaya Pradhan, and Sourav Samanta deserve special gratitude for their support in digitizing the extensive river network of the delta.

References

- Allison MA, Khan SR, Goodbred SL Jr, Kuehl SA (2003) Stratigraphic evolution of the late Holocene Ganges-Brahmaputra lower delta plain. *Sediment Geol* 155(3):317–342. doi:[10.1016/S0037-0738\(02\)00185-9](https://doi.org/10.1016/S0037-0738(02)00185-9)
- Bandyopadhyay S (1996) Location of the Adi-Ganga Palaeochannal, South 24 Parganas, West Bengal: A Review. *Geogr Rev of India* 58(2):93–109
- Bhadra T (2013) A study on fresh-water availability in Indian Sundarbans Delta. M.Phil. Dissertation, School of Oceanographic Studies, Jadavpur University, Kolkata
- Bhadra T, Hazra S, Kolay P, Sinha Roy SP (2013) Ground water—River water interaction in Deltaic West Bengal with special reference to Sundarbans. In: Abstracts of the workshop on “Sustainable Development and Management of Ground Water in West Bengal and Future of Irrigation vis-à-vis Arsenic Contamination in Ground Water”, Kolkata, 19 February 2013 (CGWA & CGWB-Eastern Region, Govt. of India), pp 138–142
- Bracken LJ, Croke J (2007) The concept of hydrological connectivity and its contribution to understanding runoff-dominated geomorphic systems. *Hydrol Process* 21:1749–1763. doi:[10.1002/hyp.6313](https://doi.org/10.1002/hyp.6313)
- Burchsted D, Daniels MD, Thorson RM, Vokoun JC (2010) The river discontinuum: applying beaver modifications to baseline conditions for restoration of forested headwaters. *Biosci* 60:908–922. doi:[10.1525/bio.2010.60.11.7](https://doi.org/10.1525/bio.2010.60.11.7)
- Burchsted D, Daniels M, Wohl EE (2014) Introduction to the special issue on discontinuity of fluvial systems. *Geomorphol* 205:1–4. doi:[10.1016/j.geomorph.2013.04.004](https://doi.org/10.1016/j.geomorph.2013.04.004)
- Chander G, Markham BL, Helde DL (2009) Summary of current radiometric calibration coefficients for Landsat MSS, TM, ETM+, and EO-1 ALI sensors. *Remote Sens Environ* 113(5):893–903. doi:[10.1016/j.rse.2009.01.007](https://doi.org/10.1016/j.rse.2009.01.007)
- Fryirs K (2013) (Dis)Connectivity in catchment sediment cascades: a fresh look at the sediment delivery problem. *Earth Surf Process Landf* 38(1):30–46. doi:[10.1002/esp.3242](https://doi.org/10.1002/esp.3242)
- Fryirs KA, Brierley GJ, Preston NJ, Spencer J (2007) Catchment scale (dis)connectivity in sediment flux in the upper Hunter catchment, New South Wales, Australia. *Geomorphol* 84(3):297–316. doi:[10.1016/j.geomorph.2006.01.044](https://doi.org/10.1016/j.geomorph.2006.01.044)
- Gole CV, Vaidyaraman PP (1966) Salinity distribution and effect of freshwater flows in the Hooghly River. In: Proceedings of 10th conference on coastal engineering, Tokyo, Japan, September 1966 (American Society of Civil Engineers, New York), pp 1412–1434
- Goodbred SL Jr, Kuehl SA (2000) The significance of large sediment supply, active tectonism and eustasy on margin sequence development: late Quaternary stratigraphy and evolution of the Ganges-Brahmaputra Delta. *Sediment Geol* 133(3):227–248. doi:[10.1016/S0037-0738\(00\)00041-5](https://doi.org/10.1016/S0037-0738(00)00041-5)

- Gopal B, Chauhan M (2006) Biodiversity and its conservation in the Sundarbans Mangrove Ecosystem. *Aquat Sci* 68:338–354. doi:[10.1007/s00027-006-0868-8](https://doi.org/10.1007/s00027-006-0868-8)
- Hazra S, Bhadra T, Ghosh S, Barman BC (2015a) Assessing Environmental Flows for Indian Sundarban: a suggested approach. *River Behav Control* 35:65–74
- Hazra S, Khan MFA, Kansal ML, Barman BC, Bhadra T, Ghosh S, Saniruzzaman S, Chandniha SK (2015b) Methodology for Assessment of Environmental Flows for The Sundarbans Ecosystem (A pilot study), IUCN-India (Unpublished Report)
- Hist FC (1915) Report on the Nadia Rivers. In: Biswas KR (ed) *Rivers of Bengal*, vol III (I). West Bengal District Gazetteers, Kolkata
- Jenkins KM, Boulton AJ (2003) Connectivity in a dryland river: short-term aquatic micro-invertebrate recruitment following floodplain inundation. *Ecol* 84(10):2708–2723. doi:[10.1890/02-0326](https://doi.org/10.1890/02-0326)
- Ji L, Zhang L, Wylie B (2009) Analysis of dynamic thresholds for the normalized difference water index. *Photogramm Eng Remote Sens* 75(11):1307–1317
- Kondolf GM, Boulton AJ, O'Daniel S, Poole GC, Rahel FJ, Stanley EH, Wohl E, Bång A, Carlstrom J, Cristoni C, Huber H, Koljonen S, Louhi P, Nakamura K (2006) Process-based ecological river restoration: visualizing three-dimensional connectivity and dynamic vectors to recover lost linkages. *Ecol Soc* 11(2):5
- Korup O, Densmore AL, Schlunegger F (2010) The role of landslides in mountain range evolution. *Geomorphol* 120:77–90. doi:[10.1016/j.geomorph.2009.09.017](https://doi.org/10.1016/j.geomorph.2009.09.017)
- Li W, Du Z, Ling F, Zhou D, Wang H, Gui Y, Sun B, Zhang X (2013) A comparison of land surface water mapping using the normalized difference water index from TM, ETM+ and ALI. *Remote Sens* 5(11):5530–5549. doi:[10.3390/rs5115530](https://doi.org/10.3390/rs5115530)
- Majumdar SC (1941) Rivers of the Bengal Delta. In: Biswas KR (ed) *Rivers of Bengal*, vol I. West Bengal District Gazetteers, Kolkata
- Mcfeeters SK (1996) The use of the normalized difference water index (NDWI) in the delineation of open water features. *Int J Remote Sens* 17(7):1425–1432. doi:[10.1080/01431169608948714](https://doi.org/10.1080/01431169608948714)
- McGinness HM, Thoms MC, Southwell MR (2002) Connectivity and fragmentation of flood plain-river exchanges in a semiarid, anabranching river system. In: Dyer FJ et al. (ed) *The structure, function and management implications of fluvial sedimentary systems*. IAHS Publ no. 276, Wallingford, UK, pp 19–26
- Quimet WB, Whipple KX, Royden LH, Sun Z, Chen Z (2007) The influence of large landslides on river incision in a transient landscape: eastern margin of the Tibetan Plateau (Sichuan, China). *Geol Soc Am Bull* 119(11/12):1462–1476. doi:[10.1130/B26136.1](https://doi.org/10.1130/B26136.1)
- Poole GC (2002) Fluvial landscape ecology: addressing uniqueness within the river discontinuum. *Freshw Biol* 47:641–660. doi:[10.1046/j.1365-2427.2002.00922.x](https://doi.org/10.1046/j.1365-2427.2002.00922.x)
- Pringle CM (2001) Hydrologic connectivity and the management of biological reserves: a global perspective. *Ecol Appl* 11(4):981–998. doi:[10.2307/3061006](https://doi.org/10.2307/3061006)
- Pringle CM (2003) What is hydrologic connectivity and why is it ecologically important? *Hydrolog Process* 17:2685–2689. doi:[10.1002/hyp.5145](https://doi.org/10.1002/hyp.5145)
- Rudra K (2008) *Banglar Nadikatha* (in Bengali). Kolkata, Sahitya Samsad, p 124
- Rudra K (2014) Changing river courses in the western part of the Ganga–Brahmaputra delta. *Geomorphol* 227:87–100. doi:[10.1016/j.geomorph.2014.05.013](https://doi.org/10.1016/j.geomorph.2014.05.013)
- Rundquist DC, Lawson MP, Queen LP, Cervený RS (1987) The relationship between the timing of summer-season rainfall events and lake-surface area. *J Am Water Resour Assoc* 23(3):493–508. doi:[10.1111/j.1752-1688.1987.tb00828.x](https://doi.org/10.1111/j.1752-1688.1987.tb00828.x)
- Tetzlaff D, Soulsby C, Bacon PJ, Youngson AF, Gibbins C, Malcolm IA (2007) Connectivity between landscapes and riverscapes—A unifying theme in integrating hydrology and ecology in catchment science? *Hydrolog Process* 21(10):1385–1389. doi:[10.1002/hyp.6701](https://doi.org/10.1002/hyp.6701)
- Ward JV (1989) The four-dimensional nature of lotic ecosystems. *J N Am Benthol Soc* 8(1):2–8. doi:[10.2307/1467397](https://doi.org/10.2307/1467397)
- Ward JV, Tockner K, Arscott DB, Claret C (2002) Riverine landscape diversity. *Fresh w. Biol* 47(4):517–539. doi:[10.1046/j.1365-2427.2002.00893.x](https://doi.org/10.1046/j.1365-2427.2002.00893.x)

- Wohl E, Beckman ND (2014) Leaky rivers: implications of the loss of longitudinal fluvial disconnectivity in head water streams. *Geomorphol* 205: 27–35. doi:[10.1016/j.geomorph.2011.10.02](https://doi.org/10.1016/j.geomorph.2011.10.02)
- Xu H (2006) Modification of normalized difference water index (NDWI) to enhance open water features in remotely sensed imagery. *Int J Remote Sens* 27(14):3025–3033. doi:[10.1080/01431160600589179](https://doi.org/10.1080/01431160600589179)

Comparative Assessment of Morphological and Landuse/Landcover Change Pattern of Sagar, Ghoramara, and Mousani Island of Indian Sundarban Delta Through Remote Sensing

Rituparna Hajra, Amit Ghosh and Tuhin Ghosh

Abstract Deltaic island systems are becoming vulnerable with frequent embankment failures, beach erosion and submergence, and flooding throughout the world. In addition to this, the alarming growth of population in this ecologically sensitive and fragile niche has posed a major threat for its very existence. The impact of sea level rise in combination with complex hydrodynamic conditions has caused severe coastal erosion in the islands of the Indian Sundarban Delta (ISD). The Sagar, Ghoramara, and Mousani Island, situated at the western part of the Indian Sundarban Delta, are the focus of this study. This study aims at the assessment of morphological changes due to the erosion and consequential land use/land cover changes. The study area is a densely populated region with 2 % growth per annum. The immediate consequences of population growth could be the decrease of agricultural land through expansion of the settlement area. Morphological changes along with high population growth create pressure on resources by lowering per capita land availability. Though having a similar environmental set up, all the three islands that are being studied have different change pattern depending on the morphological and anthropogenic activities. This study tries to compare the changes among these three islands. Assessment of the land use pattern change and the estimation of erosion have been done with the application of Remote Sensing. Temporal analysis using satellite images of 1990, 1995, 2000, 2005, 2010, and 2015 unfold the variation in the geomorphic and the land use type and help to formulate the strategic planning for the sustenance of the island.

R. Hajra (✉) · A. Ghosh · T. Ghosh
School of Oceanographic Studies, Jadavpur University, Jadavpur, India
e-mail: rituparnahajra2502@gmail.com

A. Ghosh
e-mail: ghoshamitag@gmail.com

T. Ghosh
e-mail: tuhin_ghosh@yahoo.com

Keywords Coastal erosion · Land use/land cover · Sagar Island · Ghoramara Island · Mousani Island

1 Introduction

The Ganga—Brahmaputra—Meghna (GBM) delta formed at the confluence of the river Ganges is considered to be the largest delta in world. A world heritage site and the single largest block of mangrove ecosystem, the Sundarban is a part of this delta shared between India and Bangladesh. The Indian Sundarban Delta (ISD) has a shoreline stretch of 130 km to the total 180 km length of the West Bengal coast (MOEF 2009). It comprises 102 islands of which 54 are inhabited with almost 4.6 million people. The Indian Sundarban Delta consists of 2195 km² of wetland (mangroves forest), 2069 km² of tidal river and 5366 km² of reclaimed area (Hazra et al. 2002). This unique land-water interface makes the islands of the Sundarban more dynamic in nature.

Coastal morphology has gone through significant changes due to erosion and accretion (Thomas et al. 2014). Morphological changes along with anthropogenic activities are influencing coastal ecosystems all over the world. These changes jeopardize the security and economic well-being of the coastal habitats (Malone et al. 2010). Developmental activities viz. coastal agriculture, aquaculture, port development, and urbanization have been the most frequent threats to the tropical coastal zones. Land use/land cover (LU/LC) have been continuously changing due to natural (climate forcing and change) and anthropogenic (land use conversion and other management activities) processes. Since past decade landuse/landcover change study is gaining immense importance as sustainability has become the desired goal for all developmental activities (Jayappa et al. 2006; Dinesh Kumar et al. 2007; Ghosh et al. 2001; Thomas et al. 2014).

The impact of erosion-accretion processes and sea level rise induced changes is expected to be felt mostly along the coastal zones of the island system, along the tidal creeks, and the mangroves swamps. This is expected to affect human activity and resource utilization patterns in the coastal zone (Hazra et al. 2002). Change in sea level and tidal hydraulics causes coastal erosion which is constantly reshaping islands of the Indian Sundarban Delta (WWF 2010). During 1969–2001, the Indian Sundarban Delta had a total land loss of 162.879 km² with the total submergence of a few islands like Lohachara, Bedford Island. The amount of land accretion over the past 30 years is estimated to be 82.505 km² (Hazra et al. 2002). In addition to this, an alarming growth of population in this ecologically sensitive and fragile niche has posed a major threat for its very existence. According to the report of WWF (2010), the human habited part of the Indian Sundarban Delta is witnessing an overall change in the settlement density pattern. The area under settlement with vegetation is increasing at the expense of the agricultural land. The forest area has reduced from 404.887 to 332.008 km². However, the decline in the total forest area is mostly due to coastal erosion of the forested islands (WWF 2010). This study aims

at the assessment of the land use/land cover as a result of the morphological changes due to the effects of erosion in Sagar, Mousani, and Ghoramara Island.

The islands that are being studied are situated at the confluence of the river Hooghly with the Bay of Bengal at the south-west of the Indian Sundarban Delta (ISD) (Fig. 1). Sagar Island is situated at the estuary of the river Hooghly on the south-west of the ISD, and extends from $21^{\circ} 37' 21''$ to $21^{\circ} 52' 28''\text{N}$ and $88^{\circ} 2' 17''$ to $88^{\circ} 10' 25''\text{E}$. Administratively, Sagar Island is classified as a “Block,” a collection of *mouzas* or villages which is the largest island in ISD with 206844 total population (Census 2011).

Ghoramara is located between $21^{\circ} 53' 56''\text{N}$ and $21^{\circ} 55' 37''\text{N}$ latitude and $88^{\circ} 06' 59''\text{E}$ – $88^{\circ} 08' 35''\text{E}$ longitude at the north-western part of the Sagar Island. It has faced a high rate of erosion since the 1970s. The major villages on this island are Khasimara, Baishnabpara, Hathkola, Baghpara, Raipara, Mandirtala, Chunpuri, Lakshmi Narayanpur, and Khasimara Char. Out of these, the Kashimara Char, Lakshmi Narayanpur, Kashimara and Baisnabpar have already been lost due to erosion (Jana et al. 2012; Ghosh et al. 2003). This island covers an area of 4.43 km^2 with a population of 5193 (Census 2011). Mousani Island is encircled by the

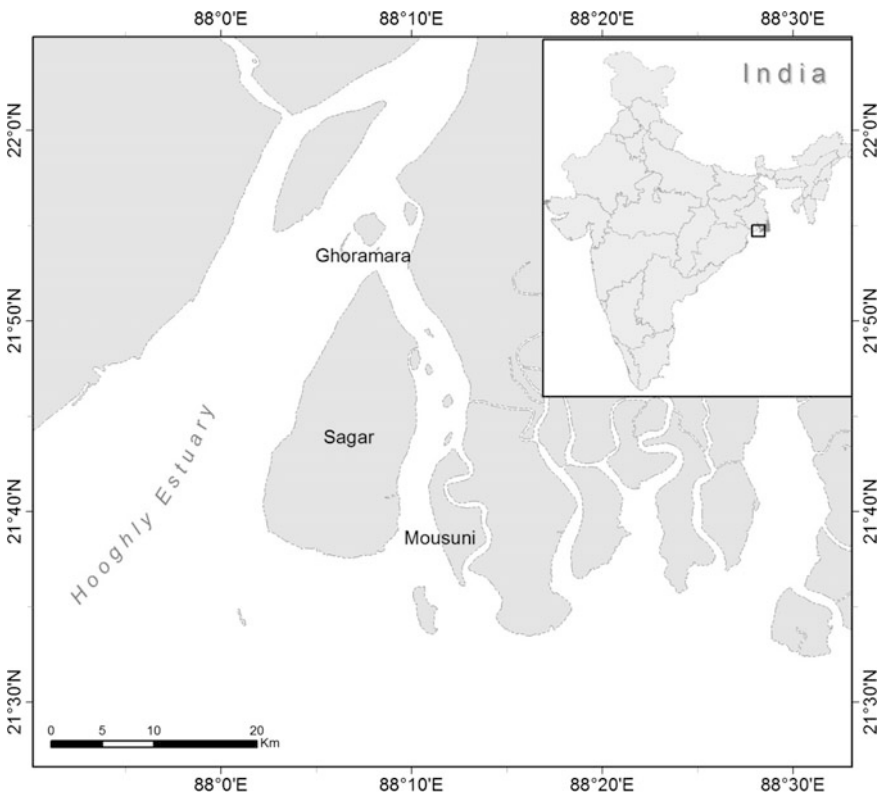


Fig. 1 Location of the study area

Muriganga/Bartala River in the west and the north-west, the Pitt's Creek/Chenayer River in the east and the Bay of Bengal in the south (WWF 2010). Mousani Island covers an area of 24 km² and is home to 22,073 people and 3340 families (Census 2011).

The reclamation of the Sagar Island from the Sundarban mangrove wetlands of the western Ganga-Brahmaputra delta was initiated in 1811 (Bandyopadhyay 1997). The elevation of these islands under study varies from 2.10 to 2.75 m above the mean sea level (Purkait 2009). The low elevation naturally makes these islands vulnerable to the threat of inundation. The Hooghly estuarine is classified as a mixed macrotidal estuary with tidal ranges of 4.64 m (Ghosh et al. 2001). The coast of the Sagar Island that falls under the tide-dominated coast, has recorded a tidal range between 5 and 6 m (Dinesh Kumar et al. 2007; Gopinath 2010). Tidal dominated coasts are geomorphically very active and environmentally very sensitive (Jayappa et al. 2006). The total land loss of the Sagar Island was estimated around 284.55 km² during the period 1951–55 and 213.83 km² in 1992 (Bandyopadhyay 1997). Ghosh et al. (2001) estimated erosion in the sectoral distribution which showed erosion was significant on both the eastern and the western face and a marginal accretion was reported in the southern portion due to the outbuilding of the delta. The rate of erosion in 1995 was 4.54 m per annum which increased to 18.75 m per annum in 1999 whereas the rate of accretion remained at the low rate of 6.25 m per annum in 1999 (Ghosh et al. 2001).

The Ghoramara Island was a part of Sagar main island up to 1881. But by 1914, the northern tip of the island was cut off from the rest of the island and subsequently, Ghoramara, Khasimara, Lohachara, and Supaibhanga have been formed (Gopinath and Seralathan 2005). The geomorphological changes observed in the Ghoramara Island are largely as a result of the changes in the estuarine hydrodynamics influenced both by natural processes and anthropogenic activities (Ghosh and Sengupta 1997). The island is under threat of severe erosion, embankment failure, cyclone, and storm surge (Hazra and Bakshi 2003; Ghosh et al. 2003). These are the main factors for habitat loss, gradual loss in ecosystem services, depreciation in well-being and the resultant migration of the people of this island. The migrated people have taken shelter in the nearby Sagar Island (Ghosh et al. 2014).

The Mousani Island has lost about 15 % of the total area whereas over almost the same period, the population has risen by about 265 % (Danda 2007). The coastal stretch of Baliara is 11.06 km long while the length of the embankment is 8.49 km of which only 1.8 km is brick-paved and the remaining 6.69 km is just exposed earthwork. The height of the embankment ranges from 4 to 6 m (WWF 2010). Erosion and embankment collapse have compelled the local people of the Mousani Island whose livelihood is dependent on agriculture to change their occupation (Danda 2007).

The land use pattern has changed with time as it influenced by human activities. Previous land use study showed a decrease in the agricultural land due to the increase in population pressure in study area (Dinesh Kumar et al. 2007; Jayappa et al. 2006). Sandy beaches and mangroves have been decreasing in these islands

mainly due to land erosion (Thomas et al. 2014). The trend of land use changes has been observed to affect negatively the agricultural land, mud flat, and marginally the dune belt (Ghosh et al. 2003). Land submergence due to sea level rise (SLR) and corresponding geomorphic changes are responsible for 66 % of land use land cover change in ISD and anthropogenic factors including population growth, conversion for quick economic return, and exploitation of the natural resources is attributed to the rest part of changes (Hazra et al. 2002). The adaptive measure including earthen embankments, cyclone shelters or planned plantation of mangrove to prevent erosion along the coast constitute only 2 % of the land use changes in the decadal level (Hazra et al. 2002).

In this context, the present study aims to assess the morphological changes due to erosion and the resulting land use pattern through Remote Sensing. The Remote Sensing data are obviously very important in detecting and monitoring change in landscape and land use pattern. Land use change detection is a data-hungry analysis which requires historical and current data which can be derived from Remote Sensing. Satellite images have been analysed to estimate the erosion and land use change pattern from 1990 to 2015. All three islands are found to be vulnerable from land erosion. As a consequence, land availability is declining thus posing a threat to the sustainability of these islands. So detail monitoring of coastal morphological changes and its impact is necessary for required policy implementation.

2 Methodology

This study aims at the detection of general trends of land use and land cover changes over the past 20 years. In this study, six broad types of suitable land use and land cover classes have been considered which are: agricultural land, mixed vegetation with settlement, mangrove forest, mudflat, sand/barren land, and water body. Natural mixed vegetation and settlement have been combined as one class since both of these are closely associated with each other in the Landsat images.

A series of Landsat (TM and OLI) images having 30 m spatial resolution acquired on different dates with a five-year interval (14 Oct 1990, 28 Jan 1995, 17 Oct 2000, 7 Oct 2005, 6 Feb 2010, and 10 Jan 2015) were used for this study. This was done keeping in mind the fact that these images provide an appropriate and cost-efficient source of information for a wide range of applications including land change mapping (Rogan and Chen 2004). The band specification of these two sensors is given in Table 1. Thermal bands were not employed in the analysis due to their coarser spatial resolution and weak signal to noise ratio (Jensen 2004).

The radiometric correction is the prerequisite for any land use change detection analysis. The Dark-Object Subtraction (DOS) radiometric correction method was applied to these images to reduce the atmospheric effects (Chavez 1988). The supervised classification method, based on the field knowledge, was employed to get the land use land cover classes. The supervised classification method can be considered more intuitive for land use land cover change detection if the required

Table 1 Band specification of Landsat images

Landsat 5 TM			Landsat 8 OLI		
Band	Wavelength	Resolution	Band	Wavelength	Resolution
Band 1—blue	0.45–0.52	30	Band 1	0.43–0.45	30
Band 2—green	0.52–0.60	30	Band 2—blue	0.45–0.51	30
Band 3—red	0.63–0.69	30	Band 3—green	0.53–0.59	30
Band 4—NIR	0.76–0.90	30	Band 4—red	0.64–0.67	30
Band 5 SWIR 1	1.55–1.75	30	Band 5—NIR	0.85–0.88	30
Band 6 thermal	10.40–12.50	120* (30)	Band 6—SWIR 1	1.57–1.65	30
Band 7 SWIR 2	2.08–2.35	30	Band 7—SWIR 2	2.11–2.29	30
			Band 8—PAN	0.50–0.68	15
			Band 9—Cirrus	1.36–1.38	30

*TM Band 6 was acquired at 120-meter resolution, but products are resampled to 30-meter pixels

training sites are properly gathered through expert knowledge and field visits (Rogan and Chen 2004). The maximum likelihood classification was used to derive six land use land cover classes for the three islands. The spectral signatures of each land use land cover class was developed based on the selected training sites and assessed for its separability using the space images feature. The combined land area in all the studied year was considered as base area to analyze the changes in land use land cover area. The area of each land use land cover class was calculated based on the cell counts of each class. Then the land use and land cover maps statistics were analyzed to determine the trend of land use and land cover change from 1990 to 2015 in these three islands. A pixel based accuracy assessment of 2015 land use land cover map was performed to check the overall all accuracy of the land cover classification. To perform the test 61 ground truth sample has been collected representing different land use land cover classes. The overall accuracy of the classification for 2015 land use and land cover map was 85 % and the Kappa coefficient was 0.79 (Table 2).

3 Results and Discussion

3.1 Erosion-Accretion Pattern at Study Islands

The study areas have suffered a bulk of land loss during the time period of 1990–2015. The images have been superimposed to estimate the land loss and shoreline change. The major coastal geomorphological landforms identified around the island during the field survey were beach, dune, and mudflats. From the five images of the different time windows, it can be said that the erosion-accretion rate is different in these islands as the land loss and the accretion were high during the periods 1995–2005 and 2010–2015 (Table 3).

Table 2 Confusion matrix for accuracy assessment of the land use land cover map of 2015

Classified pixel	Ground truth data						Total classified pixel	User's accuracy	Error of commission
	Agricultural land (x1)	Mangrove (x2)	Mixed vegetation with settlement (x3)	Mudflat (x4)	Sand/Barren land (x5)	Water (x6)			
x1	26.00	-	1.00	-	-	-	0.96	0.04	
x2	-	5.00	-	-	-	-	1	0	
x3	4.00	-	12.00	-	-	-	0.75	0.25	
x4	-	1.00	1.00	2.00	-	1.00	0.4	0.6	
x5	-	-	-	-	3.00	-	1	0	
x6	-	-	-	1.00	-	4.00	0.8	0.2	
Total ground truth pixel	30.00	6.00	14.00	3.00	3.00	5.00	61.00		
Producer's accuracy	0.87	0.83	0.86	0.67	1.00	0.80	Overall accuracy = 0.85		
error of omission	0.13	0.17	0.14	0.33	0.00	0.20	Kappa = 0.79		

Table 3 Total Land Area and Land Loss during 1990 to 2015

Island	Time window	1990–1995	1995–2000	2000–2005	2005–2010	2010–2015
Sagar	Erosion in sq km	0.43	9.35	3.8	0.55	5.79
	Accretion in sq km	17.13	1.59	0.86	7.56	0.39
Ghoramara	Erosion in sq km	0.11	0.61	0.61	0.09	0.46
	Accretion in sq km	0.35	0.00	0.02	0.29	0.05
Mousani	Erosion in sq km	0.18	2.85	0.86	0.42	1.02
	Accretion in sq km	2.48	0.05	0.45	1.21	0.37

The total area of Sagar Island has undergone dynamic changes. During 1990–1995, the land area increased from 235 to 252 km² with the highest rate of accretion of 3.34 km² per year. During 1995–2000 and 2000–2005, this island had experienced the highest land loss in the 25 year time span. The rate of erosion estimated during that period was 0.84 km² per annum. In the year 2010, the total area of the Sagar Island increased to 250 km²—there was an addition of 7.02 km² of land (Fig. 2). The estimated rate of erosion again went up to 1.02 km² per year and in the year 2015, the land area of the Sagar Island stands at 245.33 km². The overall rate of erosion has been estimated 0.2 km² during this 25 year time span at Sagar Island.

Ghoramara also experienced the highest land loss during 1995–2005 and 2010–2015 (Table 3). It can be said from the image analysis that the western, the north-western and the north eastern parts of the Ghoramara Island were the most affected during 1990–2005. This has been reported in previous studies as well (Ghosh and Sengupta 1997; Ghosh et al. 2003). But from 2005 to 2015, the erosion has affected the southern part of the island as well. This may be explained by the fact that with the change in the course of the Hooghly River and the river dynamics, the erosion pattern is also changing now.

Throughout the 25 year time span Ghoramara experienced a considerable land loss (Fig. 2). The rate of erosion was highest during 1995–2005, i.e., 0.03 km² per year. Recently Ghoramara has experienced erosion rate 0.02 km² per year, i.e., 36 % loss to total land area.

Considerable erosion was found during 1995–2000 and 2010–2015 with rate of erosion 0.14 and 0.03 km². The total area of Mousani Island was 29.75 km² in the year 1990 and it went ups and down in total amount throughout 25 year (Fig. 2). The rate of land loss was highest during 1995–2000 (Table 3). The time period of 2010–2015 is also experiencing higher erosion than accretion after the 2005–2010 time period when accretion was higher than erosion. The rate of erosion at overall 25 time span is estimated 0.08 km² per annum.

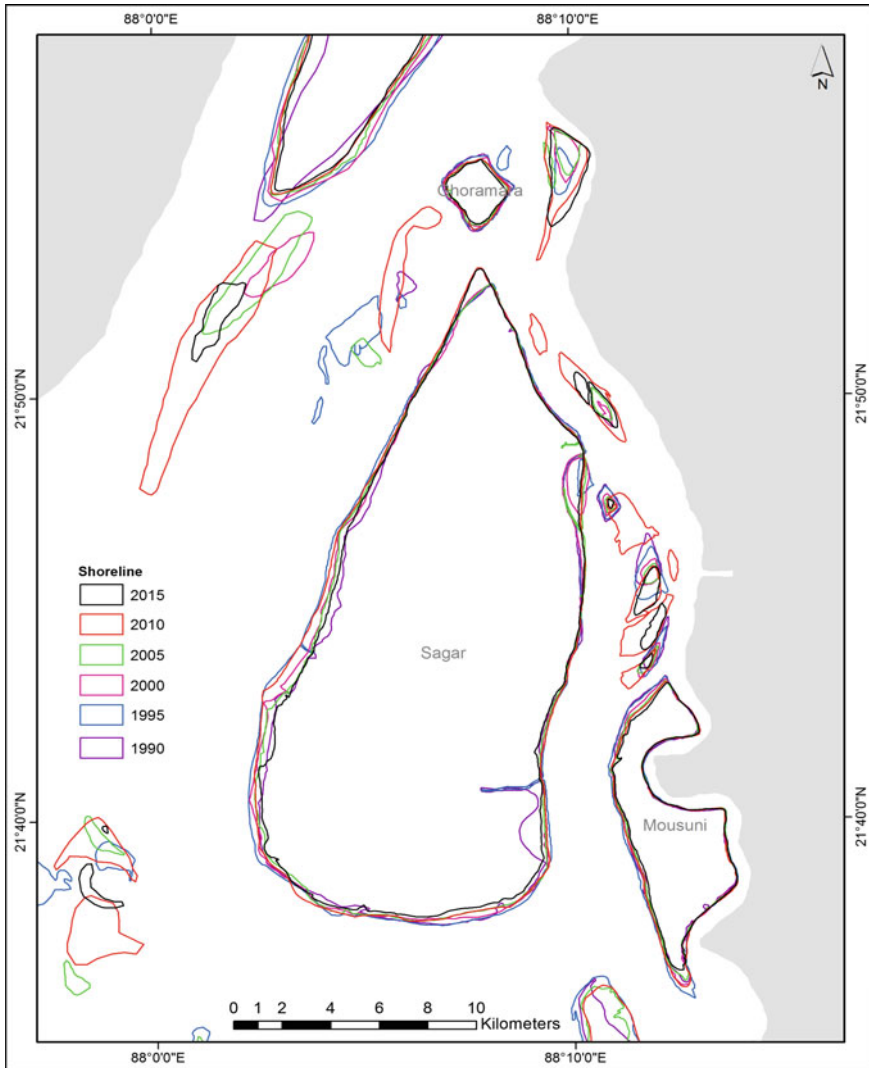
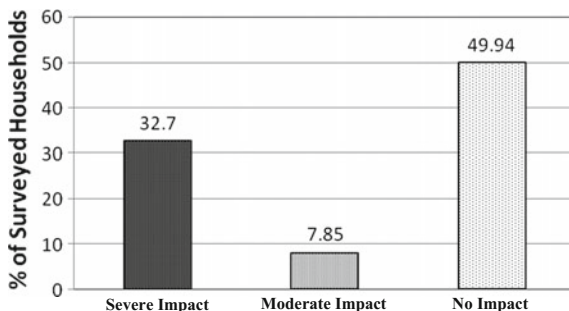


Fig. 2 Morphological change analysis to identify the extent of erosion in Study Islands (1990–2015)

It is evident from this map (Fig. 2) that the zones of erosion and accretion have changed at present from the past. Now more erosion is occurred near south-east and south-west than the northern part. Field visits help to identify the major erosional zones of the study area and correlate the data with image analysis. Sibpur, Doblal,

Fig. 3 Impact of erosion on local inhabitants during field surveys



Beguakhali, Sumatinagar, and Muriganga among 22 surveyed *mouzas* may be identified as the major erosion prone parts of the Sagar Island. The presence of the old lighthouse and the shifting of the Kapil Muni ashram are examples of coastal erosion in the Sagar Island. Mudflats have been stabilized with mangrove plantation among the surveyed *mouzas* Radhakrishnapur, Chanditala, Krishnanagar, Kastala, Sapkhali, Chemaguri.

It was found during field surveys that 24 % of the inhabitants of Sagar, Ghoramara and Mousani Island considered erosion to be a major threat. It was clear from their opinions that erosion has both a direct and an indirect impact on the lives of the local people there (Fig. 3). Direct impact includes the extreme level of suffering due to the loss of land, home, cattle and productions while indirect impact includes the suffering of the people like loss of man-days and saline water inundation due to embankment failure.

3.2 Land Use Assessment

The analysis of multi-dated satellite image has been used to estimate the change pattern of land use in these islands being studied (Figs. 4, 5, 6, 7, 8 and 9). Among these islands, Sagar being the largest has the highest population pressure. So, the settlement area expansion in this island is common. Sagar Island is having population density of 893 persons per km². The island is also a pilgrim site for the Gangasagar Mela and the Kapil Muni Ashram and consequently a good number of business activities have been developed around it though agriculture is the main source of income for the inhabitants. The consequence of the population growth in the Sagar Island is an increase of settlement area resulting in a change in the land use pattern and the expansion of the non-mangrove area.

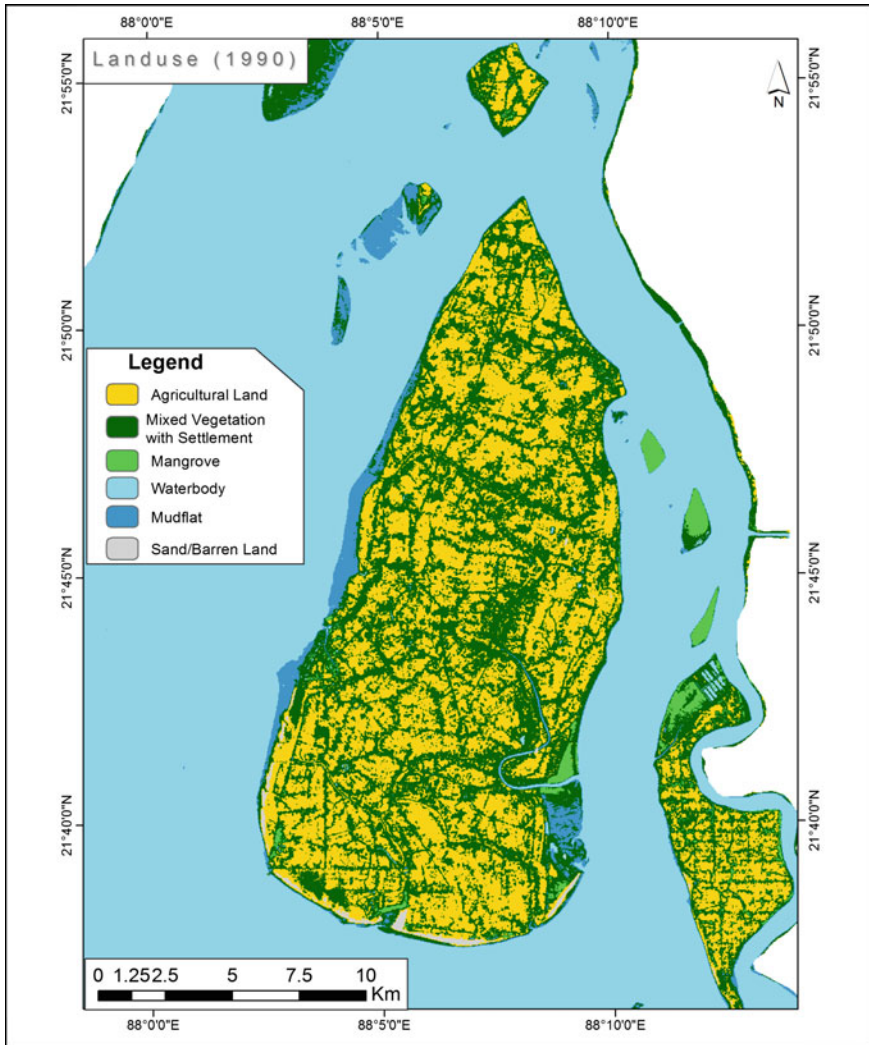


Fig. 4 Land use/land cover map of the Study Islands (1990)

Ghoramara Island has also been suffering from severe coastal erosion and areal reduction for the last three decades which has resulted in the loss of major areas on the north-west coast. As a result, numerous households have been lost along with a significant area of agricultural land. Due to the land loss, major land use patterns have also been changing in this island. The actual population growth of Ghoramara is much lower than expected which can be attributed to the migration of people due to land loss (Ghosh et al. 2014).

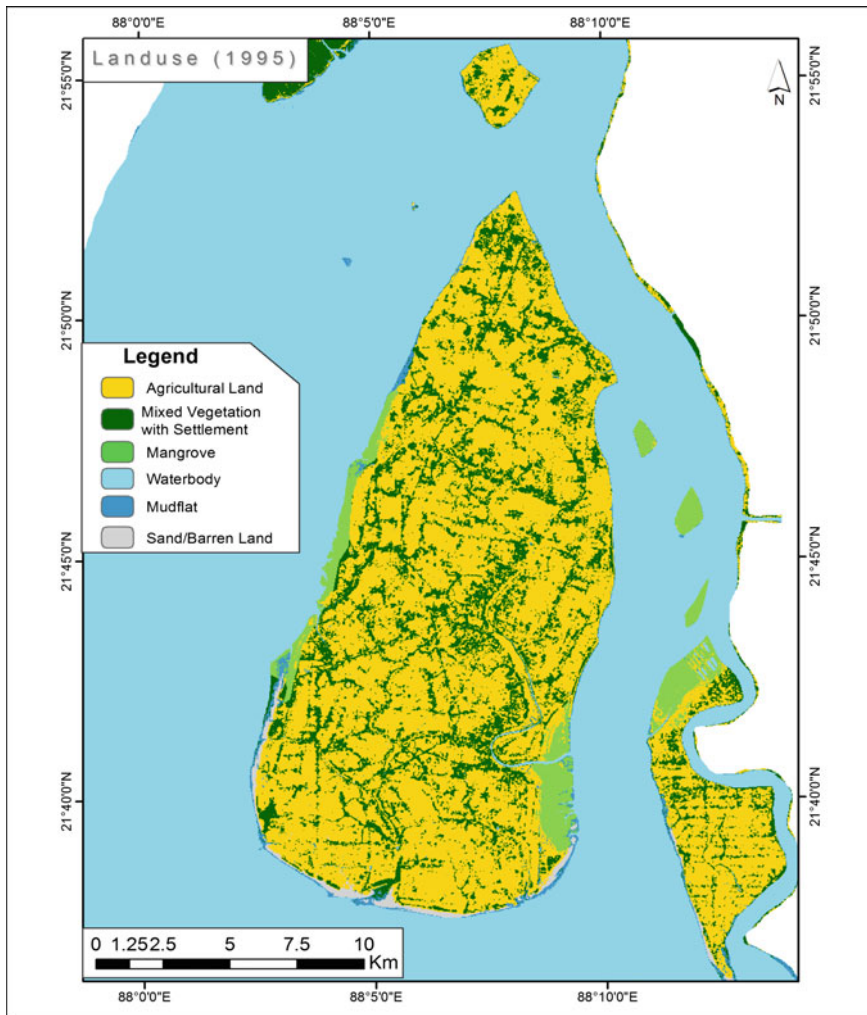


Fig. 5 Land use/Land cover map of the Study Islands (1995)

The Mousani Island is mostly flat with a very gentle slope toward the south and south-east. The images have been classified into six major land use types—agricultural land, settlement with vegetation, mangrove, water body, mud flat, and barren land (Table 4).

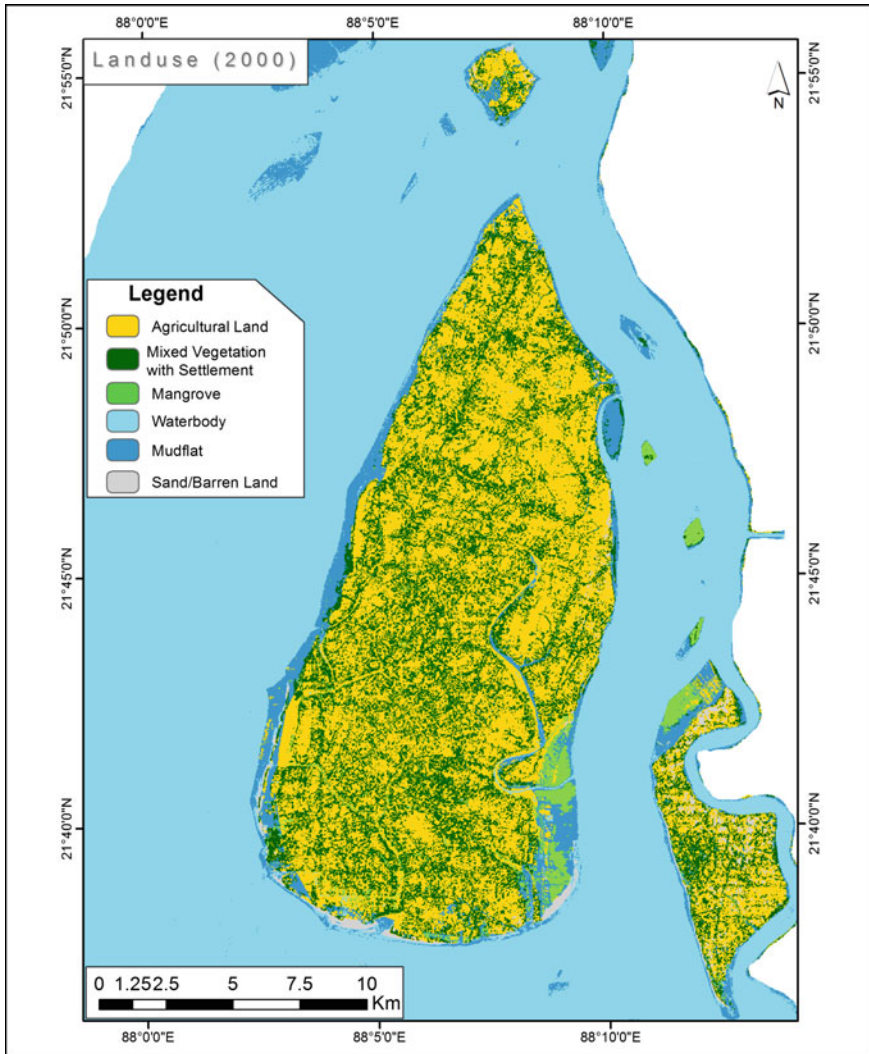


Fig. 6 Land use/Land cover map of the Study Islands (2000)

During the period of the study from 1990 to 2015, the overall trend of land cover changes that has been observed is an increase in settlement with vegetation land areas in expense of the agricultural land which is mainly due to the increase in population. A similar pattern more or less has been observed at Ghoramara and

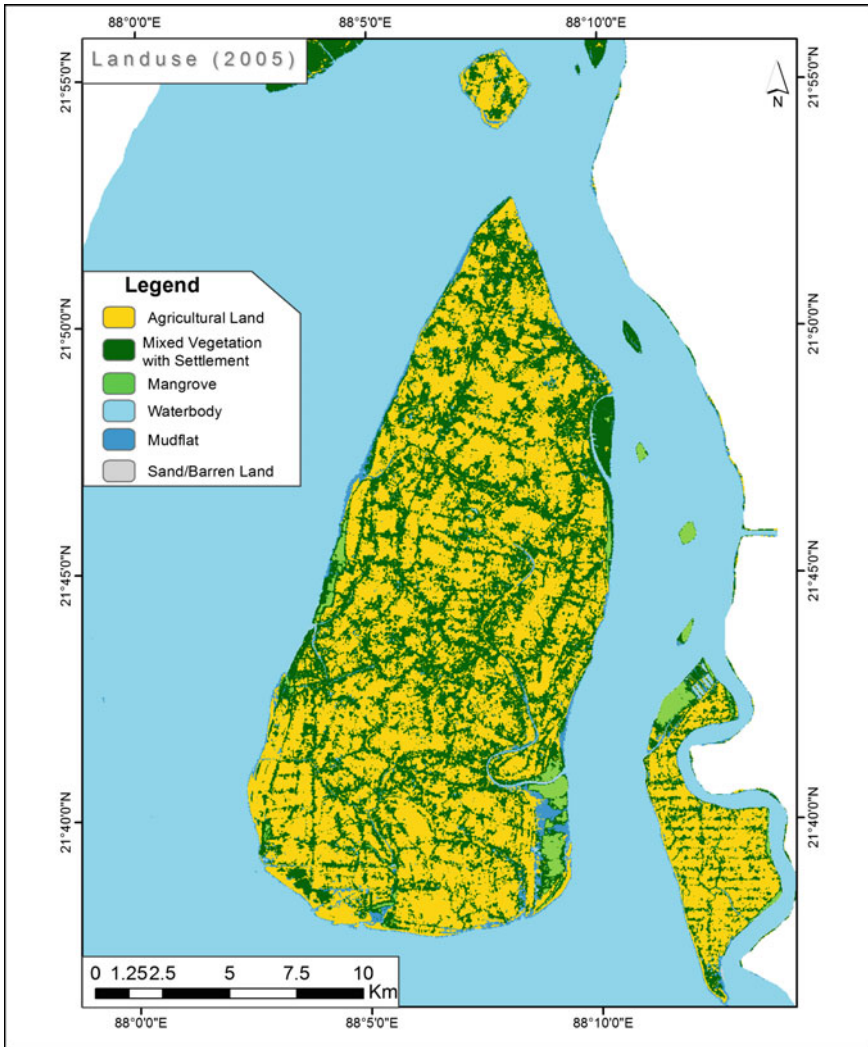


Fig. 7 Land use/Land cover map of the Study Islands (2005)

Mousani. From these images it can be suggested that mudflats have been stabilized by the mangrove plantation. It has also been found from field visits that in Sakhali, Kastala, Radhkrishnapur and Chemaguri, the mangrove plantations are growing in the mudflats.

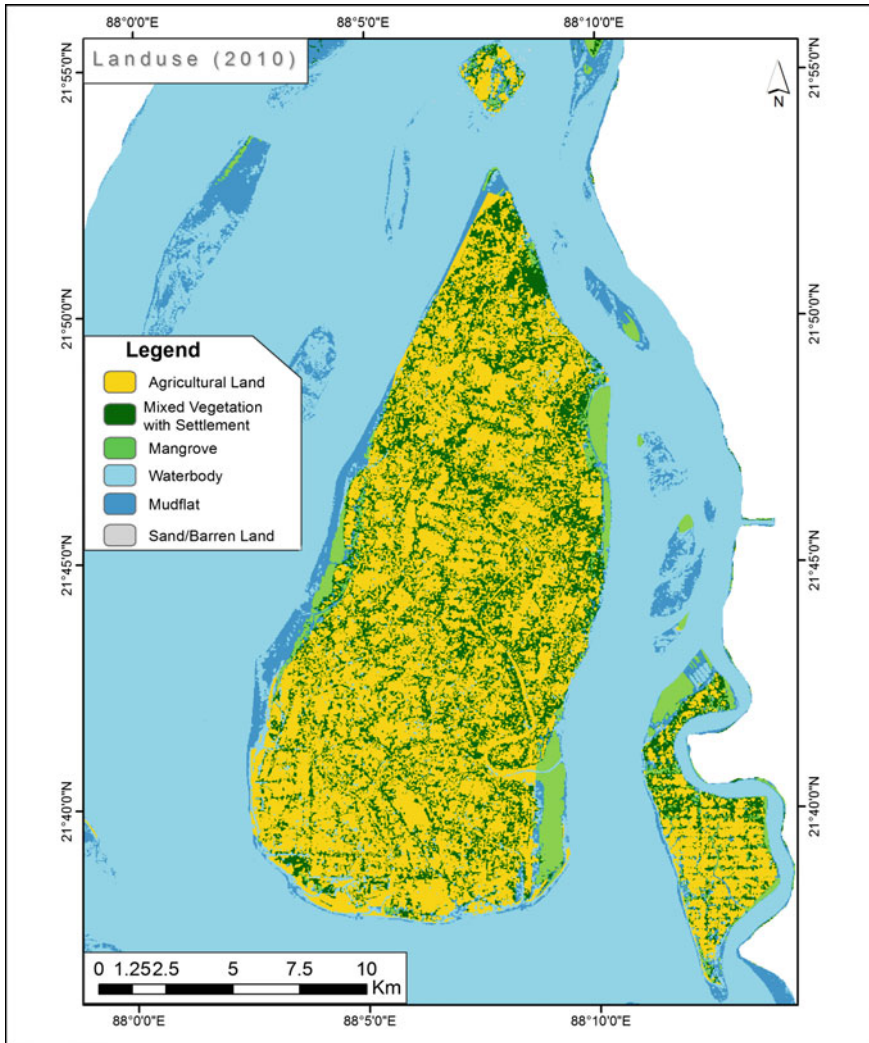


Fig. 8 Land use/Land cover map of the Study Islands (2010)

Erosion has a great impact on the Ghoramara Island. The total land area got reduced to 4.4 km² and the land use types have also been decreasing accordingly. Settlement with vegetation class had a 0.41 km² land loss and agricultural land had an increase in 2015 (Table 4). Unlike in the Sagar Island, agricultural land has not been replaced by settlement area in Ghoramara as the population growth is very low. The total population in 2010 was 5193 (Census 2011) which was 5236 in the

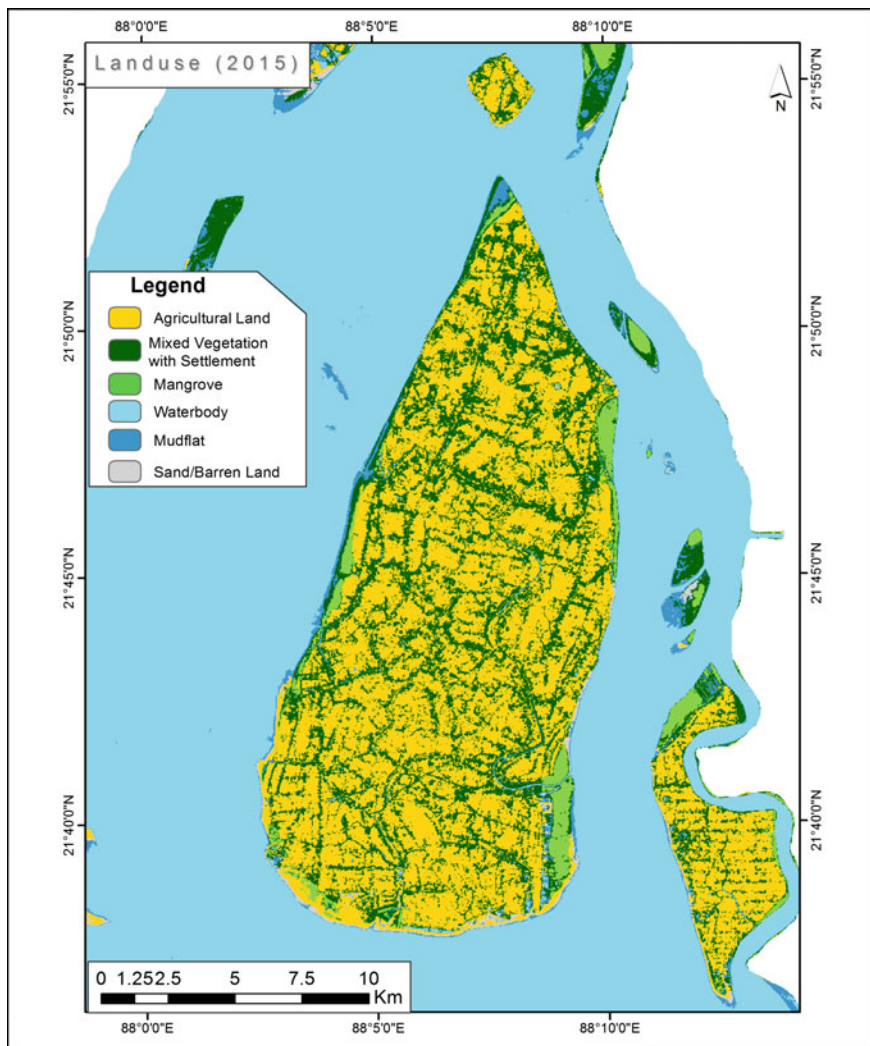


Fig. 9 Land use/land cover map of the Study Islands (2015)

year 2001 (Census 2001). So a clear positive correlation is found here between areal loss and a decrease in population influencing man induced land changes also. Significant land use or land cover changes couldn't identify in analysis but it is clear that morphological changes have great influence on land pattern change of these islands. Due to the population pressure and land loss, the per capita land availability has decreased throughout the 25 year time span.

Table 4 Landuse and landcover types in Study Islands during 1990–2015

LU/LC	1990	1995	2000	2005	2010	2015
<i>Sagar Island</i>						
Agricultural land	128.63	131.16	138.31	161.57	137.45	149.44
Mangrove	9.91	21.74	6.86	4.15	8.97	8.61
Mixed vegetation with settlement	82.23	79.26	74.95	68.7	84.02	75.12
Mudflat	12.6	7.98	20.99	6.89	13.8	5.45
Sand/Barren land	2.87	2.93	2.4	1.53	0.24	2.58
Water	21.39	14.56	14.12	14.79	13.15	16.43
<i>Ghoramara Island</i>						
Agricultural land	2.56	3.38	2.38	3.33	1.54	2.63
Mangrove	0.1	1.17	0.06	0.01	0.15	0.02
Mixed vegetation with settlement	1.23	1	1.05	1.13	1.78	1.37
Mudflat	0.93	0.2	1.39	0.49	0.73	0.12
Sand/Barren land	0.21	0.02	0.2	0.1	0.01	0.16
Water	0.9	0.16	0.85	0.87	1.72	1.63
<i>Mousani Island</i>						
Agricultural land	15.38	14.94	13.12	19.73	14.55	17.31
Mangrove	1.99	3.71	1.62	1.51	2.82	2.02
Mixed vegetation with settlement	12.6	10.23	8.22	6.53	7.58	7.2
Mudflat	0.87	1.36	4.3	0.9	3.88	1.24
Sand/Barren land	0.07	0.11	2.55	0.68	0.01	0.46
Water	1.58	2.14	2.68	3.14	3.65	4.26

3.3 Relation Between Landuse Pattern, Population Growth and Morphological Changes of Study Islands and Per Capita Land Availability

The immediate consequences of population growth can be land use pattern changes as the growing population need more land to live. The per capita land availability is decreasing due to the combine impact of erosion and population growth. It is evident from the analysis mentioned above that the settlement area increases at the expense of the other land use types. The changes in total land area due to erosion-accretion and resulted changes in land use pattern have been shown in the Fig. 10a. The graphical representation of the relation between population growth and per capita land availability (Fig. 10b) is clearly showing a decrease trend in per capita land availability. The decrease in land availability is mainly attributed to erosion. The total land area has been decreasing throughout the span of 25 years due to erosion even when the population has been increasing at the rate of 2.1 %

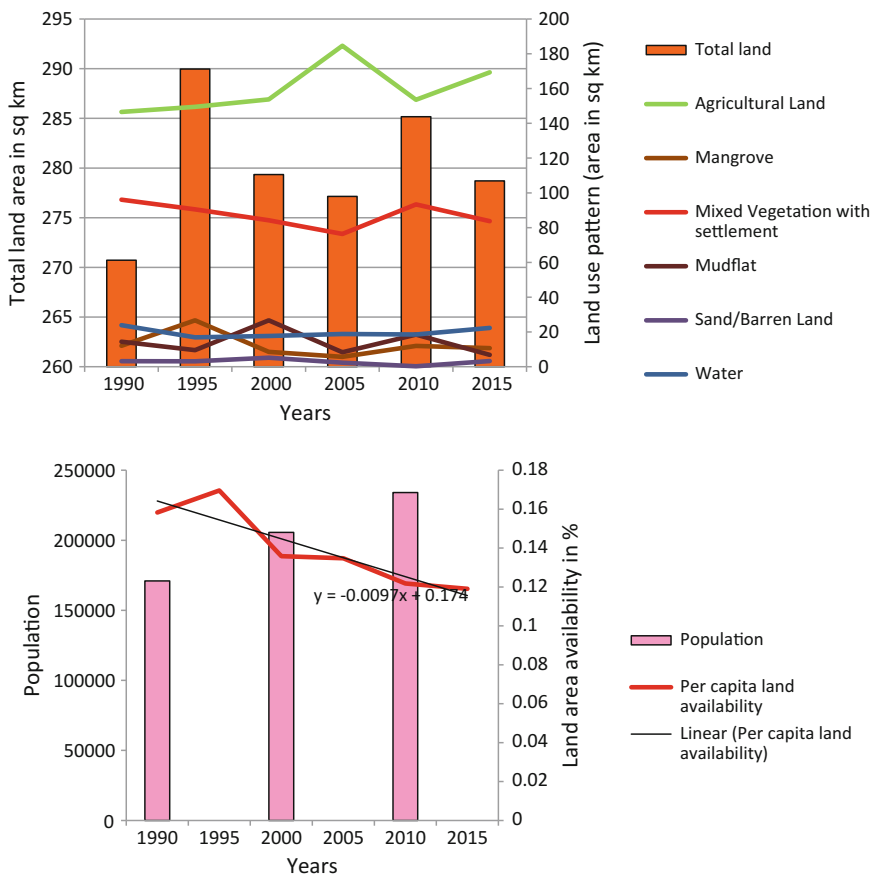


Fig. 10 a Changes in total land area and land use patterns of Study Islands (1990–2015). **b** Relation between population and per capita land availability in Study Islands

per annum. This decrease in the per capita land availability has a negative impact on the economy. The carrying capacity has also been disrupted due to the population growth which combined with the change in land use is making the whole system non-sustainable.

4 Conclusion

Land crisis is the most important issue affecting the Sundarban islanders. Land changes continuously through natural process of erosion and accretion while human intervention aggravates the problem. Remote Sensing and GIS are efficient tools to monitor the dynamism of land cover categories. Based on the analysis of satellite

data of the Sagar, Ghoramara, and Mousani islands over a period of 25 years, it has been observed that decrease in land area and increase in population pressure poses a serious threat to the sustainability of these islands. The shrinkage of agricultural land would have an impact on the food security of the region which could fail to meet demand for food of the inhabitants. Further, productivity loss that has been reported is also affecting the decline of the agricultural land.

Proper resource management and protection of marine and coastal ecosystems by 2020 has been given importance in the Sustainability Developmental Goals Post 2015. The regular maintenance of existing embankment and building stable embankments in vulnerable areas can help to protect further land loss. The pressure on resources could be relaxed by lowering the population growth though population growth is very difficult to control as a number of factors are responsible for it. The proper use of land would also minimize the problems. The implementation of modern agricultural technique could also make people interested in agriculture. Initiatives to increase productivity should be taken for the food security of the region. A detailed monitoring of the ongoing changes is important to identify the thrust areas for policy implications.

References

- Bandyopadhyay S (1997) Natural environmental hazards and their management: a case study of Sagar Island, India. *Singap J Tropol Geogr* 18(1):20–45
- Census Report of India (1991, 2001, 2011) Govt. of India
- Chavez PS (1988) An improved dark-object subtraction technique for atmospheric scattering correction of multispectral data. *Remote Sens Environ* 24(3):459–479
- Danda AA (2007) Surviving in the Sundarbans: threats and responses. Unpublished Ph.D. thesis. University of Twente
- Dinesh Kumar PK, Gopinath G, Laluraj CM, Seralathan P, Mitra D (2007) Change detection studies of Sagar Island, India, using Indian remote sensing satellite 1C linear imaging self-scan sensor III data. *J Coast Res* 23(6):1498–1502
- Ghosh T, Bhandari G, Hazra S (2003) Application of a ‘bio-engineering’ technique to protect Ghoramara Island (Bay of Bengal) from severe erosion. *J Coast Conserv* 9:171–178
- Ghosh T, Sengupta SK (1997) Morphological changes of Ghoramara Island, West Bengal: a documentation. *Indian J Geogr Environ* 2:64–65
- Ghosh T, Bhandari G, Hazra S (2001) Assessment of landuse/ landcover dynamics and shoreline changes of Sagar Island through remote sensing. Paper presented at the 22nd Asian conference on remote sensing, Singapore, 5–9 November
- Ghosh T, Hajra R, Mukhopadhyay A (2014) Island erosion and afflicted population: crisis and policies to handle climate change. In: Leal Filho W et al (eds) *International perspectives on climate change, climate change management*. Springer, Switzerland. doi:10.1007/978-3-319-04489-7_15
- Gopinath G (2010) Critical coastal issues of Sagar Island, east coast of India. *Environ Monit Assess* 160:555–561
- Gopinath G, Seralathan P (2005) Rapid erosion of the coast of Sagar Island, West Bengal—India. *Environ Geol* 48:1058–1067
- Hazra S, Bakshi A (2003) Environmental refugees from vanishing Islands. In: Bhattacharya P, Hazra S (eds) *Environment and human security*. Lancers’ Books, pp 219–227

- Hazra S, Ghosh T, DasGupta R, Sen G (2002) Sea level and associated changes in the Sundarbans. *Sci Cult* 68(9–12):309–321. ISSN 0036-8156
- Jana A, Sheena S, Biswas A (2012) Morphological change study of Ghoramara Island, Eastern India using multi temporal satellite data. *Res J Recent Sci* 1(10):72–81
- Jayappa KS, Mitra D, Mishra AK (2006) Coastal geomorphological and land-use and landcover study of Sagar Island, Bay of Bengal (India) using remotely sensed data. *Int J Remote Sens* 27 (17):3671–3682
- Jensen J (2004) *Introductory digital image processing*, 3rd edn. Pearson Prentice Hall
- Malone T, Davidson M, DiGiacomo P, Gonçalves E, Knap T, Muelbert J, Parslow J, Sweijd N, Yanagai T, Yap H (2010) Climate change, sustainable development and coastal ocean information needs. *Procedia Environ Sci* 1:324–341
- MOEF (2009) MOEF-ICZM Project Report. World Bank assisted integrated coastal zone management project. Environmental and social assessment. Govt of India, centre for environment and development, Thiruvantapuram, p 303
- Purkait B (2009) Coastal erosion in response to wave dynamics operative in Sagar Island, Sundarban delta, India. *Front Earth Sci China* 3(1):21–33
- Rogan J, Chen D (2004) Remote sensing technology for mapping and monitoring land-cover and land-use change. *Prog Plann* 61(4):301–325
- Thomas JV, Arunachalam A, Rajeev Jaiswal DP, Kiran B (2014) Dynamic land use and coastline changes in active estuarine regions—a study of Sundarban delta. *ISPRS-Int Arch Photogrammetry Remote Sens Spat Inf Sci* 1:133–139
- WWF (2010) In: Danda A (ed) *Sundarbans: future imperfect climate adaptation report*

Part IV
Remote Sensing of Natural Hazards

A Comparative Evaluation of Weight-Rating and Analytical Hierarchical (AHP) for Landslide Susceptibility Mapping in Dhalai District, Tripura

Kapil Ghosh, Shreya Bandyopadhyay and Sunil Kumar De

Abstract The landslide susceptibility map delineates the potential areas of landslide occurrence which is considered to be the first step for landslide hazard management. The present study focuses on the spatial analysis of landslide susceptibility in the Dhalai district using the Geographical Information System (GIS). For this purpose, landslide susceptibility maps are prepared using weight-rating and Analytical Hierarchical Processes (AHP). To analyze landslide manifestation in the present study area, different causative factors (lithology, road buffer, slope, relative relief, rainfall, fault buffer, land-use/land-cover, and drainage density) are derived as layers. The final susceptibility zonation map of weight-rating method shows that about 1.64 and 16.68 % of the total study area falls under very high and high susceptibility zones respectively. In the AHP method, the five landslide susceptibility zones are very low which accounted 14.8 % (354.35 km²) is, low 38.91 % (932.01 km²), moderate 34.75 % (832.37 km²), high 6.03 % (144.39 km²), and very high 5.51 % (131.87 km²). Both susceptibility maps show that the high susceptibility zone is restricted within the structural hilly areas and the low susceptibility zone is in the flood plain areas of the district. Both of the susceptibility maps are validated using the existing landslide distribution in the area.

Keywords Landslide · Susceptibility · Weight-rating system · Analytical hierarchical process · GIS

K. Ghosh · S. Bandyopadhyay
Department of Geography and Disaster Management, Tripura University,
Agartala 799022, India

S.K. De (✉)
Department of Geography, North Eastern Hill University, Shillong 793022, India
e-mail: desunil@yahoo.com

1 Introduction

Landslide is one of the most destructive environmental hazards in the hilly and mountain terrains in the tropical and the subtropical regions of world. Landslides in the mountainous regions can be considered to be cancer of hill slopes. Landslide is the result of a wide variety of processes which include geological, geomorphologic and meteorological factors. Normally the most important factors are bedrock geology (lithology, structure, degree of weathering), geomorphology (slope gradient, relative relief), land-use/land-cover and hydrologic conditions. But in recent years, anthropogenic activities may be considered to be one of the most important factors for the occurrence of this hazard. Incidents of landslide have reportedly increased ever since the road and other infrastructural developments have taken greater pace in the hilly areas. In Dhalai, most of the landslides have occurred along the National Highway (NH 44) in the high terrain areas of the Ataramura and the Longtarai hills. During the monsoon season every year, the occurrences of new landslides as well as reactivation of the old landslides are mainly responsible for creating frequent disturbance to the traffic on the National Highway, which is considered to be the lifeline of Tripura. The landslides as a consequence thus naturally lead to many deep socioeconomic problems. The amount of loss of life and properties are not so high or nil because of less human habitation along the road, but it disrupts the communication system. In the year 2000, there was massive cutting of slopes for the widening of the NH 44 and occurrences of slope failure have increased as a consequence.

In 2008, 10 % of India's population was affected by natural disaster, 0.5 % were affected by occurrences of landslides (EM-DAT 2009). According to the Geological Survey of India, (GSI 2009) 490,000 km² or 15 % of the land area of this country is vulnerable to landslide hazards. Out of these, 98,000 km² is located in the Northeast region of India.

Large numbers of landslides due to intensive rainfall have been reported in the months of May and June in 2013. In Mizoram, 17 people died and 9 houses collapsed due to the massive landslides on May 11, 2013 at Laipuitlang area in the northern part of the state capital, Aizawl. A large number of villages became inaccessible, 150 houses were badly damaged and the highway was blocked after landslides triggered by heavy and incessant rains. Two people died due to the landslide at Simna in West Tripura. In Guwahati, a woman was injured and several houses were damaged due to landslides in different parts of Guwahati following incessant rains. In Nagaland, the heavy landslide (around 80 m) took place on June 15, 2013 near the Kisama Naga heritage village in between Mao (Manipur) and Kohima (Nagaland) sector of the NH 29. As a result of the landslide, vehicular movement along that route was severely affected and prices of essential commodities increased.

Thus, landslide is a major environmental and safety hazard for the people in hilly areas of northeast India. But very few numbers of researches on landslide have been carried out on this region of the country (Pandey et al. 2008; Singh et al. 2011; Phukon et al. 2012; Dutta and Sarma 2013; Lallianthanga and Lalbiakmawia 2013; Devi and Das 2013; Singh and Singh 2013).

Identification of landslide prone areas or landslide susceptibility mapping is considered to be the integral part of landslide hazard management strategy. Landslide susceptibility (Radbruch 1970; Brabb and Pampeyan 1972) map is one form of landslide hazard zonation that includes the spatial distribution of factors related to the instability processes in order to determine zones of landslide prone areas without any temporal implication. Preparation of landslide susceptibility map involves both the qualitative as well as the quantitative approaches (Soeters and Van Westen 1996; Aleotti and Chowdhury 1999; Guzzetti et al. 1999). Qualitative methods depend on expert opinions and are often useful for regional assessment (Aleotti and Chowdhury 1999; Van Westen et al. 2003). Quantitative methods are particularly based on numerical expressions of the relationship between controlling factors and landslides (Guzzetti et al. 1999; Punia and Raman 2012). Recently, different new statistical techniques such as fuzzy logic (Lee 2005; Kanungo et al. 2008) artificial neural network (Ermini et al. 2005; Kanungo et al. 2006) and neuro-fuzzy (Sezer et al. 2011) models have been used to evaluate landslide susceptibility.

In this study, conventional weighting approach and analytical hierarchy approach were used to prepare the landslide susceptibility maps of the Dhalai district in Tripura. Performances of these two methods were then compared.

2 Location of the Study Area

The Dhalai District of the state of Tripura lies between the latitudes of 23° 25' 19" N–24° 15' 37" N and longitudes of 91° 45' 01" E–92° 10' 26" E (Fig. 1). The district covers an area of 2395 km² which is about 22.25 % of the total geographical area of the state. The district has an international boundary with Bangladesh in the south and the north. The districts Khowai and Gomati are in the west while Unokoti and the North Tripura district are in the eastern part. It is categorized as one of the economically backward district in the country.

The Dhalai district was formed in the year 1995 by dividing the North and South Tripura districts and named after the local river Dhalai with Ambassa as its headquarter. The district is characterized by a structural hilly topography which alternates with the narrow river valley. The important hill ranges are Atharamura, Langtarai, and Sakhantlang. These hill ranges are tightly folded and trending North–South direction. The maximum height of the hill ranges is 770 m. The height of these ranges gradually decreases toward the west and these hill ranges have developed during Tertiary Age.

The hills are covered with a thick forest. Different types of landforms like structural hills, denudation hill, inter-hill valley, undulating plains, flood plains, etc., are found in the study area. The whole study area is mainly composed of weathered sandstone, shale, siltstone, and alluvium. Most of the rivers have formed a subparallel to parallel and dendritic drainage pattern which indicates that they are flowing through a youthful stage. The district is drained by the river systems of the

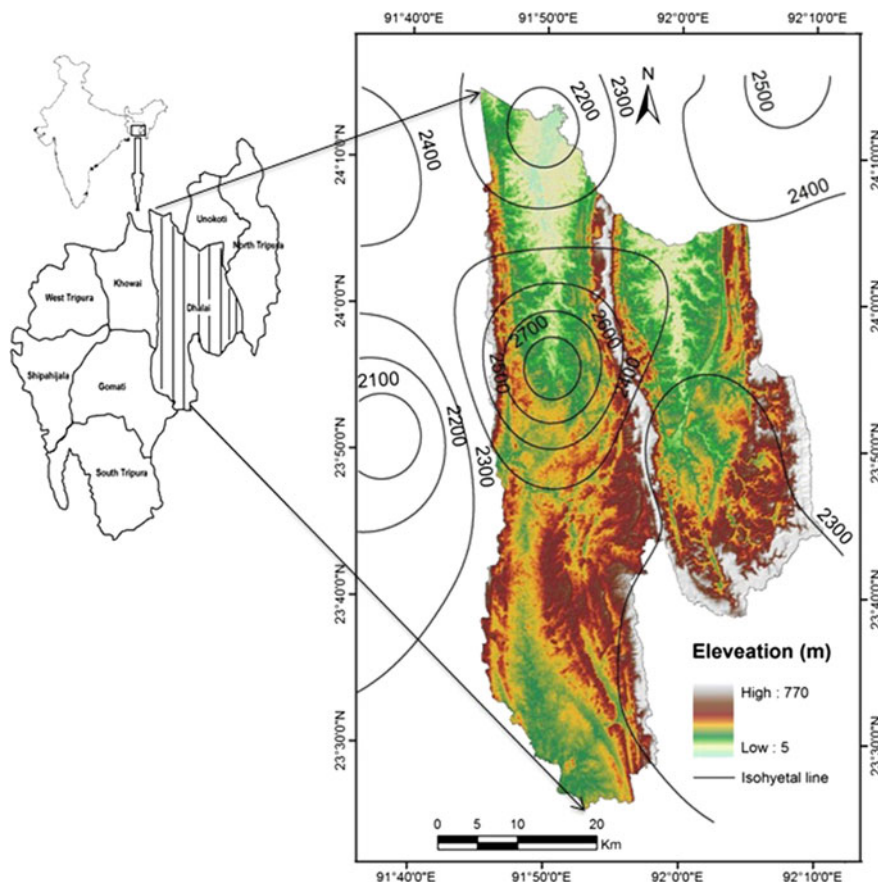


Fig. 1 Location map of the study area with iso-hyetal line

Dhalai, the Manu, the Gomati, the Khowai, and their tributaries which are perennial in nature. These river systems have originated from the Atharamura, the Longtarai, and the Sakhantlang ranges. In general, drainage pattern is structurally controlled and is in conformity with the topography.

The climate of the Dhalai district is mostly warm and humid with moderate temperatures. The area receives rainfall mainly from the southwest monsoon which commences in the month of May and lasts till September. Storms and thunder showers are common during the pre-monsoon season. The annual average rainfall is very high (2194 mm) in the study area and about 70 % of the total annual rainfall occurs during the monsoon season (between June and September). In general, the temperature varies from 20 to 34 °C. Maximum and minimum temperatures recorded during the year 2010 were 34.1 °C (in April) and 9.2 °C (in January) respectively. The texture of the soil ranges between sandy clay loamy to sandy-loamy and is acidic in nature in general.

The pH of the soil ranges from 4.50 to 6.5. About 70 % of the total study area is under dense to moderately dense forest cover.

3 Materials and Methods

In order to prepare the landslide susceptibility maps, different types of primary as well as secondary data have been used. Some of the data were amenable to satellite Remote Sensing while some prepared or obtained from field survey or other sources. Landslide susceptibility involves analysis of all the thematic data layers that have been considered to be the causative factor for landslide occurrences in the present study area. All the thematic data layers were prepared using the Geometrica 10.1 and the Arc-GIS 9.3 software. The data used in the present study are satellite images (IRS P6-LISS-III, Path—111, Row—055, date—19/12/2007), SRTM data with 90 m spatial resolution, Google Earth images, geological maps (from the Geological Survey of India), Survey of India (SOI) topographical sheets (78P/16, 73D/4, 79 M/14, 79 M/15, 84A/1 and 84A/2, scale 1: 63360) and rainfall data (IMD) of a time period of 10 years (2000–2010).

3.1 Data Layers

In the present study, eight parameters such as relative relief, slope, geological formation, and distance from fault, drainage density, land-use/land-cover, average annual rainfall, and distance from the road (Fig. 2) have been taken into account to prepare the landslide susceptibility map of Dhalai district, Tripura. To prepare the different data layers, the Survey of India (SOI) topographical sheets (1932–1933) and the existing maps were scanned to convert into a digital format and geo-referenced into the Universal Transverse Mercator (UTM), spheroid and datum WGS-1984 projection system.

The general topographical characteristics which include the relief and slope of the present study area have been studied through SRTM DEM data with a spatial resolution of 90 m. The slope map of the Dhalai district has been derived from the DEM using the slope function of the ArcGis 9.3 software. The slope map is in the form of a raster map with the same pixel size as the DEM. The slope map was reclassified into seven different classes by considering the slope gradient of the present study area. The relief map was classified into four classes with respect to altitudinal variation among flood plain to high structural hills in the present study area.

Lithology and fault maps were generated using the Geological Survey of India (GSI 2009) map Satellite Image (IRS P6-LISS-III, Path—111, Row—055, date—19/12/2007). Finally, the lithological map with the five formations namely Recent (Alluvium), Dupitila, Tipam, Bokabil, and Bhuban was rasterized on the ArcGis platform. To prepare the drainage density map, the entire drainage networks were digitized from the SOI topographic sheets of 1931–1932. The drainage density map

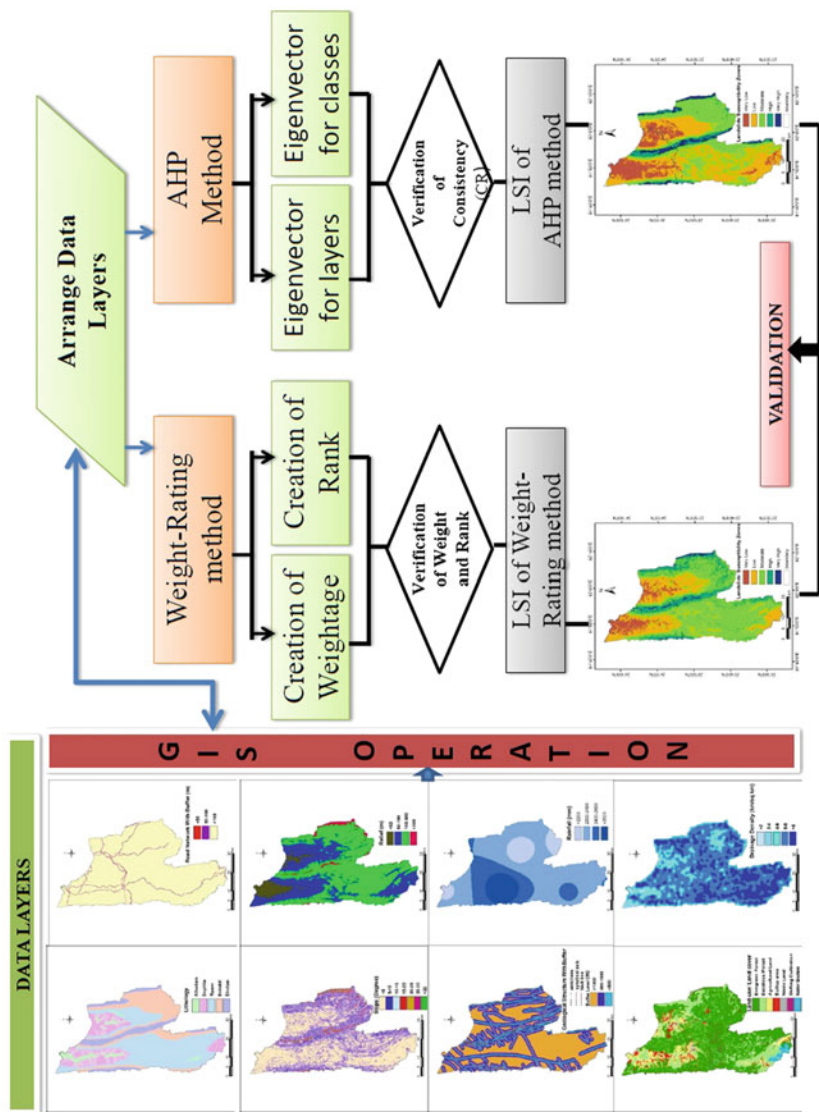


Fig. 2 Methodology adopted for landslide susceptibility mapping

(the length of drainage in km/km^2) was prepared by the Kernel method in the ArcGis 9.3 (pixel size of 30×30 m) software and reclassified into six classes with equal intervals. To generate the rainfall distribution map, the rainfall data of Ambassa, Kailashahar, Kamalpur, Chawmanu, Gandachhara, Teliamra, and Khowai, all of which are located in and around the study area, was collected for a 10 year period (2001–2010) from the meteorological department of Tripura.

Most of the available GIS software includes the Inverse Distance Weighting (IDW), kriging, spline, polynomial trend, and natural neighbor interpolation methods. In this study, the Inverse Distance Weighted (IDW) interpolation method, which is available in ArcGIS 9.3, was used for preparing this map. The road map of this study area was prepared by on-screen digitization from the Google images of 2010 and the road buffer map was prepared for susceptibility zonation mapping. The land use/land cover map of the study area was prepared from satellite data (IRS P6-LISS-III, Path—111, Row—055, date—12/19/2007) along with intensive ground truth verification with the help of the GPS. The supervised classification technique was used and the study area was classified into seven land-use/land-cover categories namely agricultural land, built-up area, deciduous forest, evergreen forest, shifting cultivation, wasteland, and water bodies. To verify the result of the study, the landslides location point was collected using the GPS and the landslide location map was then prepared.

In order to prepare the landslide susceptibility maps, eight parameters namely relative relief, slope, geological formation, distance from fault, drainage density, land-use/land-cover, average annual rainfall and distance from road were taken into account. All the thematic layers were integrated using the conventional weighting approach and the AHP approach and the landslide susceptibility maps were then produced.

3.2 Conventional Weighting Approach

Conventional weighting approach is based on the relative importance of the thematic maps that have been adopted for landslide susceptibility zonation (LSZ). The methodology is based on the guidelines of the LSZ mapping (Anbalagan 1992; BIS 1998). LSZ map of the present study area has been prepared on the basis of varying degrees on the estimated significance of the causative factors of instability such as lithology, structure, slope morphometry, land-use/land-cover and the hydrogeological condition. All the thematic layers (lithology, road buffer, slope, relative relief, rainfall, fault buffer, land-use/land-cover, and drainage density) were arranged according to their relative importance or probable influence on landslide and a weighting number (from 1 to 8) was assigned based on the multiple criteria decision-making techniques. Similarly, rating was assigned for each class within a layer which ranges from 0 to 9. GIS is an ideal tool to analyze and solve multiple criteria problems (Belton and Stewart 2002). The relative score of each thematic unit in a theme was calculated by multiplying the weight of the theme with the rank of the thematic unit. Finally using multi-criteria decision technique in GIS, a cumulative score of weight-rating index known as Landslide Susceptibility Index (LSI) was calculated.

The weight and rank of each layer is given in Table 2. All the thematic maps were overlaid using the spatial analyst tool of Arc GIS 9.3 to generate a Landslide Susceptibility Zone (LSZ) map. The resultant map was classified into high, moderate, low and very low susceptibility zones. This final LSZ map was verified in the cross checking method using the recent landslides inventory. The following equation was used for the LSZ mapping using a multi-criteria decision-making technique.

$$LSI = \sum [(Wt_1) * (Rt_1) + (Wt_2) * (Rt_2) + (Wt_3) * (Rt_3) + \dots (Wt_8) * (Rt_8)] \quad (1)$$

Where W is the weight of the theme, R is the rank of the theme, and $t_1, t_2, t_3, \dots, t_8$ are the theme numbers.

3.3 Analytical Hierarchy Process (AHP)

For the present study, the AHP method has also been used. This method was developed by Thomas Saaty at the Wharton School of Business in the 1970s (Saaty 1980). AHP is a multi-objective, semi-quantitative method that deals with the multi-criteria decisions approach. This method was used for the pair-wise comparison of all causative factors and to determine the priorities or the factor weights of the themes which have been considered for the susceptibility mapping. The AHP method is a semi-quantitative method, which includes the hierarchical structuring of the eight parameters and different classes of individual parameter, pair-wise comparison, redundant judgments, eigenvector calculation for deriving weightage and rating of the factors and the different classes of individual factors, and estimation of consistency level. In the AHP method, the relative importance (Weightage) of individual factor for preparing the landslide susceptibility map has been calculated by comparing individual factor with other factors. These comparisons were done by assigning numerical relative values between 1 and 9. The value for every individual parameter was adopted from Table 1 (Saaty 2000).

Table 1 Scale of preference between two parameters in AHP (Saaty 2000)

Degree of preferences	Numerical scales	Explanation
Equally	1	Two activities contribute equally to the objective
Moderately	3	Experience and judgment slightly to moderately favor one activity over another
Strongly	5	Experience and judgment strongly or essentially favor one activity over another
Very strongly	7	An activity is strongly favored over another and its dominance is showed in practice
Extremely	9	The evidence of favoring one activity over another is of the highest degree possible of an affirmation
Intermediate values	2, 4, 6, 8	Used to represent compromises between the preferences in weights 1, 3, 5, 7, and 9
Reciprocals	Opposites	Used for inverse comparison

In order to generate the pair-wise comparison matrix of the all parameters, each factor was rated against every other factor by assigning values between 1 and 9 when the factor on the horizontal axis was more important than the factor on the vertical axis. Conversely, the value also ranges between the reciprocals $\frac{1}{2}$ and $\frac{1}{9}$ for inverse comparison.

In this method, the consistency of the matrix can be checked using the consistency ratio (CR). The consistency ratio generally depends on a number of parameters and is ratio between the consistency index (CI) and average random consistency index (RI). This can be expressed as

$$CR = \frac{CI}{RI} \times 100. \quad (2)$$

The Consistency Index (CI) can be defined as

$$CI = \frac{\lambda_{\max} - n}{n - 1}. \quad (3)$$

Where λ_{\max} is the largest eigenvector value of a preference matrix and n is the number of parameters.

According to Saaty (1977), if the value of the CR is greater than 10 %, the subjective judgment of the matrix is inconsistent and needs to be revised. In this method the CR must be less than 10 %.

In this study, the LSZ map of the Dhalai district has been prepared by using the AHPmethod in the GIS platform. After preparing all the thematic layers, the LSI value for each considered pixel was computed. The LSI value of each pixel was calculated by multiplying the weight (eigenvector of causative factors) with the rating (eigenvector of the classes of the causative factors). Finally, the cumulative score of each pixel known as the LSI value was calculated.

$$LSI = \sum_{i=1}^n (W_i * R_i) \quad (4)$$

Where LSI is the landslide susceptibility index of the given pixel, R_i is the class weight (or rating value), and W_i is the factor weight for factor i and n is the total number of factors.

4 Results and Discussion

A number of trial and error methods were attempted to assign the weightage and rating in conventional weighting method to fixing the weightage and rating and to build the comparison matrix in AHP method. By altering the weightage of each layer and fixing the range for each class, the errors of the result were considerably reduced. This was because the reliability of this map was not only based on the information value calculation but also on the weightage given to layers. The final LSZ has been prepared by integrating all (relative relief, slope, geological

formation, distance from the fault, drainage density, land use/land cover, average annual rainfall, and the distance from the road) the parameters that have been considered as landslide causative factor for the present study.

4.1 Conventional Weighting Approach

In the conventional weighting method, all the thematic layers have been arranged according to their relative importance and the weighting number (from 1 to 8) was assigned (Table 2). Similarly, rating was assigned for each class within a layer which ranges from 0 to 9 using multi-criteria decision technique in the GIS and the cumulative score of the weight-rating index known as the Landslide Susceptibility Index (LSI) was calculated. The highest rating is given to the factors which are more important for landslide.

The landslide susceptibility map (Fig. 3) was generated on the basis of the cumulative LSI values assigned to the different features of the thematic layers in the GIS. The susceptibility map shows that LSI values are varying within the range of 70–255 in the study area. The LSI value of 132 is found to have the highest frequency of 1660, whereas the highest LSI value of 255 is found to have a frequency of only 2. From the LSI frequency distribution diagram (Fig. 4), it was found that only 0.74 % of the total frequency have an LSI value of more than 200. The LSI value of less than 100 was also found in only 6.56 % of the total frequency. The study revealed that more than 90 % of the total frequency has an LSI value of 100–200. The LSI threshold values of 100, 130, 160, and 190 were used for categorizing the susceptibility map into five zones namely very low, low, moderate, high, and very high. The respective area under these five zones is shown in Table 6.

The LSZ map shows that very high and high LSI values has been found on the structural hilly areas where landforms are characterized by a comparatively high degree of slope ($>25^\circ$), Bhuban formation and a high relative relief. Some very high to high LSI values were also found along the road sections because high weightage (i.e., 7) was given to this parameter. The higher LSI values indicate a greater instability of the slope where more attention is needed to bring about stability. The final susceptibility zonation map shows that only 1.64 and 16.68 % of the total study area fall under the very high and the high susceptibility zones respectively.

Moderate LSI values (130–160) were found mainly in the catchment area of the Dhalai and the Manu rivers which covered the majority of the southern portion of the present study area. Moderate LSI values were also found in the hill side slopes of the Ataramura and the Longtarai. The moderate susceptible zone is characterized by Tipam and Bokabil formation, 10° – 25° slopes, moderate to high drainage density and comparatively moderate (100–300 m) relative relief. The moderate susceptibility zones accounted for 49.11 % of the total study area.

Low and very low LSI values were found in the flood plain areas of the district. Low LSI values indicate very less probability of slope failure. The low to very low susceptible areas are characterized by gentle to very gentle slope and very little altitudinal difference. This zone is mainly composed of Dupitila and Alluvium formation. Low and very low susceptibility zones accounted for 25.2 and 7.38 % of the total study area respectively.

Table 2 Thematic maps, weightage, and rating for landslide susceptibility zonation study

Factor	Classes	Weightage	Rating	Remarks
Lithology	Alluvium Dupitila Tipam Bokabil Bhuban	8	2 3 5 7 8	Bhuban lithological units assign maximum rating value because this formation is characterized by thinly bedded repetition of sandstone moderate to highly weathered shale sandstone shale
Road Buffer (m)	<50 50–100 >100	7	9 5 3	Maximum rating value is assigned at <50 m distance from the road because unscientific cutting of hill side slope for widening and construction of roads, by which adherence capacity of the soil particles is lost
Slope (°)	<5° 5–10° 10–15° 15–20° 20–25° 25–30° >35°	6	2 3 4 5 6 7 8	High slopes (>35°) are highly prone to landslide due to the higher shear induced by gravity, but the slope below 15° have low susceptibility to the absence of debris over the slope surface
Relief (m)	<50 50–100 100–300 >300	5	2 4 6 8	Terrain height more than 300 m is highly prone to landslide, because the presence of debris and fragments etc.
Rainfall (mm)	<2200 2200–2400 2400–2600 >2600	4	5 6 7 8	The infiltration of water and gradual decay of pore water succession play major roles in triggering rain induce failures
Fault buffer (m)	<500 500–1000 >1000	3	7 5 3	The closeness to the fault lines in a formation showed high potential to landslides. Less than 500 m distance from the fault or lineament is assigned as the maximum rating value
Land-use/land-cover	Evergreen forest Agricultural land Water body Waste land Deciduous forest Build up area Shifting cultivation	2	1 2 1 6 4 8 9	Improper land-use such as scrub land, agricultural land, and vegetation has a higher susceptibility to landslides. Reserved/protected forest due to the presence of deep root bindings has lower susceptibility
Drainage density (km/km ²)	0–2 2–4 4–6 6–8 >8	1	1 2 3 5 7	When drainage is less, there is more possibility of infiltration, thereby increasing the pore pressure to result in landslide

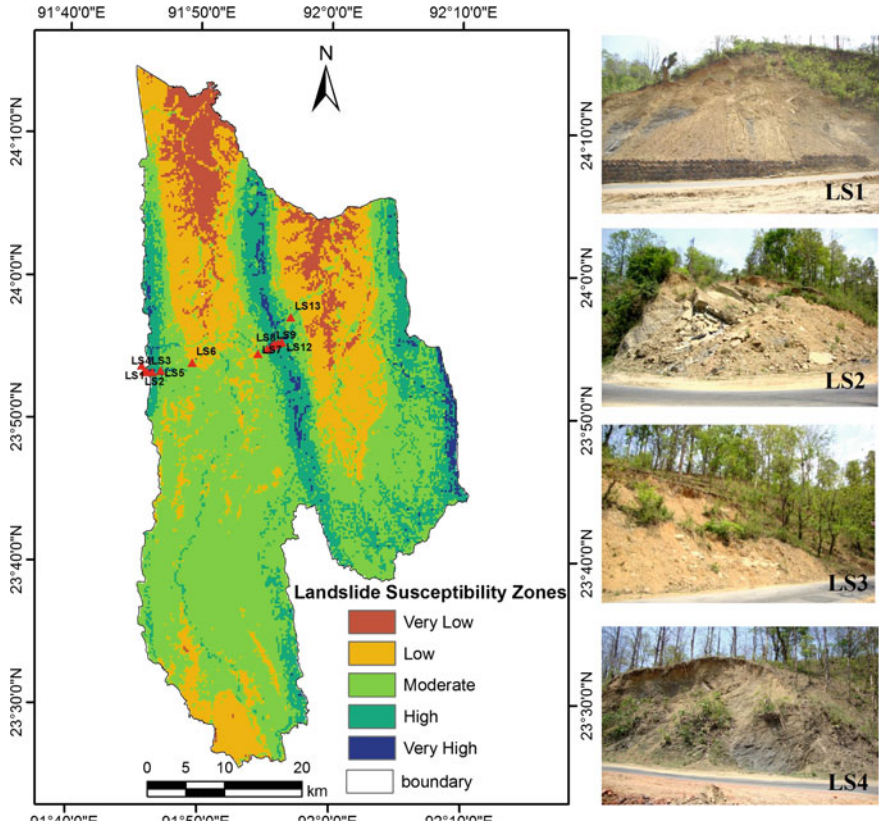


Fig. 3 Landslide susceptibility zonation (weight-rating) map of the study area

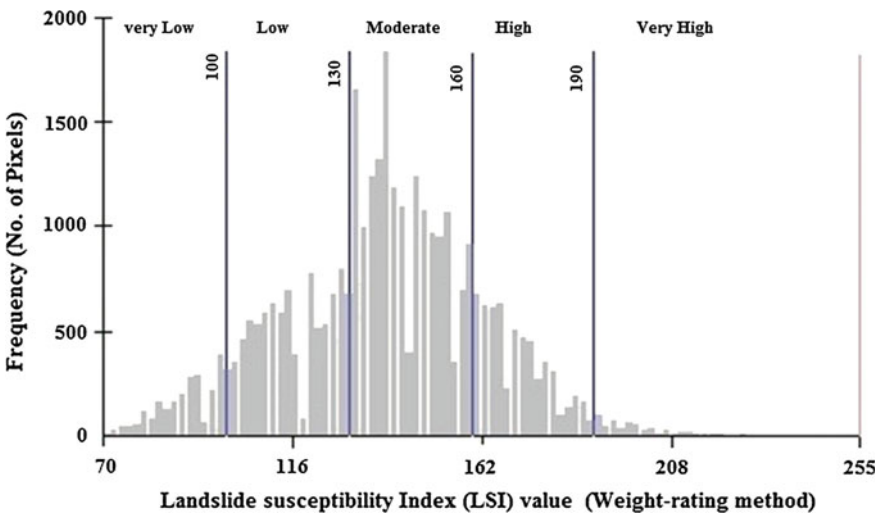


Fig. 4 Landslide susceptibility index (LSI) and frequency distribution (weight-rating method)

4.2 Analytical Hierarchy Process (AHP)

The LSZ map of the AHP method was also prepared by integrating all the parameters that have been considered as landslide causative factors for the present study. All the thematic layers were arranged according to their relative importance to the occurrence of landslide. This was done by assigning relative dominant values ranging from 9 (highest) to 1 (equal) and 1/9 (lowest). These values are assigned at the researcher's discretion by comparing each pair of parameters and the square reciprocal comparison matrixes are then generated. The normalized eigenvector values are calculated, which are termed as weightage values for landslide causative factors and rating values for different classes of individual causative factors.

The pair-wise comparisons of matrix for causative factors are shown in Table 3. In the pair-wise comparison matrix of causative factors, the first column of the matrix compares the lithology with the other factors. Lithology is mentioned in the first column because lithological formation plays the most vital role in the comparison with other factors for landslide in the present study area. The second column compares the road buffer with the remaining factors. The road factor has been taken as second-most important factor because most of the landslides in this district have occurred due to the unscientific cutting of hillside slopes for widening existing roads or constructing new roads.

The other factors are compared in the same way as the previous two factors according to their relative importance of landslide occurrence. In the pair-wise comparison matrix, the factor on the vertical axis is more important than the factor on the horizontal axis, the value varies between 1 and 9. Conversely, if the factor on the horizontal axis is more important than the factor on the vertical, then the values ranges between the reciprocals 1/2 and 1/9. Since we have used eight parameters, the comparison matrix has sixty-four boxes. It is important to mention that only the lower triangular part of the matrix is given because the values in the upper triangular part of the matrix are reciprocals of the lower triangular part. The eigenvector or the rating values of the different classes of individual factors are calculated by arranging similar comparison matrices (Table 4). The lithology gets the highest

Table 3 Original pair-wise comparison matrix for causative factors data layers

Data layers	(1)	(2)	(3)	(4)	(5)	(6)	(7)	(8)	Eigenvector (weightage)
(1) Lithology	1	3	4	5	7	6	8	9	0.331
(2) Road buffer	1/3	1	2	3	5	7	6	8	0.202
(3) Slope	1/4	1/2	1	2	3	4	6	7	0.133
(4) Lineament density	1/5	1/3	1/2	1	2	2	5	7	0.114
(5) Relief	1/7	1/5	1/3	1/2	1	3	5	7	0.108
(6) Land-use/land-cover	1/6	1/7	1/4	1/2	1/3	1	3	5	0.049
(7) Drainage density	1/8	1/6	1/6	1/5	1/5	1/3	1	5	0.041
(8) Rainfall	1/9	1/8	1/7	1/7	1/7	1/5	1/5	1	0.012

Table 4 Pair-wise comparison matrixes and principal eigenvectors of the class of respective data layers

Data layer		(1)	(2)	(3)	(4)	(5)	(6)	(7)	Eigenvector (rating)
Lithology	(1) Alluvium	1							0.05418741
	(2) Dupitila	3	1						0.10526890
	(3) Tipam	4	2	1					0.16766764
	(4) Bokabil	4	3	2	1				0.25933451
	(5) Bhuban	5	4	3	2	1			0.41354155
Road buffer (m)	(1) <50	1							0.76075974
	(2) 50–100	1/7	1						0.19119095
	(3) >100	1/9	1/7	1					0.04804931
Slope (°)	(1) <5°	1							0.29469
	(2) 5–10°	2	1						0.04334
	(3) 10–15°	3	2	1					0.057303
	(4) 15–20°	4	3	3	1				0.107055
	(5) 20–25°	5	4	4	2	1			0.160468
	(6) 25–30°	6	5	5	3	2	1		0.240204
	(7) >30°	8	7	6	4	3	2	1	0.363168
Relief (m)	(1) <50 m	1							0.05528549
	(2) 50–100 m	3	1						0.11750425
	(3) 100–300 m	5	3	1					0.26220121
	(4) >300 m	7	5	3	1				0.56500905
Rainfall (mm)	(1) <2200	1							0.1280599
	(2) 2200–2400	1	1						0.1379890
	(3) 2400–2600	2	2	1					0.2561198
	(4) >2600	4	3	2	1				0.4778314
Fault buffer (m)	(1) <500	1							0.6250131
	(2) 500–1000	1/3	1						0.2384871
	(3) >1000	1/4	1/2	1					0.1364998
Land-use/land-cover	(1) Water body	1							0.03124205
	(2) Evergreen forest	2	1						0.04308909
	(3) Deciduous forest	3	2	1					0.06470923
	(4) Agricultural land	4	3	2	1				0.09222643
	(5) Waste land	5	4	3	3	1			0.15274067
	(6) Build up area	5	5	4	4	3	1		0.25656521
	(7) Shifting cultivation	7	6	5	4	4	2	1	0.35942732
Drainage density (km/sq. km)	(1) 0–2	1							0.06176665
	(2) 2–4	2	1						0.09725359
	(3) 4–6	3	2	1					0.15992286
	(4) 6–8	4	3	2	1				0.26251761
	(5) >8	5	4	3	2	1			0.41853929

Table 5 Number of parameters (n), largest eigenvector of the performance matrix (λ_{max}), consistency index (CI), random consistency index (RI) (Satty 1977) and consistency ratio (CR) for the landslide causative factors

Causative factors	n	λ_{max}	CI	RI	CR (%)
All	8	8.86	0.087	1.41	8.71
Lithology	5	5.14	0.035	1.12	3.13
Road buffer	3	3.08	0.040	0.58	6.89
Slope	7	7.24	0.040	1.32	3.03
Relief	4	4.12	0.040	0.90	4.44
Rainfall	4	4.01	0.003	0.90	0.37
Fault buffer	3	3.02	0.010	0.58	1.72
Land-use/land-cover	7	7.39	0.065	1.32	4.92
Drainage density	5	5.07	0.016	1.12	1.56

weightage of 0.331 and rainfall gets the lowest weightage of 0.012. Consistencies of all causative factors as well as the classes within the factors have been checked. The Consistency Ratio (CR) shows the acceptable result (<10 %) for the parameters and classes within the parameters (Table 5).

Using the AHP, the LSI values were computed. From the calculation, it was found that the LSI had a minimum value of 0.05 a maximum value of 0.366, an average value of 0.132, and a standard deviation of 0.039. The LSI represents the relative susceptibility of a landslide occurrence. Therefore, the higher the index, the more susceptible the area is to landslide.

In order to prepare the LSZ using the AHP method, the LSI values were categorized into five classes by considering the threshold values of 0.105, 0.140, 0.181, and 0.229 (Fig. 5) for very low, low moderate high, and very high categories

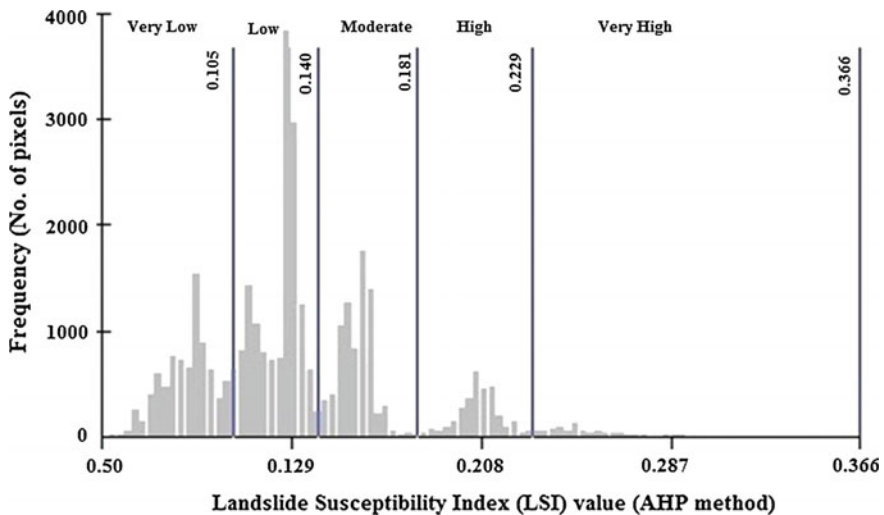


Fig. 5 Landslide susceptibility index (LSI) and frequency distribution (AHP method)

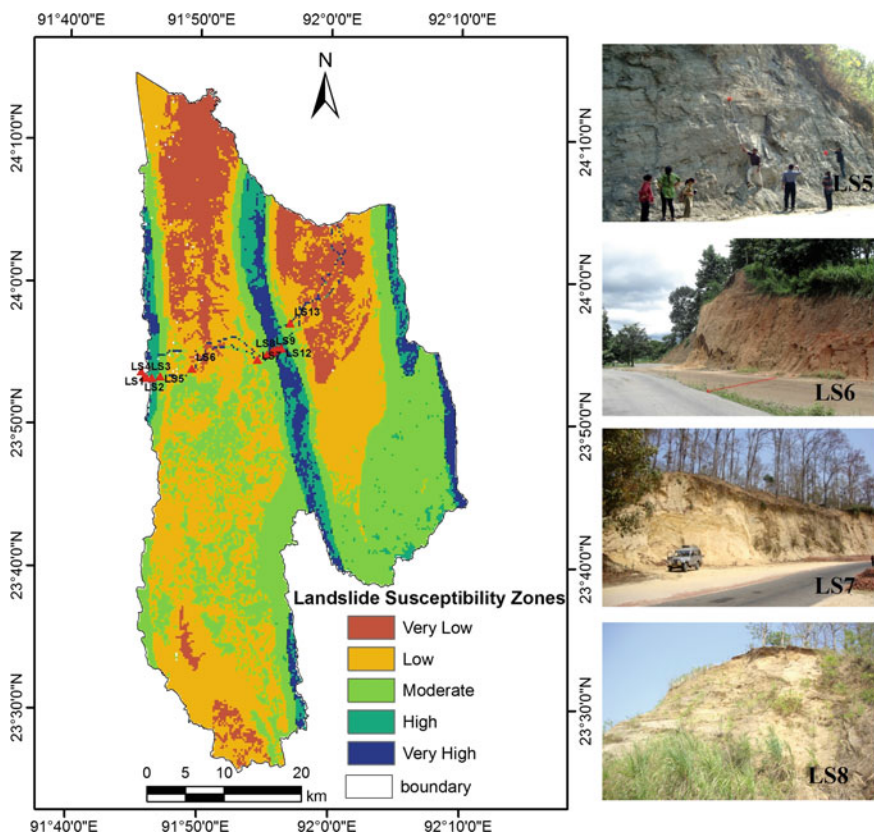


Fig. 6 Landslide susceptibility zonation (AHP) map of the study area

Table 6 Distribution of landslide susceptibility zones and area normalized incidence

Landslide susceptibility zone	Weight-rating method			AHP method		
	Area (%)	No. of landslides	Incidence per km ²	Area (%)	No. of landslides	Incidence per km ²
Very low	7.38	0	0	14.8	0	0
Low	25.20	0	0	38.91	0	0
Moderate	49.11	6	0.004	34.75	4	0.003
High	16.68	6	0.015	6.03	7	0.025
Very high	1.64	1	0.024	5.51	2	0.027

respectively. These are the five different zones in the landslide susceptibility map (Fig. 6). The five landslide susceptibility classes of the LSZ map are: very low 14.8 % (354.35 km²), low 38.91 % (932.01 km²), moderate 34.75 % (832.37 km²), high 6.03 % (144.39 km²), and very high 5.51 % (131.87 km²) (Table 6).

4.3 Comparison and Validation

The present LSZ maps have been prepared based upon the parameters which have been considered as the landslide occurrence factors. Thus, validity test is important in order to justify the result. The 13 recent landslides occurrences, which have been identified during field survey using the GPS have been used to validate the landslide susceptibility maps of the present study. A spatial layer containing these recent landslide locations has been prepared. This layer was overlaid on the landslide susceptibility maps and by cross verifying the frequency of landslides and area normalized incidence has derived. The observation has been given in Table 6.

The validation of the result shows satisfactory agreement between the susceptibility maps and the existing data of landslide locations. From the study, it was found that most of the identified landslide points fall into high to moderate zones of the susceptibility map. Therefore, it can be said that the adopted methods and classification scheme perfectly match with the reality in the present study area.

In the weight-rating-based model based on the distribution of the 13 recent landslides, it was found that 1 of them fell in the very high zone, 6 of them in the high zone and the remaining 6 in the moderate zones. No landslide event is found in the very low or the low susceptible zones. The value of area normalized incidence shows that it has increased from moderate (0.004) to very high (0.024) zones. In the AHP method, the area normalized incidence values have also increased toward the very high landslide susceptibility zone. Since no historical record of landslide incidence is available, the present study was carried out on the basis of the existing landslide events detected from the field. However, the reliability of this study is directly dependent on the quality and quantity of the collected data as well as the methods and skill for conceptual landslide prediction.

5 Conclusion

Remote Sensing and Geographical Information System are very useful tools for landslide susceptibility zonation mapping. They facilitate the integration of numerous thematic data layers which are required to generate the landslide susceptibility zonation maps. The present research revealed that lithology and road had more influence than any other considered factor on the occurrence of landslides in the present study area.

Most of the landslides have occurred along the road side slopes in the Tipam and the Bhuban formation. Roads on the high hilly terrain are being constructed unscientifically and without taking the local geological, lithological, and hydrological information into consideration. The final susceptibility zonation maps have been categorized into very high, high, moderate, low, and very low class. The susceptibility maps were verified with the landslide inventory and satisfactory results were found. The weight and the rating values of all causative factors and

classes of the respective factors were assigned based on relative importance of the factors, which strongly depends on the researcher's choice and knowledge. The AHP method for landslide susceptibility gives greater flexibility for checking the consistency of the result. The results of these two methods slightly vary with each other. Thus, the combination of the two results can give us a more acceptable susceptibility zonation map which can be used as basic data to assist slope management, road construction and land-use planning. All this information, however, is not sufficient to reduce the potential risk of landslides in a given area. Therefore, site-specific studies of different landslides are required wherever local geological and geographic heterogeneities are found.

References

- Aleotti P, Chowdhury R (1999) Landslide hazard assessment: summary review and new perspectives. *Bull Eng Geol Environ* 58(1):21–44
- Anbalagan R (1992) Landslide hazard evaluation and zonation mapping in mountainous terrain. *Eng Geol* 32:269–277
- Belton V, Stewart T (2002) Multi criteria decision analysis: an integrated approach. Kluwaer Academic Publishers, Bostan
- BIS (1998) Guideline for preparation of landslide hazard zonation maps in mountains terrains; draft proposal of the Bureau of Indian Standards 2:1–15
- Brabb EE, Pampeyan, EH (1972) Preliminary map of landslide deposits in San Mateo County, California. US Geological Survey Miscellaneous Field Studies, Map MF-360, scale 1:62,500. (Reprinted in 1978)
- Devi D, Das K (2013) Landslide hazard zonation along NH-39 from Kangpokpi to Mao, Manipur, India. *Int J Econ Environ Geol* 2(1):30–35
- Dutta PJ, Sarma S (2013) Landslide susceptibility zoning of the Kala-Pahar Hill, Guwahati Assam state (India), using a GIS based heuristic technique. *Int J Remote Sens Geosci* 2(2):49–55
- EM-DAT (2009) Emergency management disaster database. www.emdat.be/maps-disaster-types
- Ermini L, Catani F, Casagli N (2005) Artificial neural networks applied to landslide susceptibility assessment. *Geomorphology* 66:327–343
- GSI (2009) Geological survey of India report. www.portal.gsi.gov.in
- Guzzetti F, Cardinali M, Reichenbach P, Carrara A (1999) Comparing landslide maps: a case study in the upper Tiber River Basin, central Italy. *Environ Manag* 25:247–363
- Kanungo DP, Arora MK, Gupta RP, Sarkar S (2008) Landslide risk assessment using concepts of danger pixels and fuzzy set theory in Darjeeling Himalayas. *Landslides* 5:407–416
- Kanungo DP, Arora MK, Sarkar S, Gupta RP (2006) A comparative study of conventional, ANN black box, fuzzy and combined neural and fuzzy weighting procedures for landslide susceptibility zonation in Darjeeling Himalayas. *Eng Geol* 85:347–366
- Lallianthanga RK, Lalbiakmawia F (2013) Landslide hazard zonation of Mamit town, Mizoram, India using remote sensing and GIS techniques. *Int J Geol Earth Environ Sci* 3(1):184–194
- Lee S (2005) Application of logistic regression model and its validation for landslide susceptibility mapping using GIS and remote sensing data. *Int J Remote Sens* 26:1477–1491
- Pandey A, Dabral PP, Chowdary VM, Yadav NK (2008) Landslide hazard zonation using remote sensing and GIS: a case study of Dikrong river basin, Arunachal Pradesh, India. *Environ Geol* 54:1517–1529
- Phukon P, Chetia D, Das P (2012) Landslide susceptibility assessment in the Guwahati city, Assam using analytic hierarchy process (AHP) and geographic information system (GIS). *Int J Comput Appl Eng Sci* 2(1):1–6

- Punia M, Raman R (2012) The application of GIS-based bivariate statistical methods for landslide hazards assessment in the upper Tons river valley, Western Himalaya, India. *Georisk: Assess Manag Risk Eng Syst Geo Hazards* 6(3):145–161
- Radbruch DH (1970) Map of relative amounts of landslides in California, US Geological Survey Open-File Report 70-1485, pp 36, map scale 1:500,000. US Geological Survey Open-File Report, 85-585
- Saaty TL (1977) A scaling method for priorities in hierarchical structures. *J Math Psychol* 15:234–281
- Saaty TL (1980) *The analytical hierarchy process*. McGraw Hill, NY, p 350
- Saaty TL (2000) *Models, methods, concepts and application of the analytical hierarchy process*. Kluwer Academic Publishers, Boston
- Sezer EA, Pradhan B, Gokceoglu C (2011) Manifestation of an adaptive neuro-fuzzy model on landslide susceptibility mapping: Klang valley, Malaysia. *Expert Syst Appl* 38:8208–8219
- Singh CD, Behera KK, Rochoy WS (2011) Landslide Susceptibility along NH-39 between Karong and Mao, Senapati District, Manipur. *J Geol Soc India* 78:559–570
- Singh CD, Singh J (2013) Landslides caused due to ignorance—case studies from northeast India. *J Geol Soc India* 82(1):91–94
- Soeters R, Van Westen CJ (1996) Slope instability recognition, analysis, and zonation. In: Urner AK, Schuster RL (eds) *Landslides: investigation and mitigation*, vol 247. National Academy Press, Washington, D.C, pp 129–177
- Van Westen CJ, Rengers N, Soeters R (2003) Use of geomorphological information in indirect landslide susceptibility assessment. *Nat Hazard* 30:399–419

Micro Level Vulnerability Assessment of a Community Living in Mousuni Island in the Indian Sundarban: An Integrated Study Employing Geoinformatics

Bimalesh Samanta, Shouvik Das and Sugata Hazra

Abstract Climate change literature mentions that the Indian Sundarban is under accelerating threat of climate change-related impacts. This can be of disastrous consequences as the Sunderban is the world's largest repository of mangrove and mangrove-associated flora and fauna with the highest species diversity. It is also home to nearly 4.6 million human population Mousuni island, one of the 54 islands in the Indian Sundarban to have been occupied by settlers of the early nineteenth century, is highly vulnerable due to severe coastal erosion, repeated breach of embankments, cyclones, storm surge, and inundation causing loss of lives, properties and displacement and migration of families. From the perspectives of climate change-related coastal hazards, Composite Vulnerability (VR_c) which is a product of physical as well as socioeconomic vulnerability at community level has been computed. The estimated VR_c indicates overall vulnerability of each family having its geographical position determined by the GPS. The physical vulnerability characterizes relative vulnerability to physical changes of the island in quantifiable manner, whereas socioeconomic vulnerability illustrates the locally relevant socioeconomic components that further quantify the degree of vulnerability of the island community. Geoinformatics techniques have been employed to integrate both the physical and the socioeconomic components of vulnerability in order to identify and locate the most vulnerable families. This will help in planned adaptation that can be taken up by administrators and policymakers for reducing the risks due to climate change.

Keywords Sundarban · Disaster · Migration · Vulnerability · Geoinformatics · Climate change adaptation

B. Samanta

Department of Science and Technology, Government of West Bengal, Kolkata, India

S. Das · S. Hazra (✉)

School of Oceanographic Studies, Jadavpur University, Jadavpur, India

e-mail: sugata_hazra@yahoo.com

© Springer International Publishing Switzerland 2017

S. Hazra et al. (eds.), *Environment and Earth Observation*,

Springer Remote Sensing/Photogrammetry, DOI 10.1007/978-3-319-46010-9_13

1 Introduction

The Indian Sundarban is the world's largest transboundary repository of mangrove and mangrove-associated flora and fauna with the highest species diversity (Mandal and Nandi 1989; Mandal and Naskar 2008). It is also home to nearly 4.6 million human population but has been suffering from severe coastal erosion, frequent high intensity cyclones and surge, repeated breach of embankments and saline water encrustation. These have resulted in disastrous consequences like damage of crops, land loss, submergence of islands, and forced displacement of families (Hazra et al. 2002; Hazra and Bakshi 2003). Besides these, a very high density of human population, the prevalence of alarming poverty, low level of coping capacity, and inadequate disaster resiliencies force island communities to live under high degree of physical vulnerability together with socioeconomic vulnerability (Hazra et al. 2009).

The Indian Sundarban spreads over 9630 km² area together with 4260 km² forest tract in 48 islands and 5370 km² human colonized part in 54 islands extending between 21° 30' 00"N and 22° 40' 49"N latitude and 88° 02' 35"E–89° 08' 04"E longitude. It is demarcated by the Hugli estuary in the west, Harinbanga–Raimangal–Ichamati Rivers in the East, the Bay of Bengal in the South, and the Dampier-Hodges line in the North. The area to the South of this line, closely corresponds to the Kakdwip–Basirhat–Dhaka morpho-structural lineament (Chakraborti 1995) and is interspersed with innumerable river distributaries and tidal creeks that shape the Sundarban with group of islands. The area is an estuarine part of the Ganga–Brahmaputra Delta developed by the river-borne quaternary sediments (2500–5000 YBP) rapidly reworked by fluvial, fluvio-tidal and marine coastal sediments (Chakraborti 1991; Allison et al. 2003).

In the present day scenario, the Sundarban region has become the abandoned part of the delta and is probably in its destructive phase. Human colonized islands like Ghoramara, Sagar, Mousuni, Namkhana, G-Plot, as well as the mangrove islands like Dhanchi, Bulcheri, Dulibhasani, Dalhousie, Bhangduni, and Jambudwipare have experienced land loss. The land area of the Indian Sundarban has reduced by 257.03 km² at the rate of 5.97 km² per year over 44 years (1968/69–2012). The erosion has been the most dominant in the recent decade, registering a land loss of 89.32 km² during 2001–2012, at the rate of 8.12 km² per year (Hazra et al. 2010). Large numbers of families are being displaced due to erosion. Three islands viz. Lohachara, Bedford, and Suparibhanga have already vanished into sea turning its inhabitants into migrants and refugees (Hazra and Bakshi 2003; Hazra et al. 2010).

The previous study by Unnikrishnan and Sankar (2007) reported that the sea level rise value in the North Indian Ocean is close to 2.0 mm per year and in case of the northeastern part of the Bay of Bengal, it is more than 4 mm per year. The recent study of Hazra et al. (2010) estimates that the relative mean sea level is rising at the rate of 12 mm per year in the Bay of Bengal and the sea surface temperature rise rate is 0.0453 °C per year. Increasing trend in the frequency of high to very

high intensity cyclonic storms (increased 20–26 %; Singh et al. 2001; Singh 2007), rising trend of salinity regime in estuarine water (Hoque et al. 2006), shifting of high rainfall months, loss of forest cover and floral/faunal diversity indicate that the Sundarban Deltaic region is under serious threats of climate change-related impacts.

It is evident that the Sundarban is being adversely affected by high intensity events like Sidr, 2007 and Aila, 2009. The damage estimated due to Aila, based on Radarsat 2 and IRS P6 LISS IV satellite data and GPS survey, show that more than 1457 segments of protective embankments were breached, 305 km of land was washed away and 553 km of land was severely damaged. As a result, 600 villages were inundated affecting the lives of 2.6 million people. The estimated damage to crops was ₹336.74 crores due to the inundation of 211,090 ha of the cropland. The damage to infrastructure was ₹15.55 crores (source: Directorate of Irrigation and Waterways, Govt. of WB 2009a; Dept. of Disaster Management, Govt. of WB 2009b).

In this context, a micro level vulnerability assessment has been conducted in Mousuni island, one of the small islands suffering from severe coastal erosion, frequent embankment breaching, inundation, and displacement of families along with very high density of population, alarming poverty, inadequate disaster resiliencies, and low level of coping capacity. The island has registered 16 % land loss during the 1968/69–2012 period. Yet the island is home to 3340 families and 20,013 people (Fig. 1).

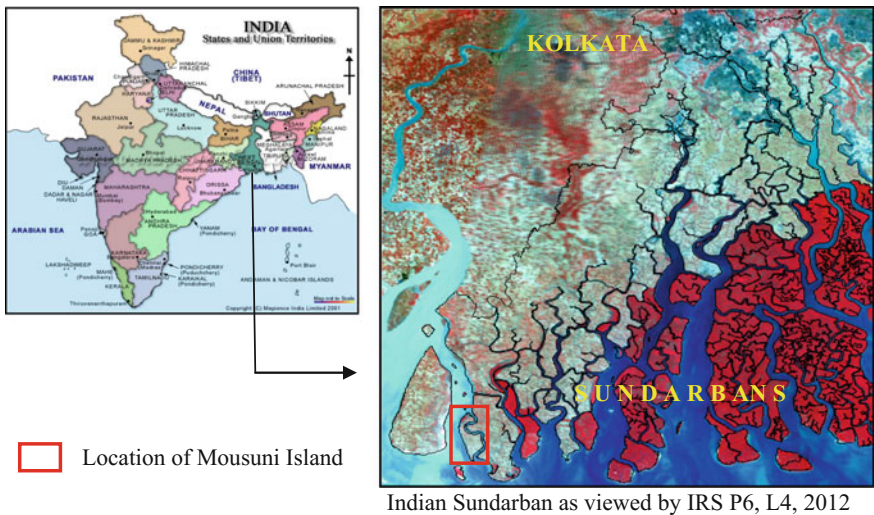


Fig. 1 Location map of study area

2 Methodology

Coastal vulnerability assessments from the perspective of climate change have been governed largely by IPCC-CZMS (1992), IPCC Technical Guidelines for Assessing Climate Change Impacts and Adaptations (Carter et al. 1994), UNDP Handbook on Methods for Climate Change Impact Assessment (Feenstra et al. 1998) and the IPCC third Assessment Report (2001). These documents provide the general frameworks to assess impacts of climate change by identifying key vulnerabilities. The researchers have evaluated the merits of applicability of these methodological frameworks and have redefined integrated frameworks (Yamada et al. 1995; Harvey et al. 1999; Wu et al. 2002). It has been observed that the definitions of vulnerability often differ and are motivated by different objectives (Patwardhan 2006). Moreover, the focus on community-based research is underemphasized and little attention has been paid to community-based attributes (Riedlinger and Betkes 2001; Jones 2001).

The National Action Plan on Climate Change (2008) has introduced eight National Missions of disaster-specific vulnerability assessment at macro levels viz. state and district level. The Government of West Bengal in its Action Plan on Climate Change (2012) has recommended studies on vulnerability in the Indian Sundarban Delta as a special region from the perspective of climate change, where specific guidelines of vulnerability assessment need to be framed.

2.1 *Micro Level Vulnerability Assessment*

In this study, vulnerability has been computed using multiplicative method of physical and social vulnerabilities which include computation of structural vulnerability of the dwelling hut (HV), topographic vulnerability (TV), vulnerability due to proximity of embankment (PV), economic vulnerability (EV), and social vulnerability (SV). The physical vulnerability characterizes relative vulnerability to physical changes of the island in quantifiable manner, whereas socioeconomic vulnerability depends on the locally relevant socioeconomic components that further quantify the degree of vulnerability of the island community. The Geographical Information System (GIS) has been employed to integrate both physical and socioeconomic components.

Composite Vulnerability Rank (VR_c) is an integration of physical and social vulnerabilities and that examines the interactions between human and their physical and social surroundings. It has been developed using the concepts of Coastal Vulnerability Index (CVI) that was introduced by Gornitz et al. (1994).

The geometric mean equation has been applied for calculating both vulnerability rank (VR) and composite vulnerability rank (VR_c) at the family level in the study area.

$$G.M = \sqrt[n]{x_1 \times x_2 \times \dots \times x_n}$$

Geometric Mean of a group of n observations is the n th root of their product. It is defined only when all observations have the same sign, and none of them is zero.

The geometric average of different vulnerability ranks viz. Vulnerability of the dwelling Hut (HV), Topographic Vulnerability (TV), Social Vulnerability (SV) and Economic Vulnerability (EV) has been derived to get the vulnerability rank of a family. The vulnerability rank (VR) has been computed as follows:

$$VR = \sqrt[4]{HV * TV * SV * EV}$$

The Positional Vulnerability (PV) is determined by the proximity/distance from the fast eroding embankment which has been used with relatively more emphasis for the final calculation of Composite Vulnerability Rank. Composite Vulnerability Rank (VRc) has been computed as follows:

$$VRc = \sqrt{VR * PV}$$

The computed VR_c indicates the overall vulnerability of each family. The family with VR_c value <1.5 is considered as less vulnerable, VR_c value $1.5-2.0$ is considered as moderately vulnerable, and VR_c value >2.0 is considered as highly vulnerable (Fig. 2 and Table 1).

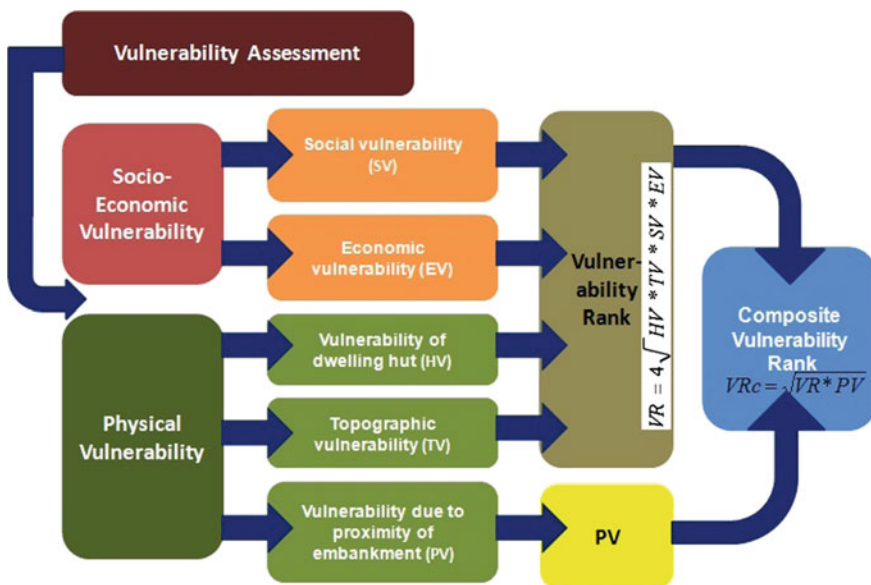


Fig. 2 Schematic diagram for assessing composite vulnerability rank

Table 1 Vulnerability descriptions and ranking

Components of vulnerabilities		Descriptions	Vulnerability ranks	
Physical vulnerability	Vulnerability of dwelling hut (HV)	The dwelling hut that are made of bricks having >0.6 m. floor height—usually not flooded or at low risk of flooding	Rank-1	
		The dwelling hut that are made of partially brick and partially mud (earthen) having 0.3–0.6 m. floor height- subject to flooding	Rank-2	
		The dwelling hut that are made of mud having <0.3 m floor height very often flooded	Rank-3	
	Topographic vulnerability (TV)	Includes the families that are settled on elevation zone of >2 m above msl	Rank-1	
		Includes the families that are settled on elevation zone of 1.5–2 m above msl	Rank-2	
		Includes the families that are settled on elevation zone of <1.5 m above msl	Rank-3	
	Vulnerability due to proximity of embankment (PV)	Includes the families that are positioned beyond 100 m distance from the fast eroding embankment and may not be forced to shift within one decade considering the current rate of coastal erosion of the area	Includes the families that are positioned between 20 and 100 m distance from the fast eroding embankment and may be forced to shift within one decade considering the current rate of coastal erosion of the area	Rank-1
			Includes the families that are positioned between 20 and 100 m distance from the fast eroding embankment and may be forced to shift within one decade considering the current rate of coastal erosion of the area	Rank-2
			Includes the families that are positioned within 20 m distance from the fast eroding embankment and may be forced to shift within 5 years considering the current rate of coastal erosion of the area	Rank-3
			Includes the families that are positioned within 20 m distance from the fast eroding embankment and may be forced to shift within 5 years considering the current rate of coastal erosion of the area	Rank-3

(continued)

Table 1 (continued)

Components of vulnerabilities		Descriptions	Vulnerability ranks
SocioEconomic vulnerability	Economic vulnerability (EV)	Families belong to upper level of APL (Above Poverty Line)—holding 3 acres irrigated or 6 acres nonirrigated agricultural, valuable assets—pump set/fishing boat/T.V./radio/mobile phones, insurance and educated member (s). Monthly family income more than Rs. 5000/- either from service or business or agriculture or various sources	Rank-1
		Families belonging to lower level of APL or upper level of BPL (Below Poverty Line)—without pump set/fishing boat/T.V./radio/mobile phones and medium landholding—less than 3 acres irrigated or less than 6 acres nonirrigated agricultural land having medium family income—Rs. 2000–5000/- per month	Rank-2
		Mainly BPL families are included in these ranks that do not possess pump set/boat/T.V./radio/mobile phone. Often they do not have agricultural land or possess a very small agricultural land and family income is significantly low	Rank-3
Social vulnerability (SV)		No physically challenged members/well educated/having <50 % women/ <30 % old age or child member	Rank-1
		Families which do not fit into the criteria of rank 1 and 3 are included in rank 2	Rank-2
		Families those members are illiterate/having >50 % women members/ >30 % old aged or child members/physically handicapped member (s)	Rank-3

Rank 1 Less vulnerable, 2 Moderately vulnerable, 3 Highly vulnerable
 Poverty Line: According to World Bank, purchasing power parity (PPP) of \$1.25 per person per day accepted internationally (Ravallion et al. 2008)

Family positions have been surveyed by NAVSTAR Global Positioning System (GPS) using Garmin 12 channels instrument. The position of family is plotted on the base map which has been prepared using IRS Resourcesat (P6) L4 satellite data in Universal Transverse Mercator (UTM) projection with World Geodetic System datum, 1984 (WGS-84) on scale 1:5000. The Geographic Information System has been used to integrate spatial data, i.e., point data of family position with non-spatial data, i.e., information of family collected through the household survey. The close-grid (100 × 100 m) RL survey has been conducted (using Auto Level Instrument) to develop the micro level elevation model. The coastal erosion has been estimated using the topographical map of 1968/69 as base line map and the satellite images of Landsat TM, 1986; IRS IC L3, 2001; IRS P6 L4, 2007 and IRS P6 L4, 2012 aided by field checks. The height of the embankment above mean sea level was also determined by the survey. The conditions of embankment have been assessed under 3 categories, viz. stable, vulnerable, and breached, based on the slope of the embankment (stable = gentle = <30°, subvertical = vulnerable), the height of the embankment (safe = at least 3 ft free board above high tide mark), the repeated occurrence of breach points and the presence of fringe mangroves. Householder's interviews have been conducted related to house type, kind of impacts of the coastal hazards/disasters they had faced, economical status and possession of assets, and social impediments. The respondents were mostly adult household heads.

3 Results and Discussion

3.1 *Physical Vulnerability*

Time series analysis of shoreline change reveals that Mousuni island is gradually getting reduced in size. The island area has reduced by 15.63 % and the estimated loss is 5.24 km² over the last 44 years (1968–2012). The shifting of high water line due to erosion was estimated at an interval of 500 m from North to South along the West coast and East Coast of two on the southern portion, viz. Kusumtala and Baliara shows that the coastal erosion is alarming in the West Coast. Embankment breaching is also a recurrent phenomenon in this area, whereas the East Coast of the island is comparatively stable with the presence of stable embankment with fringe mangroves (Fig. 3).

The island is protected by earthen embankments which are 28.77 km long except a narrow stretch of 5.38 km which is brick pitched. The height of the embankments vary between 3.5 and 6.5 m maintaining a slope of 30° to subvertical. About to 47 % (13.43 km) of the embankments is found to be vulnerable. The breach of embankment frequently threatens the islanders (Table 2).

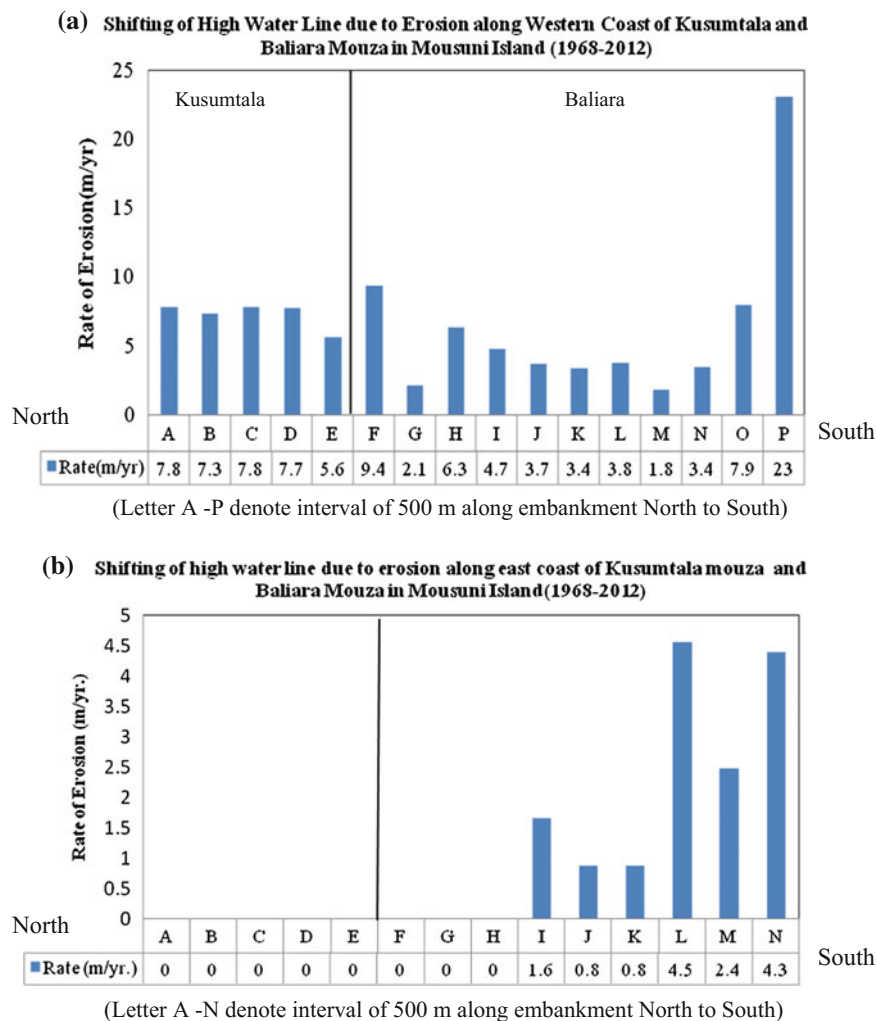


Fig. 3 **a** Shifting of high water line due to erosion along western coast of Kusumtala *mouza* and Baliara *mouza* in Mousuni island (1968–2012). **b** Shifting of high water line due to erosion along east coast of Kusumtala *mouza* and Baliara *mouza* in Mousuni island (1968–2012)

Table 2 Land loss (sq. km.) in Mousuni Island

Years	1968/69	1986	2001	2007	2012
Area (Sq. Km)	33.52	29.92	28.93	28.46	26.44
Estimated land loss (Sq. Km)	–	3.6 (0.21)	1.1 (0.07)	0.47 (0.08)	2.02 (0.40)

The Mousuni Island is characterized by very gentle slope toward the South and the Southeast. The highest elevation (3.90 m) has been marked on survey pillar established by the Survey of India (1922) exhibiting only one Bench Mark (BM) near the old collector building (the erstwhile GP office) located in the central part of the island. The micro level elevation models developed for two villages viz. Kusumtala and Baliara exhibit three zones of topographic vulnerabilities: (i) Less vulnerable zone: elevated area: >2.5 m high (ii) moderately vulnerable zone: moderately elevated area: 2.0–2.5 m high and (iii) highly vulnerable zone: low lying area: <2.0 m high. The entire island is, however, subject to flooding due to embankment failure as the tidal level remains high during the monsoon months.

Micro level physical vulnerabilities have been estimated with the components of topographic vulnerability (TV), vulnerability due to proximity to embankment (PV) and structural vulnerability of the dwelling hut (HV) of communities in the villages of Baliara and Kusumtala.

3.1.1 Topographic Vulnerability (TV)

In Baliara village, according to family location on different zones of elevation, it is found that 51 % of the families reside at low elevated areas of < 2.0 m high, 37 % are at moderately vulnerable areas with an elevation of 2.0–2.5 m and 12 % in the less vulnerable areas as they stay in a comparatively elevated zone of 0 > 2.5 m (Fig. 4).

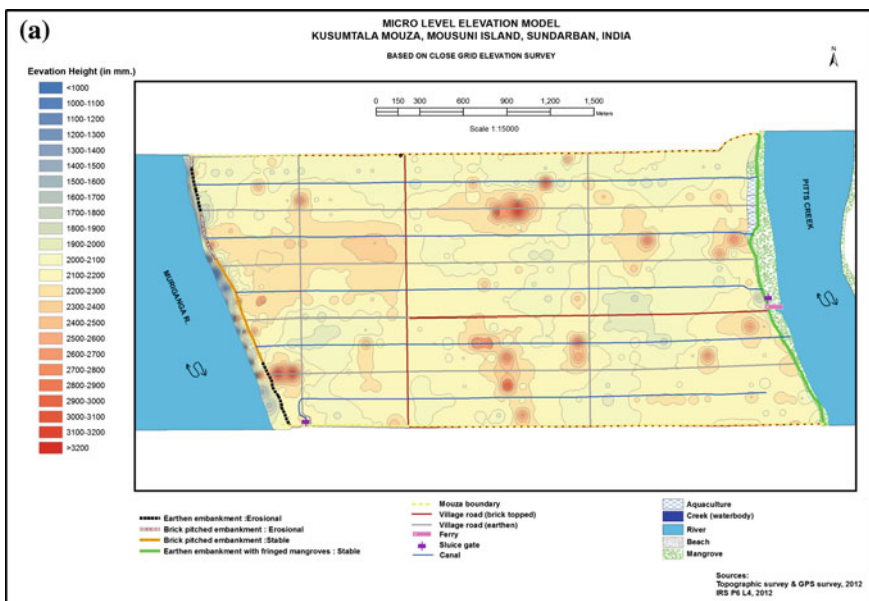


Fig. 4 a Micro level elevation map of Kusumtala mouza. **b** Micro level elevation map of Baliara mouza

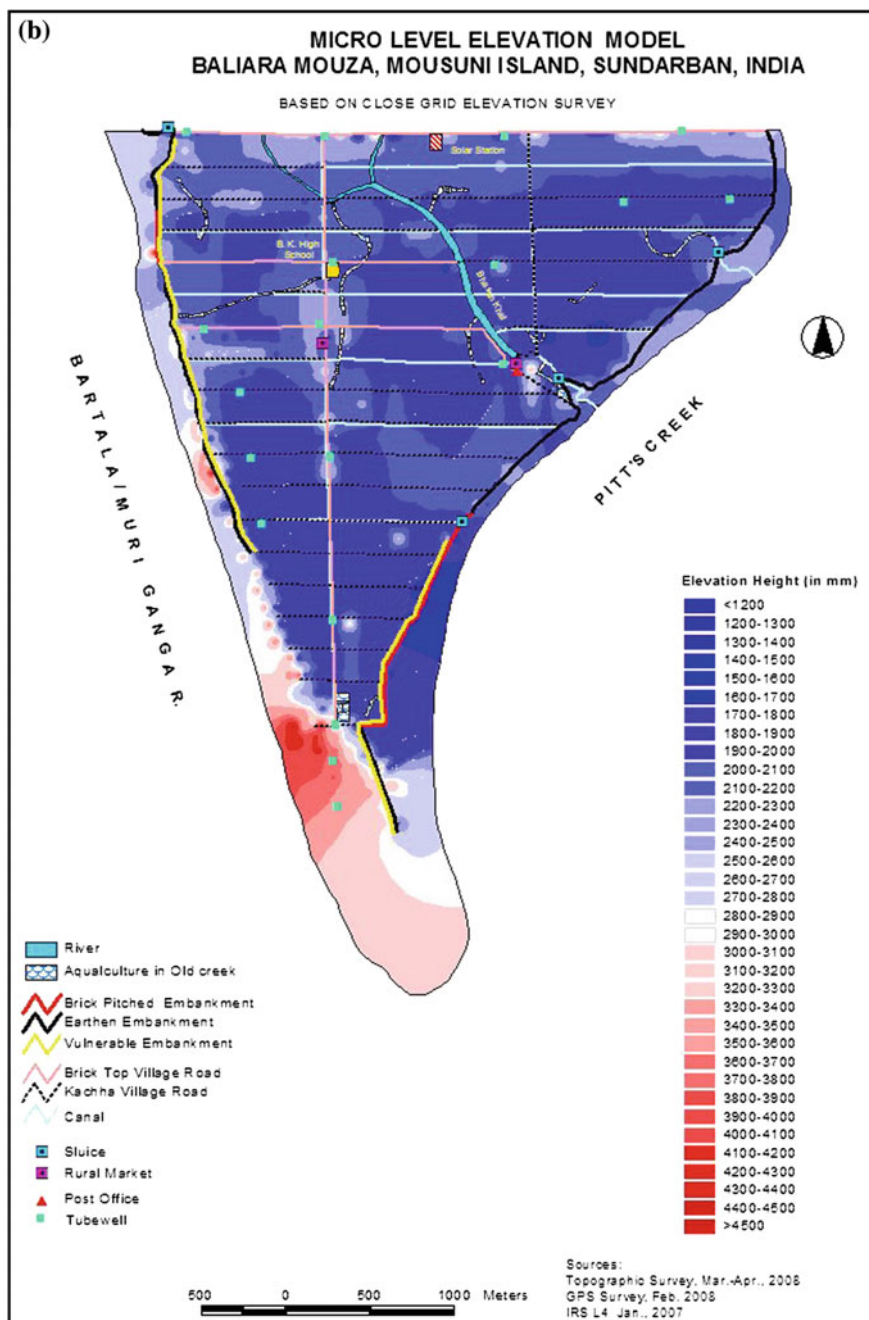


Fig. 4 (continued)

The families of village Kusumtala are moderately vulnerable as compared to the southern village of Baliara. Only 0.83 % of the families who reside in a zone of <2.0 m elevation are found to be highly vulnerable while 92.41 % are moderately vulnerable living within zones of 2.0–2.5 m elevated area and 6.76 % are less vulnerable located within zones elevated >2.5 m.

3.1.2 Vulnerability Due to Proximity to Embankment (PV)

The vulnerability due to proximity to fast eroding embankment has been computed based on the current rate of erosion. Based on the distance from the eroding embankment, 11 % families are highly vulnerable, 87 % families are less vulnerable, and only 2 % families are moderately vulnerable in Baliara village. In case of Kusumtala village, it has been identified that 3.98 % families are highly vulnerable, about 94.82 % families are less vulnerable, and only 1.20 % families are moderately vulnerable.

3.1.3 Vulnerability of Dwelling Hut (HV)

The islanders mostly reside in *kutchcha* houses made of mud. The family survey report shows that only 1 % of the families live in huts made of bricks, whereas 99 % of them live in huts made of mud. Based on the type and the condition of dwelling unit, it has been identified that in Baliara village, about 80 % families are living in highly vulnerable huts which subject to collapse during floods or storms and only 2 % of them are less vulnerable, while the rest are moderately vulnerable. In Kusumtala village, 24 % of the families are living in huts which exhibit high vulnerability, 10 % in relatively less vulnerable conditions and 66 % under conditions of moderate vulnerability.

3.2 Social Vulnerability

3.2.1 Socioeconomic Condition

As per the primary survey, it is evident that most of the people are unskilled small or marginal landowners belonging to the poorest economic strata below the poverty line and lack education. More than 20 % of people are socially backward in the Mousuni island. Most of them have to go outside the state, mainly to Kerala, for earning a livelihood.

The Gram *Panchayat* (local self-government) office reported that there are 68.15 % families belonging to the Below the Poverty Line (BPL) category (\$1.25 per day income on purchasing power parity) in Mousuni island. Significant percentages of families (50.55 %) are agricultural landless laborers of which 37.65 % belong to the BPL category. According to the GP report, 56.80 % of the families have an income which is either seasonal or marginal. Only 2.45 % of them are engaged in organized sectors. Agriculture and allied activities are otherwise the main sources of family income. The socioeconomic vulnerabilities in the villages Baliara and Kusumtala have been assessed at family level, taking the economic and social components into consideration.

3.2.2 Economic Vulnerability (EV)

In Baliara village, 64 % of the families are found to be highly vulnerable in terms of economic condition. Among those families, 59 % are from the BPL category and 5 % belong to the Above Poverty line (APL) category. Families with moderate economic vulnerability comprise 33 % of the total families. 26 % of them belong to the APL and 7 % to the BPL categories respectively.

Only 3 % of them belong to the less vulnerable category and all are APL category. The villagers of Kusumtala register comparatively better economic condition than Baliara. In Kusumtala, 31 % families are identified as economically highly vulnerable of which 30 % belong to the BPL category. Families with moderate economic vulnerability comprise 55 % of the total families of which 4.35 belong to the BPL category. Less vulnerable families have a percentage share of 13.44 % of which 12.99 % belong to the APL category.

3.2.3 Social Vulnerability (SV)

According to assessment result, it was found that a significant percentage (24 %) of families in Baliara village belongs to the highly vulnerable category in terms of social challenges. These families also belong to the BPL category. About 28 % of the families are moderately vulnerable, of which 23 % belong to the BPL and 5 % to the APL categories, respectively. The percentage of less vulnerable families is 48 % which includes 35 % from the APL and 18 % from the BPL category.

Kusumtala registers a comparatively lesser percentage of social vulnerability. Only 3.60 % of the families are considered as highly vulnerable of which 2.18 % belong to the BPL category. More than 75 % of the families are moderately vulnerable, with 33.26 % belonging to the BPL category and 42.79 % to the APL category. 19.37 % of the families are considered to be less vulnerable and belong to the APL category.

3.3 Composite Vulnerability (VR_c)

Composite Vulnerability Rank (VR_c) has been computed considering physical vulnerabilities like PV, HV, TV, and social vulnerabilities like EV and SV. The resultant VR_c value indicates the overall vulnerability of the families.

3.3.1 Vulnerability in Village Kusumtala, i.e., Middle Part of Mousuni Island

The study covering each family (total 1332 families) in Kusumtala village shows that 3.9 % of the families are highly vulnerable. Of these, 2.7 % of the families belong to the BPL category and 1.2 % belong to the APL category. 8.8 % of the families are considered to be moderately vulnerable, of which 5.1 % of them belong to the BPL category and 3.7 % to the APL category. The village Kusumtala has a high percentage (86.18) of families that are less vulnerable comparatively, belonging to 51.5 % of the APL category and 34.68 % of the BPL category. 53 families, however, are considered to be highly vulnerable and are likely to be displaced within the period of the next 5 years. Further, it has been identified that 36 of these families belong to the BPL category. Another 16 families are identified to be vulnerable due to coastal erosion and may get displaced within the next 10 years. The Bhanganpalli and Gathanpalli hamlets situated in the western parts of the village are identified as communities with a high degree of vulnerability and need immediate attention (Table 3).

Table 3 (a) Vulnerable families in Kusumtala village (based on VR_c). (b) Vulnerable families in Baliara village (based on composite vulnerability)

VR_c Rank	No of Family	APL Family	BPL Family
(a)			
Less vulnerable: $VR_c < 1.5$	1148	686	462
Moderately vulnerable: $VR_c 1.5-2.0$	117	49	68
Highly vulnerable: $VR_c > 2.0$	53	17	36
Unclassified	14	–	–
(b)			
Less vulnerable: $VR_c < 1.5$	651	419	231
Moderately vulnerable: $VR_c 1.5-2.0$	729	47	682
Highly vulnerable: $VR_c > 2.0$	171	62	109

Source GPS-based primary survey

3.3.2 Composite Vulnerability of Baliara Village in Southern Part of Mousuni Island

The composite vulnerability has been computed for each family (1551 families in total) in Baliara village. The VRc identifies that 11 % of the families are highly vulnerable, of which 7 % belong to the BPL category and 4 % belong to the APL category. 47 % of the families are moderately vulnerable, 44 % of who belong to the BPL category and 3 % to the APL category. 42 % of the families in the village are less vulnerable, of whom 27 % belong to the APL category and 15 % belong to the BPL category. With the current rate of erosion, it has been identified that 171 families are highly vulnerable who are likely to be displaced within the period of

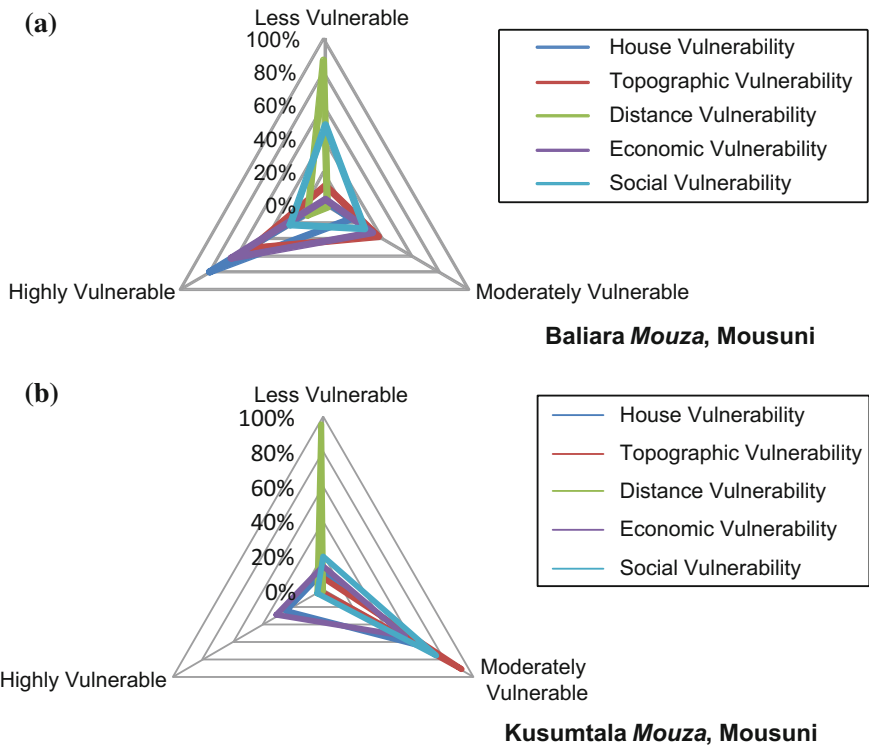


Fig. 5 a and b Radar diagram showing vulnerability of Baliara *mouza* and Kusumtala *mouza* in Mousuni Island

next 5 years. The study reveals that 202 families (13 %) may be forced to migrate within the next 5–10 years. It was observed that clusters like Narayanpalli, Indrapalli, and Ganga Yamuna Palli situated in the southern and western parts of the island are the most vulnerable and need immediate adaptive measures or planned resettlement.

The micro level study shows that Baliara village on southern part of the island has a very high degree of vulnerability compared to the Kusumtala village in the middle part of the island. The southern part is comparatively low lying and severely eroding. It comprises communities that are very vulnerable socioeconomically and also a high percentage of BPL families (69.57 %). On the other hand, the middle part being comparatively elevated comprises a higher percentage of APL families (59.30 %) (Figs. 5 and 6).

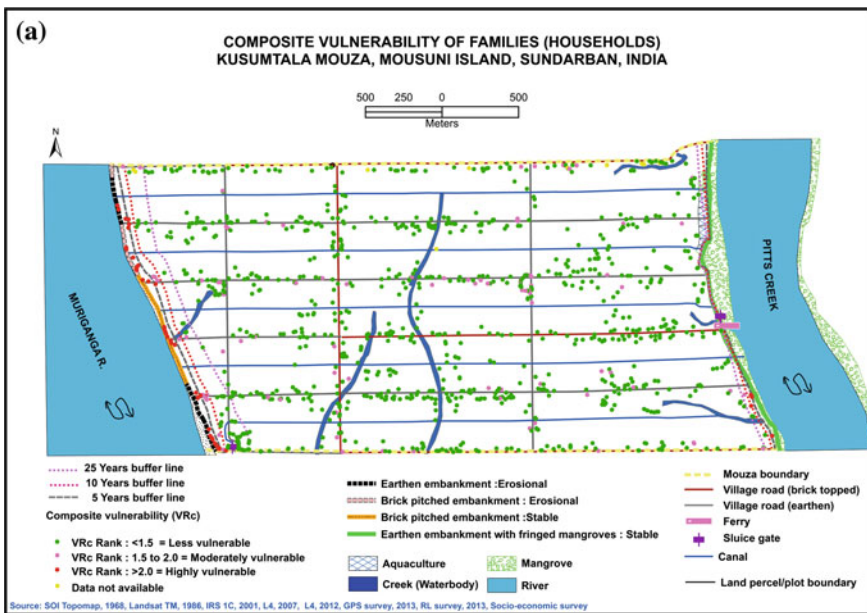


Fig. 6 a Composite Vulnerability of Kusumtala mouza in Mousuni island. **b** Composite vulnerability of Baliara mouza in Mousuni island

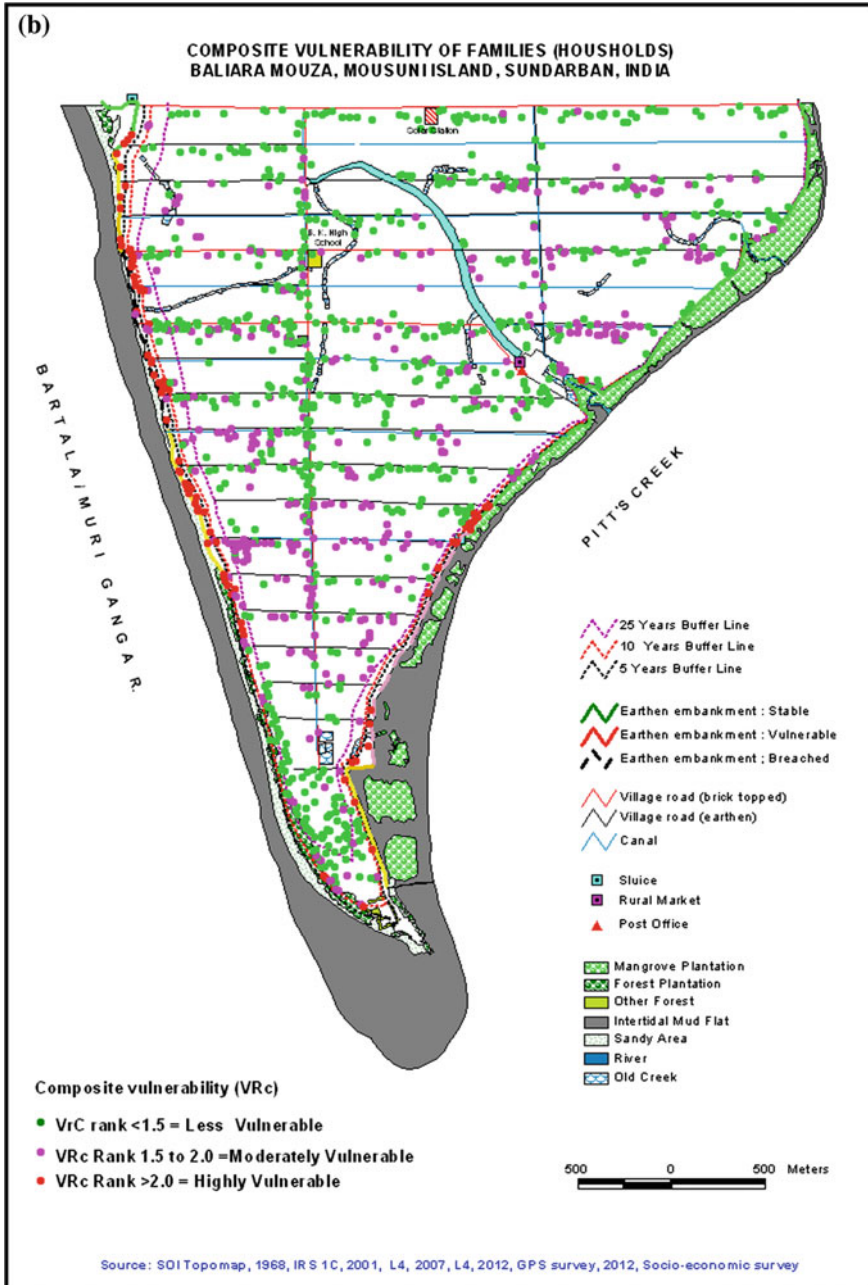


Fig. 6 (continued)

4 Conclusion

The Composite Vulnerability Rank (VR_c) reveals the interface of various dimensions of vulnerabilities. It quantitatively demonstrates that the most disadvantaged people socially and economically are forced to live in conditions of utmost physical vulnerability. People, who are without viable alternative occupations and are less literate, are forced to live in vulnerable huts near or on the embankments that experience the brunt of natural hazards. This observation also points to the extreme importance of the rebuilding and maintenance of the embankments. The designing of strategies for reduction of risk by planned migration and resettlement of the threatened population also become important in this regard.

Acknowledgments The authors are highly indebted to Dr. A.A. Danda, Head, Sundarban Programme Office, WWF for providing support to conduct the field surveys. Sincere thanks to the Secretary, DST, Govt. of WB for kind permission to publish. Views in this paper are primarily of the author's own and not necessary of the organization to which they belong.

References

- Allison MA, Khan SR, Goodbred SL, Kuehl SA (2003) Stratigraphic evolution of the late Holocene Ganges-Brahmaputra lower delta plain. *Sediment Geol* 155(3–4):317–342
- Carter TR, Parry MC, Nishioka S, Haraswa H (1994) Technical guidelines for assessing climate change impacts and adaptations. University College London, England and Centre for Global Environment Research, Tsukuba, Japan, p 59
- Chakraborti P (1991) Morphostratigraphy of the coastal quaternaries of West Bengal and Subarnarekha delta, Orissa. *Indian J Earth Scs* 18(3–4):219–225
- Chakraborti P (1995) Evolution history of the coastal quaternaries of the Bengal plain, India. *Proc Indian Natl Sci Acad* 61(5):343–354
- Feenstra JG, Burton I, Smith JB, Tol RSJ (1998) Handbook on methods for climate change impact assessment and adaptation strategies. United Nations Environment Program, Nairobi, Institute for Environment Studies, Amsterdam
- Gornitz VM, Daniels RC, White TW, Birdwell KR (1994) The development of a coastal risk assessment database: vulnerability to sea level rise in the US southeast. *J Coast Res SI* 12:327–338
- Government of West Bengal (2009a) Damage of embankment due to Aila damage report. Directorate of Irrigation and Waterways
- Government of West Bengal (2009b) Aila damage report. Department of Disaster Management
- Government of India (2008) National action plan of climate change. Prime Minister's Council on Climate Change, New Delhi, India, p 51
- Government of West Bengal (2012) West Bengal state action plan on climate change, Kolkata, p 330
- Harvey N, Clouston B, Carvalho P (1999) Improving coastal vulnerability assessment methodologies for integrated coastal zone management: an approach from South Australia. *Aust Geogr Stud* 37(1):50–69
- Hazra S, Ghosh T, Dasgupta R, Sen G (2002) Sea level and associated changes in the Sundarban. *J Sci Cult* 68(9–12):309–321

- Hazra S, Bakshi A (2003) Environmental refugees from vanishing Islands. In: Bhattacharya P, Hazra S (eds) Environment and human security. Lancers Books Publications, India, pp 219–227
- Hazra S, Dasgupta R, Samanta K (2009) Climate change–sea level rise- and socio economic impact on Sundarban, West Bengal. In: Ghosh S (ed) Global warming in context to the Indian sub-continent. Humboldt Club, Calcutta, pp 27–35
- Hazra S, Samanta K, Mukhopadhyay A, Akhand A (2010) Temporal change detection (2001–2008) of the Sundarban-Final Report. School of Oceanographic Studies. Jadavpur University and WWF-India, Sundarban Programme, Kolkata, p 128
- Hoque MA, Sarkar MSKA, Khan SAKU, Moral MAH, Khurram AKM (2006) Present status of salinity rise in Sundarban area and its effect on Sundari (*Heritiera fomes*) species. *Res J Agric Biol Sci* 2(3):115–121
- IPCC CZMS (1992) A common methodology for assessing vulnerability to sea level, 2nd revision, global climate change and the rising challenge of the sea, IPCC response strategies working group: coastal zone management subgroup. Intergovernmental Panel on Climate Change, The Hague, Netherlands
- IPCC (2001) Climate change: impacts, adaptation and vulnerability, contribution of working group II. Third assessment report. Cambridge University Press, New York, p 1032
- Jones RN (2001) An environment risk assessment management framework for climate change impact. *Nat Hazards* 23:197–230
- Mandal AK, Nandi NC (1989) Fauna of Sundarban mangrove ecosystem, West Bengal, India. Fauna of Conservation Areas, Zoological Survey of India, Government of India, p 116
- Mandal RN, Naskar KR (2008) Diversity and classification of Indian mangroves: a review. *Trop Ecol* 49(2):131–146
- Ravallion M, Chen S, Sangraula P (2008) Dollar a day revisited, policy research working paper 4620. Development Research Group, The World Bank, pp 16–18
- Patwardhan A (2006) Assessing vulnerability to climate change: the link between objectives and assessment. *Curr Sci* 90(3):276–383
- Riedlinger D, Betkes F (2001) Contribution of traditional knowledge to understanding climate change in the Canadian Arctic. *Polar Rec* 37(203):315–328
- Singh OP, Khan TMA, Rahman MS (2001) Has the frequency of intense tropical cyclones increased in the North Indian Ocean? *Curr Sci* 80(4):575–580
- Singh OP (2007) Long term trends in the frequency of severe cyclone of Bay of Bengal: observation and simulations. *Mousam* 58(1):59–66
- Unnikrishnan AS, Sankar D (2007) Are sea level rise trends along the coasts of North Indian Ocean consistent with global estimates? *Glob Planet Change* 57(3–4):301–307
- Wu SY, Yarnal B, Fisher A (2002) Vulnerability of coastal community to sea-level rise: a case study of Cape May County, New Jersey, USA. *Clim Res* 22(4):255–270
- Yamada K, Nunn PD, Mimua N, Machida S, Yamamoto M (1995) Methodology for assessment of South Pacific island countries to sea-level rise and climate change. *J Glob Environ Eng* 1:101–125

Analyzing Trends of Urbanization and Concomitantly Increasing Environmental Cruciality—A Case of the Cultural City, Kolkata

Richa Sharma, P.K. Joshi and Sandip Mukherjee

Abstract The environment in the city of Kolkata has suffered an extensive damage at hands of urban expansion. This study investigates the urban expansion in Kolkata over the last few decades and assesses its impact on environmental criticality using satellite derived parameters. An Environmental Cruciality Indicator (ECI) was developed using the vegetation indices and the land surface temperature (LST). Landsat TM and ETM+ data for the years 1989, 2006, and 2010 have been employed for this study. Land use land cover (LULC) maps were prepared using supervised classification with an accuracy of 86–90 % (0.82–0.87 kappa). Urban expansion amounting up to 109 km² was observed in the city over the past two decades. These changes modified some other environmental variables such as the moisture intensity of the surface, LST, greenness, and the built-up intensity. These changes further impact the quality of environment that was analyzed using the ECI. The indices used were Normalized Difference Vegetation Index (NDVI), Normalized Difference Water Index (NDWI), and Normalized Difference Built-up Index (NDBI). Satellite derived ECI shows a degrading trend for environment in larger parts of the city. The magnitude and spatial extent of higher environmental cruciality are coherent with the urbanization (sparse and dense settlement) patterns in and around the city. LULC has been an important factor determining the health of the environment and hence influencing the local climate.

R. Sharma (✉) · P.K. Joshi · S. Mukherjee
Department of Natural Resources, TERI University, New Delhi 110 070, India
e-mail: richa.sharma85@gmail.com

R. Sharma
National Institute of Urban Affairs, New Delhi 110 003, India

P.K. Joshi
School of Environmental Sciences, Jawaharlal Nehru University,
New Delhi 110 067, India

R. Sharma
Vlaamse Instelling Voor Technologisch Onderzoek (VITO), Boeretang 200,
Mol 2400, Belgium

Keywords Urban expansion · Environmental cruciality index · Vegetation indices · Land surface temperature · Land use land cover

1 Introduction

The urbanization process creates urban ecosystems characterized by impervious surfaces and built structures that alter the local climate in more ways than one (Ganeshan et al. 2013). These impervious areas exhibit diminished evapotranspiration, increased run off, enlarged storage, and transfer of sensible heat (Kato and Yamaguchi 2005). The built structures predominantly in cities often alter the urban geometry and albedo of the area (Akbari et al. 2009). These changes have an adverse impact on the local climate, environment and environmental variables such as land surface temperatures (Amiri et al. 2009), hydrology (O'Driscoll et al. 2010; Chelsea Nagy et al. 2012), human health (Tomlinson et al. 2011), landscape (Buyantuyev and Wu 2010), biodiversity (Biamonte et al. 2011) and quality of life. Given the current pace of urbanization globally as well as in India, cities continue to grow at a rapid pace. Thus, it becomes crucial to monitor the urban environment and control any potential threat of degradation.

Assessing the urban LST conditions is imperative to monitor the quality of urban environments, as temperature is a key parameter that controls a number of biological, physical and chemical processes of an ecosystem. LST is often used to study the thermal conditions of a region of an area. A lot of studies have focused on utilizing ground-based measurements for analyzing the thermal environments. Such measurements are good for studying the temporal variations. However, they show limited utility when it comes to spatial coverage and also suffer from lack of spatial continuity. With advances in remote sensing technology over the past few years, researchers have been able to use satellite data for thermal related studies at varying scales of both space and time.

Some of the satellites-based thermal data are provided by the National Oceanic and Atmospheric Administration's (NOAA's) Advanced Very High Resolution Radiometer (AVHRR), Moderate Resolution Imaging Spectroradiometer (MODIS) and Advanced Spaceborne Thermal Emission and Reflection Radiometer (ASTER) and Landsat's Thematic Mapper (TM), Enhanced Thematic Mapper plus (ETM+) and Thermal Infrared Sensor (TIRS) (Joshi et al. 2013). All these varying in their spatial, temporal and spectral response functions, define their wide ranging utility for different types of studies. AVHRR, for instance, is more suitable for continental or global temperature mapping due to its 1 km spatial resolution. ASTER and MODIS provide multiple thermal bands that make these data more suitable for LST studies at various spatial scales. However, among all of these, MODIS is again more suitable for studies done at continental and global scales. Though ASTER is better to study the regional scale LST, these products are extremely expensive which serves as a deterrent in terms of availability. Landsat data is available free of

cost from NASA (<http://earthexplorer.usgs.gov/>) and have the satisfactory spatial resolution to study LST at the regional or local level (Li et al. 2012).

Normalized Difference Vegetation Index (NDVI) is another related feature that is closely linked with urbanization, as it is a direct indicator of greenness including the density and health of the green cover. Vegetation is an important component of the urban ecosystem. It influences the biological environment by supporting biodiversity and improving air quality. It also impacts the physical environment through selective absorption, reflection of incident radiations and the regulation of the sensible heat balance. Typical urban materials used in buildings and urban structures exhibit a reverse impact on both the biological and physical environment. The urban materials in general tend to absorb more heat and retain it for longer duration that gradually heats up the local environment resulting in formation of the Urban Heat Island (UHI). Normalized Difference Built-up Index (NDBI) has often been employed by researchers to study, identify, and extract built-up land features (Xu 2007). NDBI is also important for identifying and studying surface UHIs. Water is another crucial factor influencing the local climate as it plays an important role in energy exchange and balance. Normalized Difference Water Index (NDWI) is often used for delineating water bodies and studying the moisture status in the area of interest (Gao 1996). However, within a water body, NDWI values might not be constant as the reflectance may vary depending upon the depth and quality of water. With development of such indices (for instance NDVI and NDBI), and further improvement and modifications, researchers have been trying to study various aspects of environment and climate.

Based on the essential indices for vegetation (NDVI), built-up intensity (NDBI) water (NDWI) and LST, this study proposes a new index measuring the cruciality of the urban environment. The primary focus of this research is to map the urbanizing landscape of the city of Kolkata and to examine its impacts on the local environment. These impacts are studied using a set of indicators that are the green cover, built-up intensity, moisture intensity, and land surface temperature. The secondary objective of the study is to propose the Environment Cruciality Indicator (ECI) to understand the state of the physical environment of the landscape.

1.1 Data and Methods

1.1.1 Study Region

The area of interest for this study is the metropolitan city of Kolkata, formerly known as Calcutta. The city is the capital of the state of West Bengal, India. It is situated at 22.567° north latitude and 88.367° east longitude (Fig. 1) covering an area of 900 km². The city has been experiencing continuous growth since its inception in 1690. Kolkata is situated on the banks of river Hooghly. It is an important cultural center of India. This study is confined to the Kolkata Municipal Corporation (KMC) jurisdiction area and the surrounding suburbs taking a buffer of

5 km with a total areal extent of 1750 km². The city experiences tropical wet and dry climate with extremely hot and humid summers (temperatures soaring to 40 °C) and short winters when temperatures dip to 9 °C. The city experiences an annual rainfall of 1640 mm and often encounters cyclones as it falls in a cyclone prone region. Kolkata's land cover in past has been dominated by wetland ecosystems but with increasing pressure due to population explosion, much of these wetlands have been transformed into various urban land uses.

1.1.2 Data Used

Geometrically and radiometrically corrected Landsat data (TM and ETM+) images of Kolkata city (path/row: 138/44) used in this study were taken in the GeoTIFF format from the Earth Resources Observation and Science (EROS) Data Centre of the U.S. Geological Survey (USGS) (<http://eros.usgs.gov/>). The data were projected in the UTM projection (zone 45) and WGS84 datum. The datasets used were acquired on January 19, 1989, January 26, 2006, and January 21, 2010. The data consists of seven bands; the first three of these are visible bands (red, green, blue). The fourth band is near-infrared, the fifth and the seventh bands are shortwave infrared and the sixth is a longwave infrared thermal band (Table 1). ETM+ data differs from TM in terms of enhanced spatial resolution of thermal band (band 6) and that it possess an additional panchromatic band.

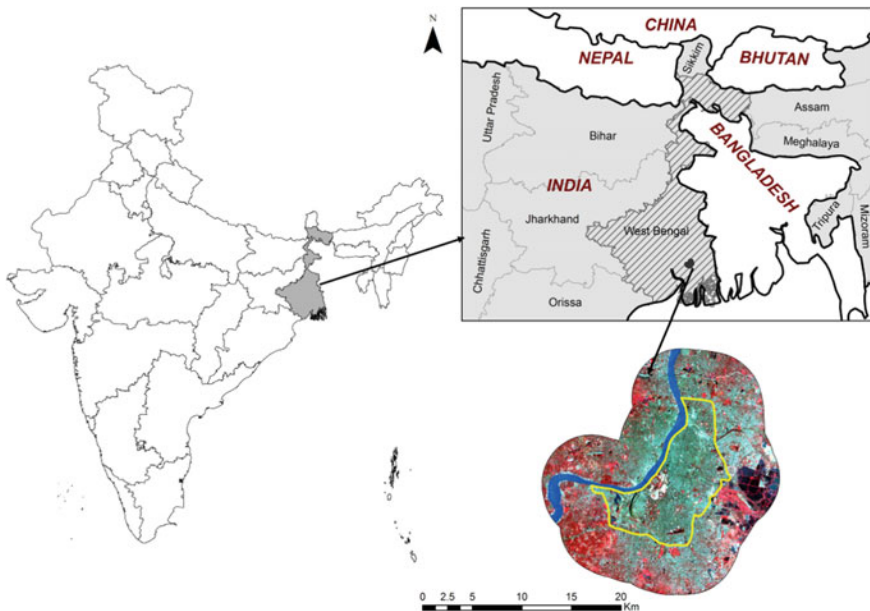


Fig. 1 Location of the study area

Table 1 Indices and their calculation

Index	Indicator of	Formula
NDVI	Greenness or vegetation	$\frac{NIR - R}{NIR + R}$
NDBI	Built-up intensity	$\frac{MIR - NIR}{MIR + NIR}$
NDWI	Water or moisture status	$\frac{NIR - MIR}{NIR + MIR}$
LST	Land surface temperature	Mono-window algorithm
ECI	Environment cruciality or criticality	$\frac{LST + NDBI}{NDVI + NDWI}$

1989 and 2010 data were TM datasets with 30 m spatial resolution for band 1 (blue), band 2 (green), band 3 (red), band 4 (NIR), band 5 (MIR1) and band 7 (MIR2), and band 6 (TIR) with 120 m. The bands had spectral resolutions of 0.45–0.52, 0.52–0.60, 0.63–0.69, 0.76–0.90, 1.55–1.75, 10.4–12.5, and 2.08–2.35 μm, respectively. ETM+ data bands possessed the same spectral resolutions. The spatial resolution was also 30 m for all the bands except band 6 which had a resolution of 60 m. ETM+ data had an extra panchromatic band having 15 m spatial and 0.45–0.90 μm spectral resolution.

1.1.3 Derivation of Variables

Since different wavelengths provide information about different parameters of land environment, different bands and diverse band ratios were computed to retrieve information about various environmental parameters. The greenness of the area under study was estimated using the NDVI, which extracts information from red and near infrared (NIR) bands. The built-up intensity represented by NDBI (Zhang et al. 2009) and wetness characterized by the NDWI (Gao 1996; Jackson et al. 2004) were calculated using the NIR and the shortwave mid-infrared (MIR) band which is the fifth band. The land surface temperature for the area was retrieved from the thermal infrared (TIR) band (Chen et al. 2006) using Qin et al.’s (Qin et al. 2001) mono-window algorithm (Sun et al. 2010) and the emissivity correction was done using NDVI to obtain the final LST images.

With rapid urbanization, more and more vegetation is being replaced with impervious urban structures. Concrete urban structures such as buildings and pavements have a tendency to absorb more heat and store it for a longer time resulting in elevated land surface temperatures. High LST manifests itself in the form of the development of the Urban Heat Island or UHI in the city. UHI in turn has adverse implications for human health, biodiversity, and energy demand especially in a hot and humid city like Kolkata. Thus, as the LST increases, the condition of the local environment becomes more critical.

Scattering or reflectance from the spongy mesophyll cells in plants exhibit high leaf reflectance in the NIR. Thus greater the number of leaf layers in a healthy, mature canopy, the greater is the infrared reflectance. Also, due to chlorophyll absorption in red band and due to very high reflectance in NIR, a healthy green leaf has a very low reflectance in red. Thus more and healthier the vegetation is, higher is the NDVI. With urbanization, there is a greater loss of green cover causing the decrease of reflectance in the near-infrared band and an increase in the red band resulting in lower NDVI values. Loss of vegetation has more direct impacts on the local climate with an increase in temperature, air pollution and a loss of habitat of local biodiversity. Thus, a decreasing NDVI in urban area indicates a degrading environment.

MIR is sensitive to water and soil moisture and very effective in distinguishing water pixels. With increasing moisture content, the MIR reflectance decreases and the NDWI thus increases. Presence of water bodies and vegetation moisture increases the NDWI. However, with increase in impervious urban structures and decrease in vegetation with urban sprawl, the NDWI would decrease indicating deterioration of the local environment.

Urban structures are low in moisture content and tend to have high MIR values with a low NIR reflectance. Thus, higher the built-up intensity of an area, more is the NDBI value. A higher NDBI that represents a higher built-up intensity is also indicative of depleting moisture content in the area. Increasing NDBI would thus be a fair indication of critical urban environments.

1.1.4 ECI Computation

An integrated Environment Cruciality Index was calculated using the various indicators discussed above. According to this index, an urban environment with a high LST and NDBI and a low NDVI and NDWI are more crucial and exhibit high ECI values. A lesser crucial urban environment would have a low LST and NDBI with a high NDVI and NDWI values. Based on this information, ECI was developed as given in Table 1. All the variables were normalized to a range of 0–255 for this purpose.

1.1.5 LULC Mapping

An insight into the land use and land cover changes is highly crucial for understanding different environmental changes taking place in an area. Supervised classification (Jensen 2015) was applied to map LULC for 1989, 2006, and 2010 Landsat datasets using parametric classifier with maximum likelihood based on Mahalanobis metric algorithm. Eight LULC classes were recognized that include: (i) water, (ii) wetland water, (iii) wetland vegetation, (iv) agricultural fallow, (v) vegetation, (vi) open area, (vii) built-up (Table 2).

Table 2 LULC classification scheme

LULC class	Description
Water	This class is covered by River Hooghly that crosses through the study area along with other water bodies such as tanks or ponds
Wetland water	This class consists of water present in wetland area towards western parts of study area
Wetland vegetation	Land covered with vegetation in wetland area
Agricultural fallow	This is comprised of agricultural land that is presently fallow or harvested
Vegetation	Vegetation class encompasses all kinds of vegetation except that related to agricultural activities and wetland vegetation
Open area	Open area in this classification scheme refers to large open playground, airport and other vast stretches of land that are not covered by vegetation or built-up structures
Built-up	This is comprised of land parcels under human settlement including buildings and other man-made constructions

2 Results

2.1 Lulc and Land Transformations

The temporal LULC maps of different time periods (1989, 2006, and 2010) were utilized to study the urban expansion. The overall accuracy of the LULC maps for 1989, 2006, and 2010 are 90, 88, and 86 %, respectively. The Kappa statistics for 1989, 2006, and 2010 are 0.8726, 0.8455, and 0.8212, respectively. The LULC statistics for different years are given in (Table 3).

The statistics show significant changes in LULC distribution areas over time. The built-up in and around the city is 88.7 km² in 1989, 144.6 km² in 2006, and 197.7 km² in 2010, thus showing an increase of 109 km² in the two decades. Maps show that the expansion has been more towards the eastern and south-eastern parts of the city engulfing the peri-urban agricultural regions and surrounding the wetlands in the process (Fig. 2).

Table 3 LULC distribution in the study area

LULC class	1989	2006	2010
Water	19.0	19.6	19.9
Wetland water	20.0	15.4	14.1
Wetland vegetation	34.2	21.2	15.0
Agricultural fallow	49.9	37.1	21.2
Vegetation	178.4	164.1	109.8
Open area	20.2	8.3	32.8
Built-up	88.7	144.6	197.6

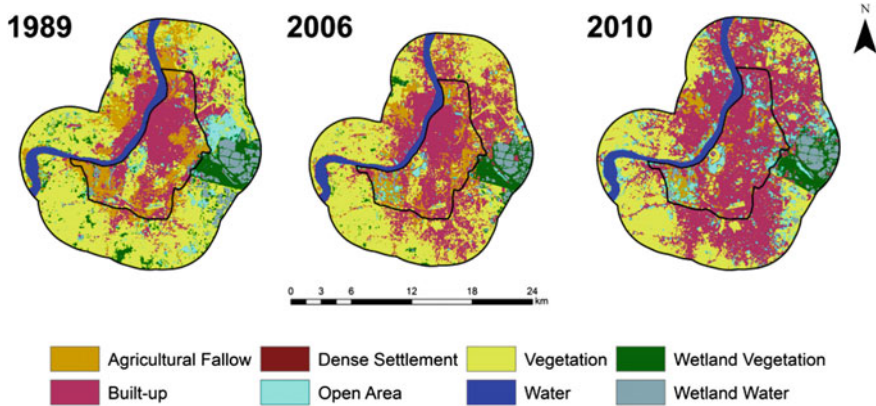


Fig. 2 Land use/land cover maps 1989, 2006, and 2010 (Sharma et al. 2015)

2.2 Spatiotemporal Patterns of Variables

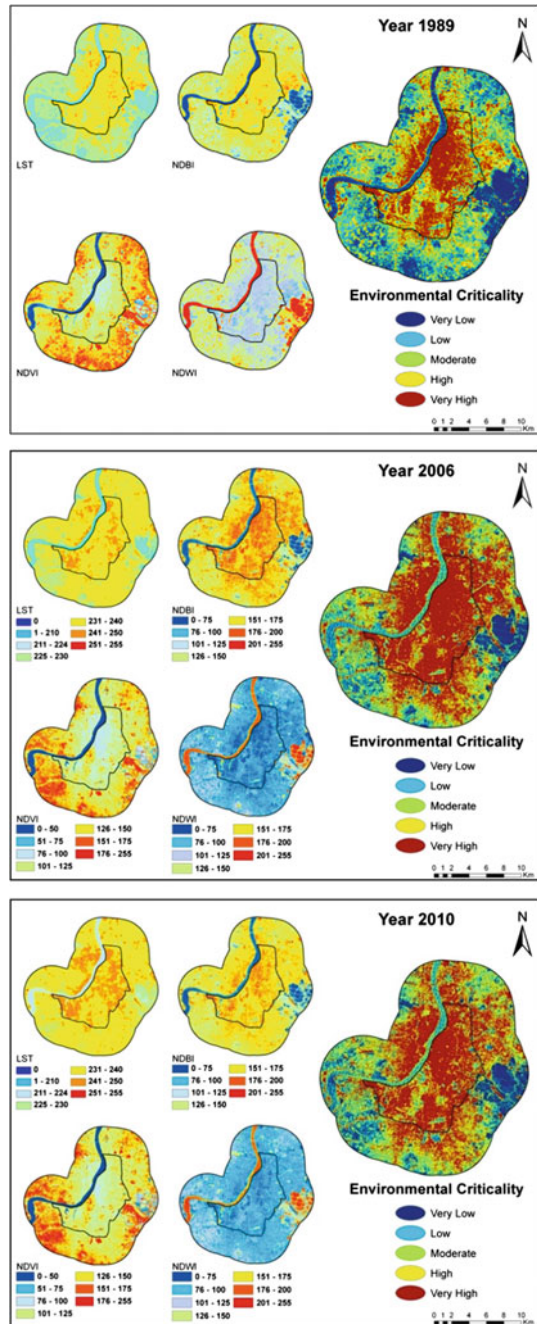
The forms of surface components, their distribution and their spatial complexities often have an impact on the local air and surface temperature. Thus, the land transformations taking place in the study region have also influenced the LST distribution in the city. The LST values in the area have been increasing over the years. The mean surface temperature in 1989 was 27.4 °C, which increased to 30.0 °C in 2006 and finally to 33.0 °C in 2010. Similarly, the minimum temperature and maximum temperature values for the study region are 18.5 and 38.4 °C, 20.0 and 39.5 °C, and 19.4 and 42.0 °C for the years 1989, 2006, and 2010, respectively. The magnitude and extent of the estimates of LST are observed to be in consistency with the urbanization pattern of the city. The NDBI values were also found to follow the same pattern, while the NDVI and the NDWI followed a reverse pattern (Fig. 3).

2.3 Dynamics of Environmental Cruciality

To assess the impact of urbanization on the environmental health, ECI computation was processed for the three years (Fig. 3). Analysis of the LULC and other variables indicated that the wetlands are particularly at threat due to rapid land transformations. This is because wetland ecosystems are highly sensitive.

In order to study the impact of urban land transformations particularly on wetland ecosystem, the ECI changes were studied for the areas that have been reclaimed from wetland. Subtracting latter year's ECI from former one assessed ECI changes for the two time periods. A greater damage to environment is indicated by greater ECI change. ECI changes in the time period 1989–2006 are more evident and are of greater magnitude (~ 2.2) and are larger in spatial extent. However, from

Fig. 3 Environmental cruciality for Kolkata; 1998, 2006, and 2010



2006 to 2010, the ECI changes are less intense and spread in smaller patches. These changes are confined to a range of 0.1 to 1.5. This indicates that massive degradation in the environmental health of wetlands had taken place in earlier time period (Fig. 4). This could, however, also be due to the smaller time frame that has been considered in the latter instance (4 years) as compared to the former one (17 years). Also, on 31st March 2006, The East Kolkata Wetlands (Conservation and Management) Act, 2006, was passed by Government of West Bengal, which seems to have contributed to minimizing the damage and increasing the protection and conservation of these wetlands.

The ECI varied on the basis of the LULC of the surface. In order to understand the variation of ECI based on the LULC, ECI images were classified into 5 zones: zone 1 (0–1), zone 2 (1–2), zone 3 (2–3), zone 4 (3–4), and zone 5 (>4). These zones were then used to study the impact of variation in land use on the environmental quality using the doughnut charts (Fig. 5).

Water class was mainly dominated by zone 2 (95–98 %). Only a small fraction of water land use class is influenced by zone 3 in 2006 (2 %) and 2010 (4 %) and a very small fraction (2 %) came under zone 1 in 1989. A similar pattern is observed for the vegetation class. Agricultural fallow and built-up classes were dominated by ECI zone 2. However, the two categories are fundamentally different from each other. Agricultural fallow is a temporary land use which when it gets covered with crops in another season, automatically moves back into zones 1 and 2. On the contrary, built-up is a more permanent land use and hence it always remains confined to higher classes of ECI.

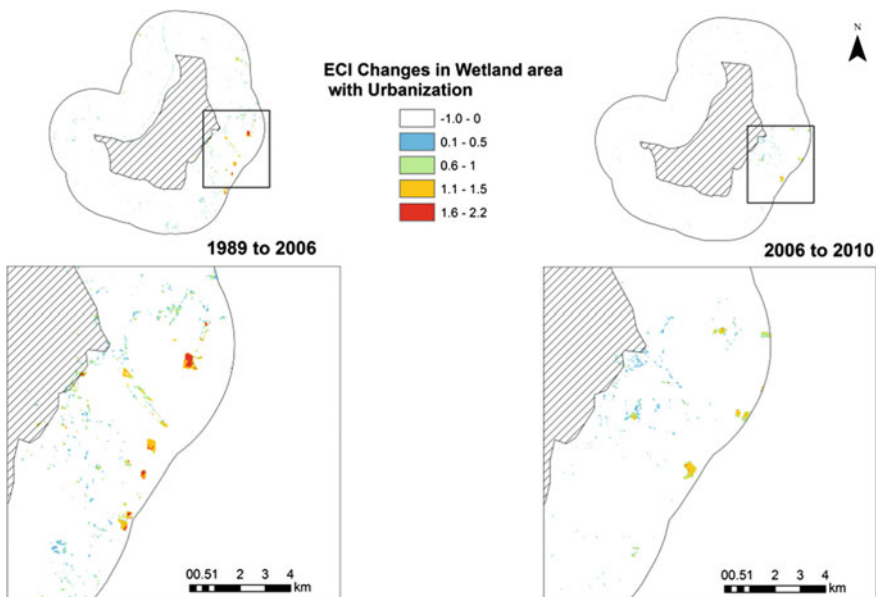


Fig. 4 Dynamics of ECI

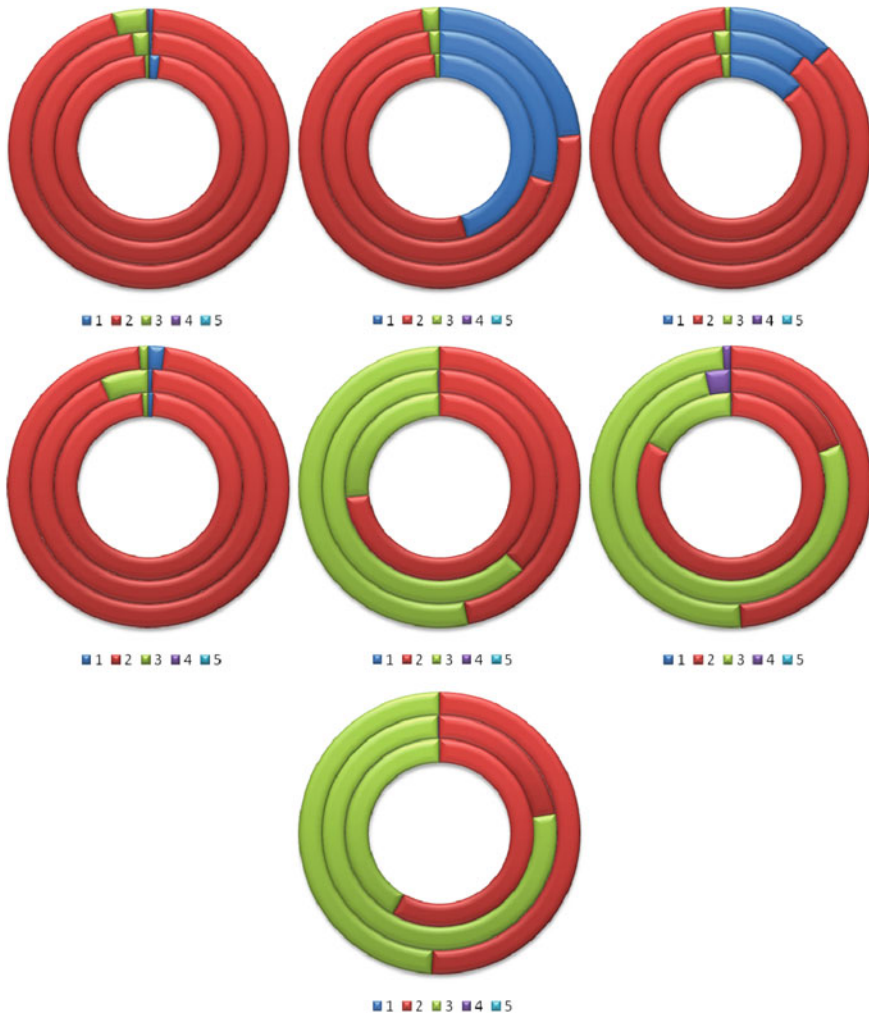


Fig. 5 ECI zone and LULC statistics for water, wetland water, wetland vegetation, vegetation, agricultural fallow, open area, and built-up (The inner most layer of doughnut represents year 1989, middle one represents year 2006 and outermost is for year 2010)

Wetland water (25–45 %) and wetland vegetation (11–13 %) are the only two LULC classes that have huge fractions that come under ECI Zone 1. This further reinforces the fact that wetland ecosystems help maintain the environmental health and quality. But as we move from the inside of doughnut to the outer layers i.e. from the year 1989 to 2010, we find that the proportion of wetland water and vegetation in the ECI zone 1 decreases, indicating an increasing disturbance in these sensitive ecosystems over the years.

3 Conclusion

LULC is an important aspect influencing the environmental quality of an area. Kolkata city has witnessed tremendous urban expansion in over the past two decades. This urban expansion has been accompanied with changes in the environmental variables of the area, namely, temperature, soil moisture, and vegetation cover. Satellite derived biophysical variables used in this study indicate that the LST (measuring surface temperature) and the NDBI (indicative of built-up intensity) is increasing, while the NDVI (representing vegetation intensity and health) and the NDWI (assessing the moisture status) have been decreasing. These disturbances have adversely impacted the environment. The Environment Cruciality Index measures how the transforming land use is influencing the local environment. Wetlands more specifically have been found to be deteriorating and disappearing to provide land for urbanization.

However, urbanization in silos could be dangerous not only for the environment but also for humans as well. Thus, a more interdisciplinary approach towards urbanization is required that can drive cities towards a more sustainable development that would be in harmony with the social and natural systems. Urban planners need to give special attention to sensitive areas such as wetlands while planning to ensure that the process of urbanization does not cause any disturbance to the cities. The governments and policy makers also need to come up with more stringent policies and laws while dealing with encroachment issues in such sensitive ecosystems as urbanization causes irreversible changes in land use and the damage to ecosystem is permanent. Thus, a more precautionary approach is required in this context.

References

- Akbari H, Menon S, Rosenfeld A (2009) Global cooling: increasing world-wide urban albedos to offset CO₂. *Clim Change* 94:275–286
- Amiri R, Weng Q, Alimohammadi A, Alavipanah SK (2009) Spatial–temporal dynamics of land surface temperature in relation to fractional vegetation cover and land use/cover in the Tabriz urban area, Iran. *Remote Sens Environ* 113:2606–2617
- Biamonte E, Sandoval L, Chacón E, Barrantes G (2011) Effect of urbanization on the avifauna in a tropical metropolitan area. *Landsc Ecol* 26:183–194
- Buyantuyev A, Wu J (2010) Urban heat islands and landscape heterogeneity: linking spatiotemporal variations in surface temperatures to land-cover and socioeconomic patterns. *Landsc Ecol* 25:17–33
- Chelsea Nagy R, Graeme Lockaby B, Kalin L, Anderson C (2012) Effects of urbanization on stream hydrology and water quality: the Florida Gulf Coast. *Hydrol Process* 26:2019–2030
- Chen X-L, Zhao H-M, Li P-X, Yin Z-Y (2006) Remote sensing image-based analysis of the relationship between urban heat island and land use/cover changes. *Remote Sens Environ* 104:133–146
- Ganeshan M, Murtugudde R, Imhoff ML (2013) A multi-city analysis of the UHI-influence on warm season rainfall. *Urban Clim* 6:1–23

- Gao B-C (1996) NDWI—a normalized difference water index for remote sensing of vegetation liquid water from space. *Remote Sens Environ* 58:257–266
- Jackson TJ, Chen D, Cosh M et al (2004) Vegetation water content mapping using Landsat data derived normalized difference water index for corn and soybeans. *Remote Sens Environ* 92:475–482
- Jensen JR (2015) *Introductory digital image processing: a remote sensing perspective*. Pearson Education
- Joshi P, Ghosh A, Chakraborty A et al (2013) Landsat again—continuing remote sensing, monitoring, mapping and measuring. *Curr Sci* 105:761–763
- Kato S, Yamaguchi Y (2005) Analysis of urban heat-island effect using ASTER and ETM+ data: separation of anthropogenic heat discharge and natural heat radiation from sensible heat flux. *Remote Sens Environ* 99:44–54
- Li Y, Zhang H, Kainz W (2012) Monitoring patterns of urban heat islands of the fast-growing Shanghai metropolis, China: using time-series of Landsat TM/ETM+ data. *Int J Appl Earth Obs Geoinf* 19:127–138. doi:[10.1016/j.jag.2012.05.001](https://doi.org/10.1016/j.jag.2012.05.001)
- O’Driscoll M, Clinton S, Jefferson A et al (2010) Urbanization effects on watershed hydrology and in-stream processes in the southern United States. *Water* 2:605–648
- Qin Z, Dall’Omo G, Karnieli A, Berliner P (2001) Derivation of split window algorithm and its sensitivity analysis for retrieving land surface temperature from NOAA-advanced very high resolution radiometer data. *J Geophys Res Atmos* 106:22655–22670
- Sharma R, Chakraborty A, Joshi PK (2015) Geospatial quantification and analysis of environmental changes in urbanizing city of Kolkata (India). *Environ Monit Assess* 187:1–12
- Sun Q, Tan J, Xu Y (2010) An ERDAS image processing method for retrieving LST and describing urban heat evolution: a case study in the Pearl River Delta Region in South China. *Environ Earth Sci* 59:1047–1055
- Tomlinson CJ, Chapman L, Thorne JE, Baker CJ (2011) Including the urban heat island in spatial heat health risk assessment strategies: a case study for Birmingham. UK. *Int J Health Geogr* 10:42
- Xu H (2007) Extraction of urban built-up land features from Landsat imagery using a thematic oriented index combination technique. *Photogramm Eng Remote Sens* 73:1381–1391
- Zhang Y, Odeh IO, Han C (2009) Bi-temporal characterization of land surface temperature in relation to impervious surface area, NDVI and NDBI, using a sub-pixel image analysis. *Int J Appl Earth Obs Geoinf* 11:256–264

Part V
Remote Sensing of Wild Habitat

Habitat Suitability Modelling for Sambar (*Rusa unicolor*): A Remote Sensing and GIS Approach

Ekwal Imam

Abstract The concept of wildlife species conservation starts with the identification of their suitable habitat as it provides essential information for wildlife refuge design and management. In this study, multiple logistic regression is integrated with remote sensing and geographic information system to evaluate the suitable habitats available for sambar (*Rusa unicolor*) in Chandoli Tiger Reserve, Maharashtra, India (17° 04' 00"N to 17° 19' 54"N and 73° 40' 43"E to 73° 53' 09"E). Satellite imageries of LISS-III of IRS-P6 of study area were digitally processed. To generate collateral data topographic maps were analysed in a GIS framework. Layers of different variables such as land use land cover, forest density, proximity to disturbances and water resources and a digital terrain model were created from satellite imageries and topographic maps. These layers along with GPS location of sambar presence/absence and multiple logistic regression (MLR) techniques were integrated in a GIS environment to model habitat suitability index of sambar. The results indicate that approximately 69.92 km² (24 %) of the forest of tiger reserve was least suitable for sambar, whereas 82.60 km² (28 %) was moderately suitable, 88.25 km² (30 %) suitable and 54.01 km² (18 %) was highly suitable. The accuracy level of this model was 80.2 %. The model advocates that forests of this area are most appropriate for declaring it as a reserve for sambar conservation.

Keywords Sambar · Habitat suitability index · Multiple logistic regression · Modelling · Remote sensing

1 Introduction

Conservation and management of threatened animal species need an understanding of the relationship between the spatial distribution of animals and their habitats (Lecis and Norris 2003). Remote Sensing and GIS can play greater role in

E. Imam (✉)

Department of Wildlife Sciences, Aligarh Muslim University, Aligarh, Uttar Pradesh, India
e-mail: ekwalimam01@gmail.com

evaluating the habitat preference of wildlife species by integrating various habitat variables of both spatial and non-spatial nature (Davis and Goetz 1990). The outputs of such models are usually simple, easily understandable and can be used for the assessment of environmental impacts or prioritisation of conservation efforts in a timely and cost-effective manner (Kushwaha et al. 2004; Zarri et al. 2008).

Sambar (*Rusa unicorn*) is the largest and most widely distributed of all Indian deers. Its large, rugged antlers are typically rusine, the brow tines being simple and the beams forked at the tip, so that they have only three tines. The antlers are typically up to 110 cm long in fully adult individuals. As with most deer, only the males have antlers. The shaggy coat can be from yellowish-brown to dark grey in colour. Sambars are found in a variety of habitats, from around 10,000 ft in the Himalayan foothills to the uplands of Central India. They range from the wet forests of the North East to the arid thorn scrub of Gujarat and Rajasthan. Sambars are present throughout peninsular India including the wet evergreen forests of the Western Ghats and also in Sri Lanka. In fact, its range extends across southeast Asia. Sambars are found in habitats ranging from tropical seasonal forests (tropical dry forests and seasonal moist evergreen forests), subtropical mixed forests (conifers, broadleaf deciduous and broadleaf evergreen tree species) to tropical rainforests. They are seldom found far from water. They are hardy animals found in all places ranging from the sea level up to 3500 m in Taiwan, Myanmar, and the foothills of the Himalayan Mountains. Sambars primarily live in the woodlands and feed on a wide variety of vegetation including grasses, foliage, browse, fruit, and water plants depending on the local habitat. They also consume a great variety of shrubs and trees. (Prater 2005; Timmins et al. 2008). Sambars have been declared as vulnerable by the IUCN (2012) and protected by the Wildlife (Protection) Act, 1972 as Schedule III animals (WPA 1991). They also happen to be the favourite prey for tigers and lions. Considering this, it is important to conserve them at the local as well as the country level.

The present study is a small effort in this direction. The first step towards significant wildlife conservation is habitat evaluation (Kushwaha 2002). Geospatial technology using satellite imagery, geographical information systems (GIS), and statistics may assist in quantifying available habitat for animal species (Johnson 1990). A suitability index provides us with the data of how much area is suitable for a particular species. The higher the value, the chances of a particular location being suitable for the occurrence of that species become significantly better. In this model, regression is used on several environmental parameters to calculate an index of species occurrence (Clark and Evans 1954; Schadt et al. 2002).

The concept of wildlife habitat analysis started with the development of habitat evaluation procedure (HEP). First evolved in 1976, HEP has been modified significantly and US Fish and Wildlife Service has developed as many as 157 habitat suitability models for large number of fish and other wildlife in the past 20 years (USFWS 1981). Encouraged by the results, Lyon (1983) used LANDSAT image classifications in predictive modelling for nesting sites of the American kestrel (*Falco sparverius*). In 1984, Bright used remotely sensed data along with other ecological parameters to assess the habitat of the elk (*Cervus canadensis*). Homer

et al. (1993) created a model that accurately predicted suitable habitat for the sage grouse (*Centrocercus urophasianus*), whereas Andries et al. (1994) used SPOT remotely sensed data for spatial modelling of the barn owl habitat. In 1997, Brian and West modelled the elk calving habitat in the prairie environment using GIS and Remote Sensing techniques. Furthermore, Store and Jokimaki (2003) used the geographic information system integrated with the multi-criteria evaluation approach to produce geo-referenced ecological information about the habitat requirements of different species.

Impressed with the utility of remote sensing and habitat modelling, this technique right from 1980s has been widely used in India. In 1986, Parihar et al. (1986) evaluated the habitat of Indian one-horned rhinoceros using remotely sensed data from LANDSAT, while Roy et al. (1995) used this technology for habitat suitability analysis of *Nemorhaedus goral*. Similarly Porwal et al. (1996) analyzed suitable habitat for the muntjac (*Cervus unicolor*) in the Kanha National Park using remote sensing data. During 2004, Kushwaha and Hazarika (2004) used Landsat-TM imagery and IRS-1D, LISS-III imagery to assess the habitat loss of the elephant in Arunachal Pradesh and Assam in India. In 2005, Unial evaluated the habitat of the lion using remote sensing and GIS in the Palpur Kuno proposed Lion Sanctuary.

A further improvement in the H.S.I. technique was recorded after application of multiple logistic regression (MLR). MLR is a relatively new statistical technique for predictive modelling. Binomial logistic regression is a form of regression which is used when the dependent variable is dichotomous and independent variables are continuous. For MLR analysis, statistical package SPSS has been used (SPSS 1988). MLR applies maximum likelihood estimation after transforming the dependent variable into a logit variable. In this way, the multiple logistic regression estimates the probability of a certain event occurring. Habitat models using presence/absence (dichotomous dependent variable) data and multiple logistic regressions is useful in formalising the relationship between the environmental conditions (independent habitat variables) and the species habitat requirements, thus quantifying the amount of potential habitat available (Imam et al. 2009).

Multiple logistic regression, integrated with remote sensing and GIS has gained momentum in different parts of the world for predictive and habitat suitability index modelling. During 1997, De La et al. carried out a habitat suitability analysis to outline potential areas for conservation of the grey wolf (*Canis lupus*) using logistic regression and geospatial techniques. Palma et al. (1999) used logistic regression to analyse the Iberian lynx habitat and its distribution. On the other hand, Hirzel et al. (2001) assessed habitat suitability models using multiple logistic regression in the Bern Alps (Switzerland) for virtual species, whereas Bio et al. (2002) used binomial logistic regression for predicting the plant species distribution in the lowland river valleys of Flanders (Belgium). Much later, Dendoncker et al. (2006) used multiple logistic regression (MLR) for modelling of land-use suitability maps.

In India recently, Kushwaha et al. (2004), Singh (2004), Braunisch et al. (2008) and Zarri et al. (2008) have used multiple logistic regression to analyse the habitat suitability for the *Cervus unicolor* at Ranikhet, muntjac in the Binsor Wildlife

Sanctuary, the tiger in the Corbett Tiger Reserve, edge effect on two population of the capercaillie (*Tetrao urogallus*) and the Nilgiri laughing thrush (*Garrulax cachinnans*) in the Western Ghats. Similarly, Imam et al. (2009) used multiple logistic regression, Remote Sensing and GIS for evaluating the suitable habitat for the tiger in the Chandoli national park. On the other hand, Singh and Kushwaha (2010) improved the logistic regression technique and used it for the wildlife habitat suitability modelling of the muntjak and goral in the Central Himalayas in India.

2 Materials and Method

2.1 Study Area

The Chandoli Tiger Reserve is situated mainly along the crest of the North Sahyadri Range of the Western Ghat (17° 04' 00"N to 17° 19' 54"N and 73° 40' 43"E to 73° 53' 09"E) (Fig. 1).

The Chandoli Tiger Reserve is situated in the bio-geographic province of the Western Ghats along the crest of the Sahyadris. The topography of the entire reserve is undulating, with steep escarpments, often with exposed rock. The average elevation is 816.5 msl, with the lowest point at 589 msl and the highest point at 1044 msl. A distinct feature of the study area is the presence of numerous barren rocky lateritic plateaus, locally called the *sadda*. Geological foundation of the area is the Deccan trap; the soils are mostly lateritic on the plateau while on the hill

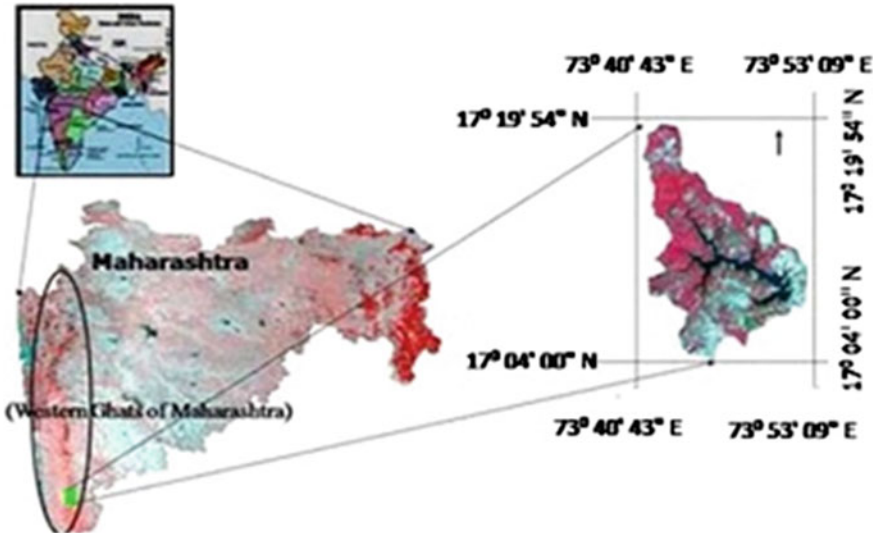


Fig. 1 Study area map

slopes, they are of mixed origin and reddish brown in colour. The area has a moderate climate with a maximum temperature of 38 °C in summer and a minimum of 7 °C in winter. Mean annual rainfall is 3500 mm.

According to Champion and Seth (1968), the forest types include western tropical hill forests, semi-evergreen forests, and southern moist mixed deciduous forests. Dominant tree species are Anjani (*Memecylon umbellatum*), Jamun (*Syzyium cumini*) with associates Pisa (*Actinodaphe angustifolia*), Katak (*Bridelia retusa*), Nana (*Lagerstroemia lanceolata*), Kinjal (*Terminalia paniculata*), Kokam (*Gravinia indica*), Phanasi (*carallia brachiata*), Ain (*Terminalia tamentosa*), Amla (*Emblca officinalis*), Umbar (*Ficus hispida*), Harra (*Terminalia chebula*), etc., whereas Bangala (*Andropogon*), Dongari (*Crysopogon fulvas*), Kalikusli (*Hetropogon canturtus*), Anjan grass (*Sanerus silaris*), Karad (*Thimedo quadri-valvis*), Saphet-kusli (*Aristida funiculate*), and Kalak (*Bambusa bambos*). The Warna River originates in the reserve and numerous other perennial and seasonal streams also drain into the reservoir.

2.2 Methodology

2.2.1 Collection of Collateral Data

The study was started with collection of topographic maps of the area. Topographic maps of scale 1:50000 were collected from the wildlife wing of the Forest Department of Maharashtra, and with the help of forest officials the boundary of the protected area was marked on these sheets. Since the study area was encompassed by four topographic maps, all toposheets were scanned separately and exported to *ERDAS IMAGINE 8.7* in the image format (.img) for mosaicing (*ERDAS IMAGINE 2004*). Before mosaicing, it is mandatory to georeference it to the Geographic Lat-Long Projection up to the sub-pixel level accuracy. The common uniformly distributed Ground Control Point's (GCP) were marked with the root mean square error of one-third of a pixel and images were re-sampled by the nearest neighbour method. After georeferencing, all topographic maps were mosaiced and re-projected into the UTM WGS-84 projection for further analysis. Then, the re-projected image was exported to *ERDAS IMAGINE 8.7* to vectorize and polygonize using a clean-build operation. A study area extent AOI was built around the tiger reserve boundary to produce a rectilinear map and the area of PA was calculated for verification.

2.2.2 Collection of Satellite Data

Satellite data of the study area of IRS-P6, LISS-III dated 2005 was acquired from the National Remote Sensing Centre, Hyderabad, India. The satellite data was imported to *ERDAS IMAGINE 8.7* software in an image format for geometric

correction. The LISS data was co-registered with the already rectified enhanced thematic mapper (ETM) satellite data of 1999 considering it as a reference coordinate system and re-projected in the UTM WGS-84. Distortion was corrected using 20 well distributed prominent features as Ground Control Points (GCP) and the precision level was brought up to 0.2 (of RMSE) to make it sufficiently accurate (Thakur et al. 2008). Since study area lies in two scenes of 095-60 and 095-61 (of LISS III), both images were treated separately and after rectification, these scenes were mosaiced together using *ERDAS IMAGINE 8.7* software. From the mosaiced data, a subset of area of interest (AOI) was prepared and displayed in False Colour Composite (FCC) using three bands (3, 2, 1) for further analysis.

2.2.3 Field Survey

The field survey was carried out for the period of 15 days from 18–30 October 2005. Ground truthing was done by taking GPS location of different habitats and matching with the features found on FCC using tone, pattern, texture, association, shape and size of the features. Besides this, opportunistic transects were used to collect data on the presence/absence of the wild species as the forested area was not accessible due to the high density of trees, under growth, and absence of tracks or roads in the area. A total of 312 points locations of the wild animal's presence/absence were recorded with the help of the GPS. Slope, aspect, elevation, and distances to roads, settlements and drainage were not recorded as they would be more accurately derived through processing of satellite/collateral data in a GIS framework.

2.2.4 Creation of Database Using Remote Sensing and GIS

It is important to prepare the land use land cover map of an area as it can give the pattern of land utilisation and also helps in evaluating the earth surface. Therefore, the map was accordingly prepared through the digital analysis of satellite data using the supervised maximum likelihood classification technique. Supervised classification is a procedure for identifying spectrally similar areas on an image by identifying 'training' sites of known targets and then extrapolating those spectral signatures to other areas of unknown targets. Supervised classification relies on the previous knowledge of the location and identification of land cover types that are in the image. In the present study, it was achieved through fieldwork. Training areas, usually small compared to the full image, are used to 'train' the classification algorithm to recognise land cover classes based on their spectral signatures, as found in the image. The maximum likelihood classifier (MLC) assumes that the training statistics for each class have a normal or 'Gaussian' distribution. The classifier then uses the training statistics to compute a probability value of whether

it belongs to a particular land cover category class. This allows for within-class spectral variance. The MLC usually provides the highest classification accuracies (Lillesand and Kiefer 1994). Using this technique, the study area was categorised into eight classes of land cover, viz. Evergreen forest, *Malkiland forest* (secondary/rejuvenated forest), Scrub, *Sada* (laterite rock), Grass land, Agriculture, Sand and River (water). While preparing the land use land cover map, it is also important to know its classification accuracy. In mapping from remotely sensed data, the term accuracy is used typically to express the degree of ‘correctness’ of a classification. A map derived with a classification may be considered accurate if it provides an unbiased representation of the land cover of the region it portrays. Therefore, classification accuracy is typically taken to mean the degree to which the derived image classification agrees with reality or conforms to the ‘truth’ (Campbell 1996). In the present study overall accuracy of 83.6 % was recorded (Table 1) which revealed that correctness of LULC is only 16.4 % away from idle.

The forest crown density map is of particular importance as it provides vital information on the status of forests. The normalized difference vegetation index (NDVI) was used to prepare a forest density map that was categorised into four canopy density classes: <10 % (non-forest), 10–40 % (open), 40–70 % (medium) and >70 % (dense). The group of pixels having NDVI values from 0 to 0.3 were categories under the canopy density class of <10 %, 0.3–0.5 as the canopy density class of 10–40 %, and 0.5–0.7 were categorised as 40–70 %. The group of pixels having the NDVI value 0.7–0.9 were kept under the canopy density class of >70 %.

It is important to quantify forest fragmentation because the spatial structure of habitats in which an organism lives influences their population dynamics and community structure (Johnson et al. 1992). For this, FRAGSTATS (Mc Garigal et al. 2002) was used to derive indices such as Contagion index and Aggregation index (Table 3).

2.2.5 Variables Selected

Habitat suitability analysis requires the generation of an accurate database on various life support systems and the potential disturbance factors affecting the habitat. Therefore, variables (Table 2) such as elevation, slope, distance from settlements, distance from drainage, distance from roads, forest type and canopy density were selected as input layers. As mentioned above, satellite imagery was used to create variables like land use land cover map and the forest crown density map while the continuous surfaces of distance from the settlement and the drainage were generated from the topographic map for proximity analysis. Elevation, aspect, and slope layers were created from the Digital Elevation Model (DEM). Distance variables like settlements and drainage were log transformed to enforce normality. All these input layers were co-registered with the sub-pixel accuracy.

Table 1 Error matrix resulting from classifying training set pixel for land use land cover

Classification accuracy	Training set data										Row total
	Evergreen forest	Malkiland	Scrubland	Grassland	Agriculture	Sand	Sada	Water			
Evergreen forest	313	0	40	0	0	0	0	0	0	0	353
Malkiland	0	342	38	79	0	0	0	0	0	0	459
Scrubland	0	0	387	0	0	0	16	0	0	0	403
Grassland	38	60	24	359	0	0	0	0	0	0	481
Agriculture	0	0	0	22	58	0	0	0	0	0	80
Sand	0	0	0	0	21	51	12	17	0	0	101
Sada	0	0	20	0	0	14	73	0	0	0	107
Water	5	0	0	0	0	0	0	480	0	0	485
Column total	356	402	509	460	79	65	101	497	0	0	2469

Overall accuracy = $[(313 + 342 + 387 + 359 + 58 + 51 + 73 + 480)/2469] \times 100 = 83.6$

Table 2 List of input database layers created for sambar habitat suitability modelling

SN	Name of layers	Format of layers	Source	File type	Software used
1	Aspects	Polygon	GIS derivative	Image file	ERDAS Imagine 8.7
2	Slope	Polygon	GIS derivative	Image file	ERDAS Imagine 8.7
3	Elevation	Polygon	GIS derivative	Image file	ERDAS Imagine 8.7
4	Drainage	Line	Topographic map	Shape file	ArcView 3.2a
5	Settlement	Point	Topographic map	Shape file	ArcView 3.2a
6	Road	Line	Topographic map	Shape file	ArcView 3.2a
7	Forest type	Polygon	Satellite imagery	Image file	ERDAS Imagine 8.7
8	Forest density	Polygon	Satellite imagery	Image file	ERDAS Imagine 8.7

3 Results and Discussion

3.1 Sambar H.S.I.

Distribution of animal species is largely determined by the availability of preferred forage and other environmental factors such as elevation, slope, distance from water, aspect, etc. Therefore, these factors (given in Table 2) were also considered for the sambar habitat suitability index analysis (Kushwaha et al. 2004; Zarri et al. 2008). After preparation of the layer maps (Table 2), the modelling process for the habitat suitability index for the sambar was started (Fig. 2).

GPS locations of the sambars’ presence/absence obtained from the field survey were transferred into ArcView 3.2 (1999) and attached as attributes to all the locations. All independent variables were transferred into raster themes and used for further analysis. Values for the land use land cover map and forest canopy density were recorded and specified as categorical variables. The points of animal detection were then intersected with all the input layers to produce the habitat use-environmental variables matrix. This worksheet was employed for further statistical analysis. Here, cases of animal sightings were taken as Boolean (presence/absence) and the multiple logistic regression was run for the H.S.I. modelling. The computer software uses the following formula for analysing the probability:

$$\ln(\text{ODDS}) = \ln\left(\frac{\hat{Y}}{1 - \hat{Y}}\right) = a + bx$$

where \hat{Y} is the predicted probability of the event which is coded with 1 (presence) rather than with 0 (Absence), $1 - \hat{Y}$ is the predicted probability of the other decision and x is predictor variable.

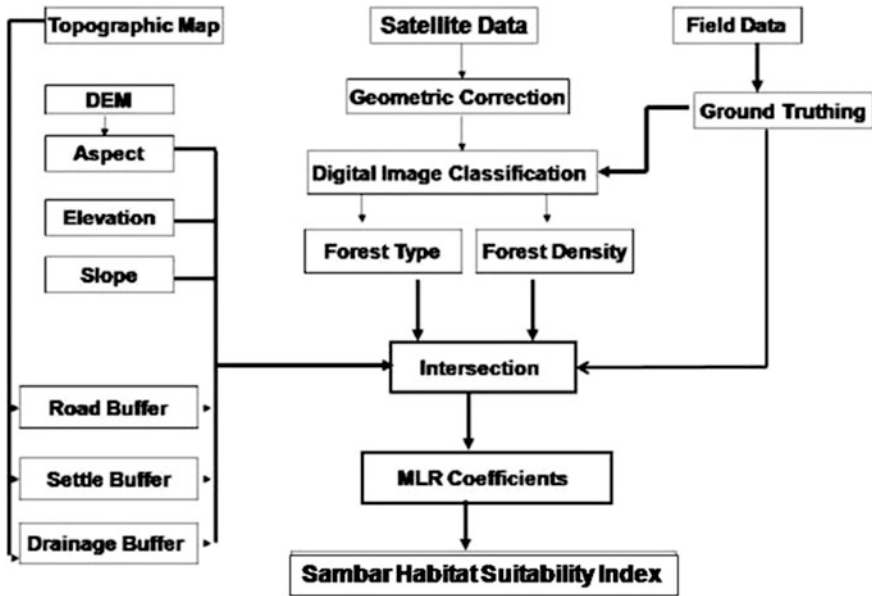


Fig. 2 Paradigm of Sambar habitat suitability analysis in Chandoli Tiger Reserve, India

The simplified formula for developing habitat suitability index will be

$$= \frac{\{\exp(FT * C) + (FD * C) + (EL * C) + (FI * C) + (Constant)\}}{\{1 + \exp(FT * C) + (FD * C) + (EL * C) + (FI * C) + (Constant)\}}$$

Where

- exp Exponential
- FT Forest type
- FD Forest density
- EL Elevation
- DD Drainage distance
- RD Road distance
- SD Settlement distance
- AS Aspect
- FI Fragmentation index
- C Coefficient value

The coefficients derived from the multiple logistic regression (Table 3) were used as weight for the variables to integrate all the layers in the GIS domain (as shown below) to arrive at the probability/suitability map.

Table 3 Coefficients derived for sambar using multiple logistic regressions

Variables	Coefficient
Land use land cover (sada)	-0.031
Land use land cover (grassland)	0.091
Land use land cover (water)	0.0081
Land use land cover (scrub)	0.038
Land use land cover (agriculture)	-1.130
Land use land cover (malkiland forest)	0.124
Land use land cover (sand)	-0.816
Land use land cover (evergreen forest)	03.13
Altitude	0.037
Aggregation index	0.089
Contagion index	-6.514
Constant	-17.89

Formula for H.S.I. of Sambar

$$\frac{\{ \exp(\text{LULC (sada)} * (-0.031) + \text{LULC (grassland)} * (0.91) + \text{LULC (water)} * (0.0081) + \text{LULC (scrub)} * (0.038) + \text{LULC (agriculture)} * (-1.130) + \text{LULC (malkiland forest)} * (0.142) + \text{LULC (sand)} * (-0.816) + \text{LULC (evergreen forest)} * (3.13) + \text{Altitude} * 0.037 + \text{CON} * (-6.514) + \text{AI} * (0.089) + \text{CONSTANT} * (-17.89)) \}}{1 + \exp(\text{LULC (sada)} * (-0.031) + \text{LULC (grassland)} * (0.91) + \text{LULC (water)} * (0.0081) + \text{LULC (scrub)} * (0.038) + \text{LULC (agriculture)} * (-1.130) + \text{LULC (malkiland forest)} * (0.142) + \text{LULC (sand)} * (-0.816) + \text{LULC (evergreen forest)} * (3.13) + \text{Altitude} * 0.037 + \text{CON} * (-6.514) + \text{AI} * (0.089) + \text{CONSTANT} * (-17.89))}$$

Where

- exp Exponential
- LULC Land use land cover
- CON Contagion index
- AI Aggregation index

The estimated log-odds image was then logit transformed to produce the intended probability map. As the log-transform squashed lower values and exaggerated the higher values, the classification accuracies were calculated at a cut-off of 0.5. The output map was sliced to be not suitable at value lower than 0.5 and suitable at values higher than that. Suitability map was further categorised into four classes of highly suitable, suitable, moderately suitable and least suitable. Predicted probability value

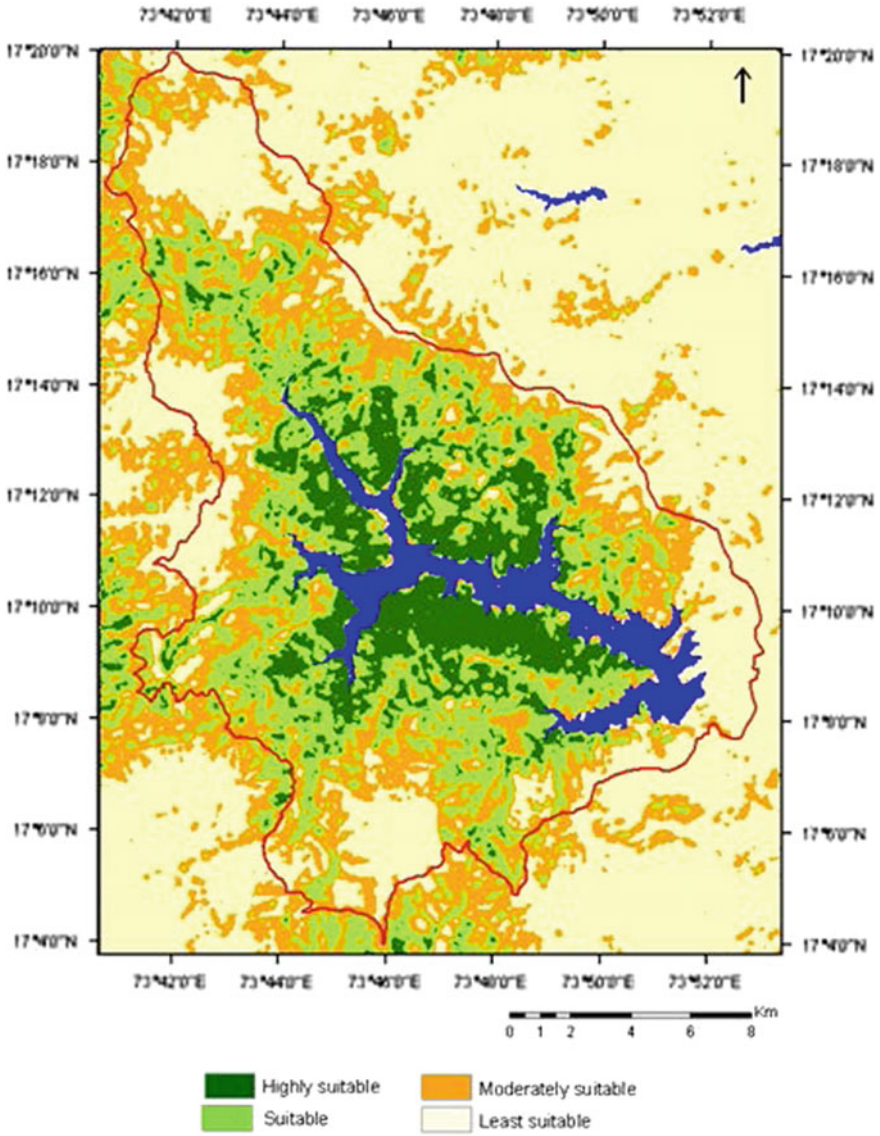


Fig. 3 Habitat suitability map for Sambar in Chandoli Tiger Reserve, India

of 0.0056–0.214 was categorised as least suitable habitat for sambar, 0.214–0.476 as moderately suitable, 0.476–0.719 as suitable and 0.719–0.876 as highly suitable, respectively.

The model, habitat suitability map of the sambar is given in Fig. 3. For the sambar, an overall classification accuracy of 80.2 % was observed with a

Table 4 Classification accuracy for sambar (HSI model) in Chandoli Tiger Reserve, India

Observed	Sambar		
	Predicted		
	Absent (1)	Present (2)	Percentage Correct
Absent (0)	93	26	78.2
Present (1)	19	88	82.2
Overall percentage			80.2

Table 5 Area under different categories of suitability for sambar in Chandoli Tiger Reserve, India

Name of species	Highly suitable habitat	Suitable habitat	Moderately suitable	Least suitable
Sambar	54.01 km ²	82.60 km ²	88.25 km ²	69.92 km ²

probability cut-off value at 0.5 (Table 4), which depicts that model is only 19.8 % away from ideal.

The results revealed that 54.01 km² (18 %) of forest area was most suitable, 82.60 km² (28 %) was moderately suitable, 88.25 km² (30 %) was suitable and 69.92 km² (24 %) was the least suitable for the sambar (Table 5).

The modelling revealed that 46 % of study area is suitable (highly suitable + suitable) for the sambar and its major portions are confined along the reservoir. Rests of the highly suitable habitats are present in fragmented form scattered in other parts of the PA. The major intact portions of the suitable habitats are lying along the southern bank of the reservoir (in the central part of protected area), whereas along the northern bank of the reservoir 3–4 small intact patches of suitable habitats are present.

It was observed during field visits that northern part of the reserve was well-protected and had corridor connectivity with the other neighbouring forest areas. In spite of that these areas are not preferred by the sambar. This is contrary to other studies (Ramesh et al. 2012; Kushwaha et al. 2004). Southern part of the reserve is exposed to more anthropogenic activities and has more cattle grazing pressure than northern portion of the reserve. Before declaration of this forest as a protected area, some of the forest patches around the river were privately owned by village and during evacuation; these forests were destroyed completely by villagers. However, these changes do not have much impact on sambar as they have developed adaptability towards disturbances caused by direct and indirect changes in their habitats (Kushwaha et al. 2004).

In due course of time, these areas transformed into grasslands, primary forests and scrub land. Therefore, these areas are highly preferred by the sambar as they got here more foliage to be eaten. The other reasons may be the presence of karvi shrub (*Strobilanthes callosus*), which are highly preferred by sambar (Geist 1998).

Karanth et al. (2010) suggested that presence of forest cover negatively influence species extinction, but human population density has positive influence on local extinction of animal species. At the time of establishment, 32 villages were present

inside the protected area and approximately 78 in the periphery of 10 km with a human population of 7900 and 10,150 respectively (Census of India 1981). It is a well-known fact that the presence or absence of a species in a particular habitat is outcome of the size/structure of fragments and also from the characteristics of the surrounding landscape, therefore, population of sambar in this reserve is very low (Zarri et al. 2008; Anonymous 2005).

However, protected areas have a significant role in the conservation of wild animals. Karanth et al. (2004) provided evidence that protected natural reserve areas are critical for reducing the local extinction probabilities of most Indian large mammals so that in spite of all pressure, local average extinction probability estimated for sambar across a 100-year time-frame is very low. The study suggested that status of this forests area improved after declaring it as reserve, and privately owned forest which were completely destroyed coming up as primary and rejuvenated forests, whereas evacuated village areas are sprouting into grass lands (Imam 2011). Although very few wild animals were seen during the field visits, but indirect evidences of their presence indicated that wild animals are thriving here after getting conservational attention. These developments are in line with recommendation of Karanth et al. (2004), that is creation of new protected areas and interconnection of existing protected areas will be required through conservation policy and management if many of mammalian species are to persist into the future.

Therefore, evaluation of new potential area for a particular wild species may be considered as one of the most important steps towards conservation. Extensive field work, sound database, statistical treatment of data and modelling technique will be helpful in predicting the potentiality of a habitat for wild animals. The study highlighted the role of Remote Sensing, GIS, and GPS in evaluation of wild animal's habitats with acceptable accuracy.

Acknowledgements The author is thankful to Prof. SPS Kushwaha, former Head, Forestry and Ecology Division and the Dean, Indian Institute of Remote Sensing (IIRS), Dehradun, India for supervision and GIS-laboratory facilities. I am also thankful to Prof. H.S.A. Yahya, Dean Faculty of Life Science & former Chairman, Department of Wildlife Sciences, AMU, Aligarh (India) for encouraging and providing opportunity to work with IIRS, Dehradun. Thanks are also due to Aditya Singh, Dr. Mohammed Irfan (formerly from ATREE) and Director and forest staffs of Chandoli Tiger Reserve, Maharashtra, India for their technical and logistic supports during my field studies.

References

- Andries AM, Gulinck H, Herremans M (1994) Spatial modeling of the barn owl *Tyto alba* habitat using landscape characteristics derived from SPOT data. *Ecography* 17:278–287
- Anonymous (2005) Management plan of Chandoli National Park. Kolhapur Forest Division, Maharashtra, India
- ArcView 3.2 (1999) Environmental Systems Research Institute. Redlands, CA, USA
- Bio AMF, Becker PD, Bie ED, Huybrechts W, Wassen M (2002) Prediction of plant species distribution in lowland river valleys in Belgium: modelling species response to site conditions. *Biodivers Conserv* 11:2189–2216

- Braunisch C, Bullmann K, Graf RF, Hirzel AH (2008) Living on the edge—modeling habitat suitability for species at the edge of their fundamental niche. *Ecol Model* 214(2–4):153–167
- Brian L, West E (1997) GIS modeling of elk calving habitat in a prairie environment with statistics. *Photogram Eng Remote Sens* 63:161–167
- Bright LR (1984) Assessment of elk habitat for resource management and planning activities from Landsat mapping products. *Am Soc Photogram Remote Sens Renew Resour Manag*. Falls Church, Virginia, USA, pp 101–108
- Campbell JB (1996) Introduction to remote sensing, 2nd edn. London, Taylor and Francis
- Census of India (1981) Population census of India. Ministry of Home Affairs, Government of India, Delhi, India
- Champion HG, Seth SK (1968) A revised survey of the forest types of India. Government of India, Delhi, India
- Clark PJ, Evans FC (1954) Distance to nearest neighbor as a measure of spatial relationships in populations. *Ecology* 35:445–453
- Davis FW, Goetz S (1990) Modeling vegetation pattern using digital terrain data. *Landscape Ecol* 4:69–80
- De La Ville N, Cousins S, Bird C (1997) Habitat suitability analysis using logistic regression and gis to outline potential areas for conservation of the Grey Wolf (*Canis lupus*). In: proceeding of conference, GIS Research, University of Leeds, Leeds, UK. pp 9–11
- Dendoncker N, Bogaert P, Rounsevell M (2006) A statistical method to downscale aggregated land use data and scenarios. *J Land use Sci* 1(2–4):63–82
- ERDAS IMAGINE 8.7 (2004) Leica geosystems GIS and mapping. <http://gis.leicageosystems.com>
- Geist V (1998) Deer of the world: their evolution, behaviour, and ecology. Stackpole Books, pp 73–77
- Hirzel AH, Helfer V, Metral F (2001) Assessing habitat-suitability models with a virtual species. *Ecol Model* 145:111–121
- Homer CG, Edwards TC, Ramsey RD, Price KP (1993) Use of remote sensing methods in modelling sage grouse winter habitat. *J Wildl Manag* 57:78–84
- Imam E (2011) Use of geospatial technology in evaluating landscape cover type changes in Chandoli National Park, India. *Comput Ecol Softw* 1(2):95–111
- Imam E, Kushwaha SPS, Singh A (2009) Evaluation of suitable tiger habitat in Chandoli National Park, India, using multiple logistic regression. *Ecol Model* 220:3621–3629
- IUCN (2012) Red list of threatened species. Version 2012.1. Available online: <http://www.iucnredlist.org>
- Johnson LB (1990) Analyzing spatial and temporal phenomena using geographical information systems. *Landscape Ecol* 4:31–43
- Johnson AR, Milne BT, Wiens JA, Crist TO (1992) Animal movements and population dynamics in heterogeneous landscapes. *Landscape Ecol* 7:63–75
- Karanth KU, Nichols JD, Kumar NS, Link WA, Hines JE (2004) Tigers and their prey: predicting carnivore densities from prey abundance. *Proc Nat Acad Sci U.S.A.* 101:4854–4858. doi:10.1073/pnas.0306210101
- Karanth K, Nichols JD, Karanth KU, Hines JE, Christensen NL (2010) The shrinking ark: patterns of large mammal extinctions in India. *Proc. R. Soc. B* 277:1971–1979. doi:10.1098/rspb.2010.0171
- Kushwaha SPS (2002) Geoinformatics for wildlife habitat characterization. Map India. www.GISdevelopment.net
- Kushwaha SPS, Hazarika R (2004) Assessment of habitat loss in Kameng and Sonitpur elephant reserves. *Curr Sci* 87:1447–1453
- Kushwaha SPS, Khan A, Habib B, Quadri A, Singh A (2004) Evaluation of sambar and muntjac habitats using geostatistical modelling. *Curr Sci* 86(10):1390–1400
- Lecis R, Norris K (2003) Habitat correlates of distribution and local population decline of the endemic Sardinian new *Euproctus platycephalus*. *Biol Conserv* 115:303–317
- Lillesand TM, Kiefer RW (1994) Remote sensing and image interpretation. Wiley, New York

- Lyon JG (1983) Landsat derived land cover classifications for locating potential kestrel nesting habitat. *Photogram Eng Remote Sens* 49:245–250
- Mc Garigal K, Cushman SA, Neel MC, Ene E (2002) FRAGSTATS: spatial pattern analysis program for categorical maps, computer software program produced by the authors at the University of Massachusetts, Amherst. Available from <http://www.umass.edu/landeco/research/fragstats/fragstats.html>
- Palma L, Beja P, Rodrigues M (1999) The use of sighting data to analyse Iberian lynx habitat and distribution. *J Appl Ecol* 36:812–824
- Parihar JS, Panigrahy S, Parihar JS (1986) Remote sensing based habitat assessment of Kaziranga National Park. In: Kamat DS, Panwar HS (eds) *Wildlife habitat evaluation using remote sensing techniques*. Indian Institute of Remote Sensing/Wildlife Institute of India, India, pp 157–164
- Porwal MC, Roy PS, Chellamuthu V (1996) Wildlife habitat analysis for sambar (*Cervus unicolor*) in Kanha National Park using remote sensing. *Int J Remote Sens* 17:2683–2697
- Prater SH (2005) *Book of Indian animals*. Oxford University Press, UK
- Ramesh T, Sankar K, Qureshi Q, Kalle R (2012) Group size, sex and age composition of chital (*Axis axis*) and sambar (*Rusa unicolor*) in a deciduous habitat of Western Ghats. *Mamm Biol* 77:53–59
- Roy PS, Ravan SA, Rajadnya N, Das KK, Jain A, Singh S (1995) Habitat suitability analysis of Nemorhaedus goral—a remote sensing and geographic information system approach. *Curr Sci* 69:685–691
- Schadt SE, Wegand T, Knauer F, Kaczensky P, Moser UB, Bufka L, Cerveny J, Koubek P, Huber T, Stanisa C, Trepl L (2002) Assessing the suitability of Central European landscapes for the reintroduction of Eurasian lynx. *J Appl Ecol* 39:189–203
- Singh A (2004) *Wildlife habitat analysis and vulnerability assessment of the Binsar wildlife sanctuary, Uttarakhand*. Dissertation, Indian Institute of Remote Sensing, Dehradun, India
- Singh A, Kushwaha SPS (2010) Refining logistic regression models for wildlife habitat suitability modeling—a case study with muntjak and goral in the Central Himalayas, India. *Ecol Model* 222(8):1354–1366
- SPSS-10 (1988) *SPSS-X user's guide*. 3rd edn. SPSS Inc., Chicago, USA
- Store R, Jokimaki J (2003) A GIS-based multi-scale approach to habitat suitability modelling. *Ecol Model* 169:1–15
- Thakur AK, Sing S, Roy PS (2008) Orthorectification of IRS-P6 LISS-IV data using Landsat ETM and SRTM datasets in the Himalayas of Chamoli district, Uttarakhand. *Curr Sci* 95:1459
- Timmins RJ, Steinmetz R, Baral HS, Kumar NS, Duckworth JW, Islam MdA, Gimán B, Hedges S, Lynam AJ, Fellowes J, Chan BPL, Evans T (2008) *Rusa unicolor*. In: IUCN 2012, IUCN red list of threatened species, Version 2012.1. www.iucnredlist.org
- Unial DP (2005) *Habitat suitability analysis of Lion in proposed Palpur Kuno sanctuary using Remote Sensing and GIS*. Dissertation, Indian Institute of Remote Sensing, Dehradun, India
- USFWS (1981) *Standards for the development of habitat suitability models for use in the habitat evaluation procedures*. USDIFWS, ESM 103, Washington, DC
- WPA (1991) *Wildlife protection act of India*. Natraj Publisher, Dehradun, India
- Zarri AA, Rahmani AR, Singh A, Kushwaha SPS (2008) Habitat suitability assessment for the endangered Nilgiri Laughingthrush: a multiple logistic regression approach. *Curr Sci* 94:1487–1494

Snow Leopard Habitat Modeling Using Neuro-Fuzzy Technique and a Comparative Analysis Between Traditional Overlay and Neuro-Fuzzy Technique—A Case Study of Chamoli and Pithorgarh District of Uttarakhand

S. Sen, G. Areedran and C.K. Singh

Abstract Snow leopard (*uncia uncia*) is the elusive, mysterious predator of the Himalayan region, found in the 5 Himalayan states of Jammu and Kashmir, Himachal Pradesh, Uttarakhand, Sikkim, and Arunachal Pradesh in India. The species is classified as endangered as per the International Union for Conservation of Nature's (IUCN) Red List. India, has 10 % of the snow leopard population in less than 5 % of its habitat area which faces serious danger from several natural and anthropogenic factors. Moreover, the animal is not restricted to wildlife sanctuaries only but is also found spread across the whole area. In the following work, habitat suitability modeling for snow leopards has been undertaken to accommodate this behavior of the cats. The study has been carried out in the state of Uttaranchal using the neuro-fuzzy technique. A comparison with the general weighted overlay method has been drawn to analyze which model is more accurate to predict the habitat suitability surface. Landsat images of ETM+ as well as TM have been used to extract the land use land cover of the study area. ASTER DEM has been used to find the slope, relief, aspect, and ruggedness index of the area. Prey citation data along with the snow leopard citation data further completes the database that is required for snow leopard habitat modeling. Finally, a neuro-fuzzy model has been developed using the MATLAB ANFIS editor to determine the suitable habitat zones for snow leopards in the Himalayan state. The surface generated has been

S. Sen (✉)

HERE Solutions India Private LTD, Mumbai, India

e-mail: senjutisen.kol@gmail.com

G. Areedran

IGCMC, WWF-India, New Delhi, India

C.K. Singh

Department of Natural Resources, TERI University, New Delhi, India

© Springer International Publishing Switzerland 2017

S. Hazra et al. (eds.), *Environment and Earth Observation*,

Springer Remote Sensing/Photogrammetry, DOI 10.1007/978-3-319-46010-9_16

then divided into six suitability zones, ranging from very high suitability to very low suitability areas, depending upon the combination of various input parameters. The model has been finally validated with ground observation data and has been compared with the traditional weighted overlay method. It was seen that while the neuro-fuzzy modeling has successfully defined specific suitability zones, the weighted overlay technique has given a much more general idea about the suitability of the area for the snow leopard habitat. Though this technique is being used for studies including landslide susceptibility and pollution vulnerability, implementing it in habitat modeling is a comparatively new endeavor. Since it takes into consideration the fact that in reality, there exist a range of possibilities, it has the ability to provide a more realistic approach toward habitat modeling. Thus, geospatial techniques used here will give a cost effective solution toward conservation of these elusive yet endangered cats.

Keywords Habitat suitability · Neuro-fuzzy model · ANFIS editor · Ruggedness index · Membership functions · Weighted overlay technique

1 Introduction

Snow Leopards (*Uncia uncia*/*Panthera uncia*), the mysterious, solitary cat, and the apex predator of the high mountainous regions are an endangered species as stated by the IUCN's Red List (Version 3.1) in 2001. The report was adapted by International Union for Conservation of Nature's (IUCN) Council in February 2000. Found in the harsh cold climate of highlands of India, Afghanistan, Bhutan, China, Kazakhstan, Kyrgyzstan, Mongolia, Nepal, Pakistan, Russia, Uzbekistan, and Tajikistan, the total global population of this big cat species is estimated to be around 4080–6590. They spread across an area of 2 million km² with most of them being found in China, followed by Mongolia and India (Project Snow Leopard, Ministry of Environment and Forest 2009). With respect to the situation in India, as stated by the IUCN, the total estimated population of snow leopards in India ranges somewhere between 200 and 600 and is found in the alpine and subalpine zones of the five Himalayan states of Himachal Pradesh, Uttaranchal, Ladakh, Jammu Kashmir, and Sikkim. The animal favors a rugged terrain interspersed with steep slopes, ridges, gullies, and rocky outcrops, mostly at an elevation of 3000–4500 m.

Thus, it is seen that the present status of snow leopards, both globally and nationally, makes it critical for conservation. Though Project Snow Leopard was launched by MoEF in 2004, snow leopards still remain a neglected species for conservation. Moreover, the habitat of this cat is in the vulnerable ecosystem of the Himalayas which faces the threats of climate change and global warming, making it all the more precarious. Apart from these, the developmental activities and

pastoralism puts pressure on this already fragile ecosystem, making the habitat and the cats all the more susceptible to endangerment.

In this study, habitat suitability modeling and mapping have been undertaken to help in better conservation of snow leopards in Uttarakhand, India. Habitat analysis and suitability models are the need of the hour in the face of rising numbers of endangered species due to various environmental factors, anthropogenic causes, and climate change. It helps in conservation and protection of those species along with its dominant prey type and the conservation of the environment in which they reside, thus helping in preserving the ecology. Habitat suitability mapping started with the use of aerial photographs for extraction of habitat factors at a small scale (Palma et al. 1999) and gradually adopted the use of different satellite imagery (Jessica et al. 2012) for large scale mapping as well as statistical techniques like Bayesian technique (Tucker et al. 1997), autologistic regression (Osborne et al. 2001), etc. Fuzzy logic, developed by Zadeh in 1965, describes that there exist a range of possibilities as against which is defined by the traditional bivalued logic. This is particularly true, especially in modelling environmental factors and phenomena. Empirical models developed for such kind of works are mostly suitable for the areas in which they are developed. Moreover, their output produces crisp values which fail to model the gradual transition between various phenomena and the overlapping between various factors in nature. It helps in incorporating the ambiguous situation (Navas et al. 2011).

A number of works regarding the application of fuzzy logic in marine environment have been noted like “marine eutrophication, water pollution, benthic faunal community mapping, vulnerability of marine areas to scuba diving and marine fishes to fishing and assessing impacts of marine fish farming” (Navas et al. 2011). A neuro-classifier is a fuzzy classifier obtained by a learning procedure which is used when interpretation and the employment of prior knowledge is required neuro-fuzzy techniques can learn a systems’ behavior from sufficiently large data sets and automatically generate fuzzy rules and fuzzy sets to a pre-defined level of accuracy (Dixon 2004). Neuro-fuzzy methodology has also been used within GIS to determine suitable sites for the locations of public golf courses, modeling groundwater vulnerability (Dixon 2004), soil erosion assessment and for irrigation (Valdes et al. 2003). It had been also used in modelling the environmental vulnerability of finfish aquaculture in the fjords of Ireland and for determining the landslide susceptibility of Cameron highlands in Malaysia (Pradhan et al. 2010).

In this study, neuro- fuzzy model has been developed to assess the location and extent of suitable habitat zones for snow leopards in Uttarakhand, India. It has been compared with weighted overlay technique to understand how and which model performs above the other when validated with ground observation. The four parameters for developing the habitat suitability model are land use, land cover, slope and aspect, and ruggedness index.

2 Study Area

As seen in Fig. 1, Uttarakhand lies in the northern part of India, bounded by Himachal Pradesh in the north-west, Uttar Pradesh in the south, Nepal in the east and China in the north. The locational extent of Uttarakhand is from $77^{\circ} 34' 22''\text{E}$ to $81^{\circ} 02' 22''\text{E}$ and $28^{\circ} 53' 24''\text{N}$ to $31^{\circ} 27' 50''\text{N}$. Physiography of Uttarakhand ranges from the plains of Haridwar to the lofty Himalayan ranges. Specifically, the northern portion of Uttarakhand was used as the study area as the habitat preference for snow leopards can be originally found here. Moreover, it coincides with the area specified by PSL (2006) with respect to Uttarakhand. Below, a short description on each of the subdivisions of the area has been given:

Chamoli: Situated in the Himalayas, it is bounded by Tibet in the north and the districts of Uttarkashi in the north-west, Pithorgarh in the east, Almora in the south east and Garhwal in the south west ,and Tehri Garhwal in the west. The subdivisions of Chamoli and Josirmath were chosen as the study area mainly because both these subdivisions were 3000 m above MSL, which has already been specified by PSL in 2006 to be included for areas under snow leopard conservation.

Pithorgarh: The district lies in the north eastern part of the Kumaon Division, extending from $29^{\circ} 27'\text{N}$ to $30^{\circ} 40'\text{N}$ and $79^{\circ} 50'\text{E}$ to $81^{\circ} 3'\text{E}$. It is bounded by Tibet in the north, Nepal in the east, Almora in the south and Almora and Chamoli

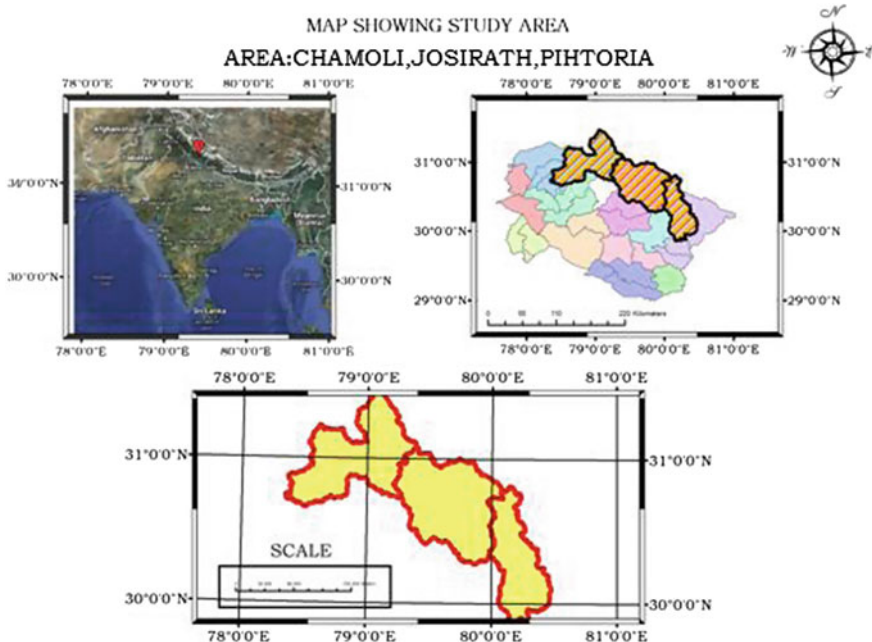


Fig. 1 Location map of study area

in the west. Pithoria subdivision of this district was chosen as the study area due to same reason as stated above.

Moreover, these districts house the Askot wildlife sanctuary, Valley of flower national park, Nanda Devi biosphere reserve and the area between Munsiari and Dung, which has been surveyed for snow leopard according to the report on Snow Leopard Conservation in Uttarakhand and Himachal Pradesh.

3 Materials Used

3.1 Satellite Data Used

Landsat™ satellite images (2010–2011) at 30 m resolution were used for deducing the land use land cover map and ASTER DEM, at 30 m resolution was used to derive the terrain parameters of slope, aspect, and ruggedness Index.

3.2 Software Used

ERADS, ENVI has been used for image processing and classification. ARC GIS was used for deriving terrain parameters, extracting, and exporting data and for creating maps. MATLAB was used for modelling technique (ANFIS Editor) and R has been used for handling the huge databases.

4 Methodology

4.1 Literature Review and Documentation of Habitat Parameters for Snow Leopards

Habitat (Hall 1997) can be defined as “resources and conditions present in an area that produce occupancy, including survival and reproduction by a given organism and as such, imply more than vegetation and vegetation structure. It’s the sum of specific resources that are needed by an organism.” A suitable habitat for any species is governed by the number of favorable factors that it can support. Snow leopards are characteristically shy and introvert cats unlike their other cousins. They prefer solitude and live a secluded life. After various literature reviews and reports (Anon 2008; Maheshwari and Sharma 2010), it was concluded that for constructing the habitat suitability model for snow leopards, a landscape level approach should be undertaken rather than a species level approach. This is because snow leopards are not restricted to wildlife sanctuaries alone and are spread across the whole area.

Primarily, four habitat factors were enlisted to construct the snow leopard habitat suitability model. They are:

1. Land use Land cover
2. Slope
3. Ruggedness Index
4. Aspect.

Snow Leopards prefer cold and arid or semi-arid scrubland, grassland, and barren lands as their habitat with average elevation of the areas being 3000 m above MSL. Steep, cliff-like slopes ranging from 30° to 60° are preferred by the snow leopards rather than low and gentle ones. They favor difficult and rugged terrain which helps them to camouflage themselves, which in turn facilitates the prey hunting and protects them against poachers. It was also noted in a study that snow leopards choose the eastern aspect of the slopes more than the northern and southern.

4.2 Image Processing and Classification

LandsatTM and ETM data of Uttaranchal were downloaded, geometrically rectified and preprocessed followed by Land use land cover classification. The data was projected to UTM projection with Zone number 44N and WGS 84 as the datum and the study area was extracted. A supervised classification technique was used in ENVI for extracting the land use and land cover of the study area followed by an accuracy assessment on the same. The extracted LULC had an accuracy of 97.68 %. Uttaranchal was divided into eight classes, namely: dense forest, open forest, alpine scrub, permanent, and seasonal snow, settlement, and water bodies. Figure 2 provides the reference for the same.

ASTER DEM having a spatial resolution of 30 m was downloaded and pre-processed for extracting the terrain parameters. Slope, aspect, and ruggedness index were calculated in ARC GIS and the following classification scheme for each of the variable was applied. Tables 1, 2 and 3 provides a description of the classification of terrain parameters.

4.3 Habitat Suitability Modeling Using Neuro-Fuzzy Technique

The habitat suitability model was created in MATLAB with the help of an ANFIS editor which applies a hybrid neuro- fuzzy model for teaching a *Takagi-Sugeno* type fuzzy system. The advantage of ANFIS is that it itself decides the membership functions and rules. It is a hybrid method wherein the *gradient method* is used for

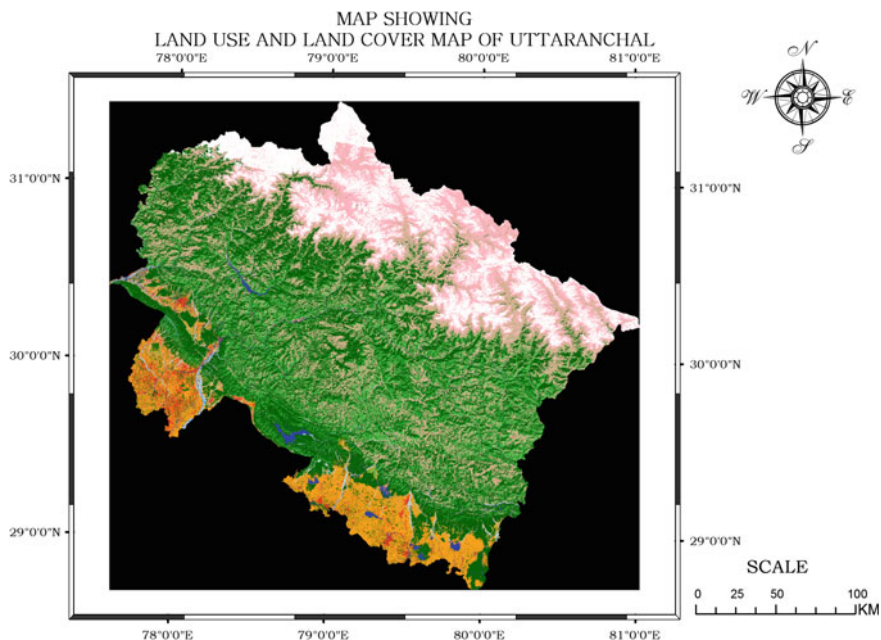


Fig. 2 Landuse and land cover map of Uttarakhand showing the eight classes of LULC

Table 1 Classification scheme for slope

Slope	Range (°)	Class
Low to gentle	0–20	1
Moderate to steep slope	20–45	2
Precipitous to cliff like slope	45–90	3

Table 2 Classification scheme for ruggedness index

Ruggedness	Ranges (m)	Class
Low to level ruggedness	Below 200	1
Intermediate to moderate ruggedness	200–500	2
Steep to very steep and rugged terrain	500 to highest	3

Table 3 Classification scheme for aspect

Aspect	Ranges (°)	Class
Northern	0–40	1
North eastern and eastern	40–110	2
Southern and western	110–359	3

the input function parameter and *least square* is used for the output function parameter and uses a *weighted mean* for *defuzzification* method. ANFIS, thus, helps in optimizing the parameter scheme that best fits the data with the help of neural network.

For preparing the data for MATLAB, the pixel values of the sites pertaining to all the habitat factors, where the snow leopard ground data was observed, were extracted using ARC GIS. This is also known as sample extraction. Since most of the ground data was concentrated in the Chamoli district, this was used as the training data. This was followed by the creation of the habitat suitability index in which the parameter classes pertaining to the training sites were extracted and classified depending on their suitability under expert supervision.







Neuro- fuzzy modelling: After loading the training data, a fuzzy inference system for MATLAB was generated using the grid partitioning method wherein triangular membership function was chosen for the input parameters. The training data was reiterated with 40 epochs and with an error tolerance of zero. It was seen that after 40 epochs, the error stabilizes at the point of nearly 15 epochs at 0.3697.

4.4 Post Training: Predicting Habitat Suitability Surface

Evaluating the fuzzy inference structure yielded the suitability values for each pixel of the training set. The resulting FIS was then used to predict the suitability values for the rest of the areas, i.e., Pithorgarh and Josirmath. The values were exported and plotted against their respective spatial location using R programming language as it has the capacity to handle huge databases that were the resultant output of MATLAB ANFIS. This was finally interpolated in ARC GIS (natural neighbor technique) to generate the habitat suitability surface which was reclassified into 6 six zone. The classification scheme followed has been described below with reference to Table 4:

Not suitable: Areas consisting of dense forest, water bodies, agriculture, and settlement are included in this class. Even if the other three factors, i.e., slope, terrain ruggedness and aspect range from being moderate to highly suitable, the probability of these areas being suitable enough to be a habitat for the snow leopard habitat has been negated due to the type of the land cover present.

Table 4 Classification scheme for habitat suitability zones

Codes	Suitability	Symbology
1	Not suitable	
2	Very low suitability	
3	Low suitability	
4	Moderate suitability	
5	High Suitability	
6	Very high suitability	

Very Low suitability: These areas mostly have open forests and one of the terrain parameters are low to moderately suitable which varies according to the spatial locations.

Low suitability: Areas which are contiguous to the alpine scrublands and are a continuation of the open forest are included in this zone. Since the areas in this zone gradually merge into the alpine scrubland, they have a low probability of being suitable for the snow leopard. Moreover, among the terrain parameters, these areas mostly portray the northern aspect which, according to the ground observation carried out, is not preferred by the snow leopard. But since slope and ruggedness index can be suitable in this zone, this zone has a low potential of being a suitable habitat with only one or two of the habitat factors being favorable.

Moderately suitable: The areas of seasonal snow and alpine scrubland are included in this zone. The land cover is suitable for snow leopards but the other three factors remain moderately suitable. This zone is characterized by the fact that at a given time, either two or three factors are moderately suitable.

High suitability: The areas of permanent snow cover, seasonal snow cover, or alpine scrublands with moderate to steep slopes and moderate to steep ruggedness are considered to be highly suitable for snow leopards. These areas can have any other aspect other than the northern.

Very high suitability: Only those areas where land cover is permanent snow, slope is moderate to very steep and the terrain is very rugged are considered to be highly suitable for the snow leopard. These aspect in these areas is north eastern, eastern or south eastern. The reason for the areas being highly suitable for snow leopard habitats is that the habitat parameters exactly coincide with the ones preferred the most by the snow leopards.

4.5 *Weighted Overlay*

After classifying the parameters, they were provided weights according to their respective importance as habitat parameters. Land use and land cover (LULC) was weighted the most and aspect the least whereas slope and ruggedness index were given equal importance on a scale of 0–1. Weighted overlay analysis was carried out in ARC GIS and the suitability map was reclassified on the same scale as the surface generated by ANFIS.

(It has to be noted that while deciding the habitat parameters, land cover was given the most importance as it becomes a deciding factor for snow leopard habitats. This can be concluded from the fact that it was observed during ground observation that even when the slope, ruggedness, and aspect of a particular area were found to be suitable, no snow leopards could be spotted if the land cover was not appropriate. The information for preferences for slope and ruggedness gathered from ground observation data and through surveys carried out in Ladakh region showed the

preference for eastern aspect, but since, in general, the number of snow leopards spotted has been low, the preference of other aspects could not be ruled out.)

4.6 Validation and Comparative Analysis

The resultant surface generated from both the techniques, were validated with the help of ground data that contained snow leopard presence/absence as well as prey data.

4.7 Comparative Analysis

A comparative analysis was drawn in the end between the habitat suitability surfaces generated by neuro-fuzzy technique as well as traditional weighted overlay technique.

5 Results and Discussions

5.1 Validation

The habitat surfaces generated with the help of both the neuro- fuzzy model and the weighted overlay technique were validated with the ground reference data as received from WWF-India. Of all the 13 points that were collected, 11 were seen to be in the high to very high suitability zone, 7 being in high, and the other 4 being in very high suitability zone. The model had an accuracy of 84.61 % correctly, i.e., the neuro-fuzzy model predicted ~85 % (84.61 %) of the habitat suitability surfaces correctly. The error can be attributed to the fact that the ground observation was fewer in number and contained direct as well as indirect evidence. The less density of ground observation data in high suitability zones could also be attributed to the fact that the evidence from these areas have been difficult to collect due to its harsh environment as well as the shy nature of snow leopards.

5.2 Habitat Suitability Zonation and Analysis

After the models were validated, the six habitat suitability zones in all the three subdistricts of Pithoria, Josirmath, and Chamoli were quantitatively as well as

qualitatively analyzed. Below is a detailed study of the habitat suitability zones in each of the subdistricts:

Not Suitable Zone: Areas with dense forest and unsuitable terrain parameters in all the three subdistricts were recognized as unsuitable habitat zone for snow leopards. While in Pithoria, the area under this zone amounted to 20.79 %, in Josirmath it was 12 %. The highest percentage of not suitable zone for snow leopard habitat was found to be in Chamoli with a percentage of 22.84 % of the total area of the subdistrict.

Very Low Suitability Zone: This area, in all the three subdistricts, was seen to coincide with regions contiguous to open forests having moderate ruggedness index with a northern slope. While Pithoria witnesses this habitat zone in a linear fashion in the northern part and in patches in the southern part of itself with an area of 15.19 %, in Josirmath, this habitat zone has a coverage of 18 %. It was seen that in Josirmath, the land cover type had a profound effect of making the 18 % of its area fall in this category of habitat suitability zone than the other terrain factors. Chamoli has an area of 8–10 % in very low suitability zone.

Low Suitability Zone: Pithoria has an area of 12.82 %, especially in the northern and western parts of it, categorized as low suitability zone for snow leopard habitat where a transition of open forests to alpine scrublands is seen along with a northern aspect. Josirmath has an area of 22 % under this habitat suitability zone and Chamoli has an area of 8.89 % of its area under this habitat zone.

Moderate Suitability Zone: This zone shows the characteristics of having alpine scrubland as their land cover type in all the three subdistricts with moderately rugged terrain and moderately suitable slope and aspect. Pithoria has 18.98 % of its area in this zone, mainly concentrated in the central part of itself like the veins of leaf. Here the slope is dominantly gentle and aspect ranges from southern to western. In Josirmath, a total of 30 % of area is moderately suitable for snow leopards whereas in Chamoli, only 10.75 % of area falls under this category.

High Suitability Zone: 25.65 % of area in Pithoria was seen to be categorized by the neuro- fuzzy model as highly suitable for snow leopards. The highest occurs in Chamoli wherein an area of 48.20 % was predicted to fall under this class of habitat suitability zone. Josirmath is predicted to have the least with an area of only 5.53 %. These areas in Pithoria, Josirmath and Chamoli have seasonal snow or alpine scrubland as their dominant land cover. In northern Pithoria, it is present in bold patches.

Very High Suitability Zone: Chamoli has been predicted to have the highest percentage of area in the very high suitability zone amounting to 15.92 % followed by Josirmath which has an area of 12.55 % and lastly, Pithoria, having an area of only 4.32 %. In all the three subdistricts, this region portrays a combination of highly favored terrain factors with permanent snow as their land cover.

After the detailed analysis of each habitat suitability zone in each of the three subdistricts as predicted by the neuro-fuzzy model, a comparative analysis of the same was done with the habitat suitability surfaces predicted by simple weighted

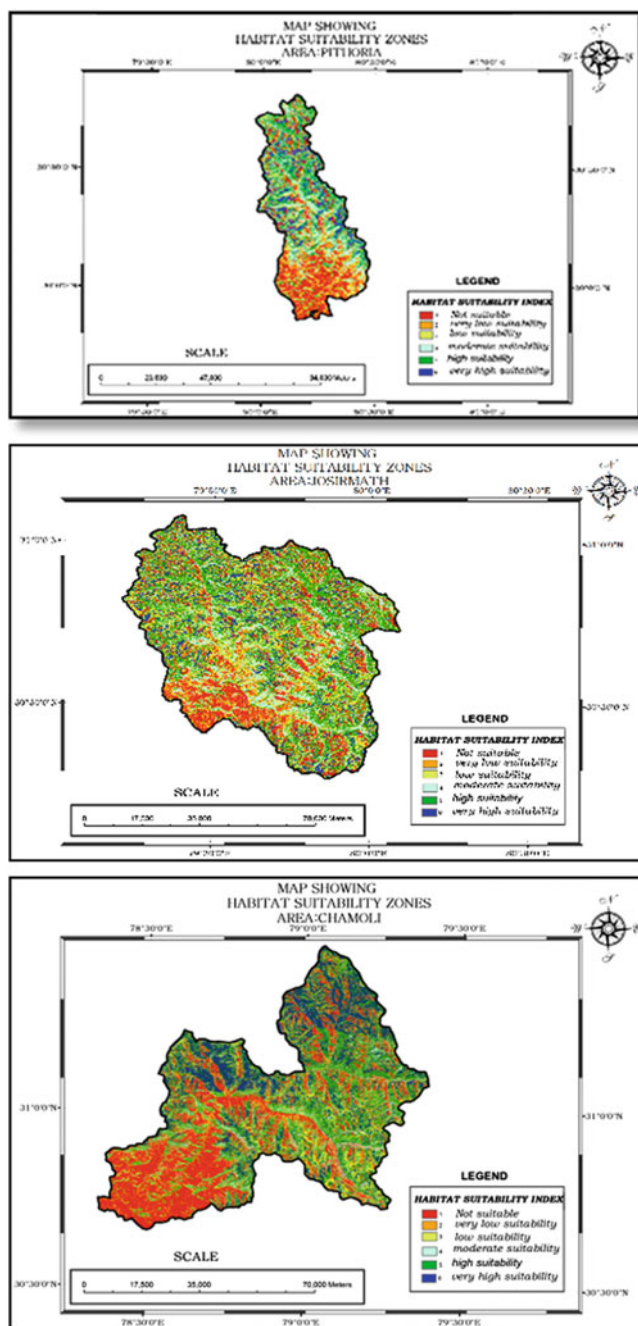


Fig. 3 Habitat suitability maps for Pithoria, Josirmath and Chamoli

overlay technique carried out in ArcGIS. Figure 3 shows the habitat suitability zones in each of the areas.

5.3 Comparative Analysis

Weighted overlay is a simple traditional technique and gives a very general idea about the suitability of the area for the snow leopard. It fails in categorizing the study area into suitable classes of snow leopard habitat with range of possibilities. It was seen that while the neuro-fuzzy technique was successful in predicting the surface areas which could be reclassified easily into subsequent habitat zones mentioned above, simple weighted overlay fails to do so. It does not help in predicting the exact extent of suitability areas and neither enables to categorize the habitat suitability surface into the above defined habitat zones. It, in fact, overestimates most of the areas to be very highly suitable which does not match with the reality. Nevertheless, it was seen that on a broader scale, both the outputs match even though the degree of habitat suitability surfaces predicted by the neuro-fuzzy model is far more accurate. The same classification technique and suitability indices have been followed for both the techniques. Figure 4 shows the comparative analysis between habitat suitability surfaces generated by weighted overlay technique and Neuro-fuzzy model.

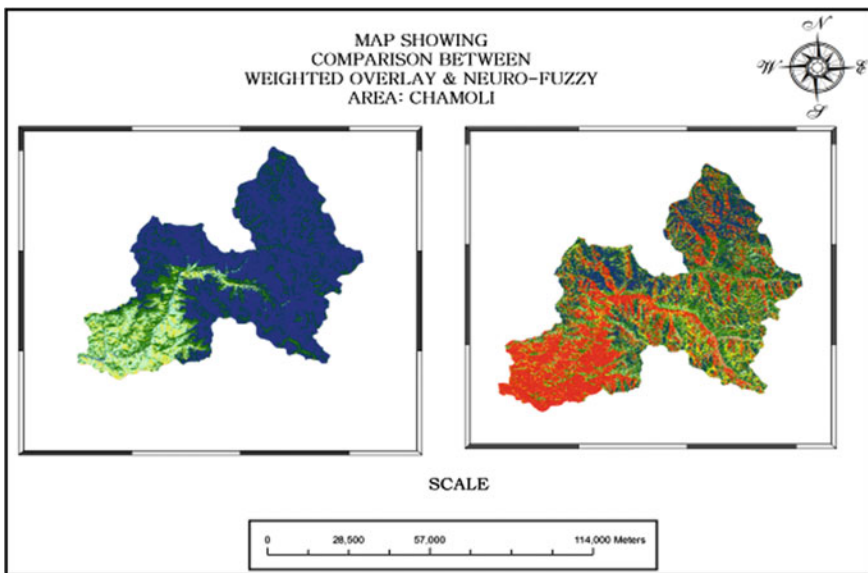


Fig. 4 Map showing comparison between habitat suitability surfaces generated by weighted overlay technique and Neuro-fuzzy model

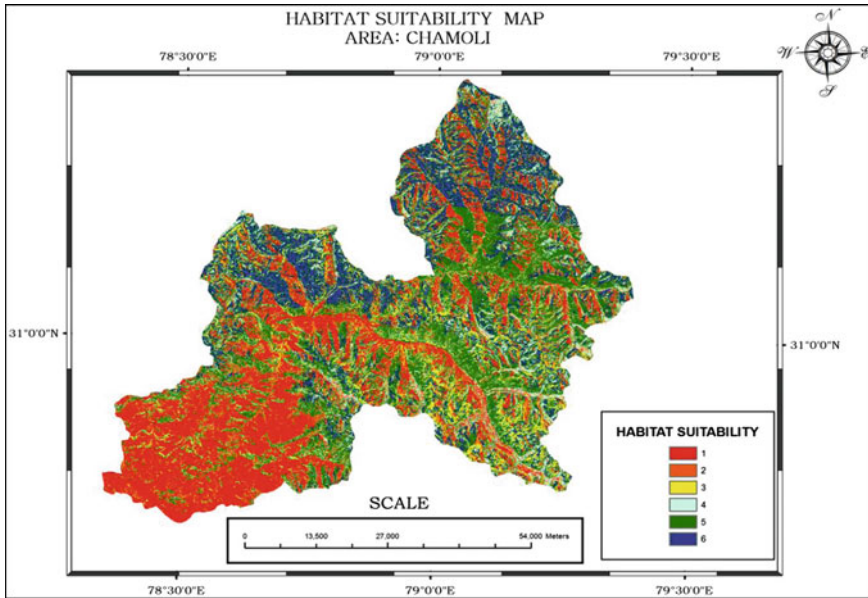


Fig. 5 Map showing the habitat suitability surface as generated by trapezoidal membership function in neuro-fuzzy model

5.4 Sensitivity Analysis

MATLAB ANFIS is helpful since it is capable of deciding independently the membership values on the basis of the membership functions chosen by the user. But while doing so, it also inherits the danger of not being able to give optimum results as the membership function chosen might not be suitable for the dataset. To check this, habitat suitability analysis was done for the second time (only in Chamoli) using a Trapezoidal membership function and the final map was validated against the ground observation points. It was seen that there was not much difference between the accuracy of the two results. While triangular membership function resulted in an accuracy of 84.61 %, trapezoidal membership function gave an accuracy of 81.29 %. Figure 5 provides reference for the same.

6 Conclusion

The neuro-fuzzy technique is comparatively newer and its use in habitat modeling has been very limited. This work attempts to use this technique in predicting and modeling the habitat of a lesser known, endangered species of the cat family. It was seen that the model was able to predict the habitat surface with the capacity of moving beyond the traditional binary approach. It resulted in a surface with varying

degree of suitability, which is comparable with the real world, where between the most and the least suitable habitats, there remains the possibility of the existence of a range of moderately suitable habitats. This becomes clearer when the results are compared with the conventional overlay approach.

With regard to the quantitative analysis related to the areas under different suitability zones, it was seen that while Chamoli had the greatest area under suitable zone, Josirmath had more area under potentially suitable zone (Suitable zone is the summation of total area with high to very high suitability index and potentially suitable zone is the summation of the total area with moderate to low suitability indices). In terms of all the aspects, Pithoria had the lowest amount of suitable area for snow leopards. With respect to policy formulation, it can be said that since Chamoli has the most area under suitable habitat zone, it is more prone to poaching and therefore, special attention should be paid to this subdistrict. In general, areas with very high or high suitability need immediate attention for habitat preservation. Areas with low to moderate conservation should be protected with policies in such a way that in the future, their potential for sheltering snow leopards should increase. Habitats which are not at all suitable or have a very low suitability index should be given least importance during consideration for conservation or during policy formulation.

Few of the challenges that this study encountered has been described below:

1. The model does over predict in few instances, especially in predicting the unsuitable areas of Chamoli. The neuro-fuzzy model over predicts the unsuitable areas of habitat in Chamoli district, i.e., it shows that the percentage of unsuitable areas in Chamoli district is more than what it is in reality. The relatively small number of ground observation could be a major reason.
2. The snow leopard, being mysterious in character, and an animal of harsh terrain and environment, its citation becomes a major obstacle. This prevents us from understanding the animal's behavior in a more comprehensive way, which is essential for realizing the preferences for habitats.

The study also opens up an immense future scope for further study. A comparison with fuzzy technique, multi logistic regression and AHP can be done to estimate the most accurate technique for habitat prediction. Modeling can also be done on multi scale that will help in policy formulation and actual implementation. Moreover, different membership functions can be incorporated into the model apart from the triangular membership functions to see which membership functions provide a better and accurate result. Moreover, the work can be carried out in several other parts of India especially in the eastern Himalayas to predict habitat suitability zones for snow leopards in those areas. A comparison can be made between the western Himalayas and the eastern Himalayas with respect to the habitat suitability of snow leopards in India.

Acknowledgments The authors are highly thankful to Dr. P. K. Joshi, Head, Dept. of Natural Resources, TERI university and Dr. Oinam Bakim Chandra, Assistant Professor, Shiv Nadar University, Noida for their constant support and valuable guidance.

References

- Anon (2008) The project snow leopard. Ministry of Environment and Forests, Government of India New Delhi
- Areendran G, Raj K, Mazumdar S, Munshi M, Govil H, Sen PK (2011) Geospatial modelling to assess elephant habitat suitability and corridors in Northern Chhattisgarh, India. *Trop Ecol* 52 (3):275–283
- Belongie CC (2008) Using GIS to create a gray wolf habitat suitability model and to Assess Wolf Pack Ranges in the Western Upper Peninsula of Michigan. *Resource Analysis*, 10:15
- Cruz A (2009) ANFIS: Adaptive neuro-fuzzy inference systems. IM, UFRJ, Mestrado NCE
- Dixon B (2004) Applicability of neuro-fuzzy techniques in predicting ground-water vulnerability: a GIS-based sensitivity analysis. *J Hydrol* 2004:1–22
- Forrest JL, Wikramanayaka E, Areendran G, Shreshtha R, Gyetshen K, Maheshwari A, Mazumdar S, Naidoo R, Thapa GJ, Thapa K (2012) Conservation and climate change: assessing the vulnerability of snow leopard habitat to treeline shift in the Himalaya. *Biol Conserv* 129–135
- Hall et al (1997) The habitat concept and a plea for standard terminology. In: *Wildlife society bulletin*, vol 25, No 1. International issues and perspectives in wildlife management. Spring, 1997, pp 173–182
- Hansen MJ, Franklin SE, Woudsma CG, Peterson M (2000) Caribou habitat mapping and fragmentation analysis using Landsat MSS, TM, and GIS data in the North Columbia Mountains, British Columbia, Canada. *Remote sens Environ* 77(2001):50–65
- Hong TP, Lee CY (1995) Induction of fuzzy rules and membership functions from training examples. *Fuzzy Sets Syst* 84:33–47
- Jessica L et al (2012) Conservation and climate change: assessing the vulnerability of snow leopard habitat to treeline shift in the Himalaya. *Biol conserv* 150:129–135
- Kushwaha SPS, Roy PS (2002) Geospatial technology for wildlife habitat evaluation. *Trop Ecol* 43(1):137–150
- Maheshwari A, Sharma D (2010) Snow leopard conservation in Uttarakhand and Himachal Pradesh. WWF-India, New Delhi
- Maheshwari A, Takpa J, Sandeep K, Shawl T (2010) An investigation of carnivore-human conflicts in Kargil and Drass areas of Jammu and Kashmir. Report submitted to Rufford Small Grant
- McDermid GJ, Franklin SE, Ledrew EF (2005) Remote sensing for large-area habitat mapping. *Prog Phys Geogr* 29(4):449–474
- Navas MJ, Telfar TC, Ross LG (2011) Spatial modeling of environmental vulnerability of marine finfish aquaculture using GIS-based neuro-fuzzy techniques, *Mar Pollut Bull* 1786–1799
- Newland FT et al (1996) Neurofuzzy extraction of wind data from remotely sensed images. In: *Third international winds workshop*, Ascona, Switzerland, p 18
- Osborne PE, Alonso JC, Bryant RG (2001) Modelling landscape-scale habitat use using and remote sensing: a case study with great bustards. *J Appl Ecol* 38:458–471
- Palma et al (1999) The use of sighting data to analyse Iberian lynx habitat and distribution. *J Appl Ecol* 36
- Pereira MC, Itami Robert M (1991) GIS-based habitat modeling using logistic multiple regression: a study of the Mt. Graham red squirrel, *Photogram Eng Remote Sens* 57(11):1475–1486
- Pradhan B, Sezer EA, Gokceoglu C, Bruchroithner MF (2010) Landslide susceptibility mapping by neuro-fuzzy approach in a landslide-prone area (Cameron Highlands, Malaysia). *Geosci Remote Sens* 48
- Sperduto MB, Congalton RG (1996) Predicting rare orchid (Small whorled pogonia) habitat using GIS. *Photogram Eng Remote Sens* 62(11):1269–1279
- Store R, Jokimaki J (2003) GIS-based multi-scale approach to habitat suitability modelling. *Scie Direct Ecol Model* 169:1–15

- Tucker K, Rushton SP, Sanderson RA, Martin EB, John B (1997) Modelling bird distributions—a combined GIS and Bayesian rule-based approach. *Landscape Ecol* 12(2):77–93
- Valdes et al (2003) Phytoplankton photopigments as indicators of estuarine and coastal eutrophication. *Biosci* 53(10):953–964
- Wieland R, Mirschel W (2008) Adaptive fuzzy modeling versus artificial neural networks. *Environ Model Softw* 23(2): 215–224

Index

A

Agriculture, 7, 27, 36, 48, 51, 84, 87, 92, 154, 156, 162, 171, 201, 207, 237, 241, 254
Air-sea exchange, 124, 125, 128, 130–132
Analytical hierarchical process, 2, 5, 18, 181–183, 187, 189–192, 261
ANFIS editor, 251, 252
AVHRR, 37, 125, 127, 130, 132, 133, 216
AWiFS, 74, 76, 77

B

Bay of Bengal, 7, 100, 124, 125, 128, 130, 131, 133, 139, 155, 156, 196

C

Change detection, 109, 157
Chlorophyll-*a*, 125, 127, 128, 131
Climate change, 36, 48, 57, 58, 61, 68, 100, 107, 197, 198, 248, 249
Climate change adaptation, 198
Coast, 3, 7, 9, 11, 13, 36, 100, 101, 104, 124, 125, 127, 130, 133, 154, 156, 158, 162, 163, 171, 196–198, 200, 202, 203, 208
Coastal erosion, 100, 104, 154, 162, 196, 197, 200, 202, 208
Crop identification, 74, 78, 84

D

Disaster, 176, 196–198, 202
Downscaling, 38–41, 43–45, 47, 51, 58, 60, 61, 63, 64, 68
Drought, 36, 47, 48, 51, 74, 88
Dug well (Kapil Dhara), 88–94

E

Earth observation, 249, 255, 256, 260, 261
Environment, 2, 4, 6, 10, 11, 13, 17, 18, 25, 27, 36, 37, 42, 47, 48, 50, 60, 88, 138, 149,

156, 176, 216, 217, 219, 220, 222, 225, 232, 233, 239, 248, 249, 256, 261

F

Forestry, 27, 244
FSC, 76, 78, 83–85
Fugacity of CO₂, 127–133

G

GCM, 39, 58, 60, 61, 64, 68
Geo-informatics, 137, 195
Ghoramara Island, 155, 156, 160, 163, 167, 169
GIS, 5, 18, 24, 25, 27, 28, 32, 33, 88–90, 92, 93, 95, 114, 170, 179–181, 183, 184, 198, 231–233, 236, 239, 244, 249, 252, 254, 255

H

Habitat suitability, 232–234, 237, 239, 240, 242, 249, 251, 252, 254, 256, 258, 259, 261
Habitat suitability index, 233, 239, 240, 254
Hierarchical process, 2, 5

I

Indian Sundarban Delta, 154, 155, 157

L

Landscape, 41, 43, 44, 47, 48, 157, 217, 244
Landslide, 176, 177, 179–187, 189, 191, 249
Land surface temperature, 36, 216, 217, 219
Land use/land cover, 4, 7, 9, 17, 18, 24, 25, 51, 74, 78, 80, 81, 89, 92–94, 154–157, 162, 164–169, 181, 183, 220, 222, 237, 239, 249, 251, 252, 255
LRD, 24, 27, 28, 31

M

- Mangrove, 98, 100, 101, 104, 114, 124, 138, 154, 156, 157, 159, 162, 164, 166, 169, 196, 202
- Membership functions, 79, 252, 260, 261
- MGNREGA, 88, 89, 92, 94
- Migration, 156, 163, 212
- MNDWI, 141, 142, 144, 145, 149
- Modelling, 36, 39, 232, 233, 239, 243, 244, 249, 251, 254, 260
- MODIS, 37, 41, 47, 50, 74, 125, 127, 130, 132, 133, 216
- Mousani Island, 155, 156, 160, 162, 164, 169, 171
- Multi-criteria-decision-making, 4, 5, 18
- Multiple logistic regression, 233, 239, 240

N

- Natural hazards, 49, 212
- Natural resources, 27, 34, 157
- NCEP and HADCM3, 60
- NDVI, 40, 41, 43, 45, 74, 76, 78, 81, 82, 84, 98, 99, 110–112, 117, 217, 219, 220, 222, 226, 237
- NDWI, 141, 142, 217, 219, 220, 222, 226
- Neuro-fuzzy model, 249, 252, 254, 256, 257, 259, 261

O

- Ocean, 124, 128, 196, 216
- Open-source, 24, 28, 32, 47

R

- Reflectance, 41, 78, 81, 84, 98, 110, 141, 142, 146, 217, 220
- Remote sensing, 24, 25, 36, 38, 47, 74, 84, 85, 89, 92, 94, 95, 98, 99, 109, 125, 133, 140, 149, 157, 170, 179, 191, 231, 233, 236, 244
- River discontinuity, 138, 149
- Ruggedness index, 249, 251–253, 255, 257

S

- Sagar Island, 100, 101, 155, 156, 160, 162, 167
- Saline blank, 100, 101, 105
- Sambar, 232, 239, 241–245
- SDSM, 58, 60, 61, 63–68
- Soil moisture, 7, 36, 42, 47, 48, 50, 51, 89, 220, 226
- Suitability analysis, 4, 18, 233, 237, 240, 260
- Suitability mapping, 249
- Sundarban, 98–102, 104, 106, 124, 138, 140, 154, 156, 170, 196–198, 212
- Susceptibility, 177, 179–181, 183–186, 189–191, 249
- Sustainability, 88, 91, 94, 154, 157, 171
- Sustainable development, 1, 24, 26, 226
- Synthetic color composite, 110, 112, 114, 115

T

- Thermal remote sensing, 37, 49

U

- Urban heat island, 48, 51, 217, 219
- Urbanization, 154, 216, 217, 219, 222

V

- Vegetation cover, 40, 110, 112, 117, 226
- Vulnerability, 196–199, 201, 202, 204, 206–210, 212, 249

W

- Watershed, 12, 23, 24, 26, 32, 34, 88, 89, 91, 92, 94, 95
- Weightage matrix, 2, 6, 7, 12, 15, 17
- Weighted overlay technique, 249, 256, 259
- Weight-rating system, 181, 184, 186, 190, 191
- Wild habitat, 232, 234
- WRD, 24, 25, 27, 28, 31, 33